



HAL
open science

Influence of wood flour and cellulose on the properties and the stability of formulations based on polyolefins and bio-based polymers

Alessia Quitadamo

► **To cite this version:**

Alessia Quitadamo. Influence of wood flour and cellulose on the properties and the stability of formulations based on polyolefins and bio-based polymers. Matériaux. Université de Lyon; Università degli studi La Sapienza (Rome), 2019. Français. NNT : 2019LYSEI015 . tel-03098435

HAL Id: tel-03098435

<https://theses.hal.science/tel-03098435>

Submitted on 5 Jan 2021

HAL is a multi-disciplinary open access archive for the deposit and dissemination of scientific research documents, whether they are published or not. The documents may come from teaching and research institutions in France or abroad, or from public or private research centers.

L'archive ouverte pluridisciplinaire **HAL**, est destinée au dépôt et à la diffusion de documents scientifiques de niveau recherche, publiés ou non, émanant des établissements d'enseignement et de recherche français ou étrangers, des laboratoires publics ou privés.



SAPIENZA
UNIVERSITÀ DI ROMA



INSA

2019LYSEI015

UNIVERSITÉ
FRANCO
ITALIENNE

UNIVERSITÀ
ITALO
FRANCESE

PhD in Joined Agreement

Sapienza, University of Rome

Department of Chemical Engineering Materials Environment

Electrical, Materials and Nanotechnology Engineering (EMNE)

(XXXI cycle)

INSA, University of Lyon

Polymer Material Engineering

Material

(ED 34)

Alessia Quitadamo

Influence of wood flour and cellulose on the properties and the stability of formulations based on polyolefins and bio-based polymers

2019, March 14th

In front of the jury composed of :

Bemporad, Edoardo, Professeur, Università degli studi Roma Tre Reviewer

Nanni, Francesca, Associate Professor, Università degli studi di Roma Tor Vergata, Reviewer

Robin, Jean-Jacques, Professeur, Institut Charles Gerhardt Montpellier, Examiner

Bergeret, Anne, Professeur, Ecole des Mines, Examiner

Valente, Marco, Associate Professor, Sapienza Università di Roma, PhD Supervisor

Massardier, Valérie, Maître de Conférences HDR, INSA-Lyon, PhD Supervisor

Département FEDORA – INSA Lyon - Ecoles Doctorales – Quinquennal 2016-2020

SIGLE	ECOLE DOCTORALE	NOM ET COORDONNEES DU RESPONSABLE
CHIMIE	CHIMIE DE LYON http://www.edchimie-lyon.fr Sec. : Renée EL MELHEM Bât. Blaise PASCAL, 3e étage secretariat@edchimie-lyon.fr INSA : R. GOURDON	M. Stéphane DANIELE Institut de recherches sur la catalyse et l'environnement de Lyon IRCELYON-UMR 5256 Équipe CDFA 2 Avenue Albert EINSTEIN 69 626 Villeurbanne CEDEX directeur@edchimie-lyon.fr
E.E.A.	ÉLECTRONIQUE, ÉLECTROTECHNIQUE, AUTOMATIQUE http://edeea.ec-lyon.fr Sec. : M.C. HAVGOUDOUKIAN ecole-doctorale.eea@ec-lyon.fr	M. Gérard SCORLETTI École Centrale de Lyon 36 Avenue Guy DE COLLONGUE 69 134 Écully Tél : 04.72.18.60.97 Fax 04.78.43.37.17 gerard.scorletti@ec-lyon.fr
E2M2	ÉVOLUTION, ÉCOSYSTÈME, MICROBIOLOGIE, MODÉLISATION http://e2m2.universite-lyon.fr Sec. : Sylvie ROBERJOT Bât. Atrium, UCB Lyon 1 Tél : 04.72.44.83.62 INSA : H. CHARLES secretariat.e2m2@univ-lyon1.fr	M. Philippe NORMAND UMR 5557 Lab. d'Ecologie Microbienne Université Claude Bernard Lyon 1 Bâtiment Mendel 43, boulevard du 11 Novembre 1918 69 622 Villeurbanne CEDEX philippe.normand@univ-lyon1.fr
EDISS	INTERDISCIPLINAIRE SCIENCES-SANTÉ http://www.ediss-lyon.fr Sec. : Sylvie ROBERJOT Bât. Atrium, UCB Lyon 1 Tél : 04.72.44.83.62 INSA : M. LAGARDE secretariat.ediss@univ-lyon1.fr	Mme Emmanuelle CANET-SOULAS INSERM U1060, CarMeN lab, Univ. Lyon 1 Bâtiment IMBL 11 Avenue Jean CAPELLE INSA de Lyon 69 621 Villeurbanne Tél : 04.72.68.49.09 Fax : 04.72.68.49.16 emmanuelle.canet@univ-lyon1.fr
INFOMATHS	INFORMATIQUE ET MATHÉMATIQUES http://edinfomaths.universite-lyon.fr Sec. : Renée EL MELHEM Bât. Blaise PASCAL, 3e étage Tél : 04.72.43.80.46 infomaths@univ-lyon1.fr	M. Luca ZAMBONI Bât. Braconnier 43 Boulevard du 11 novembre 1918 69 622 Villeurbanne CEDEX Tél : 04.26.23.45.52 zamboni@maths.univ-lyon1.fr
Matériaux	MATÉRIAUX DE LYON http://ed34.universite-lyon.fr Sec. : Stéphanie CAUVIN Tél : 04.72.43.71.70 Bât. Direction ed.materiaux@insa-lyon.fr	M. Jean-Yves BUFFIÈRE INSA de Lyon MATEIS - Bât. Saint-Exupéry 7 Avenue Jean CAPELLE 69 621 Villeurbanne CEDEX Tél : 04.72.43.71.70 Fax : 04.72.43.85.28 jean-yves.buffiere@insa-lyon.fr
MEGA	MÉCANIQUE, ÉNERGÉTIQUE, GÉNIE CIVIL, ACOUSTIQUE http://edmega.universite-lyon.fr Sec. : Stéphanie CAUVIN Tél : 04.72.43.71.70 Bât. Direction mega@insa-lyon.fr	M. Jocelyn BONJOUR INSA de Lyon Laboratoire CETHIL Bâtiment Sadi-Carnot 9, rue de la Physique 69 621 Villeurbanne CEDEX jocelyn.bonjour@insa-lyon.fr
ScSo	ScSo* http://ed483.univ-lyon2.fr Sec. : Viviane POLSINELLI Brigitte DUBOIS INSA : J. Y. TOUSSAINT Tél : 04.78.69.72.76 viviane.polsinelli@univ-lyon2.fr	M. Christian MONTES Université Lyon 2 86 Rue Pasteur 69 365 Lyon CEDEX 07 christian.montes@univ-lyon2.fr

*ScSo: Histoire, Géographie, Aménagement, Urbanisme, Archéologie, Science politique, Sociologie, Anthropologie

List of figure	i
List of table	vi
Riassunto	I
Introduzione	I
Bibliografia	III
Blend polimerici	III
Compositi con filler naturali	IX
Résumé	XIV
Introduction	XIV
Bibliographie	XV
—Mélanges de polymères	XVI
Composites avec charges naturelles	XXIII
Introduction	1
References	2
1. State of the art	1
1.1 Wood-plastic composites	4
1.2 Waste paper as filler in thermoplastic composites	11
1.2.1 References	Erreur ! Signet non défini.
1.3 Bio-derived thermoplastic polymers	15
1.3.1 Polylactic Acid (PLA)	16
1.3.2 Soy Protein Isolate (SPI)	22
1.4 Thermoplastics blends	25
References	Erreur ! Signet non défini.
1.5 Biodegradability	30
1.5.1 References	40
2 Materials and Methods	47
2.1 Materials	47
2.1.1 Polymers	47
2.1.2 Additives	51
2.1.3 Natural Fibres	52
2.1.4 Production process	53
2.2 Methods	54
2.2.1 Tensile tests	57
2.2.2 Optical Microscopy	57

2.2.3	Scanning electron microscopy (SEM)	57
2.2.4	Quartering	58
2.2.5	Differential Scanning Calorimetry (DSC)	59
2.2.6	Thermogravimetric Analysis (TGA)	60
2.2.7	Rheological measurements (ARES G2)	61
2.2.8	Infrared Analysis Attenuated Total Reflection (ATR-FTIR)	64
2.2.9	Size Exclusion Chromatography (SEC)	65
2.2.10	Composting Tests	66
3	Waste paper treatment and application in WPC	70
3.1	From waste paper to useful fillers	70
3.1.1	Superfine grinding mill type SF	70
3.1.2	Knife mill SM 300	73
3.2	Recycled waste paper fibres in HDPE and WPC	80
3.3	References	87
4	Polymer Blends	88
	Elaboration of PLA based blend	88
4.1	Effect of compatibilizer on PLA	88
4.1.1	Tensile tests	88
4.1.2	Scanning electron microscopy (SEM)	89
4.1.3	Size Exclusion Chromatography (SEC)	90
4.1.4	Differential scanning calorimetry (DSC)	90
4.1.5	ATR-FTIR	92
4.2	HDPE-PLA blend	94
4.2.1	Tensile Test	94
4.2.2	Scanning Electron Microscopy (SEM)	98
4.2.3	Differential Scanning Calorimetry (DSC)	99
4.2.4	Thermogravimetric Analysis (TGA)	101
4.2.5	Infrared Analysis Attenuated Total Reflection (ATR-FTIR)	102
4.3	Elaboration of SPI based blends	104
4.4	Effect of compatibilizer on SPI	104
4.4.1	Tensile tests	105
4.4.2	Rheological measurements	107
4.4.3	Scanning Electron Microscopy (SEM)	108
4.4.4	Thermogravimetric Analysis (TGA)	111
4.4.5	Attenuated Total Refraction Infrared Spectroscopy	114
4.5	HDPE-SPI blend	116

4.5.1	Tensile tests	116
4.5.2	Scanning Electron Microscopy	117
4.5.3	Composting tests	120
4.6	Conclusion	123
4.7	References	125
5	Composites with Natural Fillers	127
	Wood Flour (WF)	127
5.1	Tensile tests	134
5.2	Scanning Electron Microscopy (SEM)	136
5.3	Differential Scanning Calorimetry (DSC)	138
5.4	Thermogravimetric Analysis (TGA)	142
5.5	Infrared Analysis Attenuated Total Reflection (ATR-FTIR)	144
	Recycled waste paper (P) and mix WF-P	144
5.6	Tensile tests	145
5.7	Scanning Electron Microscopy (SEM)	148
5.8	Differential Scanning Calorimetry (DSC)	151
5.9	Influence of Wood flour and Recycled waste paper on HDPE and PLA	152
5.10	Composting tests	163
5.11	Conclusion	201
5.12	References	202
6	Conclusion	206

List of figure

FIGURA 1: CURVE DI TRAZIONE PER I BLEND HDPE-PLA CON TRE DIVERSE PROPORZIONI (BLU HDPE70-PLA30, ARANCIONE HDPE50-PLA50 E GRIGIO HDPE30-PLA70)	IV
FIGURA 2: HDPE50-PLA50 BLEND (A) CON IL 3WT.% DI LOTADER AX8840 (B) AND POLYBOND 3029 (C).....	V
FIGURA 3: IMMAGINI AL MICROSCOPIO A SCANSIONE ELETTRONICA (SEM) DI PLA75-LOT25 (A) AND PLA75-POLY25 (B).	V
FIGURA 4: VISCOSITÀ DINAMICA DEL LOTADER AX8840 E DEI SUOI BLEND CON LA PROTEINA DI SOIA IN DIVERSI RAPPORTI (DA LOT75-(SPI70-GLY30)25 A LOT25-(SPI70-GLY30)75).	VI
FIGURA 5: CURVE DI TRAZIONE PER HDPE50SPI50 (GRIGIO), HDPE50(SPI70GLY30)50 (ARANCIONE) E HDPE48.5(SPI70GLY30)48.5LOT3 (BLU).	VII
FIGURA 6: IMMAGINI SEM DI HDPE50SPI50 (A), HDPE50(SPI70GLY30)50 (B), HDPE50(SPI70GLY30)50LOT3 (C)	VIII
FIGURA 7: OSSERVAZIONE VISIVA DI HDPE, PROTEINA DI SOIA ISOLATA (SPI) AND HDPE50SPI50 DURANTE TRE MESI DI COMPOSTAGGIO A 35°C AND 58°C.....	IX
FIGURA 8: VARIAZIONE DI MASSA DELL'HDPE E DEL BLEND HDPE50-SPI50 DURANTE TRE MESI DI COMPOSTAGGIO (T1= 1 MESE, T2= 2 MESI, T3= 3 MESI) A 35°C (SCALA DEI BLU) E A 58°C (SCALA DEI VERDI).	IX
FIGURA 9: IMMAGINE SEM HDPE50-PLA50-WF30 (A), HDPE50-PLA50-LOT3-WF30 (B), HDPE50-PLA50-POLY3-WF30 (C).	XI
FIGURA 10: MODULO ELASTICO (BLU), ALLUNGAMENTO A ROTTURA (GRIGIO) E CARICO DI ROTTURA (ARANCIONE) PER I COMPOSITI CARICATI CON LA FARINA DI LEGNO E LE FIBRE DI CARTA RICICLATA.	XII
FIGURA 11: IMMAGINE SEM DI A)HDPE50-PLA50-P10, PRIVO DI AGGLOMERATI E B)HDPE50-PLA50-P20, CON AGGLOMERATI.	XII
FIGURA 12: A) VELOCITÀ DI CRISTALLIZZAZIONE RISPETTO AL TEMPO PER PLA (BLU), PLA60-P40 (ARANCIONE) E PLA60WF40 (GRIGIO), B) VELOCITÀ DI CRISTALLIZZAZIONE RISPETTO AL TEMPO PER HDPE (BLU), HDPE60-P40 (ARANCIONE) E HDPE60WF40 (GRIGIO).	XIII
FIGURE 13: TRABANT CAR, PRODUCED IN 1958 IN THE GERMAN DEMOCRATIC REPUBLIC WITH MAIN PARTS MADE OF COMPOSITES WITH NATURAL FILLERS [WIKIPEDIA, TRABANT, 18/11/2016]	2
FIGURE 14: EXAMPLE OF WOOD-PLASTIC COMPOSITES APPLICATION IN DECKING MARKET [7TRUST.COM, GREEN PRODUCTS 18/11/2016].....	4
FIGURE 15: POLYPROPYLENE-GRAFTED-MALEIC ANHYDRIDE	5
FIGURE 16: WORKING MECHANISM OF POLYOLEFIN-GRAFTED-MALEIC ANHYDRIDE AS COUPLING AGENT (ELLIPTICAL SHAPE IS THE MALEIC ANHYDRIDE GRAFT): LEFT) COMPOUND FORMATION BECAUSE OF THE WEAK INTERACTION BETWEEN PLANT FIBRES (HYDROPHILIC) AND POLYMERS (HYDROPHOBIC); RIGHT) COMPOSITE FORMATION THANKS TO THE INTERACTION OF MAPP MALEATED GRAFT WITH PLANT FIBRES AND POLYMERIC MAPP CHAINS MIXING WITH POLYMER MATRIX. [ADAPTED FROM 5]	5
FIGURE 17: TENSILE STRENGTH TREND OF POLYPROPYLENE-RICE HUSK FLOUR (PP-RHF) NEAT AND WITH FIVE DIFFERENT COMPATIBILIZING AGENTS [ADAPTED FROM 24]	7
FIGURE 18: IZOD IMPACT STRENGTH TREND OF POLYPROPYLENE-RICE HUSK FLOUR (PP-RHF) NEAT AND WITH FIVE DIFFERENT COMPATIBILIZING AGENTS [ADAPTED FROM 24]	7
FIGURE 19: TENSILE MODULUS TREND OF RECYCLED HDPE FROM MILK BOTTLES, WITH 30 WT.% OF ASPEN HARDWOOD AND 2 OR 5 WT.% OF MAPP [ADAPTED FROM 25].....	8
FIGURE 21: STORAGE MODULUS OF PA11 NEAT AND WITH BEECH FIBRES (BF) (30-40-50 WT.%) MODIFIED (MOD) AND NOT [28].	11
FIGURE 22: DIMENSIONAL STABILITY OF POLYPROPYLENE (PP), HIGH-IMPACT POLYPROPYLENE (HIPP), HIGH-DENSITY POLYETHYLENE (HDPE) AND LOW-DENSITY POLYETHYLENE (LDPE) WITH DIFFERENT PERCENTAGES OF PAPER SLUDGE [ADAPTED FROM 41]	15
FIGURE 23: FLEXURAL STRENGTH OF POLYPROPYLENE (PP), HIGH-IMPACT POLYPROPYLENE (HIPP), HIGH-DENSITY POLYETHYLENE (HDPE) AND LOW-DENSITY POLYETHYLENE (LDPE) WITH DIFFERENT PERCENTAGES OF PAPER SLUDGE [ADAPTED FROM 41]	15
FIGURE 24: RING OPENING POLYMERIZATION OF LACTIDE TO PRODUCE POLYLACTIC ACID (PLA) [ADAPTED FROM WWW.INNOREX.EU]	16

FIGURE 25: INFLUENCE OF TEC (A) AND ABTC (B) ON GLASS TRANSITION TEMPERATURES OF PLA BASED BLENDS [46]	19
.....	
FIGURE 26: STRESS-STRAIN CURVES OF NEAT PLA AND PLA MODIFIED WITH FOUR DIFFERENT IONIC LIQUIDS [47]	22
FIGURE 27: FORMATION OF PEPTIDE BOND BETWEEN CARBOXYL AND AMINO GROUPS, WITH ELIMINATION OF WATER.....	23
FIGURE 28: TYPICAL PROTEIN INTERACTIONS THAT STABILIZE PROTEIN STRUCTURES.	23
FIGURE 29: THE ROLE OF PLASTICIZER ON POLYMER.....	24
FIGURE 30: EFFECT OF GLYCEROL CONTENT ON SPI FILM [58].	24
FIGURE 31: DIFFERENT SPI FILMS WITH 0-10-20-30-40 WT.% OF GLYCEROL [59].	25
FIGURE 32: THERMAL ANALYSIS RESULTS FOR LOW-DENSITY POLYETHYLENE/PLA BLEND WITH 4 PHR OF LOW-DENSITY POLYETHYLENE-GRAFT-MALEIC ANHYDRIDE [73].....	28
FIGURE 33: SEM MICROGRAPHS OF PLA80LDPE20 BLENDS WITH DIFFERENT AMOUNTS OF PE-GMA (0 TO 10 WT.%) [75].	29
FIGURE 34: EFFECT ON ELONGATION AT BREAK AND YOUNG’S MODULUS OF PE-G-MA ON LLDPE/SPI BLENDS WITH DIFFERENT AMOUNTS OF SPI [76].	30
FIGURE 35: PLA MACROSCOPICAL EFFECTS OF SOIL BURIAL TESTING (YELLOWING, BREAKAGE AND FRAGMENTATION) [78].....	32
FIGURE 36: EVOLUTION OF DIFFERENT POLYMERS AFTER 28 DAYS OF INCUBATION IN SOLID MEDIUM [79].	33
FIGURE 37: DEGREE OF BIODEGRADATION (%) FOR PURE PLA, PLA/LLDPE BLEND, PLA/LLDPE BLENDS WITH NANOCLAY (CLOISITE® 30B (30B), MMT-NA+ MODIFIED WITH BIS-(2-HYDROXYETHYL) METHYL TALLOW ALKALY AMMONIUM CATIONS AND CLOISITE® 15A (15A), MMT-NA+ MODIFIED WITH DIMETHYL, DEHYDROGENATED TALLOW, QUATERNARY AMMONIUM CATIONS) PROCESSED WITH ONE STEP OR TWO STEPS MIXING [81].....	34
FIGURE 38: TIME-DEPENDENCE OF RESIDUAL WEIGHT RW(%) FOR PURE PLA, PURE LLDPE-LDPE, PLA/(LLDPE-LDPE) 50/50 WITH AND WITHOUT 5% ORGANOPHILIC MONTMORILLONITE (ORG-MMT) [82].	36
FIGURE 39: CHEMICAL STRUCTURE OF THE MAIN CONSTITUENTS OF NATURAL FIBRES (CELLULOSE, HEMICELLULOSE AND LIGNIN).....	37
FIGURE 40: HIERARCHICAL STRUCTURE OF LIGNOCELLULOSIC FIBRES [88].....	38
FIGURE 41: CHEMICAL PROPERTIES OF DIFFERENT AMINO ACIDS RELATED TO R SIDE GROUP PRESENCE.	51
FIGURE 41: EXTRUSION EQUIPMENT (A), INJECTION MOULDING EQUIPMENT (B) AND SAMPLES OBTAINED FROM THE PRODUCTION PROCESS.	54
FIGURE 42: CYLINDRICAL STATOR AND ROTOR WITH BLADES OF THE TURBOMIXER EQUIPMENT.....	55
FIGURE 43: GENERAL PROCESS TO OBTAIN SAMPLES WITH TURBOMIXER PROCESSING: A)INTRODUCTION OF POLYMER PELLETS, B) INTRODUCTION OF NATURAL FILLERS, C) EXTRACTION OF THE MELTED CHARGE AFTER PROCESSING AT MELTING TEMPERATURE AND HIGH SPEED ROTATION, D) INTRODUCTION OF MELTED CHARGE IN THE COMPRESSION MOULDING EQUIPMENT, E) EXTRACTION OF SAMPLES.	56
FIGURE 44: TENSILE TEST EQUIPMENT USED TO EVALUATE MECHANICAL PROPERTIES.....	57
FIGURE 45: DIFFERENTIAL SCANNING CALORIMETRY EQUIPMENT USED TO ANALYSE THERMO-CHEMICAL PROPERTIES OF SAMPLES.	60
FIGURE 46: THERMOGRAVIMETRIC ANALYSIS EQUIPMENT USED TO ANALYSE THERMAL STABILITY OF OUR SAMPLES.	61
.....	
FIGURE 47: AMPLITUDE SWEEP PERFORMED TO DETECT A SOLICITATION AMPLITUDE IN WHICH THE MODULE IS INDEPENDENT OF THE DEFORMATION FOR BOTH HDPE (A) AND PLA (B)	62
FIGURE 48: RHEOLOGY EQUIPMENT USED TO PERFORM RHEOLOGICAL MEASUREMENTS.....	63
FIGURE 49: TIME SWEEP PERFORMED TO EVALUATE THE STABILITY OF PLA AT FIXED DEFORMATION (1% DERIVED FROM AMPLITUDE SWEEP) AND 10RAD/S FREQUENCY FOR 1 HOUR.	64
FIGURE 50: INFRARED ANALYSIS ATTENUATED TOTAL REFLECTION (ATR-FTIR) EQUIPMENT USED TO EVALUATE INTERACTIONS OR REACTIONS BETWEEN COMPONENTS.	65
FIGURE 51: SIZE EXCLUSION CHROMATOGRAPHY EQUIPMENT USED TO EVALUATE MOLECULAR WEIGHT OF PLA-BASED SAMPLES.	66
FIGURE 52: AQUARIA USED TO PERFORM COMPOSTING TESTS AT MESOPHILIC (A) AND THERMOPHILIC (B) CONDITIONS.....	67
FIGURE 53: AQUARIA WEIGHTED BEFORE (A) AND AFTER (B) THE ADDITION OF SOIL AND SAMPLES TO EVALUATE THE VARIATION OF WEIGHT UNDER COMPOSTING CONDITION.....	67

FIGURE 54: SAMPLES HAVE BEEN PLACED OVER 1KG OF SOIL (A) AND THEN HAVE BEEN COVERED WITH ANOTHER KG OF SOIL TO PERFORM COMPOSTING TESTS.....	68
FIGURE 42: PROCESS SCHEME OF THE MICRONIZATION PLANT.....	71
FIGURE 43: STEREOMICROSCOPY IMAGE OF MICRONIZED PAPER.....	72
FIGURE 44: OPTICAL MICROSCOPY IMAGE OF MICRONIZED PAPER.....	72
FIGURE 45: RECYCLED PAPER BEFORE MICRONIZING PROCESS.....	73
FIGURE 46:RECYCLED PAPER AFTER MICRONIZING PROCESS THROUGH SUPERFINE GRINDING MILL.....	73
FIGURE 47: SCHEME OF THE ADOPTED KNIFE MILL SM300.....	74
FIGURE 48: STEREOMICROSCOPY IMAGE AND VISUAL OBSERVATION OF RECYCLED PAPER AFTER MICRONIZING PROCESS THROUGH KNIFE MILL.....	75
FIGURE 49: STRESS-STRAIN CURVES FOR NEAT HDPE AND COMPOSITES WITH 10 WT.% AND 20 WT.% OF WASTE PAPER PROCESSED WITH SUPERFINE GRINDING MILL.....	76
FIGURE 50: STRESS-STRAIN CURVES FOR COMPOSITES WITH 20WT.% OF FILLERS FROM SUPERFINE GRINDING MILL (20S) AND KNIFE MILL(20K).....	77
FIGURE 51: SEM PICTURE OF SPECIMENS WITH 10WT.% FIBRES S.....	78
FIGURE 52: SEM PICTURE OF SPECIMENS WITH 20WT.% FIBRES K.....	78
FIGURE 53: SEM OF THE COMPOSITE PRODUCED WITH 20WT.% OF FIBRES FROM THE SUPERFINE GRINDING MILL....	79
FIGURE 54: SEM OF THE COMPOSITES PRODUCED WITH 20WT.% OF FIBRES FROM THE KNIFE MILL.....	79
FIGURE 55: STRESS-STRAIN CURVE FOR COMPOSITES WITH 10WT.% OF FIBRES (F) FROM SUPERFINE GRINDING MILL WITH 1-3-5 WT.% OF MAPE(A).....	81
FIGURE 56: COMPARISON OF WATER ABSORPTION TESTS AT DIFFERENT TEMPERATURES.....	82
FIGURE 57: TENSILE TEST RESULTS FOR HDPE BASED COMPOSITES WITH 30WT.% OF WOOD FLOUR, 10WT.% OF RECYCLED PAPER FIBRES AND A MIX OF TWO MORPHOLOGIES.....	84
FIGURE 58: TENSILE TEST RESULTS FOR HDPE BASED COMPOSITES WITH 30WT.% OF WOOD FLOUR, 30WT.% OF WOOD FLOUR AND 10WT.% OF RECYCLED PAPER FIBRES WITH AND WITHOUT MAPE.....	84
FIGURE 59: WATER ABSORPTION TESTS FOR HDPE BASED COMPOSITES WITH 30WT.% OF WOOD FLOUR (W),30WT.% OF WOOD FLOUR (W) AND 10WT.% OF RECYCLED PAPER FIBRES (F) WITH AND WITHOUT MAPE COMPATIBILIZER (A).....	86
FIGURE 60: SCANNING ELECTRON MICROSCOPY IMAGES OF PLA75-LOT25 (A) AND PLA75-POLY25 (B).....	90
FIGURE 74: DSC CURVES OF NEAT PLA (BLUE), PLA75-LOT25 (FUCSIA) AND PLA74-POLY25 (GREEN).....	91
FIGURE 61: ATR-FTIR SPECTRA OF PLA, LOTADER AX8840, POLYBOND 3029, PLA75-LOT25 AND PLA75-POLY25.....	93
FIGURE 62: NMR SPECTRA OF NEAT PLA (BLUE) AND PLA75LOT25 (RED).....	94
FIGURE 63: TENSILE TESTS RESULTS OF HDPE-PLA BLENDS WITH DIFFERENT RATIOS (BLUE HDPE70-PLA30, ORANGE HDPE50-PLA50 AND GREY HDPE30-PLA70).....	95
FIGURE 64: TENSILE TESTS RESULTS OF COMPATIBILIZED HDPE50-PLA50 BLENDS WITH 1, 3 AND 5WT.% OF LOTADER AX8840 AND POLYBOND 3029.....	97
FIGURE 65: HDPE50-PLA50 BLEND MORPHOLOGY OF CRYO-FRACTURED SURFACE.....	98
FIGURE 66: HDPE50-PLA50 BLEND WITH 3WT.% OF LOTADER AX8840 (A) AND POLYBOND 3029 (B) OF CRYO-FRACTURED SURFACE.....	99
FIGURE 67: DIFFERENTIAL SCANNING CALORIMETRY THERMOGRAMS OF NEAT PLA, HDPE AND HDPE50-PLA50.....	100
FIGURE 68: INFRARED SPECTRA (ATR-FTIR) OF A) HDPE, PLA AND HDPE50-PLA50 AND B) HDPE50-PLA50, HDPE50-PLA50-POLY3 AND HDPE50-PLA50-LOT3.....	103
FIGURE 69: TENSILE TESTS RESULTS OF LOTADER AX8840-SOY PROTEIN ISOLATE (SPI) BLEND WITH 10 AND 30 WT.% OF PLASTICIZER (GLYCEROL).....	105
FIGURE 70: DYNAMIC VISCOSITY OF LOTADER AX8840 AND ITS BLENDS WITH SPI.....	107
FIGURE 71: DYNAMIC VISCOSITY OF LOT-(SPI70-GLY30) FOR DIFFERENT BLEND RATIOS.....	108
FIGURE 72: SEM IMAGES OF A) SPI70-GLY30, B) LOT75-SPI25, C) LOT75-(SPI90-GLY10)25, D) LOT75-(SPI70-GLY30)25.....	109
FIGURE 73 : SEM IMAGES OF A) LOT35-(SPI70-GLY30)65 , B) LOT50-(SPI70-GLY30)50, C) LOT65-(SPI70-GLY30)35 , D) LOT75-(SPI70-GLY30)25 AT 120°C WITH SECONDARY ELECTRONS SE.....	110
FIGURE 74: INFLUENCE OF GLYCEROL ON SPI DEGRADATION.....	111

FIGURE 75: A) MASS VARIATION DURING DEGRADATION OF LOTADER AX8840 (GREEN), LOT75-SPI25 (BLUE) AND LOT75-(SPI70-GLY30)25 (FUCHSIA), B) DERIVATIVE WEIGHT CURVE FOR LOTADER AX8840 (GREEN), LOT75-SPI25 (BLUE) AND LOT75-(SPI70-GLY30)25 (FUCHSIA).	113
FIGURE 76 : FTIR SPECTRA OF GLYCEROL, SPI AND SPI70-GLY30	114
FIGURE 77: ATR-FTIR SPECTRA OF LOTADER AX8840 (A), LOT75-SPI25(B) AND LOT75-(SPI70GLY30)25 (B).	116
FIGURE 78: TENSILE TESTS RESULTS FOR HDPE50-SPI50 (GREY), HDPE50-(SPI70-GLY30)50 (ORANGE) AND HDPE48.5-(SPI70-GLY30)-48.5-LOT3(BLUE).	117
FIGURE 79: : SEM IMAGES OF A) HDPE50-SPI50 FRACTURE SURFACE FROM TENSILE TEST 30X, B)HDPE50-(SPI70-GLY30)50 FRACTURE SURFACE FROM TENSILE TEST 30X, C) HDPE50-SPI50 CRYO-FRACTURED SURFACE 35X, D)HDPE50-(SPI70-GLY30)50 CRYO-FRACTURED SURFACE 35X, E) HDPE50-(SPI70-GLY30)50-LOT3 CRYO-FRACTURED 35X, F) HDPE50-SPI50 CRYO-FRACTURED 100X, G) HDPE50-(SPI70-GLY30)50 CRYO-FRACTURED 100X , H)HDPE50-(SPI70-GLY30)50-LOT3 CRYO-FRACTURED 100X.	119
FIGURE 80: VISUAL OBSERVATION OF HDPE, SOY PROTEIN ISOLATE (SPI) AND HDPE50-SPI50 DURING THREE MONTHS TESTING IN SOIL AT 35°C AND 58°C.	121
FIGURE 81: MASS VARIATION MEASUREMENTS OF HDPE AND HDPE50-(SPI70-GLY30)50 DURING THREE MONTHS TESTING IN SOIL AT 35°C (BLUE-SCALE) AND 58°C (GREEN-SCALE).	121
FIGURE 82: ATR-FTIR RESULTS FOR HDPE DURING THREE MONTHS TESTING IN SOIL AT 35°C (A) AND 58°C (B).	122
FIGURE 83: ATR-FTIR RESULTS DURING THREE MONTHS OF COMPOSTING IN SOIL FOR HDPE50-(SPI70-GLY30)50 AT 35°C (A) AND 58°C (B).	123
FIGURE 84: SCANNING ELECTRON MICROSCOPY IMAGES OF A) PLA70-WF30, B) PLA70WF30IL, C) PLA52.5-LOT17.5-WF30 AND D) PLA52.5-POLY17.5-WF30	128
FIGURE 85:A) MASS VARIATION DURING DEGRADATION OF PLA (GREEN), PLA70WF30 (PURPLE), PLA70WFIL30 (RED), PLA52.5POLY17.5WF30 (BLUE, ONE DASHED LINE) AND PLA52.5LOT17.5WF30 (DASHED LINE) B) DERIVATIVE WEIGHT CURVE FOR PLA (GREEN), PLA70WF30 (PURPLE), PLA70WFIL30 (RED), PLA52.5POLY17.5WF30 (BLUE, ONE DASHED LINE) AND PLA52.5LOT17.5WF30 (DASHED LINE).	131
FIGURE 86: TENSILE TESTS RESULTS FOR HDPE50-PLA50 (RED), HDPE50-PLA50-WF20 (BLUE), HDPE50-PLA50-WF30 (GREY) AND HDPE50-PLA50-WF40 (PURPLE).	135
FIGURE 87:TENSILE TEST RESULTS FOR HDPE50-PLA50 (RED), HDPE50-PLA50-WF30 (BLUE), HDPE50-PLA50-LOT3-WF30 (GREY) AND HDPE50-PLA50-POLY3-WF30 (YELLOW).....	136
FIGURE 88: HDPE50-PLA50-WF30 COMPOSITE	137
FIGURE 89: HDPE50-PLA50-LOT3-WF30 (A) HDPE50-PLA50-POLY3-WF30 (B).....	138
FIGURE 90: DSC THERMOGRAMS OF A)HDPE50-PLA50, HDPE50-PLA50-WF20, HDPE50-PLA50-WF30, HDPE50-PLA50-WF40, B) PLA MELTING PEAK MAGNIFICATION OF HDPE50-PLA50, HDPE50-PLA50-WF20, HDPE50-PLA50-WF30, HDPE50-PLA50-WF40, C) HDPE50-PLA50, HDPE50-PLA50-WF30, HDPE50-PLA50-LOT3-WF30, HDPE50-PLA50-POLY3-WF40, D) PLA MELTING PEAK MAGNIFICATION OF HDPE50-PLA50, HDPE50-PLA50-WF30, HDPE50-PLA50-LOT3-WF30, HDPE50-PLA50-POLY3-WF40.....	142
FIGURE 91:ATR-FTIR RESULTS FOR HDPE-PLA BLENDS HDPE50-PLA50 MATRIX COMPOSITES WITH 3 WT.% OF COMPATIBILIZER AND 30 WT.% OF WOOD FLOUR.	144
FIGURE 92: TENSILE TESTS CURVES OF HDPE50-PLA50 (RED), HDPE50-PLA50-P10 (BLUE), HDPE50-PLA50-P20 (GREY), HDPE50-PLA50-P30 (YELLOW), HDPE50-PLA50-P40 (GREEN).....	147
FIGURE 93: ELASTIC MODULUS (BLUE), ELONGATION AT BREAK (GREY) AND TENSILE STRENGTH (ORANGE) TREND FOR COMPOSITES WITH WOOD FLOUR AND RECYCLED WASTE PAPER.	147
FIGURE 94: TENSILE TEST CURVES OF HDPE50-PLA50-WF40 (RED), HDPE50-PLA50-P40 (BLUE), HDPE50-PLA50-WF30-P10 (GREEN), HDPE50-PLA50-LOT3-WF30-P10 (PURPLE) AND HDPE50-PLA50-POLY3-WF30-P10 (ORANGE).	148
FIGURE 95: SEM IMAGES OF A)HDPE50-PLA50-P10 AND B)HDPE50-PLA50-P20.	149
FIGURE 96: SEM IMAGES OF HDPE50-PLA50-WF30-P10.....	150
FIGURE 97: SEM IMAGES OF A) HDPE50-PLA50-LOT3-WF30-P10 (500X), B) HDPE50-PLA50-LOT3-WF30-P10 (1000X), C) HDPE50-PLA50-POLY3-WF30-P10 (500X) AND D) HDPE50-PLA50-POLY3-WF30-P10 (1000X).	151
FIGURE 98: MALTA CROSS EVOLUTION IN PLA STUDIED WITH A THERMO-OPTICAL MICROSCOPE AT 500X MAGNIFICATION WITH POLARIZED LIGHT.	154
FIGURE 99: CRYSTALS GROWTH IN PLA WITH RECYCLED WASTE PAPER (PLA60-P40), STUDIED WITH A THERMO-OPTICAL MICROSCOPE AT 500X MAGNIFICATION WITH POLARIZED LIGHT.	155

FIGURE 100: CRYSTALS GROWTH IN PLA WITH WOOD FLOUR (PLA60-WF40), STUDIED WITH A THERMO-OPTICAL MICROSCOPE AT 100X MAGNIFICATION WITH POLARIZED LIGHT.	156
FIGURE 101: CRYSTALLINITY RATE VS TIME FOR NEAT PLA (BLUE), PLA60-P40 (ORANGE) AND PLA60-WF40 (GREY)..	157
FIGURE 102: CRYSTALS' GROWTH IN HDPE STUDIED WITH A THERMO-OPTICAL MICROSCOPE AT 500X MAGNIFICATION	158
FIGURE 103: CRYSTALS' GROWTH IN HDPE WITH RECYCLED WASTE PAPER (HDPE60-P40), STUDIED WITH A THERMO-OPTICAL MICROSCOPE AT 500X MAGNIFICATION.	158
FIGURE 104: CRYSTALS' GROWTH IN HDPE WITH WOOD FLOUR (HDPE60-WF40), STUDIED WITH A THERMO-OPTICAL MICROSCOPE AT 500X MAGNIFICATION.....	159
FIGURE 105: CRYSTALLINITY RATE VS TIME FOR NEAT HDPE (BLUE), HDPE60-P40 (ORANGE) AND HDPE60-WF40 (GREY).....	160
FIGURE 106: TUBROMIXER PROCESSING OF SAMPLES WITH HDPE, PLA, WOOD FLOUR AND RECYCLED WASTE PAPER.	161
FIGURE 107: COMPRESSION MOULDING TECHNIQUE (PLATES AT 90°C) PERFORMED ON SAMPLES PRODUCED WITH TURBOMIXER PROCESSING.	161
FIGURE 108: SAMPLES OBTAINED WITH COMPRESSION MOULDING TECHNIQUE.....	162
FIGURE 109: VISUAL OBSERVATION OF HDPE, PLA, HDPE60-WF40, PLA60-WF40, HDPE60-P40, PLA60-P40, PLA60-WF30-P10 AND HDPE30-PLA30-WF30-P10 FOR THREE MONTHS TESTING IN SOIL AT 35°C AND 58°C.	166
FIGURE 110: MASS VARIATION MEASUREMENTS OF HDPE, PLA, HDPE60-WF40, PLA60-WF40, HDPE60-P40, PLA60-P40, PLA60-WF30-P10 AND HDPE30-PLA30-WF30-P10 FOR THREE MONTHS TESTING IN SOIL AT 35°C AND 58°C....	166
FIGURE 111: MASS AVERAGE MOLECULAR WEIGHT OF PLA-BASED SAMPLES BEFORE BURYING IN SOIL (T=0) AND AFTER ONE, TWO OR THREE MONTHS BURYING (T=1, T=2 AND T=3 RESPECTIVELY) AT 35°C.....	168
FIGURE 112: MASS AVERAGE MOLECULAR WEIGHT OF PLA-BASED SAMPLES BEFORE BURYING IN SOIL (T=0) AND AFTER ONE, TWO OR THREE MONTHS BURYING (T=1, T=2 AND T=3 RESPECTIVELY) AT 58°C.....	168
FIGURE 113: ATR-FTIR SPECTRUM OF RECYCLED WASTEPAPER	171
FIGURE 114: ATR-FTIR SPECTRUM OF WOOD FLOUR.....	171
FIGURE 115: ATR-FTIR SPECTRA OF HDPE FROM TIME 0 TO TIME 3 FOR BURIED SAMPLES AT 35°C.....	172
FIGURE 116: ATR-FTIR SPECTRA OF HDPE FROM TIME 0 TO TIME 3 FOR BURIED SAMPLES AT 58°C.....	172
FIGURE 117: ATR-FTIR SPECTRA OF HDPE60-P40 AT TIME 0,1,2,3 OF THE SAMPLES PLACED AT 35 ° C.....	174
FIGURE 118: ATR-FTIR SPECTRA OF HDPE60-P40 AT TIME 0, 1, 2, 3 OF SAMPLES PLACED AT 58 ° C.	174
FIGURE 119: ATR-FTIR SPECTRA OF HDPE60-WF40 AT TIME 0,1,2,3 OF THE SAMPLES PLACED AT 35° C.	175
FIGURE 120: ATR-FTIR SPECTRA OF HDPE60-WF40 AT TIME 0, 1, 2, 3 OF SAMPLES PLACED AT 58 ° C.	175
FIGURE 121: ATR-FTIR SPECTRA OF PLA AT TIME 0, 1, 2, 3 OF SAMPLES PLACED AT 35 ° C.	176
FIGURE 122: ATR-FTIR SPECTRA OF PLA AT TIME 0, 1, 2, 3 OF SAMPLES PLACED AT 58 ° C.	176
FIGURE 123: ATR-FTIR SPECTRA OF PLA60-WF40 AT TIME 0, 1, 2, 3 OF SAMPLES PLACED AT 35 ° C.....	177
FIGURE 124: ATR-FTIR SPECTRA OF PLA60-WF40 AT TIME 0, 1, 2, 3 OF SAMPLES PLACED AT 58 ° C.....	178
FIGURE 125: ATR-FTIR SPECTRA OF PLA60-P40 AT TIME 0, 1, 2, 3 OF SAMPLES PLACED AT 35 ° C.	179
FIGURE 126: ATR-FTIR SPECTRA OF PLA60-P40 AT TIME 0, 1, 2, 3 OF SAMPLES PLACED AT 58 ° C.	179
FIGURE 127: ATR-FTIR SPECTRA OF PLA60-WF30-P10 AT TIME 0, 1, 2, 3 OF SAMPLES PLACED AT 35 ° C.	180
FIGURE 128: ATR-FTIR SPECTRA OF PLA60-WF30-P10 AT TIME 0, 1, 2, 3 OF SAMPLES PLACED AT 58 ° C.	180
FIGURE 129: ATR-FTIR SPECTRA OF HDPE30-PLA30-WF30P-10 AT TIME 0, 1, 2, 3 OF SAMPLES PLACED AT 35 ° C.	181
FIGURE 130: ATR-FTIR SPECTRA OF HDPE30-PLA30-WF30-P10 AT TIME 0, 1, 2, 3 OF SAMPLES PLACED AT 58 ° C.	181
FIGURE 131: MASS AND DERIVATIVE VARIATIONS IN WEIGHT AS A FUNCTION OF TEMPERATURE DURING DEGRADATION OF HDPE AT TIME 0, 1, 2, 3 AT 35 ° C.....	183
FIGURE 132: MASS AND DERIVATIVE VARIATIONS IN WEIGHT AS A FUNCTION OF TEMPERATURE DURING DEGRADATION OF HDPE AT TIME 0, 1, 2, 3 AT 58 ° C.....	183
FIGURE 133: MASS AND DERIVATIVE VARIATIONS IN WEIGHT AS A FUNCTION OF TEMPERATURE DURING DEGRADATION OF HDPE60-WF40 AT TIME 0, 1, 2, 3 AT 35 ° C	184
FIGURE 134: MASS AND DERIVATIVE VARIATIONS IN WEIGHT AS A FUNCTION OF TEMPERATURE DURING DEGRADATION OF HDPE60-WF40 AT TIME 0, 1, 2, 3 AT 58 ° C	185
FIGURE 135: MASS AND DERIVATIVE VARIATIONS IN WEIGHT AS A FUNCTION OF TEMPERATURE DURING DEGRADATION OF HDPE60-P40 AT TIME 0, 1, 2, 3 AT 35 ° C.....	185

FIGURE 136: MASS AND DERIVATIVE VARIATIONS IN WEIGHT AS A FUNCTION OF TEMPERATURE DURING DEGRADATION OF HDPE60-P40 AT TIME 0, 1, 2, 3 AT 58 ° C.....	186
FIGURE 137: MASS AND DERIVATIVE VARIATIONS IN WEIGHT AS A FUNCTION OF TEMPERATURE DURING DEGRADATION OF PLA AT TIME 0, 1, 2, 3 AT 35 ° C.....	187
FIGURE 138: MASS AND DERIVATIVE VARIATIONS IN WEIGHT AS A FUNCTION OF TEMPERATURE DURING THE DEGRADATION OF PLA AT TIME 0, 1, 2, 3 AT 58 ° C.....	187
FIGURE 139: MASS AND DERIVATIVE VARIATIONS IN WEIGHT AS A FUNCTION OF TEMPERATURE DURING THE DEGRADATION OF PLA60-WF40 AT TIME 0, 1, 2, 3 AT 35 ° C.....	188
FIGURE 140: MASS AND DERIVATIVE VARIATIONS OF THE WEIGHT AS A FUNCTION OF THE TEMPERATURE DURING THE DEGRADATION OF PLA60-WF40 AT TIME 0, 1, 2, 3 AT 58 ° C.....	188
FIGURE 141: MASS AND DERIVATIVE VARIATIONS IN WEIGHT AS A FUNCTION OF TEMPERATURE DURING THE DEGRADATION OF PLA60-P40 AT TIME 0, 1, 2, 3 AT 35 ° C.....	189
FIGURE 142: MASS AND DERIVATIVE VARIATIONS IN WEIGHT AS A FUNCTION OF TEMPERATURE DURING THE DEGRADATION OF PLA60-P40 AT TIME 0, 1, 2, 3 AT 58 ° C.....	190
FIGURE 143: MASS AND DERIVATIVE VARIATIONS IN WEIGHT AS A FUNCTION OF TEMPERATURE DURING DEGRADATION OF HDPE30-PLA30-WF30-P10 AT TIME 0, 1, 2, 3 AT 35 ° C.....	191
FIGURE 144: MASS AND DERIVATIVE VARIATIONS IN WEIGHT AS A FUNCTION OF TEMPERATURE DURING DEGRADATION OF HDPE30-PLA30W-F30-P10 AT TIME 0, 1, 2, 3 AT 58 ° C.....	191
FIGURE 145: DSC RESULTS FOR NEAT HDPE AFTER THREE MONTHS BURIED AT 35°C.....	192
FIGURE 146: DSC RESULTS FOR NEAT HDPE AFTER THREE MONTHS BURIED AT 58°C.....	192
FIGURE 147: DSC RESULTS FOR HDPE60-WF40 AFTER THREE MONTHS BURIED AT 35°C.....	193
FIGURE 148: DSC RESULTS FOR HDPE60-WF40 AFTER THREE MONTHS BURIED AT 58°C.....	193
FIGURE 149: DSC RESULTS FOR HDPE60-P40 AFTER THREE MONTHS BURIED AT 35°C.....	194
FIGURE 150: DSC RESULTS FOR HDPE60-P40 AFTER THREE MONTHS BURIED AT 58°C.....	194
FIGURE 151: DSC RESULTS FOR NEAT PLA DURING COMPOSTING PROCESS AT 35°C.....	196
FIGURE 152: DSC RESULTS FOR NEAT PLA DURING COMPOSTING PROCESS AT 58°C.....	196
FIGURE 153: MELTING PEAK OF PLA60-WF40 COMPOSITES DURING COMPOSTING PROCESS AT 58°C.....	198
FIGURE 154: MELTING PEAK OF PLA60-WF30-P10 COMPOSITES DURING COMPOSTING PROCESS AT 58°C.....	198
FIGURE 155: MELTING PEAK OF HDPE30-PLA30-WF30-P10 COMPOSITES DURING COMPOSTING PROCESS AT 58°C.....	199
FIGURE 156: SUMMARY OF COMPOSTING RESULTS.....	200

List of table

TABELLA 1: RISULTATI DELLE PROVE DI TRAZIONE PER I BLEND HDPE50-PLA50 CON 1, 3 E 5 WT.% DI POLYBOND 3029 O DI LOTADER AX8840.....	III
TABELLA 2: RISULTATI DELLE PROVE DI TRAZIONE PER I BLEND LOTA75-SPI25 TAL QUALE, CON IL 30 WT.% DI GLICEROLO, E DIVERSI RAPPORTI LOTADER AX8840-SPI.....	VI
TABELLA 3: TENSILE TESTS RESULTS OF SAMPLES FILLED WITH WOOD FLOUR. BLUE COLOUR IS FOR WOOD FLOUR, PURPLE FOR POLYBOND 3029 AND RED IS FOR LOTADER AX8840 ADDITION.....	XI
TABLE 4: COMPARISON BETWEEN NATURAL AND GLASS FIBRES [2].....	1
TABLE 5: MECHANICAL PROPERTIES OF SOME NATURAL FIBRES IN COMPARISON TO TRADITIONAL FIBRES AND POLYMERS [ADAPTED 5].....	2
TABLE 6: PROPERTIES OF FIVE MAPP WITH DIFFERENT MALEIC ANHYDRIDE CONTENT (MA%), MOLECULAR WEIGHT (MW) AND MELT FLOW INDEX (MFI) [ADAPTED FROM 24].....	6
TABLE 7: THERMAL PROPERTIES OF NEAT HIGH-DENSITY POLYETHYLENE (HDPE) IN COMPARISON TO HDPE WITH 20-30-40-50-60 WT.% OF WOOD [ADAPTED FROM 26].....	8
TABLE 9: DIFFERENTIAL SCANNING CALORIMETRY (DSC) RESULTS OF NEAT PLA AND PLA WITH 10 AND 20 WT.% OF RECYCLED WOOD FIBRES (RWF) AND 0.5 WT.% OF SILANE AS COMPATIBILIZING AGENT [27].....	9

TABLE 10: THERMO GRAVIMETRIC ANALYSIS (TGA) OF BEECH FIBRES AND BEECH FIBRES MODIFIED WITH ALKALINE TREATMENT [28].	10
TABLE 11: MECHANICAL PROPERTIES OF POLYAMIDE 11 (PA11) NEAT AND WITH FIBRES (MODIFIED OR NOT WITH ALKALINE TREATMENT) [28].	10
TABLE 12: MECHANICAL PROPERTIES OF POLYOLEFIN-OLD NEWSPAPER COMPOSITES COMPARED TO POLYOLEFIN-GLASS FIBRES COMPOSITES [REF. 32-35-37].	13
TABLE 13: SOME PLA MECHANICAL FEATURES IN COMPARISON TO TRADITIONAL POLYOLEFINS.	17
TABLE 14: TENSILE TEST RESULTS OF PURE PLA AS WELL AS PLA MODIFIED WITH POLYETHYLENE GLYCOL (PEG) AND ACETYL TRI-N-BUTYL CITRATE (ATBC) IN DIFFERENT PERCENTAGES [44].	18
TABLE 15: INFLUENCE OF MOLECULAR WEIGHT AS WELL AS CONTENT OF TRIETHYL CITRATE (TEC) AND ACETYL TRIBUTYL CITRATE (ATBC) ON POLYLACTIC ACID THERMAL PROPERTIES [ADAPTED FROM 46].	19
TABLE 16: THE EFFECT OF FOUR DIFFERENT IONIC LIQUIDS ON PLA MECHANICAL PROPERTIES [ADAPTED FROM 47].	21
TABLE 17: EFFECT OF FOUR DIFFERENT IONIC LIQUIDS ON PLA THERMAL PROPERTIES [ADAPTED FROM 47].	21
TABLE 18: DSC RESULTS BEFORE AND AFTER COMPOSTING FOR LLDPE, LLDPE 80WT.% AND PLLA 20WT.%, AND BLEND COMPATIBILIZED WITH 4WT.% OF LOW DENSITY POLYETHYLENE-GRAFT-MALEIC ANHYDRIDE [83].	36
TABLE 19: INGEO BIOPOLYMER 3251D TECHNICAL PROPERTIES.	47
TABLE 20: ERACLENE MP90 TECHNICAL PROPERTIES.	48
TABLE 21: TYPICAL AMINO ACIDS THAT ARE PRESENT IN PRO-FAM 974 [TECHNICAL DATA SHEET].	49
TABLE 22: TENSILE TEST RESULTS FOR NEAT HDPE AND COMPOSITES WITH 10 WT.% AND 20 WT.% OF WASTE PAPER PROCESSED WITH SUPERFINE GRINDING MILL (S).	76
TABLE 23: MAIN RESULTS OF TENSILE TESTS FOR COMPOSITES PRODUCED WITH 20WT.% OF FIBRES FROM THE SUPERFINE GRINDING (20S) AND KNIFE (20K) MILL.	77
TABLE 24: SAMPLES PRODUCED WITH 10 WT.% OF RECYCLED WASTE PAPER FIBRES AND THREE DIFFERENT PERCENTAGES OF MAPE (1, 3 AND 5 WT.%).	80
TABLE 25: MAIN TENSILE TESTS RESULTS FOR COMPOSITES PRODUCED WITH 10WT.% OF FIBRES AND THREE DIFFERENT PERCENTAGES OF POLYBOND 3029 (A).	81
TABLE 26: FAMILIES OF PRODUCED SAMPLES THROUGH TURBO MIXING. ALL SAMPLES HAVE HDPE MATRIX.	83
TABLE 27: TENSILE TEST RESULTS FOR NEAT HDPE BASED COMPOSITE WITH 30WT.% OF WOOD FLOUR, 10WT.% OF RECYCLED PAPER FIBRES AND WITH 3WT.% AND 5WT.% OF MAPE COMPATIBILIZER.	85
TABLE 28: FORMULATIONS OF PLA AND PLA-FUNCTIONAL POLYETHYLENE BLENDS TO EVALUATE THE INFLUENCE OF LOTADER AX8840 AND POLYBOND 3029 ON PLA.	88
TABLE 29: TENSILE TESTS RESULTS FOR NEAT PLA, PLA75-LOT25 AND PLA75-POLY25.	89
TABLE 30: DIFFERENTIAL SCANNING CALORIMETRY RESULTS FOR NEAT PLA, LOTADER AX8840 AND POLYBOND 3029, PLA75-LOT25 AND PLA75-POLY 25 BLENDS.	91
TABLE 31: TENSILE TESTS RESULTS OF HDPE-PLA BLENDS WITHOUT COMPATIBILIZERS.	94
TABLE 32: TENSILE TESTS RESULTS FOR HDPE-PLA BLEND WITH LOTADER AX8840 AND POLYBOND 3029 IN DIFFERENT AMOUNTS (1, 3, 5WT.%).	96
TABLE 33: DSC RESULTS FOR HDPE, PLA AND HDPE50-PLA50.	99
TABLE 34: DSC RESULTS OF HDPE50-PLA50 WITH 1-3-5 WT.% OF LOTADER AX8840 OR POLYBOND 3029.	101
TABLE 35: TGA RESULTS FOR HDPE-PLA BLENDS WITH DIFFERENT COMPATIBILIZER PERCENTAGES, HDPE50-PLA50 MATRIX COMPOSITES WITH 3 WT.% OF COMPATIBILIZER AND 20, 30 OR 40 WT.% OF WOOD FLOUR. T_{ONSET} (°C) ARE EVALUATED WITH THE EXTRAPOLATED ONSET TEMPERATURE FROM TGA CURVE. T_{DTG} (°C) ARE THE TEMPERATURES OF MAXIMUM DTG CURVES PEAKS. ΔM (%) ARE THE MASS VARIATION PERCENTAGES BETWEEN THE TOTAL AMOUNT OF SAMPLE BEFORE THE TEST AND THE RESIDUAL MASS AFTER THE TEST.	102
TABLE 36: COMPOSITION AND PROCESSING CONDITIONS FOR SOY PROTEIN ISOLATE (SPI) BASED BLEND.	104
TABLE 36: TENSILE TESTS RESULTS FOR LOTADER AX8840 SPI BLEND WITH DIFFERENT AMOUNT OF GLYCEROL.	105
TABLE 37: TENSILE TESTS RESULTS OF 30.WT% GLYCEROL PLASTICIZED SPI BLENDED WITH DIFFERENT RATIOS OF LOTADER AX8840.	106
TABLE 38: TENSILE TESTS RESULTS FOR HDPE-SPI BLEND, ANALYSING THE INFLUENCE OF GLYCEROL ADDITION AS PLASTICIZER AND LOTADER AX8840 AS COMPATIBILIZER.	117
TABLE 39: PRODUCED FORMULATIONS OF PLA, PLA COMPOSITES (PLA70-WF30) AND MODIFICATION WITH COMPATIBILIZING AGENTS (POLYBOND 3029 AND LOTADER AX8840) AND IONIC LIQUID (IL).	127

TABLE 40:TGA RESULTS FOR PLA, PLA70WF30 AND COMPATIBILIZED COMPOSITES WITH LOTADER AX8840, POLYBOND 3029 AND IL. T_{ONSET} (°C) IS EVALUATED WITH THE EXTRAPOLATED ONSET TEMPERATURE FROM TGA CURVE. T_{DTG} (°C) TEMPERATURE OF MAXIMUM DTG CURVES PEAKS. ΔM (%) IS THE MASS VARIATION PERCENTAGE BETWEEN THE TOTAL AMOUNT OF SAMPLE BEFORE THE TEST AND THE RESIDUAL MASS AFTER THE TEST.....	129
TABLE 41:PRODUCED FORMULATIONS OF HDPE50-PLA50 COMPOSITES WITH 20, 30 AND 40WT.% OF WOOD FLOUR AND 3 WT.% OF COMPATIBILIZING AGENT.....	133
TABLE 42: TENSILE TESTS RESULTS OF SAMPLES FILLED WITH WOOD FLOUR. BLUE COLOUR IS FOR WOOD FLOUR, PURPLE FOR POLYBOND 3029 AND RED IS FOR LOTADER AX8840 ADDITION.	134
TABLE 43: DSC RESULTS FOR HDPE50-PLA50 COMPOSITES WITH 20, 30 AND 40 WT.% OF WOOD FLOUR AND 3 WT.% OF COMPATIBILIZER POLYBOND 3029 OR LOTADER AX8840.	139
TABLE 44: TGA RESULTS FOR HDPE-PLA BLENDS WITH DIFFERENT COMPATIBILIZER PERCENTAGES AND HDPE50-PLA50 MATRIX COMPOSITES WITH 3 WT.% OF COMPATIBILIZER AND 20, 30, 40 WT.% OF WOOD FLOUR. T_{ONSET} (°C) IS EVALUATED WITH THE EXTRAPOLATED ONSET TEMPERATURE FROM TGA CURVES. T_{DTG} (°C) TEMPERATURE OF MAXIMUM DTG CURVES PEAKS. ΔM (%) IS THE MASS VARIATION PERCENTAGE BETWEEN THE TOTAL AMOUNT OF SAMPLE BEFORE THE TEST AND THE RESIDUAL MASS AFTER THE TEST.	143
TABLE 45:PRODUCED FORMULATIONS OF HDPE50-PLA50 COMPOSITES WITH 10, 20, 30 AND 40WT.% OF RECYCLED WASTE PAPER, MIX OF 30WT.% OF WOOD FLOUR AND 10WT.% OF RECYCLED WASTE PAPER WITH AND WITHOUT 3 WT.% OF COMPATIBILIZING AGENT.....	145
TABLE 46: TENSILE TESTS RESULTS FOR RECYCLED WASTE PAPER COMPOSITES (FROM 10 TO 40WT.%) AND MIX OF 30WT.% OF WOOD FLOUR AND 10WT.% OF RECYCLED WASTE PAPER, COMPARED WITH NEAT HDPE50-PLA50 MATRIX AND COMPOSITES WITH WOOD FLOUR.....	146
TABLE 47: DSC RESULTS FOR HDPE50-PLA50, HDPE50-PLA50-P COMPOSITES AND HDPE50-PLA50-WF-P COMPOSITES WITH AND WITHOUT COUPLING AGENTS.....	152
TABLE 48: TENSILE TESTS RESULTS OF HDPE AND PLA COMPOSITES WITH WOOD FLOUR AND RECYCLED WASTE PAPER FIBRES.....	153
TABLE 49: SAMPLES PRODUCED WITH TURBOMIXER PROCESSING.	162
TABLE 50: TENSILE TESTS RESULTS FOR SAMPLES PRODUCED WITH TURBOMIXER PROCESSING.	163
TABLE 51: FORMULATIONS OF SAMPLES FOR COMPOSTING TEST IN SOIL.	163
TABLE 52: CHARACTERISTIC PEAKS OF HDPE, CELLULOSE, HEMICELLULOSE AND LIGNIN.....	169
TABLE 53: DSC RESULTS FOR NEAT PLA DURING COMPOSTING PROCESS AT 58°C.	195
TABLE 54: DSC RESULTS FOR PLA-BASED COMPOSITES DURING COMPOSTING PROCESS AT 58°C.	197

Riassunto

Introduzione

I materiali polimerici hanno assunto nel corso degli ultimi decenni una grande importanza, e il loro utilizzo è più antico di quanto si possa immaginare. Infatti, polimeri come la seta, la lana e il cotone sono tra i primi materiali conosciuti dall'uomo, nonostante la comprensione della loro struttura sia diventata nota solo nel ventesimo secolo.

L'aumento del consumo di materiali polimerici e l'aumento dell'importanza nei confronti delle problematiche ambientali hanno diretto le ricerche verso nuove classi di materiali. Al fine di ridurre la quantità di polimero di derivazione petrolifera e di valorizzare fibre di origine naturale, si sono sviluppati i Wood Plastic Composites (WPC) [1-2]. Questa classe di materiali si è diffusa grazie a proprietà come la durabilità e la manutenzione più facile del solo legno, la possibilità di utilizzare le stesse tecniche di produzione di materiali polimerici e alla possibilità di usare materiali di scarto, valorizzandoli, per la loro produzione. I WPC sono, infatti, materiali compositi a matrice termoplastica con fibre lignocellulosiche. Lino, canapa, bambù, cotone ecc. sono alcuni esempi di fibre naturali che vengono usate frequentemente nei WPC [3-5]. In particolare, la farina di legno e le fibre di carta riciclate rappresentano due prodotti di scarto che possono essere valorizzati nei WPC. La farina di legno è un importante scarto della lavorazione del legno, caratterizzato da diverse granulometrie e di forma prevalentemente particellare. Le fibre di carta riciclate sono derivate da carta che non può essere sottoposta al tradizionale processo di riciclaggio, rappresentando quindi un rifiuto solido urbano. La proposta è quella di valorizzare questo scarto all'interno dei WPC, riducendo ulteriormente la quantità di polimero di derivazione petrolifera, aumentando le prestazioni del composito.

Un'altra strategia adottata per affrontare i problemi derivanti dall'inquinamento di polimeri di derivazione petrolifera riguarda lo sviluppo di blend polimerici di quest'ultimi con polimeri bio-derivati. Infatti, al fine di ridurre ulteriormente il quantitativo di carica non riciclabile, oltre l'introduzione di farina di legno e fibre di carta riciclate, è possibile anche l'introduzione di polimeri bio-derivati. Tra questi, l'acido polilattico (PLA) e la proteina di soia isolata (SPI) rappresentano due interessanti possibilità [6-9].

L'obiettivo della ricerca è quindi lo sviluppo di un materiale ad alto valore aggiunto, con elevato tenore di carica bio-derivata e maggiormente ecosostenibile. La strategia perseguita si basa sia

sull'introduzione di fibre naturali, sia sull'uso di un blend polimerico poliolefina/polimeri bio-derivati come matrice, riducendo così la quantità di carica non biodegradabile presente nel materiale. Dopo un'introduzione sullo stato dell'arte (capitolo 1) e la descrizione dei materiali e dei metodi utilizzati per caratterizzare i campioni (capitolo 2), la parte sperimentale del progetto è stata analizzata in quattro capitoli: produzione e utilizzo delle microfibre di carta in una matrice di poliolefina (capitolo 3), sviluppo e caratterizzazione (proprietà meccaniche, proprietà termo-chimica, morfologia e degradazione) di una miscela poliolefina-polimero bioderivato (capitolo 4), sviluppo e caratterizzazione (proprietà meccaniche, proprietà termo-chimica, morfologia e degradazione) di un composito caricato con fibre di carta e farina di legno (capitolo 5), conclusioni e prospettive future (capitolo 6).

L'HDPE è stato scelto come poliolefina in quanto rappresenta il principale polimero di riciclo sul mercato (si pensa infatti in futuro di utilizzare polimeri di riciclo invece di quelli vergini). Il PLA, essendo il polimero biodegradabile maggiormente utilizzato a livello industriale, rappresenta la scelta più intuitiva in termini di polimeri bio-derivati. Il PLA è un poliestere alifatico, prodotto a partire da polisaccaridi. Un'alternativa interessante è rappresentata da altri polimeri bio-derivati, di origine proteica. Tra questi, la proteina di soia isolata (SPI) presenta buone potenzialità essendo biodegradabile, compostabile e biocompatibile. La produzione di campioni a base SPI è generalmente basata su "processi umidi", caratterizzati da dispersione o solubilizzazione di SPI in soluzione, seguiti dall'evaporazione di solventi. Solo un'attenzione limitata è stata dedicata ai "processi a secco" come lo stampaggio a compressione, dalle polveri o per estrusione. Lo sviluppo di formulazioni attraverso l'estrusore è stata una delle originalità di questo lavoro. La farina di legno è filler naturale di largo impiego, essendo un diffuso materiale di scarto, per la produzione dei Wood Plastic Composite (materiali compositi già diffusi per la loro processabilità, le loro proprietà e le loro applicazioni). Le fibre di carta riciclata sono derivate da scarti di carta industriale, non sottoponibile al tradizionale processo di riciclo. Rappresentano quindi un ulteriore passo nella produzione di un composito verso un ridotto impatto ambientale.

L'ottimizzazione della composizione è una sfida non solo per le proprietà d'impiego di questi materiali, ma anche per la loro dismissione.

Uno dei principali limiti sia dei blend polimerici che dei compositi a matrice polimerica caricati con fibre naturali, è la diversa idrofilia tra i componenti. Al fine di fronteggiare questo problema, due agenti di accoppiamento, Lotader AX8840 e Polybond 3029, sono stati introdotti.

Bibliografia

1. Z.N. Azwa et al., A review on the degradability of polymeric composites based on natural fibres, *Mater Design*, vol 47, pp. 424-442, 2013.
2. A. Ashori, A. Nourbakhsh, Characteristics of wood-fiber plastic composites made of recycled materials, *Waste Manage*, vol 29, pp. 1291-1295, 2009.
3. S. Migneault et al., Effect of processing method and fiber size on the structure and properties of wood-plastic composites. *Compos Part A-App S*, vol 40, pp. 80-85, 2009.
4. K. Pei-Yu et al., Effects of material compositions on the mechanical properties of wood-plastic composites manufactured by injection moulding, *Mater Design*, vol 30, pp. 3489-3496, 2009.
5. M. Prambauer, C. Paulik, C. Burgstaller, The influence of paper type on the properties of structural paper- Polypropylene composites, *Compos Part A-App S*, vol 74, pp. 107-113, 2015
6. R. Thipmanee, A. Sane, Effect of zeolite 5A on compatibility and properties of linear low-density polyethylene/thermoplastic starch blend, *J. Appl. Polym. Sci.*, 126, E251–E258 (2012).
7. 29 G. Singh, H. Bhunia, A. Rajor, and V. Choudhary, "Thermal properties and degradation characteristics of polylactide, linear low density polyethylene, and their blends," *Polym. Bull.*, vol. 66, no. 7, pp. 939–953, 2011.
8. 30 N. Ploypetchara, P. Suppakul, D. Atong, and C. Pechyen, "Blend of polypropylene/poly(lactic acid) for medical packaging application: Physicochemical, thermal, mechanical, and barrier properties," *Energy Procedia*, vol. 56, no. C, pp. 201–210, 2014.
9. H. Ismail, S.T. Sam, K.M. Chin, "Polyethylene/Soy Protein-based Biocomposites: Properties, Applications, Challenges and Opportunities", in *Polyethylene-Based Biocomposites and Bionanocomposites*, Ed. P.M. Visakh, S. Luftl, 2016.

Blend polimerici

Il blend HDPE/PLA con la stessa quantità di entrambi i polimeri sembra essere il miglior compromesso tra buone proprietà meccaniche e riduzione di carica non bio-derivata (figura 1 e tabella 1).

Tabella 1: Risultati delle prove di trazione per i blend HDPE50-PLA50 con 1, 3 e 5 wt.% di Polybond 3029 o di Lotader AX8840.

Campioni	E (GPa)	σ (MPa)	ϵ (%)
HDPE50-PLA50	1.8±0.1	38.7±0.2	99.4±2.1

HDPE50-PLA50-Poly1	2.2±0.1	43.3±2.8	86.2±17.3
HDPE50-PLA50-Poly3	2.3±0.1	42.8±2.6	71.9±46.9
HDPE50-PLA50-Poly5	1.9±0.0	39.7±0.4	34.1±13.1
HDPE50-PLA50-Lot1	2.2±0.2	40.7±4.0	175.3±84.2

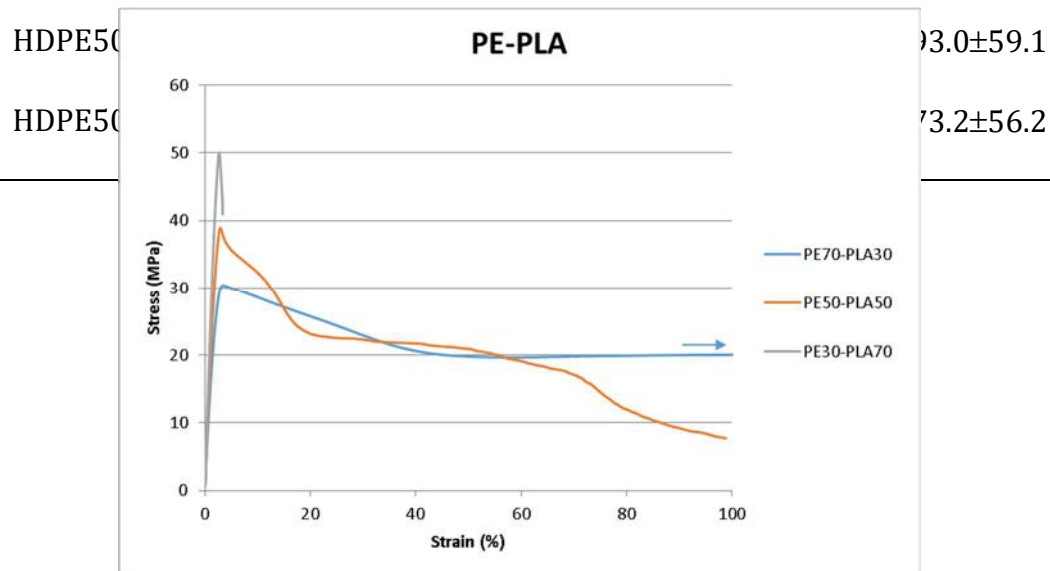


Figura 1: Curve di trazione per i blend HDPE-PLA con tre diverse proporzioni (blu HDPE70-PLA30, arancione HDPE50-PLA50 e grigio HDPE30-PLA70)

Gli agenti di accoppiamento, Lotader AX8840 e Polybond 3029, mostrano un miglioramento di omogeneità del blend. In particolare, Lotader AX8840 si è rivelato maggiormente efficace nel miglioramento della tenacità del blend rispetto al Polybond 3029. Infatti, il più alto contenuto di glicidil metacrilato (circa 8wt. %) nel Lotader AX8840 rispetto al contenuto di anidride maleica (1.5-1.7wt. %) nel Polybond 3029, può spiegare la miglior efficienza del Lotader AX8840. Le immagini SEM mostrano un comportamento tipicamente immiscibile per il blend HDPE50-PLA50 (figura 2 A), mentre l'aggiunta del Lotader AX8840 e del Polybond 3029 (figura 2 B e 2 C) mostrano una migliore omogeneità del blend.

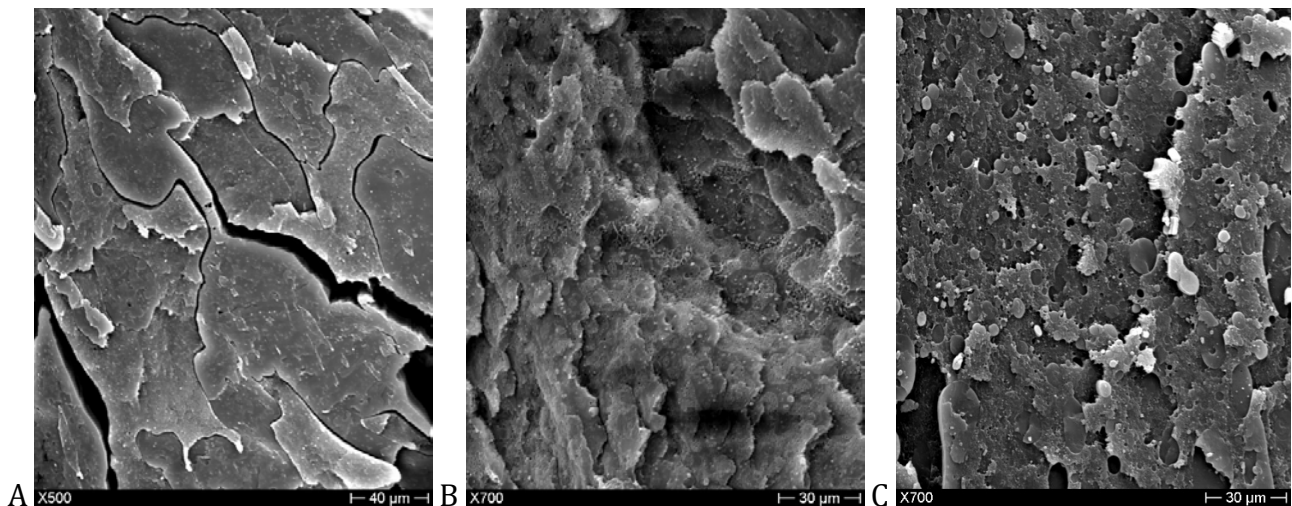


Figura 2: HDPE50-PLA50 blend (A) con il 3wt.% di Lotader AX8840 (B) and Polybond 3029 (C).

Valutazioni più accurate sono state fatte sui blend PLA-Lotader AX8840 e PLA-Polybond 3029 con un contenuto di PE funzionalizzato del 25%. Le immagini SEM mostrano una migliore dispersione e una minor dimensione della fase secondaria (agente di accoppiamento) nel caso del Lotader AX8840 (figura 3). Questo risultato è in accordo con le proprietà meccaniche dei due blend: PLA75-Lot25 ha mostrato un allungamento a rottura intorno al $193\pm 47\%$ mentre PLA75-Poly25 $28.9\pm 13\%$.

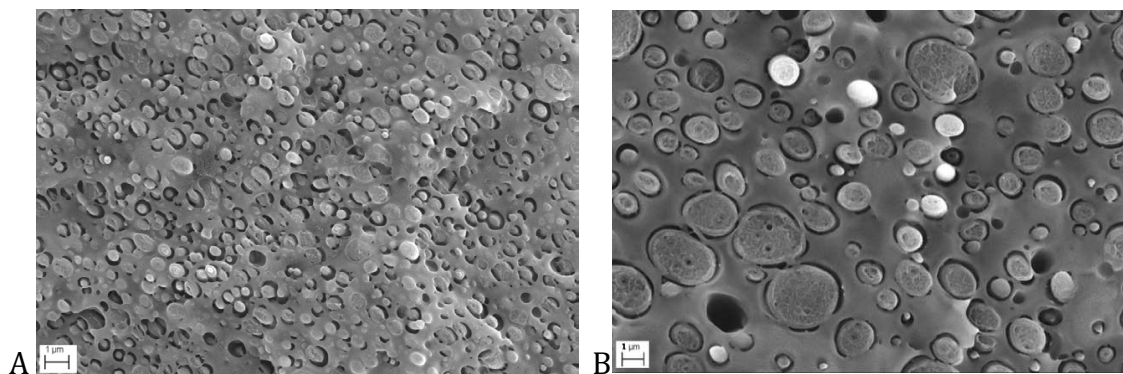


Figura 3: Immagini al microscopio a scansione elettronica (SEM) di PLA75-Lot25 (A) and PLA75-Poly25 (B).

La proteina di soia isolata (SPI) è stata studiata come possibile alternativa al PLA. Al fine di processarla, il glicerolo è stato aggiunto al 30 wt.% come plasticizzante. In particolare, sono state eseguite analisi dei blend HDPE-SPI compatibilizzati con Lotader AX8840. In prima analisi, sono stati effettuati test sui blend SPI-Lotader AX8840, per valutare gli effetti del compatibilizzante. I blend SPI-Lotader AX8840 mostrano maggior deformazione e miglior omogeneità quando il glicerolo è aggiunto al blend (tabella 2).

Tabella 2: Risultati delle prove di trazione per i blend lota75-SPI25 tal quale, con il 30 wt.% di glicerolo, e diversi rapporti Lotader AX8840-SPI.

Campioni	E (MPa)	σ (MPa)	ϵ (%)
Lot75-SPI25	185±6	9±1	22±2
Lot75-(SPI70-Gly30)25	86±4	9±1	37±1
Lot65-(SPI70-Gly30)35	169±8	8±1	12±1
Lot50-(SPI70-Gly30)50	122±13	7±1	20±4
Lot35-(SPI70-Gly30)65	117±5	9±1	26±1

Le analisi FTIR e TGA suggeriscono un'interazione unicamente fisica e non chimica tra il glicerolo e la proteina di soia, in analogia con i risultati di letteratura.

La SPI è caratterizzata da un grande incremento di viscosità in fase produttiva, confermato dalle analisi reologiche (figura 4).

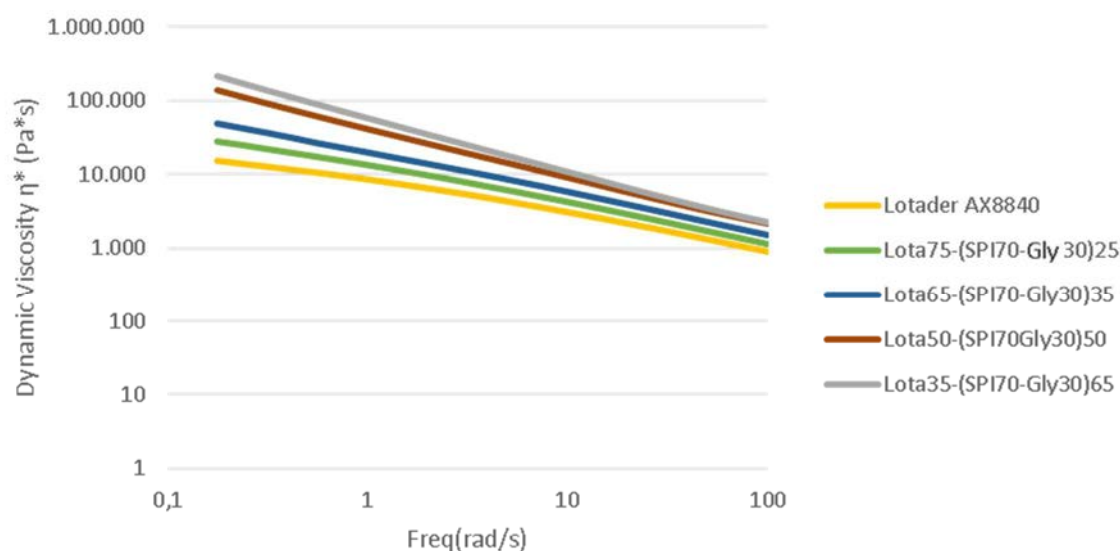


Figura 4: Viscosità dinamica del Lotader AX8840 e dei suoi blend con la proteina di soia in diversi rapporti (da Lot75-(SPI70-Gly30)25 a Lot25-(SPI70-Gly30)75).

I blend HDPE-SPI hanno mostrato un aumento delle proprietà meccaniche con l'aggiunta del glicerolo e dell'agente di accoppiamento, Lotader AX8840 introdotto al 3 wt.% (figura 5). I risultati ottenuti sono coerenti anche con le immagini SEM (figura 6).

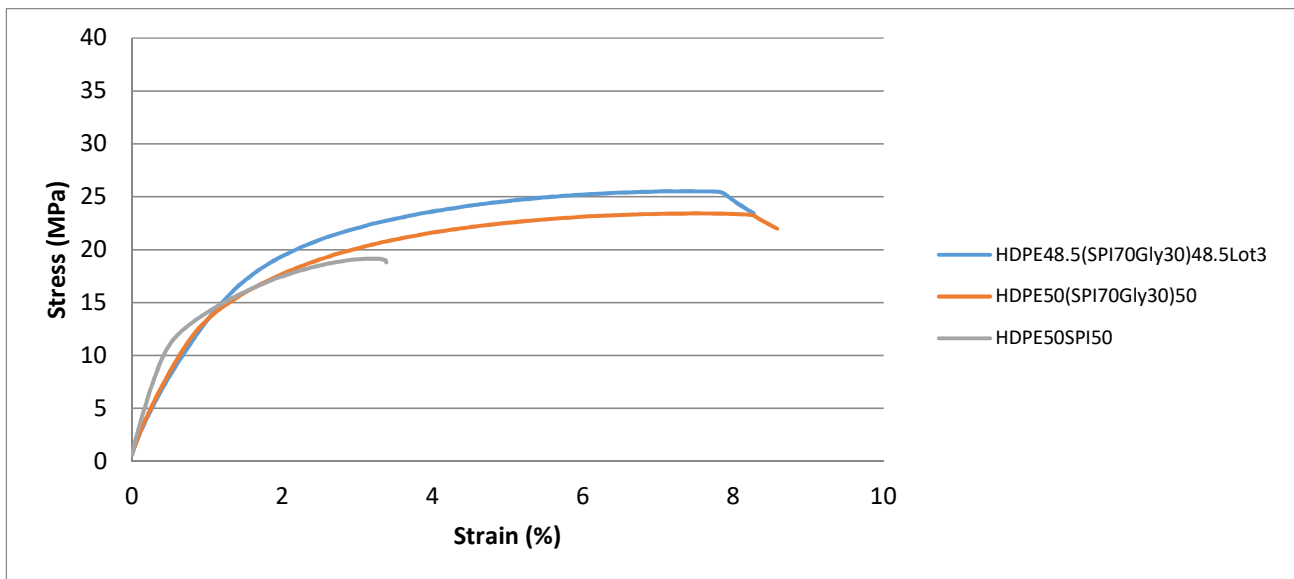


Figura 5: Curve di trazione per HDPE50SPI50 (grigio), HDPE50(SPI70Gly30)50 (arancione) e HDPE48.5(SPI70Gly30)48.5Lot3 (blu).

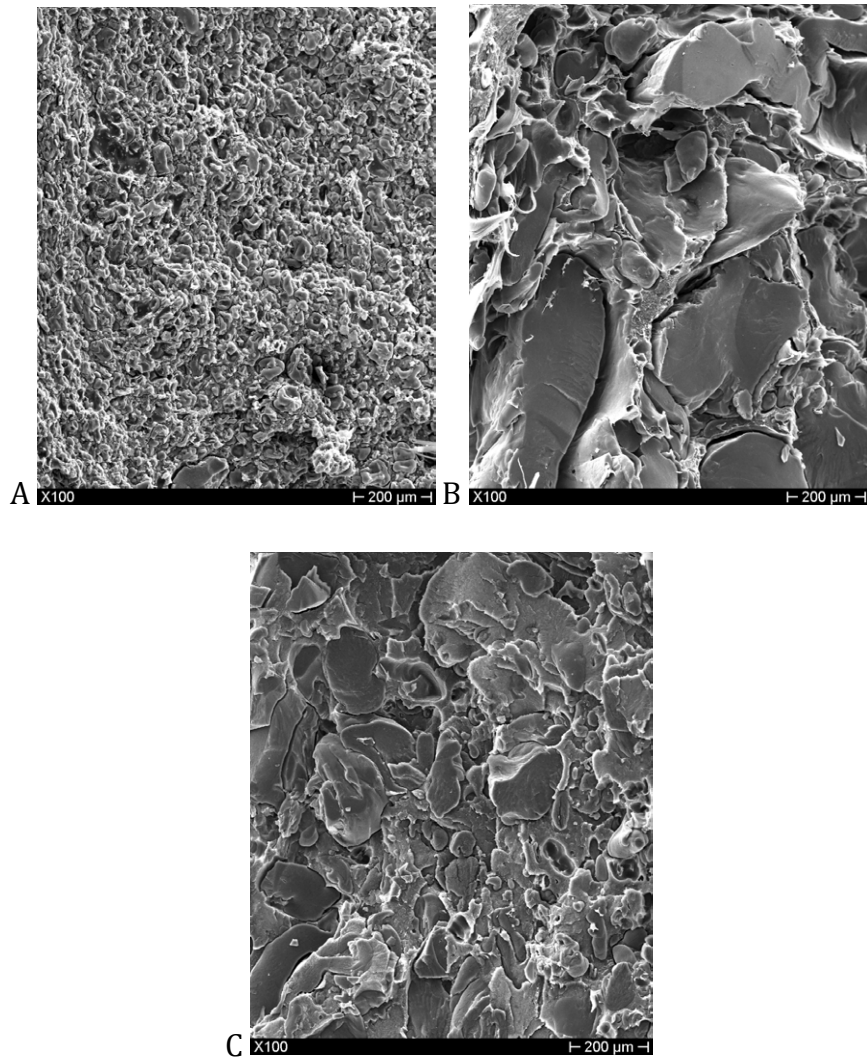


Figura 6: Immagini SEM di HDPE50SPI50 (A), HDPE50(SPI70Gly30)50 (B), HDPE50(SPI70Gly30)50Lot3 (C)

Preliminari test di compostaggio sono stati eseguiti per tre mesi a 35°C e 58°C, analizzando la variazione del peso (figura 7), dell'aspetto visivo (figura 8) e gli spettri FTIR. I risultati sono coerenti con una rapida degradazione della SPI, al contrario dell'HDPE che rimane stabile e inalterato. HDPE50-SPI50 mostra una progressione della degradazione, con una variazione di peso che arriva a quasi il 30% per i campioni compostati a 58°C.

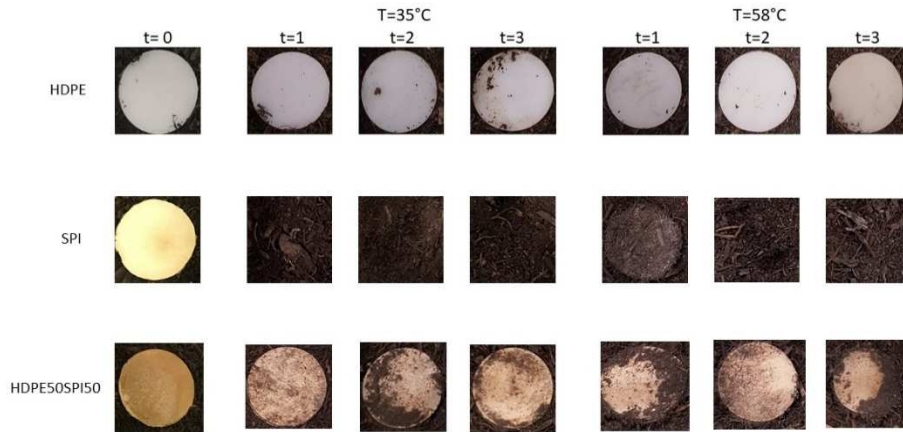


Figura 7: Osservazione visiva di HDPE, proteina di soia isolata (SPI) and HDPE50SPI50 durante tre mesi di compostaggio a 35°C and 58°C.

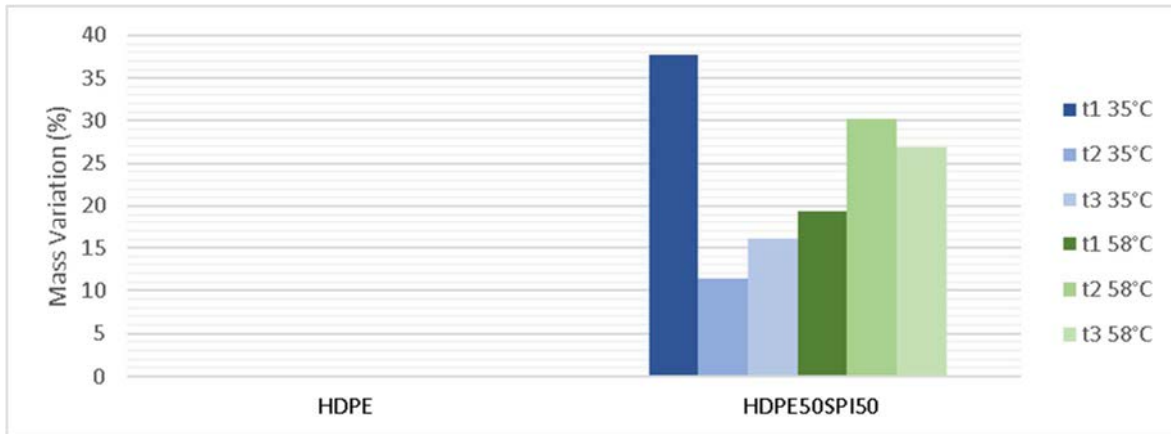


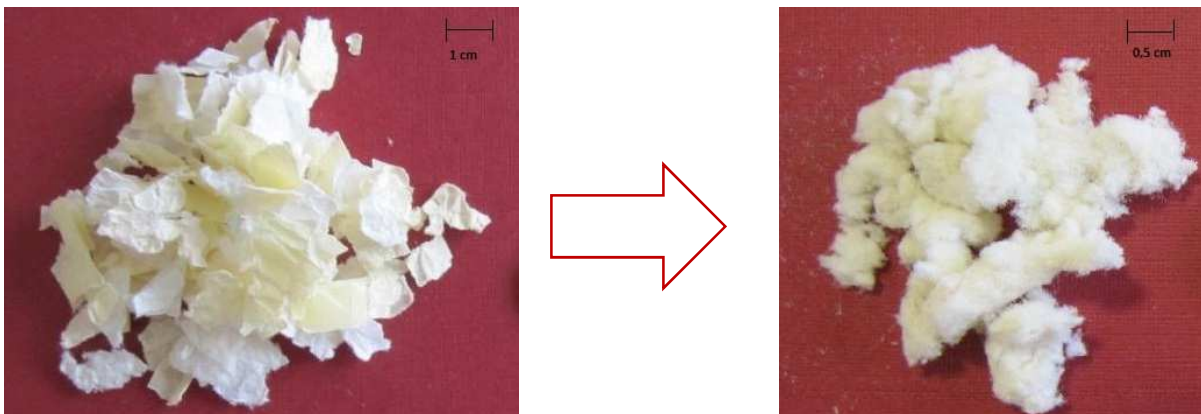
Figura 8: Variazione di massa dell'HDPE e del blend HDPE50-SPI50 durante tre mesi di compostaggio (t1= 1 mese, t2= 2 mesi, t3= 3 mesi) a 35°C (scala dei blu) e a 58°C (scala dei verdi).

Compositi con filler naturali

A partire dalle analisi precedenti, il blend HDPE50-PLA50 è stato selezionato come matrice per compositi con la farina di legno, le fibre di carta riciclata e un mix dei due filler naturali. In particolare, 20-30-40 wt.% di farina di legno e 10-20-30-40 wt.% di fibre di carta riciclata sono state additivate al blend, e il mix 30wt.% di farina di legno e 10wt.% di fibre di carta riciclata è stato selezionato come rapporto tra i due filler. Le percentuali sono state scelte al fine di introdurre il più alto quantitativo possibile di filler naturale, compatibilmente con il processo produttivo, sia per valorizzare lo scarto, sia per ridurre la quantità di polimero non bio-

derivato. Il problema dell'interfaccia fibra-matrice è stato affrontato introducendo il 3 wt.% di Lotader AX8840 o Polybond 3029.

Il consumo di carta è incrementato negli ultimi anni, e con esso i problemi connessi al suo smaltimento. Nonostante circa il 72% dei rifiuti cellulósici possa essere sottoposto al processo di riciclaggio, la restante parte rappresenta un rifiuto solido. Una proposta, al fine di ridurre l'inquinamento connesso a questo tipo di rifiuto, riguarda la micronizzazione della carta per ottenere fibre di dimensioni idonee all'applicazione in materiali compositi. In questo lavoro è stato adottato un processo di micronizzazione che lavora per impatto, attrito e turbolenza. Il processo produttivo delle fibre di carta è stato parte integrante del progetto, avendo cura di ottenere fibre di dimensioni idonee all'introduzione in compositi. La carta, dopo essere stata macinata in un mulino a martelli per ottenere frammenti di 8-10mm, è introdotta nel micronizzatore ottenendo, a seguito di una separazione fibre di $750 \pm 300 \mu\text{m}$ di lunghezza e $25 \pm 10 \mu\text{m}$ di diametro.



L'aggiunta della farina di legno consente di incrementare le proprietà meccaniche, aumentando allo stesso tempo la difettosità della matrice (tabella 3). L'aggiunta del 3 wt.% di compatibilizzante, sia Lotader AX8840 e Polybond 3029, consente di aumentare l'omogeneità della matrice.

Tabella 3: Tensile tests results of samples filled with wood flour. Blue colour is for wood flour, purple for Polybond 3029 and red is for Lotader AX8840 addition.

Campioni	E (GPa)	σ (MPa)	ϵ (%)
HDPE50-PLA50	1.8±0.1	38.7±0.2	99.4±2.1
HDPE50-PLA50-WF20	3.4±0.1	34.6±2.8	1.6±0.1
HDPE50-PLA50-WF30	4.1±0.1	34.0±1.3	1.2±0.2
HDPE50-PLA50-WF40	5.0±0.2	33.5±1.5	1.9±0.0
HDPE50-PLA50-Poly3-WF20	3.3±0.1	36.0±0.8	1.8±0.1
HDPE50-PLA50-Poly3-WF30	4.1±0.2	35.9±1.4	1.4±0.1
HDPE50-PLA50-Poly3-WF40	4.9±0.1	33.6±1.7	0.9±0.2
HDPE50-PLA50-Lot3-WF20	3.3±0.1	37.8±1.5	2.0±0.1
HDPE50-PLA50-Lot3-WF30	4.1±0.1	35.0±1.2	1.4±0.1
HDPE50-PLA50-Lot3-WF40	5.0±0.1	34.1±3.3	1.0±0.1

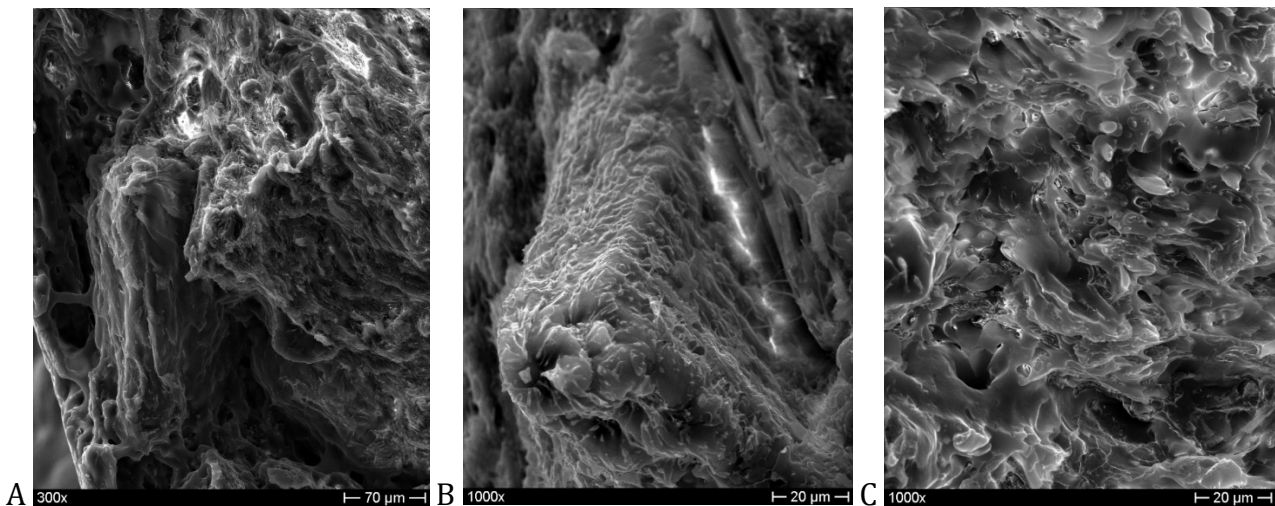


Figura 9: Immagine SEM HDPE50-PLA50-WF30 (A), HDPE50-PLA50-Lot3-WF30 (B), HDPE50-PLA50-Poly3-WF30 (C).

Le fibre di carta riciclata sono state aggiunte al blend HDPE50-PLA50. All'aumentare della percentuale delle fibre di carta riciclata aumenta il modulo elastico (figura 10), dando allo stesso tempo problemi di formazione di agglomerati per percentuali superiori al 10 wt.% (figura 11). Questa è una delle ragioni per cui è stato scelto il 10 wt.% come percentuale di fibre da aggiungere al mix con la farina di legno.

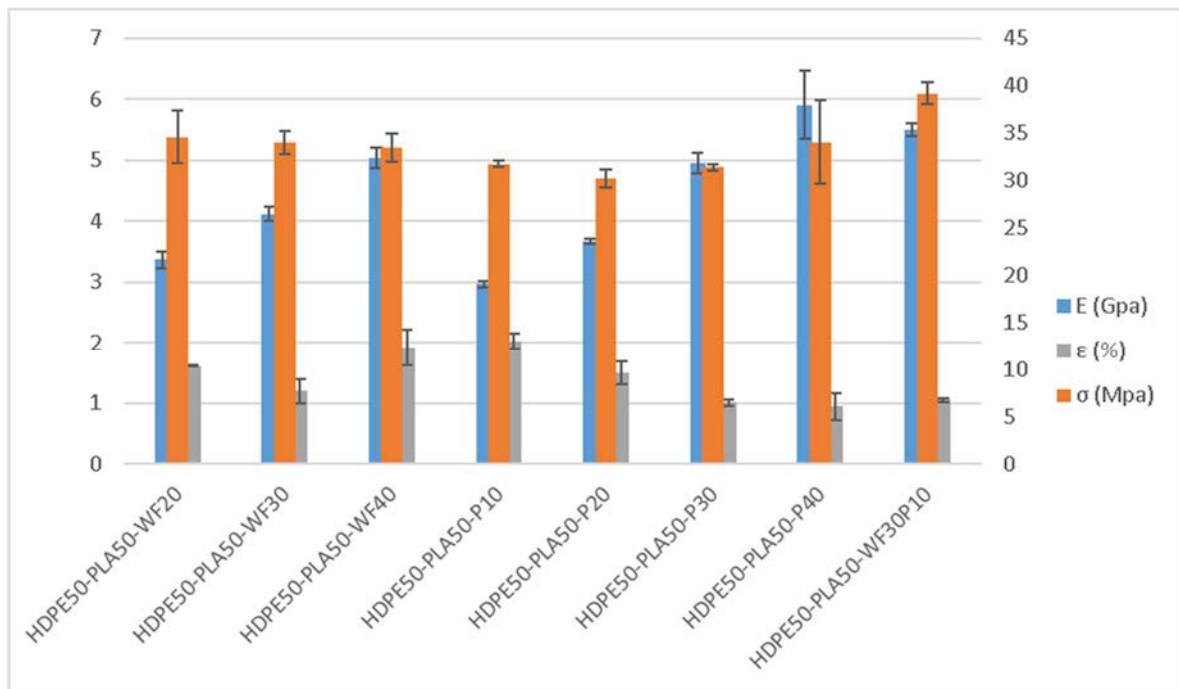


Figura 10: Modulo elastico (blu), allungamento a rottura (grigio) e carico di rottura (arancione) per i compositi caricati con la farina di legno e le fibre di carta riciclata.

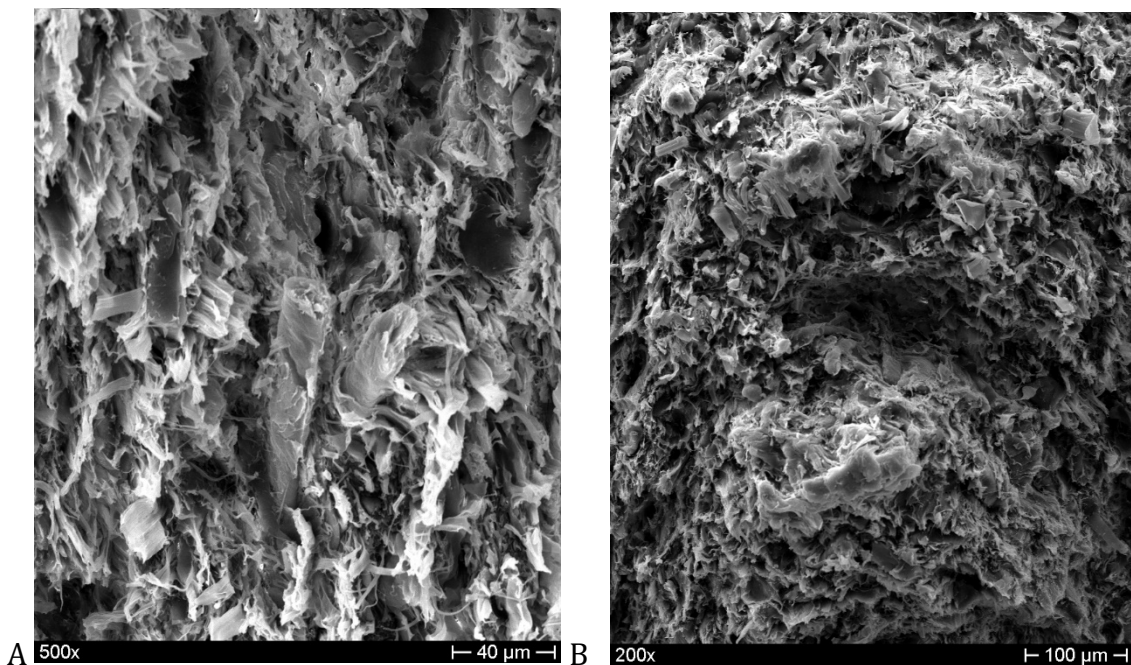
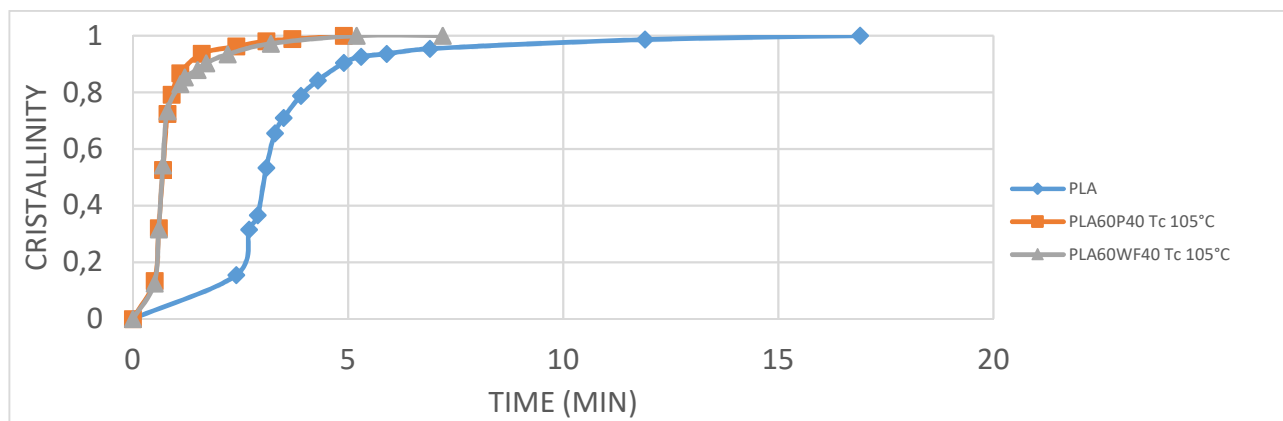


Figura 11: Immagine SEM di a)HDPE50-PLA50-P10, privo di agglomerati e b)HDPE50-PLA50-P20, con agglomerati.

Il mix 30 wt.% farina di legno e 10wt.% fibre di carta riciclata consente di incrementare il modulo elastico e il carico di rottura rispetto ai compositi con la stessa quantità (40 wt.%) di sola farina di legno o sole fibre di carta riciclata. L'aggiunta di Lotader AX8840, anche in questo caso, sembra essere più efficiente del Polybond 3029, in accordo con i risultati precedenti.

L'influenza della farina di legno e delle fibre di carta riciclata sull'HDPE e il PLA è stata analizzata attraverso l'uso del termo-microscopio ottico (TOM) e della calorimetria a scansione differenziale (DSC). TOM ha mostrato la formazione di uno strato unico di sferuliti sulla superficie delle fibre sia per l'HDPE sia per il PLA, comportamento tipico di filler con moderato effetto nucleante, in accordo con la letteratura. Le analisi DSC hanno validato tale ipotesi: sia la farina di legno sia le fibre di carta riciclata consentono di ridurre l'half-time crystallization (figure 12).

A



B

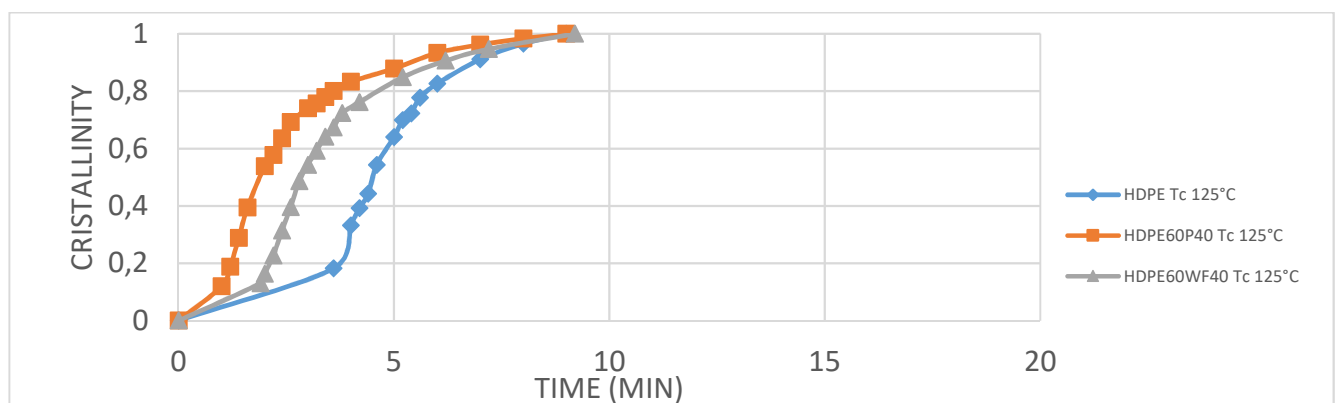


Figura 12: A) Velocità di cristallizzazione rispetto al tempo per PLA (blu), PLA60-P40 (arancione) e PLA60WF40 (grigio), B) Velocità di cristallizzazione rispetto al tempo per HDPE (blu), HDPE60-P40 (arancione) e HDPE60WF40 (grigio).

Résumé

1.1 Introduction

Les matériaux polymères ont pris une grande importance au cours des dernières décennies et leur utilisation est plus ancienne qu'on ne pourrait l'imaginer. Les polymères tels que la soie, la laine et le coton sont parmi les premiers matériaux connus par l'homme, bien que leur structure n'ait été étudiée qu'au XXe siècle.

L'augmentation de la consommation de matériaux polymères et l'importance croissante des questions environnementales ont conduit à la recherche de nouvelles classes de matériaux. Afin de réduire l'utilisation de polymères dérivés du pétrole et d'améliorer les fibres d'origine naturelle, les Composites Plastique Bois ou Wood Plastic Composites (WPC) [1-2] ont été développés. Cette classe de matériaux s'est répandue grâce à des propriétés comme durabilité et entretien plus faciles que le bois seul, la possibilité d'utiliser les mêmes techniques de production des matériaux polymère et à la possibilité d'utiliser des déchets pour leur production. En effet, les WPC sont des matériaux composites à matrice thermoplastique et à fibres lignocellulosiques. Lin, chanvre, bambou, coton, etc sont des exemples de fibres naturelles fréquemment utilisées dans les WPC [3-5]. En particulier, la farine de bois et les fibres de papier recyclées correspondent à deux déchets pouvant être valorisés dans les WPC. La farine de bois est un déchet important de la transformation du bois, caractérisé par différentes granulométries et principalement par la forme des particules. Les fibres de papier utilisées dans cette thèse sont issues de papier qui ne peut pas être soumis au processus de recyclage traditionnel, et correspond à un déchet urbain solide. Le travail a consisté à valoriser ces déchets dans des composites de type WPC avec matrice partiellement bio-sourcée, à base de poly(acide lactique) (PLA) et de protéine de soja isolée (SPI) [6-9].

L'objectif de la recherche a donc été de développer des matériaux à haute teneur en matière biosourcée (matrice et charges), a priori écologiques. Après une introduction sur l'état de l'art (chapitre 1), la description des matériaux et méthodes utilisés pour caractériser les échantillons (chapitre 2), la partie expérimentale du projet a fait l'objet de quatre chapitres : production des microfibrilles de papier et insertion dans une matrice polyoléfine (chapitre 3), élaboration et caractérisation (essais mécaniques, propriétés thermo-chimiques, morphologie et dégradation) de mélanges polyoléfines-polymères biosourcés (chapitre 4), élaboration et caractérisation (essais mécaniques, propriétés thermo-chimiques, morphologies et

dégradation) de composites chargés avec fibres de papier et farine de bois (chapitre 5), conclusion et perspectives futures (chapitre 6).

Concernant les polymères, un premier choix s'est porté sur l'HDPE car il représente de forts volumes à recycler et nos résultats (obtenus sur résines vierges) devraient pouvoir s'extrapoler sur leurs homologues à recycler en fin de vie. Le PLA, étant un polymère bio-dérivé et biodégradable parmi les plus utilisés au niveau industriel, correspond à un autre choix intéressant. Le PLA est un polyester aliphatique produit à partir de polysaccharides. Nous avons aussi choisi d'utiliser de la protéine de soja isolée (SPI), biodégradable, compostable et biocompatible. La production d'échantillons à base de SPI repose généralement sur des procédés caractérisés par une dispersion ou une solubilisation de SPI, suivis de l'évaporation de solvants. Dans la littérature, une attention limitée a été portée aux « procédés à l'état fondu » tels que le moulage par compression, à partir de poudres ou par extrusion. Nous avons pu définir des paramètres de mise en œuvre à l'état fondu de nos mélanges à base de SPI, ce qui constitue une originalité de notre travail. La farine de bois est une charge naturelle largement utilisée, déchet très répandu et adapté à la production de composites bois-plastique (matériaux composites déjà largement répandus dans le commerce du fait de leurs propriétés et leurs applications). Les fibres de papier recyclées sont issues de morceaux de papier industriel, non soumis au processus de recyclage traditionnel. Par conséquent, ils représentent une étape supplémentaire dans la production d'un composite ayant un impact environnemental réduit.

L'optimisation de la composition est un défi non seulement pour les propriétés d'utilisation des matériaux, mais également pour leur fin de vie.

L'une des principales limitations à la fois des mélanges polymères et des composites à matrice polymère chargés de fibres naturelles réside dans le caractère hydrophile différent entre les constituants. Afin de résoudre ce problème, deux agents de couplage, PE-g-GMA (Lotader AX8840) et PE-g-MA (Polybond 3029), ont été introduits.

Bibliographie

10. Z.N. Azwa et al., A review on the degradability of polymeric composites based on natural fibres, *Mater Design*, vol 47, pp. 424-442, 2013.
11. A. Ashori, A. Nourbakhsh, Characteristics of wood-fiber plastic composites made of recycled materials, *Waste Manage*, vol 29, pp. 1291-1295, 2009.
12. S. Migneault et al., Effect of processing method and fiber size on the structure and properties of wood-plastic composites. *Compos Part A-App S*, vol 40, pp. 80-85, 2009.

13. K. Pei-Yu et al., Effects of material compositions on the mechanical properties of wood-plastic composites manufactured by injection moulding, *Mater Design*, vol 30, pp. 3489-3496, 2009.
14. M. Prambauer, C. Paulik, C. Burgstaller, The influence of paper type on the properties of structural paper- Polypropylene composites, *Compos Part A-App S*, vol 74, pp. 107-113, 2015
15. R. Thipmanee, A. Sane, Effect of zeolite 5A on compatibility and properties of linear low-density polyethylene/thermoplastic starch blend, *J. Appl. Polym. Sci.*, 126, E251–E258 (2012).
16. 29 G. Singh, H. Bhunia, A. Rajor, and V. Choudhary, “Thermal properties and degradation characteristics of polylactide, linear low density polyethylene, and their blends,” *Polym. Bull.*, vol. 66, no. 7, pp. 939–953, 2011.
17. 30 N. Ploypetchara, P. Suppakul, D. Atong, and C. Pechyen, “Blend of polypropylene/poly(lactic acid) for medical packaging application: Physicochemical, thermal, mechanical, and barrier properties,” *Energy Procedia*, vol. 56, no. C, pp. 201–210, 2014.
18. H. Ismail, S.T. Sam, K.M. Chin, “Polyethylene/Soy Protein-based Biocomposites: Properties, Applications, Challenges and Opportunities”, in *Polyethylene-Based Biocomposites and Bionanocomposites*, Ed. P.M. Visakh, S. Luftl, 2016.

Mélanges de polymères

Le mélange HDPE/PLA avec la même quantité de deux polymères semble être le meilleur compromis entre de bonnes propriétés mécaniques et une réduction de matière non biodégradable (figure 1 et tableau 1).

Tableau 1: Résultats des essais de traction pour les mélanges HDPE50-PLA50 avec 1, 3 et 5% de PE-g-MA (Polybond 3029) ou de PE-g-GMA (Lotader AX8840).

Echantillons	E (GPa)	σ (MPa)	ϵ (%)
HDPE50-PLA50	1.8±0.1	38.7±0.2	99.4±2.1
HDPE50-PLA50-Poly1	2.2±0.1	43.3±2.8	86.2±17.3
HDPE50-PLA50-Poly3	2.3±0.1	42.8±2.6	71.9±46.9
HDPE50-PLA50-Poly5	1.9±0.0	39.7±0.4	34.1±13.1
HDPE50-PLA50-Lot1	2.2±0.2	40.7±4.0	175.3±84.2

HDPE50-PLA50-Lot3	2.1±0.1	41.7±1.9	193.0±59.1
HDPE50-PLA50-Lot5	1.7±0.1	34.3±1.5	173.2±56.2

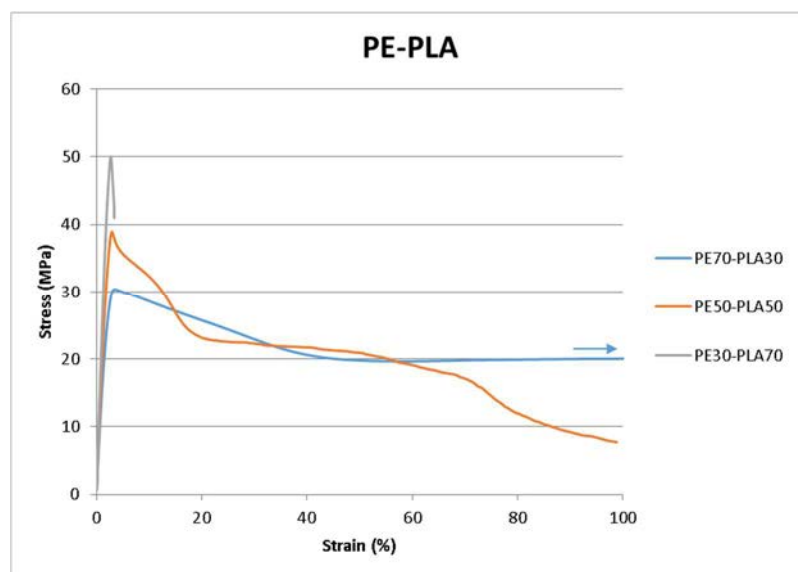


Figure 1: Courbes de traction pour les mélanges HDPE-PLA avec trois proportions différentes (HDPE70-PLA30 bleu, HDPE50-PLA50 orange et HDPE30-PLA70 gris).

Les agents de couplage, PE-g-GMA (Lotader AX8840) et PE-g-MA (Polybond 3029), montrent une amélioration de l'homogénéité du mélange. En particulier, le Lotader AX8840 a été plus efficace pour améliorer la ténacité du mélange que le Polybond 3029. En fait, la teneur en méthacrylate de glycidyle plus élevée (environ 8%) du Lotader AX8840 par rapport à la teneur en anhydride maléique (1,5-1,7%) du Polybond 3029, peut expliquer la meilleure efficacité du Lotader AX8840. Les images MEB montrent un comportement typiquement non miscible pour le mélange HDPE50-PLA50 (Figure 2 A), tandis que les ajouts de Lotader AX8840 et de

Polybond 3029 (Figure 2B et 2C) montrent une meilleure homogénéité du mélange, avec des diamètres de la phase dispersée moindres.

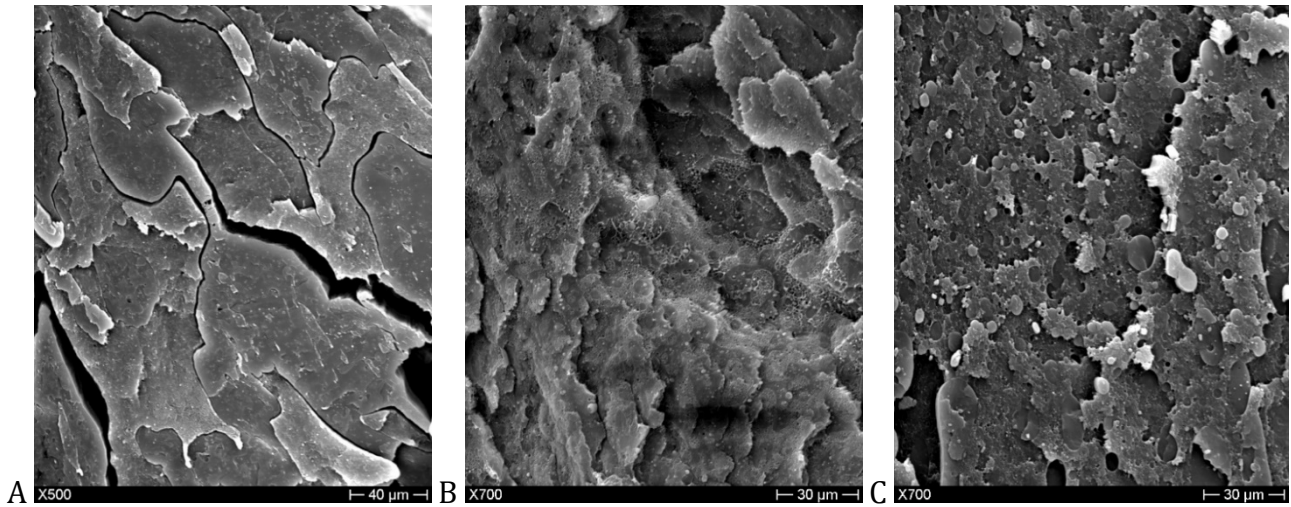


Figure 2: Mélange HDPE50-PLA50 (A) avec 3% de Lotader AX8840 (B) et Polybond 3029 (C).

Des observations avec grossissement supérieur ont été effectuées sur les mélanges PLA-Lotader AX8840 et PLA-Polybond 3029 avec une teneur en PE fonctionnalisé de 25%. Les images SEM montrent une meilleure dispersion et une taille plus petite de la phase dispersée avec le Lotader AX8840 (figure 3). Ce résultat est en accord avec les propriétés mécaniques des deux mélanges: PLA75-Lot25 a présenté un allongement à la rupture de 193 ± 47 % tandis que PLA75-Poly25 29 ± 13 %.

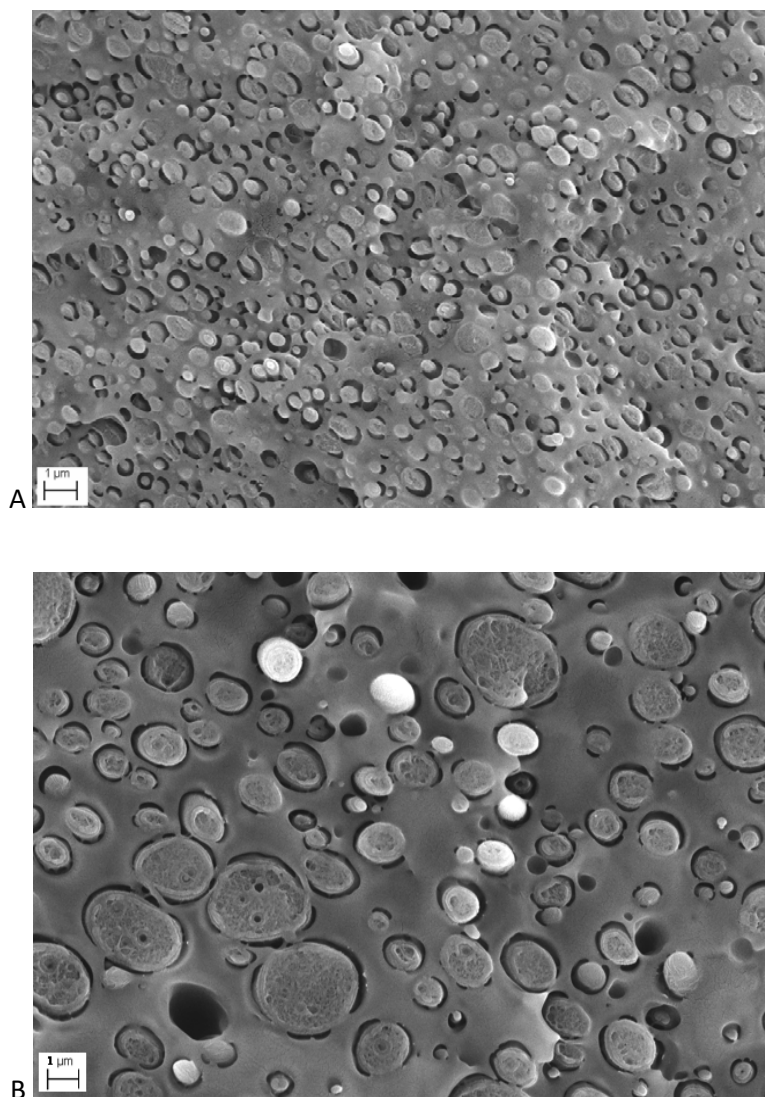


Figure 3: Images de microscopie à balayage électronique (MEB) de PLA75-Lot25 (A) et PLA75-Poly25 (B).

La protéine de soja isolée (SPI) plastifiée avec du glycérol a été étudiée comme une alternative possible au PLA. La mise en œuvre à l'état fondu de nos mélanges SPI-Lotader constitue une originalité de notre travail. En particulier, les mélanges SPI-Lotader AX8840 présentent une plus grande déformation et une meilleure homogénéité lorsque du glycérol est ajouté au mélange (en substitution du SPI), comme on le voit en comparant le Lot75-SPI25 au Lot75-(SPI70Gly30)25 (tableau 2).

Tableau 2: Résultats des essais de traction pour les mélanges Lot75-SPI25, avec 30% de glycérol et plusieurs rapports Lotader AX8840-SPI.

Echantillons	E (MPa)	σ (MPa)	ϵ (%)
--------------	------------	-------------------	-------------------

Lot75-SPI25	185±6	9±1	22±2
Lot75-(SPI70-Gly30)25	86±4	9±1	37±1
Lot65-(SPI70-Gly30)35	169±8	8±1	12±1
Lot50-(SPI70-Gly30)50	122±13	7±1	20±4
Lot35-(SPI70-Gly30)65	117±5	9±1	26±1

Les analyses FTIR et TGA suggèrent des interactions faibles entre le glycérol et les protéines de soja, en accord avec les résultats de la littérature.

L'ajout de SPI correspond à une forte augmentation de la viscosité lors de la mise en oeuvre, confirmée par des analyses rhéologiques (figure 4).

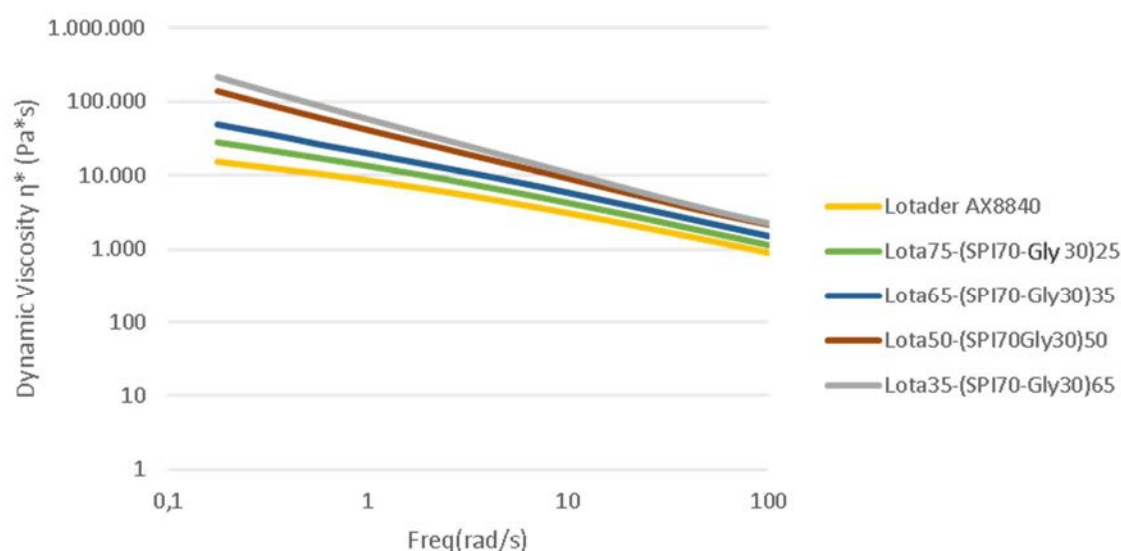


Figure 4: Viscosité dynamique du Lotader AX8840 et de ses mélanges avec la protéine de soja dans différentes proportions.

Les mélanges HDPE-SPI avec 30% de glycérol et de 3% de Lotader AX8840 présentent une très légère amélioration de l'allongement à la rupture (Figure 5), 2.78 ± 0.53 pour HDPE50SPI150 et 6.18 ± 1.98 pour HDPE48.5(SPI70Gly30)48.5Lot3. Les images MEB sont difficiles à interpréter (Figure 6).

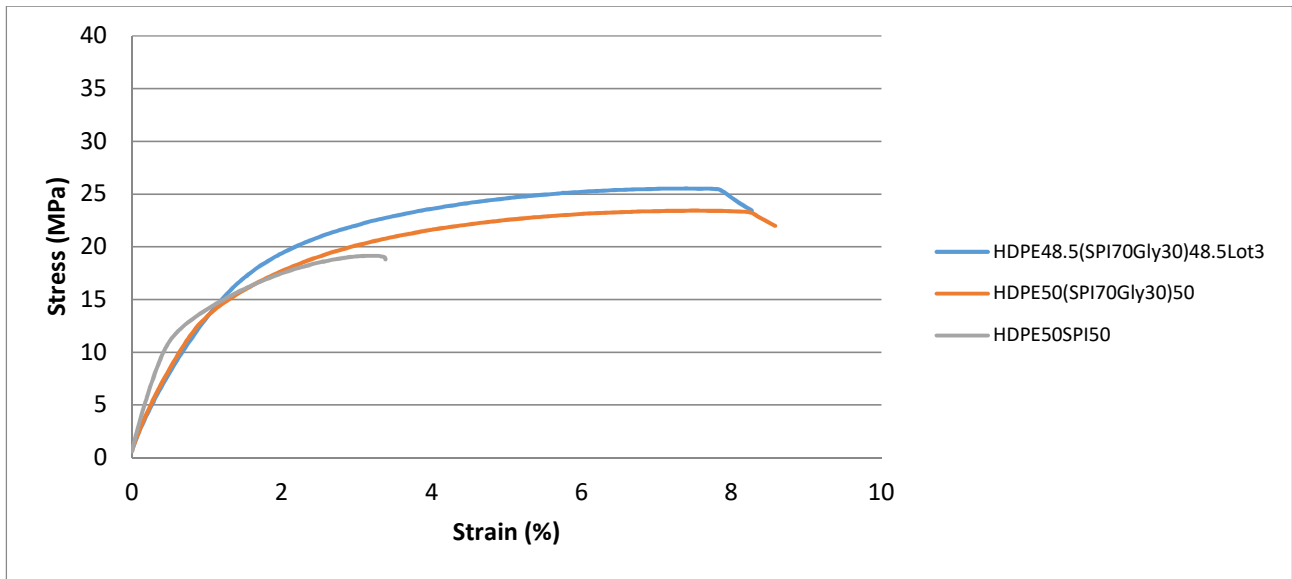


Figure 5: Courbes de traction pour HDPE50SPI50 (gris), HDPE50 (SPI70Gly30) 50 (orange) et HDPE48.5 (SPI70Gly30) 48.5Lot3 (bleu).

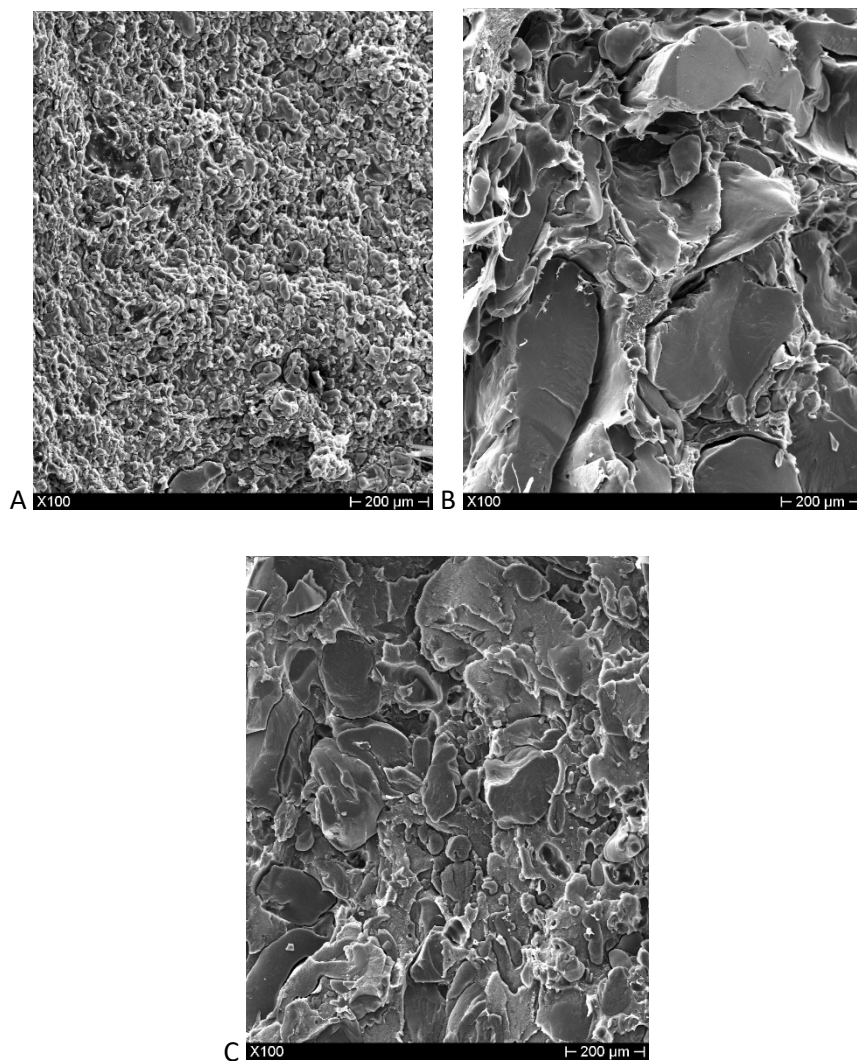


Figure 6: Images MEB de HDPE50SPI50 (A), HDPE50(SPI70Gly30) 50 (B), HDPE50(SPI70Gly30)50Lot3 (C).

Des tests préliminaires de compostage ont été effectués pendant trois mois à 35°C et 58°C, en se basant, dans un premier temps sur i) la variation de masse (Figure 7), ii) l'apparence visuelle (Figure 8) et iii) les spectres FTIR. Les résultats sont compatibles avec une dégradation rapide du SPI, contrairement au HDPE qui reste stable. HDPE50-SPI50 montre une progression de la dégradation, avec une variation de masse qui atteint près de 30% pour les échantillons compostés pendant 3 mois à 58 ° C.

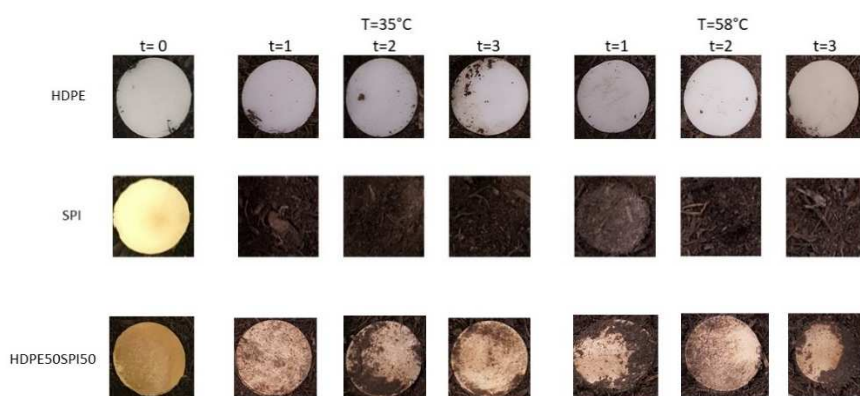


Figure 7: Observation visuelle du HDPE, de la protéine de soja isolée (SPI) et du HDPE50-SPI50 pendant trois mois de compostage à 35 ° C et 58 ° C.

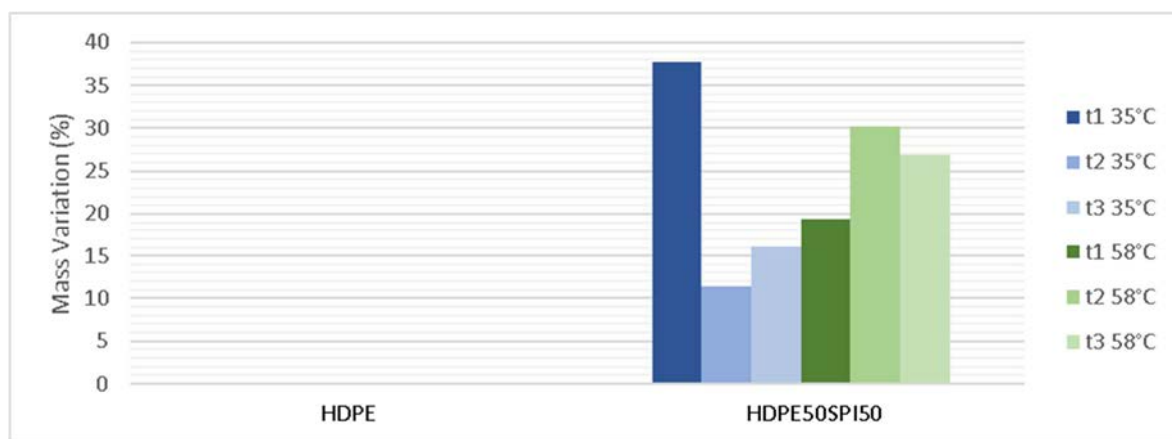
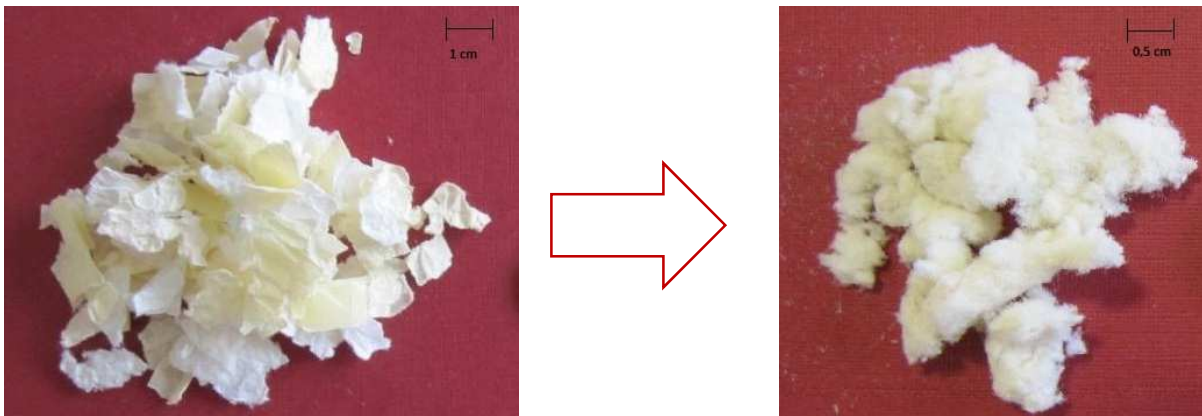


Figure 8: Variation de masse du mélange HDPE et HDPE50-SPI50 pendant trois mois de compostage (t1= 1 mois, t2= 2 mois et t3= 3 mois) à 35 ° C (échelle bleue) et à 58 ° C (échelle verte).

Composites avec charges naturelles

À partir des analyses précédentes, le mélange HDPE50-PLA50 a été sélectionné comme matrice pour les composites contenant de la farine de bois, des fibres de papier recyclé et un mélange de deux charges naturelles. En particulier, 20, 30, 40% de farine de bois et 10, 20, 30, 40% de fibres de papier recyclé ont été ajoutées au mélange. Le mélange 30% en masse de farine de bois et 10% en masse de fibres de papier recyclées a été choisi pour étudier l'influence de l'ajout de charges naturelles avec 3% de Lotader AX8840 ou Polybond 3029.

La consommation de papier a augmenté ces dernières années et, partant, les problèmes liés à son élimination. Bien que 72% environ des déchets cellulosiques soient soumis au processus de recyclage, la partie restante représente un déchet solide. Une proposition concerne la micronisation du papier pour obtenir des fibres d'une taille appropriée pour une application dans des matériaux composites. Dans ce travail, un processus de micronisation a été adopté, qui fonctionne par impact, friction et turbulence. Le papier, après avoir été broyé dans un broyeur à marteaux pour obtenir des fragments de 8 à 10 mm, est transporté dans le microniseur, en permettant d'obtenir, après un step de séparation, des fibres de $750 \pm 300 \mu\text{m}$ de long et de $25 \pm 10 \mu\text{m}$ de diamètre.



L'ajout de farine de bois permet d'augmenter le module d'Young, mais les problèmes d'interface sont sans doute à l'origine d'allongements à la rupture faibles (tableau 3).

Tableau 3: Résultats des essais de traction d'échantillons chargés de farine de bois. La couleur bleue correspond à la farine de bois sans compatibilisant, le violet avec le Polybond 3029 et le rouge avec le Lotader AX8840.

Echantillons	E (GPa)	σ (MPa)	ϵ (%)
--------------	------------	-------------------	-------------------

HDPE50PLA50	1.8±0.1	38.7±0.2	99.4±2.1
HDPE50PLA50WF20	3.4±0.1	34.6±2.8	1.6±0.1
HDPE50PLA50WF30	4.1±0.1	34.0±1.3	1.2±0.2
HDPE50PLA50WF40	5.0±0.2	33.5±1.5	1.9±0.0
HDPE50PLA50Poly3WF20	3.3±0.1	36.0±0.8	1.8±0.1
HDPE50PLA50Poly3WF30	4.1±0.2	35.9±1.4	1.4±0.1
HDPE50PLA50Poly3WF40	4.9±0.1	33.6±1.7	0.9±0.2
HDPE50PLA50Lot3WF20	3.3±0.1	37.8±1.5	2.0±0.1
HDPE50PLA50Lot3WF30	4.1±0.1	35.0±1.2	1.4±0.1
HDPE50PLA50Lot3WF40	5.0±0.1	34.1±3.3	1.0±0.1

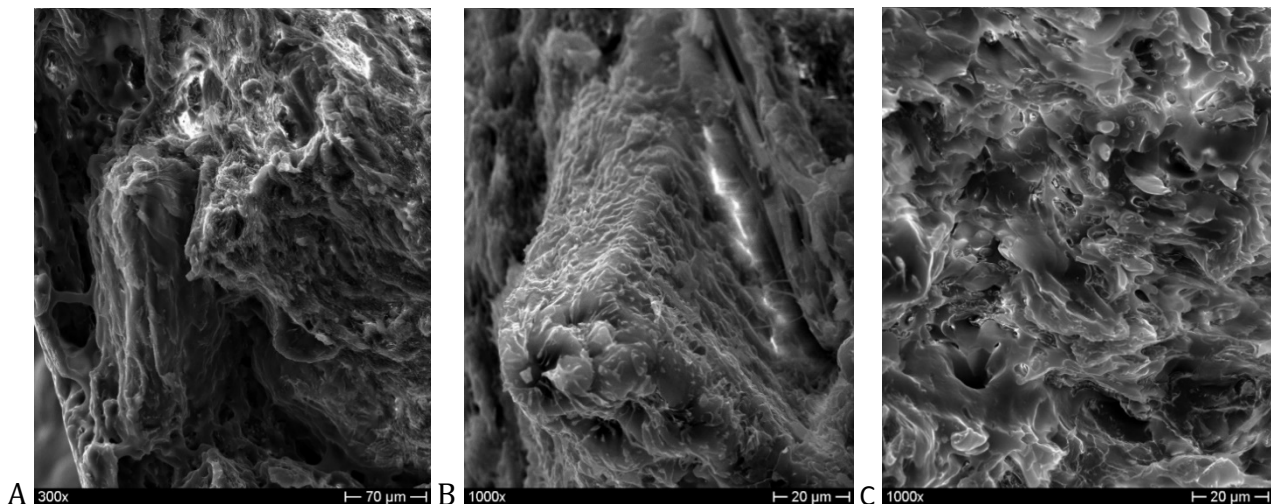


Figure 9: Image MEB HDPE50PLA50WF30 (A), HDPE50PLA50Lot3WF30 (B), HDPE50PLA50Poly3WF30 (C).

Les fibres de papier recyclées ont été ajoutées au mélange HDPE50PLA50. A mesure que le pourcentage de fibres de papier recyclées augmente, le module d'élasticité augmente (figure 10), tout en créant des problèmes d'agglomération pour des pourcentages supérieurs à 10% (figure 11). C'est l'une des raisons pour lesquelles on a choisi d'étudier plus particulièrement des mélanges avec 10% de fibres de papier, associées à la farine de bois.

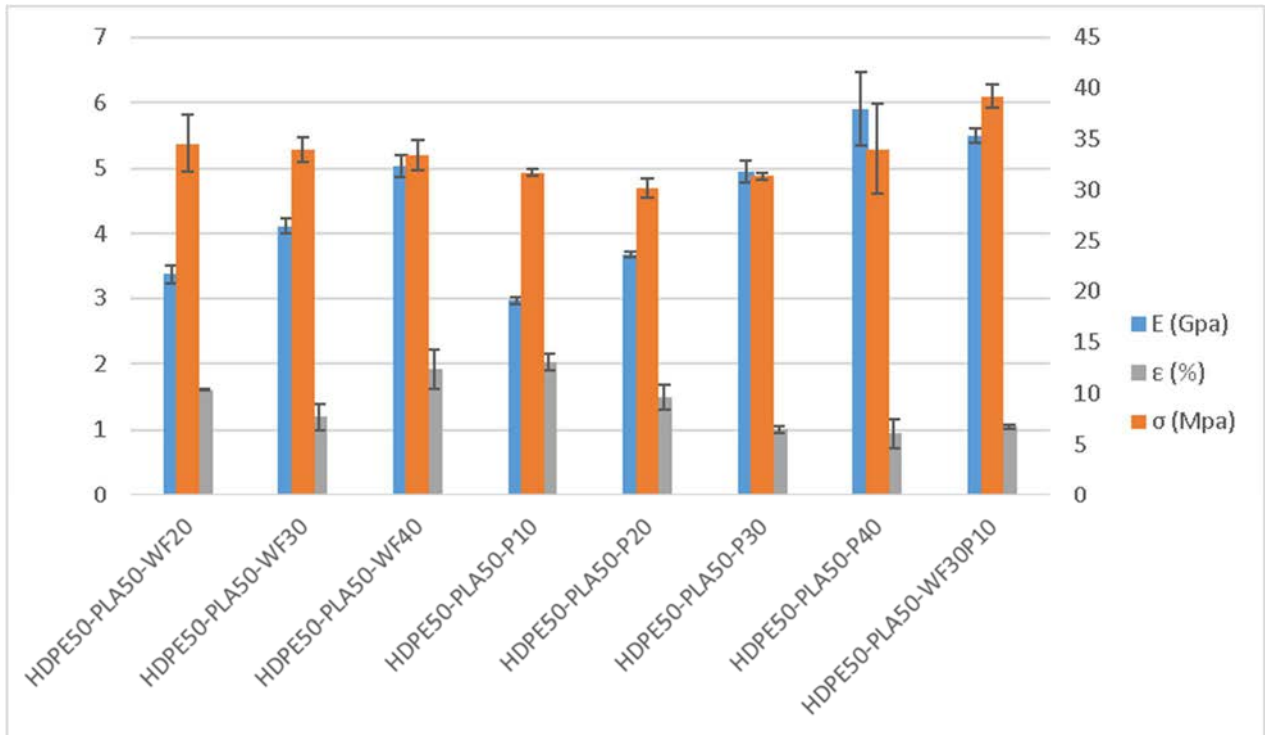


Figure 10: Module élastique (bleu), allongement à la rupture (gris) et résistance à la traction (orange) pour les composites chargés de farine de bois et de fibres de papier recyclées.

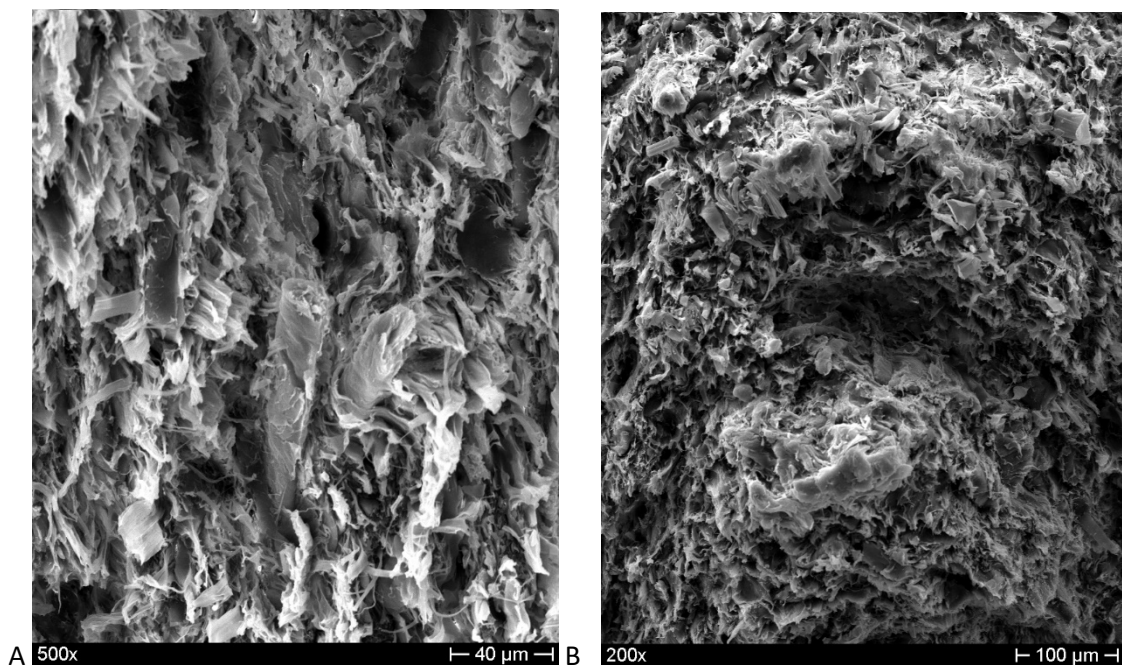


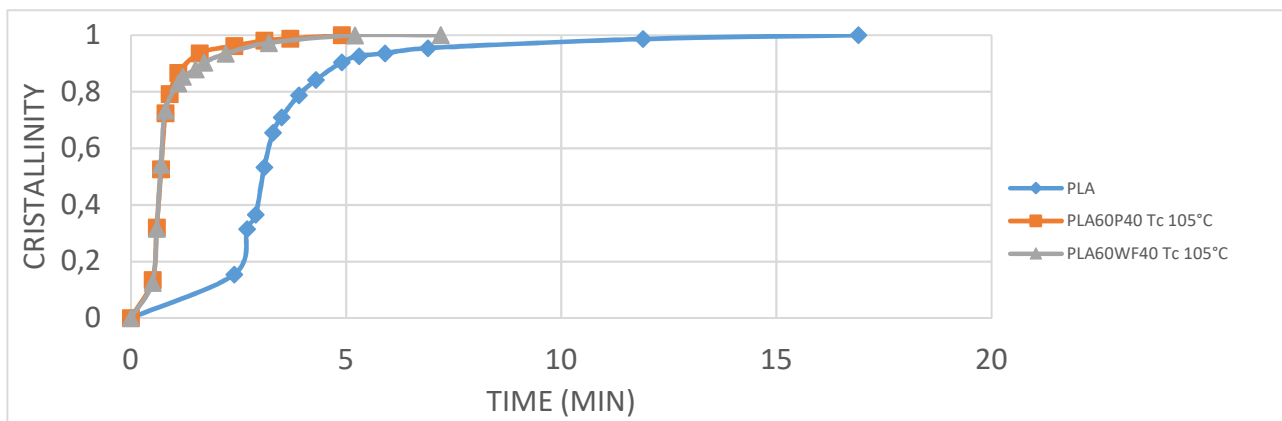
Figure 11: Image MEB de a) HDPE50-PLA50-P10, sans agglomérats et b) HDPE50-PLA50-P20, avec des agglomérats.

Le mélange avec 30% de farine de bois et 10% de fibres de papier recyclées permet d'augmenter le module élastique et la charge à la rupture par rapport aux composites contenant

40% de papier recyclé. L'ajout de Lotader AX8840, également dans ce cas, semble être plus efficace que le Polybond 3029.

L'influence de la farine de bois et des fibres de papier recyclées sur l'HDPE et le PLA a été analysée grâce à l'utilisation du thermomicroscope optique (TOM) et de l'analyse calorimétrique différentielle (DSC). Le TOM a montré la formation d'une seule couche de sphérulites à la surface des fibres, à la fois pour le PEHD et pour le PLA, comportement typique des charges à effet de nucléation modéré, selon la littérature. Les analyses DSC ont validé cette hypothèse : la farine de bois, tout comme les fibres de papier recyclées réduisent le temps de demi cristallisation du PLA (figure 12).

A



B

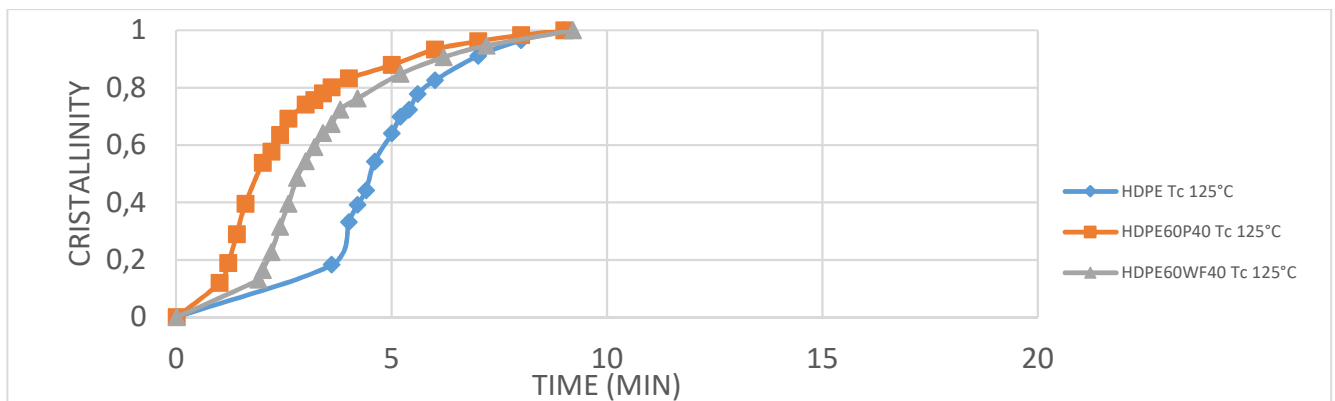


Figure 12: A) Taux de cristallisation en fonction du temps pour PLA (bleu), PLA60-P40 (orange) et PLA60WF40 (gris), B) Taux de cristallisation en fonction du temps pour HDPE (bleu), HDPE60-P40 (orange) et HDPE60WF40 (gris).

Introduction

The importance assumed by polymer materials is evident, and is more ancient than we can imagine. In fact, polymers like wood, silk, wool, cotton are among the first materials known by the men, though their deep nature has been known only in the 20th century.

Important discoveries have been done thanks to observation of nature, trying to learn from its structures and organizations, as a consequence many synthetic polymers often hydrophobic have been produced, revolutionizing our routine.

Great importance is related to thermoplastic polymers, thanks to their mechanical properties, production processes, cheapness and versatile applications. Moreover, natural polymers are mainly thermoplastic ones after plasticization process, with properties rather different from fuel-based such as their hydrophilicity.

Environmental impact is one of the biggest problems related to synthetic polymers: end-of-life of fuel-based polymers can be a problem, especially when they are dispersed in seas or on earth. Although many progresses have been done, there are still problems related to the dispersion of non-biodegradable polymer wastes.

The increasing consumption of polymer materials, and the increasing importance of environmental protection, directed researches towards new materials classes. An interesting strategy in order to face this problem could be polymeric matrix composites filled with natural waste product [1]. In this class of materials, Wood Plastic Composites (WPC) developed because of their potential recyclability and the possibility to use waste materials for their production [2]. WPC could substitute virgin wood in many applications, such as automotive, nautical, construction like windows and door frames and outdoor furniture. Moreover, WPC could be modelled through the same methods of traditional woodworking [3-4] and processed through traditional thermoplastic methods [5]. Other important properties of WPC are low moisture absorption, low density, low price, less abrasion during processing than mineral fillers [6]. In our work we used high density polyethylene as WPC matrix.

Another important source of waste product is paper, potentially useful as filler in thermoplastic matrix [7-9]. Paper couldn't always be subjected to traditional recycling process, as a consequence an interesting alternative is to properly grind this waste and recycle it in

composites. Our proposal in particular is to use this waste product as filler in WPC materials, in order to improve their properties reducing the no-ecofriendly amount of charge. In this way we use both recycled wood and recycled paper as filler in our composite.

Another strategy adopted to face pollution problems could be the introduction of bio-derived polymer. In fact, in order to further reduce the amount of no-recyclable charge, besides introducing wood flour and paper fibres, the introduction of a bio-derived polymer in the matrix is also possible: PLA and Soy Protein Isolate derived polymers were chosen. In fact, composites with biodegradable products based on agricultural materials have developed during last year [10-12].

One of the biggest problems of WPCs, because of their different nature, is low compatibility between hydrophilic filler and hydrophobic matrix. Many researches have been conducted in order to face this problem. The introduction of a coupling agent is one of the most common methods adopted. The same problem of different hydrophilicity was faced blending polyolefins and bio-derived polymers in order to obtain a thermoplastic matrix with good properties. The easiest way to improve blend's properties was the introduction of a coupling agent. As a consequence, coupling agents have to act both on natural filler-matrix interfaces and on hydrophobic-hydrophilic matrix interfaces. Among coupling agent, maleic anhydride and ethylene-glycidyl methacrylate co-polymer have been chosen.

After an introduction on the state of the art (chapter 1) and the description of the materials and methods used to characterize the samples (chapter 2), the experimental part of the project was analysed in four chapters: production and use of paper microfibrils in a polyolefin matrix (chapter 3), development and characterization (mechanical properties, thermo-chemical properties, morphology and degradation) of a biodegradable polyolefin-polymer mixture (chapter 4), development and characterization (mechanical properties, thermo-chemical properties, morphology and degradation) of a composite filled with paper fibres and wood flour (chapter 5), conclusions and future perspectives (chapter 6).

References

1. Z.N. Azwa et al., A review on the degradability of polymeric composites based on natural fibres, *Mater Design*, vol 47, pp. 424-442, 2013.
2. A. Ashori, A. Nourbakhsh, Characteristics of wood-fiber plastic composites made of recycled materials, *Waste Manage*, vol 29, pp. 1291-1295, 2009.
3. V.Mazzanti, F. Mollica, N. El Kissi, Rheological and Mechanical characterization of polypropylene-based Wood Plastic Composites. Mazzanti, *Polym Composites*, 2015.

4. M. Hietala, J. Niinimäki, K. Oksman, Processing of wood chip-plastic composites: effect on wood particle size, microstructure and mechanical properties, *Plast, Rubber Compos*, vol 40, pp. 49-56, 2011.
5. S. Migneault et al., Effect of processing method and fiber size on the structure and properties of wood-plastic composites. *Compos Part A-App S*, vol 40, pp. 80-85, 2009.
6. K. Pei-Yu et al., Effects of material compositions on the mechanical properties of wood-plastic composites manufactured by injection moulding, *Mater Design*, vol 30, pp. 3489-3496, 2009.
7. M. Prambauer, C. Paulik, C. Burgstaller, The influence of paper type on the properties of structural paper- Polypropylene composites, *Compos Part A-App S*, vol 74, pp. 107-113, 2015
8. I. Baroulaki, O. Karakasi, G. Pappa, P.A. Tarantili, D. Economides, K. Magoulas, Preparation and study of plastic compounds containing polyolefins and post used newspaper fibres, *Composite: Part A*, vol 37, pp. 1613-1625, 2006.
9. M. Mehrabzadeh, F. Farahmand, Recycling of commingled plastics waste containing polypropylene, polyethylene and paper, *J App Polym Sci*, vol 80, pp. 2573-2577, 2001.
10. K.K. Kabor et al., Chemical treatments on plant based natural fibre reinforced polymer an overview, *Compos Part B-Eng*, pp. 2883-2892, 2012.
11. X. Ma, J. Yu, J.F. Kennedy, Studies on the properties of natural fibres-reinforced thermoplastic starch composites, *Carbohyd polym*, vol 62, pp. 19-24, 2005.
12. A.A.S. Curvelo, A.J.F. de Carvalho, K.A.M. Agnelli, Thermoplastic starch-cellulosic fibers composites: preliminary results, *Carbohyd polym*, vol 45, pp. 183-188, 2003.

1. State of the art

This chapter is derived and adapted from “Oil-based and bio-derived thermoplastic polymer blends and composites”, written by A. Quitadamo, V. Massardier, M. Valente (Introduction to Renewable Biomaterials, edited by Lucian Lucia and Ali Ayoub)

During recent years, many researchers have focused their attention on natural fibres as fillers for thermoplastics composites. These kinds of fibres, in fact, are characterised by many advantages with respect to traditional glass and carbon fibres such as low cost, low density, comparable specific tensile properties, non-abrasive to the equipment, non-irritating the skin, reduced energy consumption, renewability, **potential** bio-degradability [1-2]. Table 4 shows the main feature of natural fibres, in comparison to traditional glass fibres.

Table 4: Comparison between natural and glass fibres [2]

	Natural fibres	Glass fibres
Density	Low	Twice that of natural fibres
Cost	Low	Low, but higher than natural fibres
Renewability	Yes	No
Energy consumption	Low	High
Distribution	Wide	Wide
CO ₂ neutral	Yes	No
Abrasion to machines	No	Yes
Health risk when inhaled	No	Yes
Disposal	Biodegradable	Non biodegradable

Some of the widespread applications for composites with natural fillers are aerospace, leisure, construction, sport, packaging and automotive. In fact, these industrial sectors have shown enormous interest in the development of new composites materials [3]. One of the first examples of using natural fibres instead of fuel-based ones is Trabant.

The Trabant (Figure 13) is the first known application of natural fibres in automotive industries, produced in 1958 in the German Democratic Republic. The main parts, manufactured with

phenolic resin reinforced with cotton fibres, were roof, boot lid, bonnet, wings and doors [4].



Figure 13: Trabant car, produced in 1958 in the German Democratic Republic with main parts made of composites with natural fillers [Wikipedia, Trabant, 18/11/2016]

Table 5 reports mechanical properties of some natural fibres as compared to conventional fibres and polymers [5].

Table 5: Mechanical properties of some natural fibres in comparison to traditional fibres and polymers [adapted 5]

	Density (g/cm ³)	Elongation (%)	Tensile strength (MPa)	Young's Modulus (GPa)
<i>Fibres</i>				
Cotton	1.5-1.6	7.0-8.0	278-800	5.5-12.6
Jute	1.3	1.5-1.8	393-773	26.5
Flax	1.5	2.7-3.2	345-1035	27.6
Hemps	1.5	1.6	690	70.0
Ramie	1.5	1.2-3.8	400-938	61.4-128.0
Sisal	1.5	2.0-2.5	511-635	9.4-22.0
Coir	1.2	30.0	175	4.0-6.0
Viscose (cord)		11.4	593	11.0
Soft wood (Kraft)	1.5		1000	40.0
E-glass	2.5	2.5	2000-3500	70.0
S-glass	2.5	2.8	4570	86.0
Aramid (normal)	1.4	6-8	3000-3150	100-150
Carbon (standard)	1.8-2	1.4-1.8	4000	230.0-240.0
<i>Polymers</i>				

ABS	1.05	10	55	2.8
Polycarbonate	1.22	100	62	2.3
Polyetherimide	0		105	2.8
Nylon	1.12	29	66	3.5
Polyethylene (HDPE)	0.95	30	28	1.1-1.2
Polypropylene	0.9	200	35	1.5-2
Polystyrene (high impact)	1.05	15	35	3-3.5
Epoxy resin	1.3	3-4	32	4-6

Natural fibres are a large family of fibres, including wood, cellulose, hemp, flax, jute, sisal, kenaf and many others [6]. In particular, wood-plastic composites (WPCs) are one of the commonly known families of natural fibres-thermoplastic composites. Another interesting class of materials is characterised by thermoplastic composites with cellulosic fibres derived from wastes such as newspapers, additivated paper, paper board and paper mill sludge. These two classes of composites will be deeply described.

The main drawback of composites with natural fillers is the poor compatibility between hydrophilic fibres and hydrophobic matrices: the different nature between filler and matrix causes the formation of fibre-fibre interactions instead of fibre-matrix ones. As a consequence, formation of agglomerates and lower dispersion of natural fibres is possible. These two problems, bad mixing and weak interface, will give a composite with low mechanical properties [7].

The most popular methods to improve fibre-matrix interface are the introduction of a coupling agent [8-11] as well as physical and chemical treatments [12-13].

Natural fibres present drawbacks, such as interface problems with traditional polyolefins, low temperature processes, moisture absorption and swelling fibres, supply and demand cycles based on product availability and harvest yields, quality variations based on growing sites and seasonal factors, but their advantages are much more interesting and will lead to new materials taking care of our planet.

1.2 Wood-plastic composites

Wood Plastic Composites (WPC) were born in Italy in the 1970s, and then developed as commercial products in North America in the 1990s. By the start of the 21st century they were spreading to India, Singapore, Malaysia, Japan and China [14]. The introduction of WPCs in the decking market (Figure 14) was mainly responsible for their growth. A direct result of success in the decking market is that product are now being developed and introduced for new exterior applications such as railing, fencing, roofing and siding [15].



Figure 14: Example of wood-plastic composites application in decking market
[7trust.com, green products 18/11/2016]

The WPC are defined as thermoplastics reinforced with wood or other natural fibres, principally produced from commodity thermoplastics such as polyethylene, polyvinyl chloride or polypropylene [16]. The matrix chosen for WPC production is influenced by limited thermal stability of wood: only thermoplastics that melt or can be processed under 200°C are commonly used [17].

One of the biggest problems of WPCs, because of their different nature, is the low compatibility between hydrophilic fillers and hydrophobic matrices. Many researches have been conducted in order to face this problem. The introduction of a coupling agent is one of the most common methods adopted. A variety of coupling agents used in WPC exist such as acrylates, amides and imides, anhydrides, chlorotriazines and derivatives, epoxides, isocyanates, organic acids, monomers, polymers and copolymers, inorganic agents and organic-inorganic agents (silanes, titanates).

Polyolefins grafted with maleic anhydride as coupling agents have received attention because

they allow improving mechanical properties of wood fibre-polyolefin composites. The maleic anhydride mechanism permits the formation of interactions or chemical bonds between the hydroxyl groups of natural fibres and carbonyl groups of maleic anhydride [18-21]. Figure 15 shows an example of a polypropylene-grafted-maleic anhydride (MAPP) polyolefin, and Figure 16 the mechanism of coupling agent action.

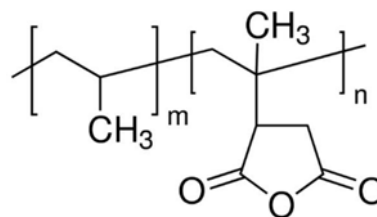


Figure 15: Polypropylene-grafted-maleic anhydride

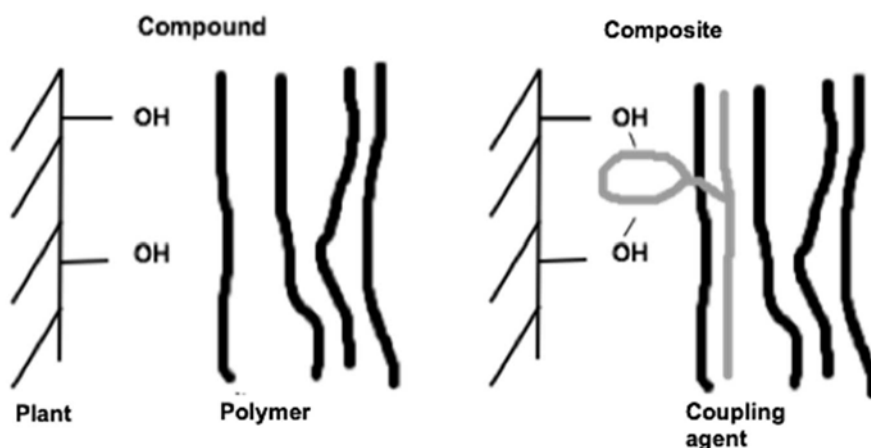


Figure 16: Working mechanism of polyolefin-grafted-maleic anhydride as coupling agent (elliptical shape is the maleic anhydride graft):

left) compound formation because of the weak interaction between plant fibres (hydrophilic) and polymers (hydrophobic); right) composite formation thanks to the interaction of MAPP maleated graft with plant fibres and polymeric MAPP chains mixing with polymer matrix. [adapted from 5]

The main effects of maleic anhydride are improving tensile and flexural modulus as well as tensile and flexural strength. However, an optimization of its concentration must be performed

[22-23].

Kim et al. [24] analysed different maleic anhydride grafted polypropylene (MAPP), and their influence on bio-flour-filled polypropylene composites. In particular, they studied rice husk flour (RHF) and wood flour (WF) as fillers (30 wt.%), and they have chosen five different MAPP with different percentages of maleic anhydride (MA) graft, molecular weight (\overline{M}_w) and melt flow index (MFI), displayed in Table 6. The amount of coupling agent was 3 wt.% with respect to the total weight of the composite (bio-flour and polypropylene).

Table 6: Properties of five MAPP with different maleic anhydride content (MA%), molecular weight (\overline{M}_w) and melt flow index (MFI) [adapted from 24]

MAPP	MA (%)	\overline{M}_w	MFI (g/10 min)	Providers
(A) Polybond 3150	0.5	46,000	20	Crompton Polybond
(B) Polybond 3200	1	42,000	104	Crompton Polybond
(C) G-3003	1.2	52,000	90	Eastman Chemical Products
(D) E-43	1.2	91,00	ND	Eastman Chemical Products
(E) Bondyram	0.8	66,000	90	Polyram

An optimization of maleic anhydride percentages and \overline{M}_w was needed in order to improve composite properties, as shown in Figure 17 and 19. Low MA content did not allow obtaining adequate interactions between bio-flour and polypropylene matrix. On the other hand, high MA content keep the coupling agent near the hydrophilic surface, preventing a good interaction with the hydrophobic matrix. Low MAPP Mw did not allow a good mixing with the polypropylene matrix, while a high Mw could provide interface problems. Because of that, G-3003 was considered as the best-optimized coupling agent, able to induce the best properties in the composite.

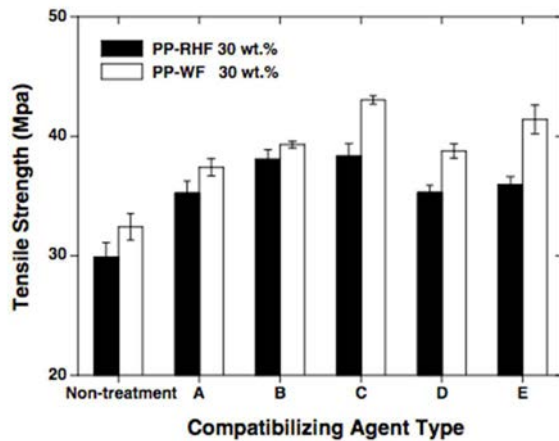


Figure 17: Tensile strength trend of polypropylene-rice husk flour (PP-RHF) neat and with five different compatibilizing agents [adapted from 24]

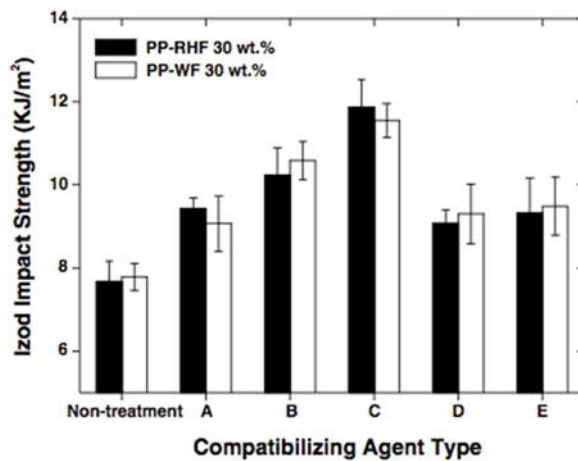


Figure 18: Izod impact strength trend of polypropylene-rice husk flour (PP-RHF) neat and with five different compatibilizing agents [adapted from 24]

Selke and Wichman, using recycled HDPE from milk bottles, with 30 wt.% of Aspen hardwood and 2 or 5 wt.% of MAPP, have developed another interesting work [25]. A good effect of MAPP addition with respect to neat HDPE was evident, and, as literature revealed, a suitable MAPP percentage is needed in order to optimize the properties of the analysed composite. The evolution of elastic modulus is reported in Figure 19.

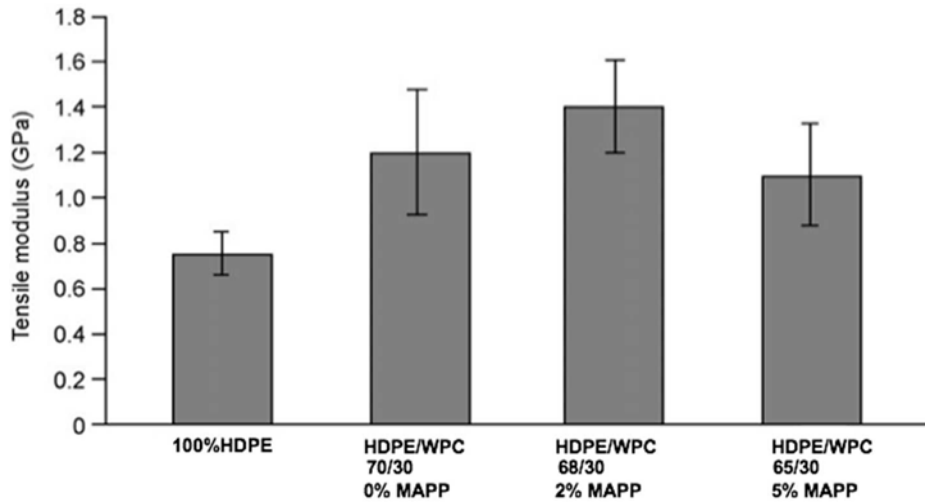


Figure 19: Tensile modulus trend of recycled HDPE from milk bottles, with 30 wt.% of Aspen hardwood and 2 or 5 wt.% of MAPP [adapted from 25]

Important analyses were also conducted about thermal stability of wood-plastic composites. Tazi et al. [26] studied the effect of wood and MAPE percentages on thermo-physical properties. They found that the addition of wood fillers and coupling agent (MAPE) to the polymer matrix resulted in an increase of the melting temperature of HDPE up to values higher than 141°C; the same phenomenon was reported in literature. Table 7 sums up their results.

Table 7: Thermal properties of neat high-density polyethylene (HDPE) in comparison to HDPE with 20-30-40-50-60 wt.% of wood [adapted from 26]

Samples (Numbers represent ratios)	T _m (°C)	ΔC _p (J/g/°C)	X (%)
HDPE 100	138.2	16.8	74.7
HDPE 80/Wood 20	142.0	14.0	76.6
HDPE 70/Wood 30	143.3	11.0	78.1
HDPE 60/Wood 40	140.0	10.0	78.5
HDPE 50/Wood 50	143.4	6.0	79.0
HDPE 40/Wood 60	140.9	4.0	86.1

Variation of heat capacity (ΔC_p) decreases while the filler amount increases: wood fillers obstruct molecular chains mobility close to melting temperature. Heat capacity is defined as the heat per amount material (mole, gram etc.) necessary to increase the temperature by one degree. Near the melting point, macromolecule chains can easily move. Wood fillers can act as nucleating agents for polymers, increasing their crystallinity, as visible also from enthalpy variation. As a consequence, due to the endothermic nature of melting peak, the variation of heat capacity is lower than neat polymer near the melting peak. Moreover, wood flour has a lower heat capacity with respect to polyethylene, as a consequence a lower heat capacity variation can be expected. [Synergy effects of wood flour and fire retardants in flammability of wood-plastic composite, Umemuraa T., Araoa, Y., Nakamurab S., Tomita Y., Tanaka T., Energy Procedia 56, 48 – 56, 2014]. Moreover, wood fillers acted as nucleating agents, increasing crystallinity of the matrix, from 74.7% to 85.1%.

Potentially biodegradable composites have been developed by Pilla et al [27], who studied a poly (lactide) (PLA)recycled wood fibre (RWF) composites compatibilized with 0.5% of GE Silicones—Silquest A-174VVR silane (gamma-methacrylox-ypropyltrimethoxysilan) silane. Differential Scanning Calorimetry (DSC) analyses (Table 8) have shown that the addition of RWF acted as a nucleating agent, in agreement with Tazi et al. work.

Table 8: Differential Scanning Calorimetry (DSC) results of neat PLA and PLA with 10 and 20 wt.% of recycled wood fibres (RWF) and 0.5 wt.% of Silane as compatibilizing agent [27].

Samples	T _{cc} (°C)	X(%)
PLA	110.5	10
PLA-10%RWF-0.5%Silane	98.8	16
PLA-20%RWF-0.5%Silane	98.8	17

Zierdt et al. [28] studied a bio-WPC produced with bio-based polyamide 11 (PA 11) and chemically modified beech fibres up to 50 wt.%. They performed chemical modification of the beech fibres in order to improve fibre-matrix interface and increase fibres thermal resistance to processing temperature. The treatment consisted of an alkaline aqueous solution of sodium

hydroxide (NaOH) at 10g/l, in which fibres were soaked for 60 min. Thermo Gravimetric Analysis (TGA) proved an increased thermal stability given by a TGA onset temperature shifted from 290 to 330 °C, as shown in Table 9.

Table 9: Thermo gravimetric analysis (TGA) of beech fibres and beech fibres modified with alkaline treatment [28].

Material	T _{onset} (°C)	T ₂₅ (°C)	T ₅₀ (°C)	ML _{600°C}
Beech fibres	290	313	353	87
Modified beech fibres	330	333	363	88

T_{onset} is the onset temperature of second decomposition stage.

T₂₅ is the temperature at 25% mass loss.

T₅₀ is the temperature at 50% mass loss.

ML_{600°C} is the mass loss at 600°C.

This improvement resulted from hemicellulose removal, as confirmed through Attenuated Total Reflection Infrared Spectroscopy (ATR-FTIR). Mechanical and thermo-mechanical analysis of the processed bio-WPC (Table 10 and Figure 20) showed an increase in both elastic and storage modulus of the composites by the chemical treatment of the fibres. This effect was attributed to an increased number of hydrogen bonds between the modified beech fibres and the PA 11 matrix. The overall mechanical properties of the investigated bio-WPCs support their use as sustainable construction materials for technical applications.

Table 10: Mechanical properties of polyamide 11 (PA11) neat and with fibres (modified or not with alkaline treatment) [28].

Material	Fibre content (%)	Elastic modulus (GPa)	Tensile strength (MPa)	Strain at break (%)	Impact strength (kJ/m ²)
PA11	0	1297±28	48±2	136.7±9.5	12.8±1
PA11/beech fibres	30	2983±75	53±1	4.2±1.3	2.8±0.1
	40	3764±69	58±1	2.9±0.4	2.8±0.4
	50	4684±184	65±2	2.2±0.2	2.4±0.2
PA11/modified beech fibres	30	3278±85	57±1	6.4±1.1	3.0±0.1
	40	4012±90	59±2	3.4±0.7	3.0±0.1

50	5049±108	65±2	2.6±0.2	2.9±0.1
----	----------	------	---------	---------

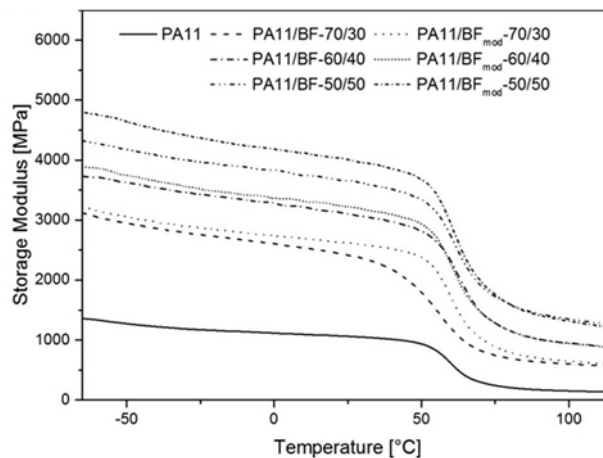


Figure 20: Storage modulus of PA11 neat and with beech fibres (BF) (30-40-50 wt.%) modified (mod) and not [28].

During last years, researchers have also oriented their works in totally biodegradable composites. These kinds of composites are characterized by biodegradable matrices with natural fillers. An interesting work in this field was published by Huda et al [29] for producing “green”/bio-based composites with poly (lactic acid) (PLA) as matrix and recycled cellulose fibres (from newsprint). They obtained composites with mechanical properties that can compete with conventional thermoplastic composites. The main results of this study can be shown in the tables below (TC 1004, R 0083 and R 0084 are the cellulosic fibres derived from newspaper/magazine or Kraft paper stock). WPCs are a well-established class of materials, with their own properties and market. However, improvement in order to increase WPC properties and environmental friendly character could still be done. The use of virgin wood for WPCs materials could overcome its usual application, moreover WPC can be processed through traditional thermoplastics processes and post processed with the same method as traditional wood.

1.3 Waste paper as filler in thermoplastic composites

Paper consumption has grown during last years, and so the problems related to its disposal. From all the cellulosic waste, around 72%, is used in recycling process, the rest is sent to incinerator for thermovalorization or is used for other applications (for example, production of energy in the fireplace) or is sent to waste dump [1-2].

Paper is the most recycled product in Europe and 54% of paper industry's raw materials come from waste paper and board [3].

Paper recycling process has advantages like raw material's lower cost, the chance to use waste as fuel for steam production, the reduction of the amount of waste, of the storage cost and trees' consumption [4].

There are also some disadvantages such as the possibility to reuse paper for a maximum of 5-6 times, after that, waste paper becomes a solid urban waste and needs disposal or the production of variable amounts of slug and waste that have to be recovered and have to be subjected to different treatments.

One of the biggest problem related to paper recycling is the use of chlorine compounds to bleach paper, which will remain in the recycled products [5]. Another pollution source is the incinerator both for the dust that developed in the process and for the residual material that has not undergone complete combustion [6-8].

Concluding, despite great economic advantages and the reduction of environmental pollution due to recycling processes, there are still problems related to the disposal of sludges and wastes, the use of incinerators and water treatment. Moreover, inked paper or additivated one (for example with polymer films) cannot be subjected to traditional recycling process without higher costs and must accordingly be disposed as special waste.

In this context, the possibility to use different kinds of cellulosic waste as dispersed phase in composite materials with HDPE matrix represents an interesting perspective.

The different hydrophilic nature between HDPE and cellulosic fibres makes necessary the use of physical or chemical treatment [9-12] to improve fibre matrix interface. In fact, interfacial adhesion is important in order to obtain satisfactory mechanical properties [13]. In this study, the introduction of maleic anhydride graft polyethylene (MAPE) as compatibilizer has been chosen [14-16], even if, in some cases, a poor effect of the additive has been seen [20].

During last years, many studies have been done on waste paper usage as filler in thermoplastic matrix composites. Different kinds of waste paper have been used like newspapers, copy papers [17], ink-eliminated waste paper sludge flour [18] and unbleached cellulosic Kraft pulp fibres [19-20]. The results were promising considering mechanical properties. In fact, waste paper composites are comparable to glass fibres composites in some cases [19] and could be suitable materials for many applications. For example, in future studies, we would introduce recycled

paper fibres to improve impact behaviour, as was investigated with glass or basalt fibres in previous works [21]. Problems related to paper disposal has grown during last year, despite paper is the most recycled product in Europe and 54% of paper industry's raw materials come from waste paper and paperboard [30]. Paper cannot always be subjected to traditional recycling processes. In fact, approximately 72% [www.euwid-recycling.com] of all the cellulosic wastes is used in recycling processes, the rest has to be sent to incinerators or landfilled as solid wastes [31]. In order to reduce environmental impact of paper industries, the possibility of introducing different kinds of waste paper is opened. Newspapers are one of the widespread sources of waste paper, and many studies have been conducted on it. Sanadi et al. proposed one of the first studies on newspaper's fibres introduction in thermoplastic composites in 1994 [32]. They introduced 40 wt.% of recycled old newspaper fibres (ONF) in polypropylene, resulting in a tensile strength of 34.1 MPa, and unnotched Izod impact strength of 112 J/m. Thanks to the addition of MAPP (3 % of the fibre weight), a 57 MPa tensile strength and a 212 J/m Izod impact strength were achieved. This study shows the positive effect of newspaper introduction in polypropylene matrix, as well as the good effect of coupling agent. More recent works [33-37] not only validate the good results obtained by newspapers fibres, but also proposed the possibility to substitute 20-30 wt.% fibreglass (GF) in polypropylene composites by 40-50 wt.% old newspaper fibres (ONF). This involves a reduction on the use of synthetic polymers, avoiding glass fibres for some applications, and exploiting the environmentally friendly character of natural fibres. Some interesting results about these works are summed up in Table 11.

Table 11: Mechanical properties of polyolefin-old newspaper composites compared to polyolefin-glass fibres composites [ref. 32-35-37].

Composites (Numbers represent ratios)	Izod impact Energy Notched (J/m)	Izod impact Energy Unnotched (J/m)	Tensile Modulus (GPa)	Tensile Strength (MPa)	Publication
PP60/ONF40	20.8±0.5	112±18	4.42±0.2	34.1±1.1	[32]
PP60/ONF40/MAPP3	21.6±0.1	212±24		57.0±0.7	[32]
PP80/ONF20			2.8±0.1		[37]
PP70/ONF30			3.8±0.1		[37]
PP60/ONF40			4.2±0.1		[37]
PP50/ONF50			5.3±0.2		[37]

PP80/GF20	4.1±0.1		[37]
PP70/GF30	5.7±0.1		[37]
PP60/GF40	7.7±0.1		[37]
PP90/ONF10/MAPP5	2.7	44	[35]
PP80/ONF20/MAPP5	3.0	50	[35]
PP70/ONF30/MAPP5	3.3	58	[35]

PP –polypropylene ONF - old newspaper fibres MAPP – polypropylene-grafted-maleic anhydride GF - glass fibre

Some interesting studies have been conducted on the introduction of paper sludge in thermoplastic composites. Sludge is an abundant waste source; about 300 kg of sludge is produced for each ton of recycled paper [38]. Properties and composition of paper sludge firstly depend on raw materials, the paper grade being manufactured, the amount of water used and the cleaning technique used for wastewater. Wood, cellulose fibres, lignin and organic binders are the main organic components, while kaolinite and calcium carbonate are the main inorganic ones [39]. Generally, paper sludge is disposed in landfills. As a consequence, many researchers focused their attention on the potential use of this waste charge in composite materials.

Hamzeh, Ashori and Mirzaei, have proposed an interesting study, introducing waste paper sludge in high-density polyethylene-wood flour composites [40]. They analysed different concentrations (20, 30, 40 and 60 wt.%) of two sludge materials: one derived from wastewater treatment used in paper industries and the other ink-eliminated sludge, derived from the recycling treatment of waste paper. This study suggests that waste sludge can be used as reinforcing filler for thermoplastic composites: in fact, composites with paper sludge addition have shown better properties (except for some samples) in terms of flexural properties and water absorption uptake. Similar results were also obtained by Son et al. [41], investigating the effect of different paper sludge's mixing ratio and types, as well as concentration of coupling agents on the physical and mechanical properties of paper sludge-thermoplastic composites. They analysed the dimensional stability of the composites, which increases with paper sludge content. By a mechanical point of view, they also confirmed the effect of paper sludge as reinforcement, regarding flexural strength. These two aspects can be seen in Figure 21 and Figure 22.

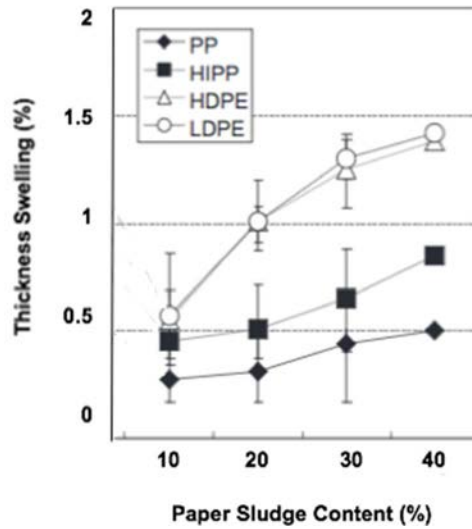


Figure 21: Dimensional stability of polypropylene (PP), high-impact polypropylene (HIPP), high-density polyethylene (HDPE) and low-density polyethylene (LDPE) with different percentages of paper sludge [adapted from 41]

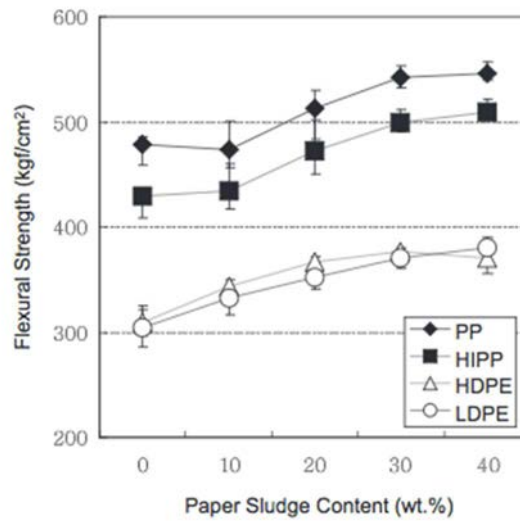


Figure 22: Flexural strength of polypropylene (PP), high-impact polypropylene (HIPP), high-density polyethylene (HDPE) and low-density polyethylene (LDPE) with different percentages of paper sludge [adapted from 41]

The extraction process adopted to obtain fibres from waste paper directly affect the properties of the resulting composites. The choice depends on the application of the produced material.

1.4 Bio-derived thermoplastic polymers

Bio-derived thermoplastic polymers developed during last decades in order to potentially substitute traditional polyolefins in their common applications such as:

- Packaging and food (films, containers, food wrapper, composting bags, plates, cutlery)
- Agricultural (planting containers, controlled release of chemicals)
- Textile (wipes, filters, geotextiles, diapers)
- Medicine (release of drugs, suture, screw, orthopaedic products)

The importance of bio-based polymers in these fields concerns the reduction of environmental impacts and the improved compatibility with organic materials. Nevertheless, hydrophilicity of bio-based polymers can be a problem, concerning the compatibility with traditional hydrophobic polyolefins.

1.4.1 Polylactic Acid (PLA)

Poly Lactic Acid (PLA) is one of the most known bio-derived polymer firstly produced through polymerization by Carothers in 1932 [42] and lately patented by Dupont in 1954. PLA is an aliphatic thermoplastic polyester, generally produced through ring-opening polymerization of lactides (Figure 23).

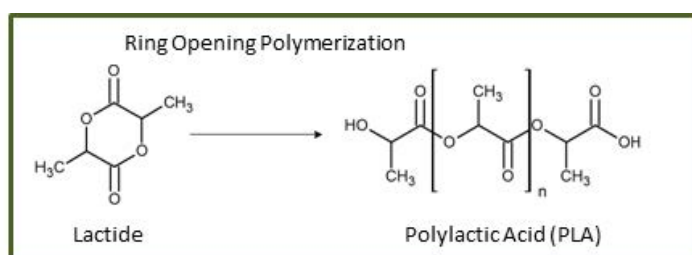


Figure 23: Ring Opening Polymerization of Lactide to produce Polylactic Acid (PLA) [adapted from www.InnoRex.eu]

Lactic Acid (LA) could be synthesized through two methods: chemical synthesis based on petrochemical feedstock, or carbohydrate fermentation. The majority of LA is produced through carbohydrate fermentation and the scheme process is shown in the graph below.

Fermentation

Monomer

Polymerization



Mechanical properties of PLA are good considering tensile modulus, tensile strength and flexural strength, comparable or higher than traditional polyolefins such as polyethylene, polypropylene and polyethylene terephthalate. Table 12 reports main mechanical features of PLA and traditional polyolefins.

Table 12: Some PLA mechanical features in comparison to traditional polyolefins.

	PLA	PET	HDPE	PP
Tensile modulus (GPa)	3.4	3.3	1.3	1.8
Tensile strength (MPa)	53	50-70	15-20	40-50
Flexural strength (MPa)	80	80	20	40
Elongation at break (%)	6	50-150	700-800	100-600
Cost (\$/lb)	1-1.5	0.70-0.72	0.27	0.28

Otherwise, one of the main drawbacks of PLA is its brittleness, in fact tensile modulus and tensile strength of PLA are comparable to PET, but PLA elongation at break limited its applications in PET fields [43].

In order to improve PLA applications, brittleness have to be decreased. During last years, researchers proposed different ways to face this problem, such as the addition of biocompatible plasticizers, blending with other polymers (developed in the paragraph thermoplastic blends) and recent studies also propose the use of ionic liquids.

Baiardo et al. [44] analysed the influence of two different plasticizers, in different percentages: acetyl tri-n-butyl citrate (ATBC) and PEGs with different molecular weights. Both acted as plasticizers, significantly increasing the elongation at break of PLA. As literature reported, the main problem of plasticizers is the decrease of tensile strength and tensile modulus; this problem was confirmed by this study and Table 13 displays these results.

Table 13: Tensile test results of pure PLA as well as PLA modified with polyethylene glycol (PEG) and acetyl tri-n-butyl citrate (ATBC) in different percentages [44]

Material	σ_b (MPa)	E (GPa)	ϵ_b (%)
Pure PLA	66	3.3	1.8
PEG 400 (wt %)			
5	41.6	2.5	1.6
10	32.5	1.2	140
12.5	18.7	0.5	115
15	19.1	0.6	88
20	15.6	0.5	71
PEG 1.5K (wt %)			
5	52.3	2.9	3.5
10	46.6	2.8	5
12.5	18.5	0.7	194
15	23.6	0.8	216
20	21.8	0.6	235
PEG 10K (wt %)			
5	53.9	2.8	2.4
10	48.5	2.8	2.8
15	42.3	2.5	3.5
20	22.1	0.7	130
ATBC (wt %)			
5	53.4	3.2	5.1
10	50.1	2.9	7
12.5	17.7	0.1	218
15	21.3	0.1	299
20	23.1	0.1	298

Martin et al. [45] analysed the effect of different plasticizers such as glycerol, PEG and Oligomeric Lactic Acid (OLA). Glycerol was the less effective plasticizer, while PEG and OLA acted as best plasticizers, decreasing glass transition temperature, melting point and increasing up to 200% the elongation at break. As expected, the plasticizer effect was also evident in a decrease in elastic modulus.

The influence of molecular weight and content of plasticizers introduction was analysed by Maiza et al. [46]. They evaluated the effect of different percentages of triethyl citrate (TEC) and acetyl tributyl citrate (ATBC) on the properties of films for food packaging made of PLA.

Increasing the plasticizers contents leads to lower Tg, melting and crystallization temperature, melting and crystallization heat. Meanwhile, an increased crystallinity was experienced with the rise of the plasticizer. Some results are shown in Table 14 and Figure 24.

Table 14: Influence of molecular weight as well as content of triethyl citrate (TEC) and acetyl tributyl citrate (ATBC) on polylactic acid thermal properties [adapted from 46]

Sample (Numbers represent ratios)	name	Crystallinity (%)	Tc (°C)	ΔH_c (J/g)	Tm (°C)	ΔH_m (J/g)
Treated PLA	TrtPLA	0.45	131.81	4.937	152.03	4.517
PLA 95/TEC 5	PLA-TEC5	2.61	120.87	16.12	148.92	18.43
PLA 90/TEC 10	PLA-TEC10	3.32	119.67	9.640	147.97	12.42
PLA 85/TEC 15	PLA-TEC15	3.84	104.42	20.19	145.94	23.23
PLA 80/TEC 20	PLA-TEC20	5.88	91.63	18.52	143.52	22.90
PLA 70/TEC 30	PLA-TEC30	7.49	70.56	10.95	138.55	15.83
PLA 95/ATBC 5	PLA-ATBC5	1.35	115.73	20.07	146.96	21.27
PLA 90/ATBC 10	PLA-ATBC10	2.68	111.56	20.77	150.08	23.02
PLA 85/ATBC 15	PLA-ATBC15	3.42	101.06	23.68	148.07	20.97
PLA 80/ATBC 20	PLA-ATBC20	4.36	92.01	19.61	146.74	22.86
PLA 70/ATBC 30	PLA-ATBC30	9.73	71.75	13.90	143.20	20.24

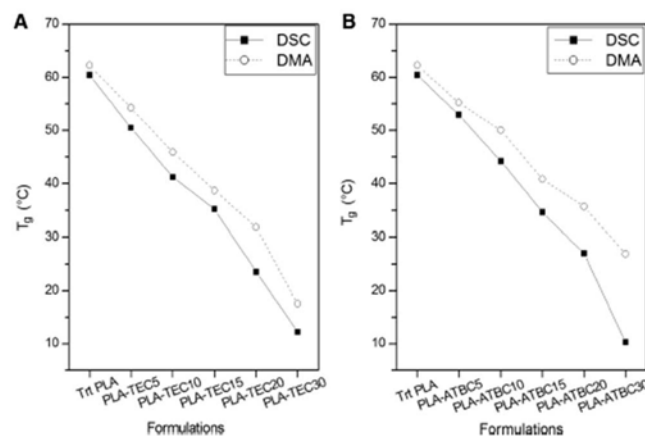


Figure 24: Influence of TEC (A) and ABTC (B) on glass transition temperatures of PLA based blends [46]

During last years, a new method of improving PLA toughness have been developed through addition of ionic liquids, which are molten salts achieving great attention because of their high thermal stability, low vapour pressure, recyclability and non-flammability; moreover, ionic liquids are considered as green solvents.

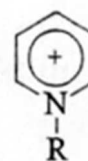
Ionic liquids are characterized by liquid in which the ions are slightly coordinated, reaching low melting points (below 100°C). Their structure is generally composed of organic cations and inorganic anions, influencing their properties. In fact, the low melting point is a direct consequence of organic cation asymmetry compared to inorganic part: in this way lattice energy is low, and so the melting point.

They are usually categorized into four different families on their cations:

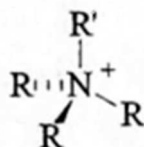
Imidazolium ion



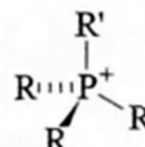
Pyridinium ion



Ammonium ion



Phosphonium ion



Chen et al. [47] studied the effect of four different ionic liquids on PLA based blends:

1-methyl-3-pentylimidazolium tetrafluoroborate ([MPI][BF₄]),

1-methyl-3-pentylimidazolium hexafluorophosphate ([MPI][PF₆]),

1-methyl-3-pentylimidazolium bis(trifluoromethanesulfonyl)imide ([MPI][TFSI]),

1,2-dimethyl-3-pentyl imidazolium bis(trifluoromethanesulfonyl)imide ([DMPI][TFSI])

Their main results are reported in Table 15, 17 and Figure 25.

Table 15: The effect of four different ionic liquids on PLA mechanical properties [adapted from 47]

Sample	Tensile strength (MPa)	Elongation at break (%)	Young's Modulus (GPa)
PLA	49.2 ± 2.6	2.5 ± 0.5	3.29 ± 0.16
PLA + 10% [MPI][BF4]	24.1 ± 1.1	26.9 ± 1.0	2.13 ± 0.23
PLA + 20% [MPI][BF4]	16.4 ± 1.6	32.8 ± 3.8	1.96 ± 0.03
PLA + 10% [MPI][BF4]	26.8 ± 1.5	29.7 ± 1.6	2.54 ± 0.16
PLA + 20% [MPI][BF4]	20.6 ± 1.3	61.6 ± 5.8	1.84 ± 0.03
PLA + 10% [MPI][TFSI]	30.9 ± 1.7	15.9 ± 1.8	1.92 ± 0.28
PLA + 20% [MPI][TFSI]	26.0 ± 1.3	28.9 ± 2.2	1.48 ± 0.06
PLA + 10% [DMPI][TFSI]	27.4 ± 1.4	16.1 ± 2.9	2.27 ± 0.04
PLA + 20% [DMPI][TFSI]	13.7 ± 1.6	34.1 ± 3.8	1.25 ± 0.08

Table 16: Effect of four different ionic liquids on PLA thermal properties [adapted from 47]

Sample	Decomposition temperature (°C)	Glass transition temperature (°C)	Melting peak (°C)
PLA	357	60.6	164.2
PLA + 10% [MPI][BF4]	364	62.8	174.1
PLA + 20% [MPI][BF4]	368	62.3	174.3
PLA + 10% [MPI][BF4]	366	63.6	174.6
PLA + 20% [MPI][BF4]	370	62.9	175.6
PLA + 10% [MPI][TFSI]	362	53.8	172.6
PLA + 20% [MPI][TFSI]	364	51.4	172.9
PLA + 10% [DMPI][TFSI]	363	59.6	173.8
PLA + 20% [DMPI][TFSI]	365	57.9	174.2

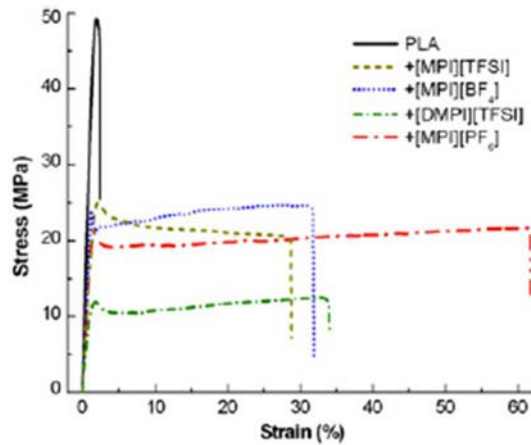


Figure 25: Stress-Strain curves of neat PLA and PLA modified with four different ionic liquids [47]

They demonstrated that ionic liquids can improve ductility of PLA, and slightly improve its thermal stability but with a considerable reduction in both tensile strength and modulus.

1.4.2 Soy Protein Isolate (SPI)

Among bio-derived polymers, Soy Protein Isolate (SPI) achieved great importance in eco-friendly materials, displaying good biocompatibility, biodegradability and compostability [48]. Many applications of SPI refer to food industry, but also drug delivery and packaging [49].

Soy protein, in general, is derived from decorticated and defatted soy, with a composition around 18-20% oil, 40-45% protein, 25-30% carbohydrates and 3% ashes [50-51].

Soy protein can be extracted from different products [52]:

- 1) Defatted Soy Flour (DSF) is the least expensive soy protein products, about 15 cent dollar/pound ¢/lb (5). In this case soy protein is decorticated and oil is removed, obtaining 56% protein and 34% carbohydrates flour.
- 2) Soy Protein Concentrate (SPC) is obtained post-leaching of water/alcohol soluble carbohydrates (about ¢ 50/lb). SPC is characterized by 65-75% of protein content and 18% of carbohydrates.
- 3) Soy Protein Isolate (SPI) is obtained by alkali extraction and acidification reprecipitation (about ¢ 130/lb). SPI is characterized by protein concentration higher than 90%, this is the main reason related to SPI development in materials science.

SPI is characterized by peptide bonds among amino acids, a covalent bond between carboxyl and amino groups of residues of adjacent amino acids (Figure 26).

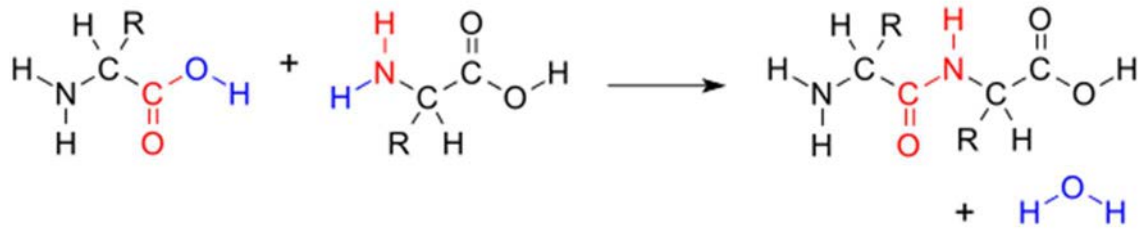


Figure 26: Formation of peptide bond between carboxyl and amino groups, with elimination of water.

SPI is composed of globulin proteins, mainly 7S (37%) and 11S (31%), characterized by polar and a-polar chains. Therefore, hydrogen bonds, dipole-dipole and hydrophobic interactions are displayed inter- and intra- chains [53] (Figure 27). Hydrogen bonds are electrostatic attractions between a hydrogen atom (which is covalently bounded to a high electronegative atom) and a close electronegative atom [54]. Hydrogen bonds, as a consequence, are weak bonds. Dipole-dipole interactions are interactions between two dipolar molecules: the partial negative part of a molecule is attracted by a partial positive part of another molecule. These interactions are weaker than covalent or ionic bonds. Hydrophobic interactions are displayed in proteins because of the presence of non-polar R groups that can be close to each other or separated by polar R-group. In this way, in aqueous environment inside the cell, hydrophobic amino acids are close to each other and try to exclude water. This is a weak interaction.

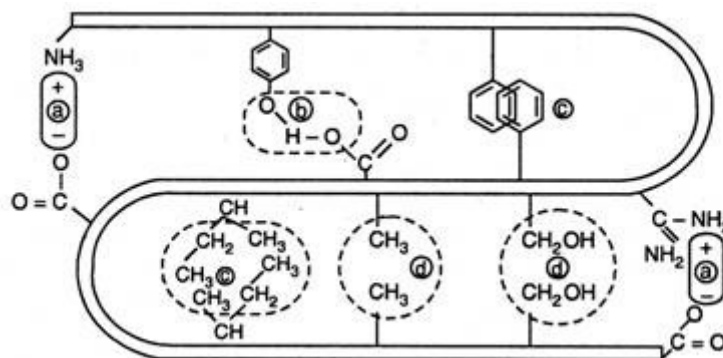


Figure 27: Typical protein interactions that stabilize protein structures. a) electrostatic interaction, b) hydrogen bonding, c) interaction of non-polar side chains d) Van der Waals interactions. [<http://www.biologydiscussion.com>, 18/07/2019]

SPI, in fact, is characterized by a complex network because of macromolecular interactions, requiring different steps in order to properly be processed:

1. Breaking of weak bonds between macromolecules;

2. Organization and orientation of macromolecules;
3. Formation of new interactions and bonds, stabilizing the final structure.

Normally, because of high molecular interactions, SPI cannot be directly melt processed. In fact, plasticizers are often added in SPI production, to obtain materials with good processability and properties [55]. The plasticizer is a little molecule with low volatility, which allows reducing macromolecules interactions by increasing their free volume and mobility [56]. The most used plasticizers are water, glycerol and sorbitol [57]. In literature, glycerol use for SPI plasticization is deeply studied, and frequently the optimal percentage of glycerol is around 30 wt.%.

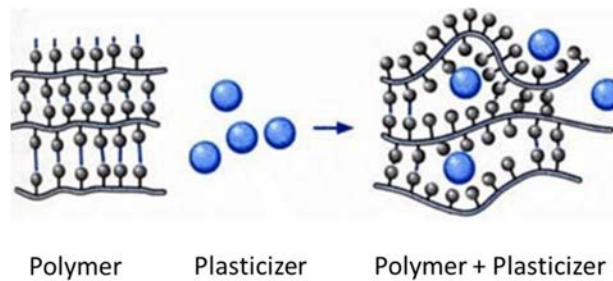


Figure 28: The role of plasticizer on polymer.

Kurose et al. [58] reported the effect of glycerol content on mechanical properties of SPI.

Glycerol content directly affected tensile strength, suggesting the typical behaviour of a plasticizer: the higher glycerol percent, the lower tensile strength. The elongation at break suggests the need to optimize glycerol content: at least 20% of glycerol content must be added in order to switch from brittle to ductile behaviour obtaining considerable elongation at break (120%) with 30% of glycerol (Figure 29), in coherence with other literature works. Interesting studies have been performed by Guerrero et al. [59], analysing the effect of both different production processes for SPI-based materials and glycerol amount. In particular, they analysed, through infrared spectroscopy and thermal analyses, SPI features processed by casting and compression moulding. The best balance of mechanical and technological properties has been obtained with 30-40 wt.% of glycerol (Figure 30).

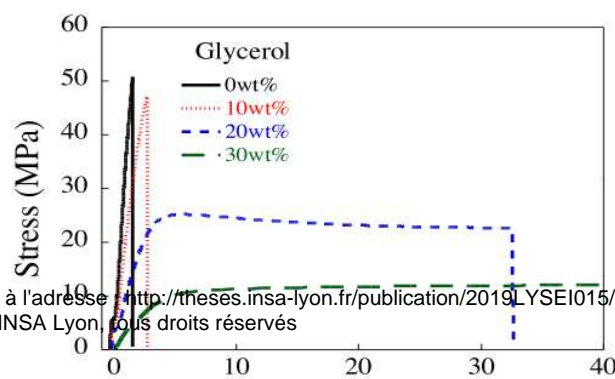




Figure 30: Different SPI films with 0-10-20-30-40 wt.% of Glycerol [59].

Mechanical results displayed a reduction in tensile strength and an improvement in elongation at break, in agreement with the plasticizer effect. In fact, glycerol reduces intermolecular interactions between protein chains, increasing macromolecular mobility.

Compression seemed to be the best process in order to obtain high elongation at break, keeping good tensile strength. Moreover, this is a conventional production process, used in many industries, requiring short time period to produce SPI films.

Production of SPI-based samples is usually based on processes characterized by dispersion or solubilization of SPI in solution, followed by evaporation of solvents [60]. Only limited attentions have been displayed on melt processes such as compression moulding, from powders, or extrusion [61]. Traditionally, extrusion represents one of the most widespread processing techniques for plastics. As a consequence, studies have been done in order to use these techniques for SPI-based blends [62]. The possibility to use extrusion for SPI materials allows increasing versatility of these products.

1.5 Thermoplastics blends

Polymer blending is an easy method in order to obtain polymers with modified properties and versatile applications. In fact, polymeric blends production was half of all plastic production in 2010 [63].

Different kinds of polymer blends exist, but, in this paragraph, we are going to discuss on thermoplastic blends, focusing on oil-based and bio-derived thermoplastic polymers.

Generally speaking, a polymer blend is a mixture of two or more different polymers. They can be miscible, partially miscible or immiscible, depending on free energy of mixture. As a consequence, the polymer in the lower amount goes to assume the geometric shape more thermodynamically stable, a sphere. In fact, considering the thermodynamic second law, in order to have miscible blends mix polymers, the variation of free energy has to be negative.

$$\Delta G = \Delta H - T\Delta S \quad (1)$$

where ΔG is the variation of free energy, ΔH is the variation of enthalpy, T is the temperature and ΔS is the entropy.

ΔH is negative just in case the affinity between polymers is higher than affinity of the polymer itself: thus ΔH is generally positive. ΔS is inversely proportional to polymerization degree, which for polymers is generally very high. As a consequence, the variation of free energy is generally positive, causing immiscible blends between polymers [64].

In order to predict the solubility between two polymers, the use of Flory and Huggins theory is often used. They studied this question in the early 1940, and proposed a model based on the following equation:

$$\chi_{AB} = \frac{V_{ref}(\delta_A - \delta_B)^2}{RT} \quad (2)$$

where χ_{AB} is the Flory-Huggins interaction parameter, V_{ref} is a reference volume, generally 100 cm³/mol, δ is the solubility parameter of the polymer, R is the gas constant and T the temperature. The higher is χ_{AB} , the lower is the miscibility between both polymers [65]. The solubility parameter was also deeply studied by Bicerano in his book "Prediction of polymer properties"[66] because of its importance for compatibility and permeation prediction, bulk and solution properties of polymers [67]. Hildebrand theories [68-69] provides definition of δ depending on energy of total evaporation

$$\delta = \frac{\sqrt{\Delta H_{vap}}}{V} \quad (4)$$

in which ΔH_{vap} is the energy of evaporation and V is the molar volume of the solvent. This δ expression is valid only for regular solutions (aliphatic and non-polar solvents). Hansen [70] extends δ proposing a multidimensional solubility parameter

$$\delta = \sqrt{\delta_D^2 + \delta_H^2 + \delta_P^2} \quad (5)$$

where δ_D refers to nonspecific intermolecular interactions related to dispersion forces, δ_H refers to specific intermolecular interactions such as hydrogen bonding, acid-base interaction ...) and δ_P refers to dipole-dipole forces.

One of the parameters that govern miscibility between polymers is the interfacial tension: the higher the interfacial tension, the higher the immiscibility between polymers [71].

Having high interfacial tension leads to particles formation, which could coalesce, decreasing mechanical properties. The general rule to achieve good blends is, like chemicals say, 'similar dissolves similar'. Polymers with similar polarity are easier to blend than polymers with different polarities. Other important features are:

- Specific group attractions: polymers with groups that could provide bonds or attraction between polymer chains are easier to blend.
- Molecular weight: polymers with low molecular weight are easier to mix, facilitating miscibility. As said before, polymers with similar molecular weight are more miscible.
- Ratio: the mutual amount of polymers affects the possibility of mixing. A low amount of polymer could be soluble in another polymer, while a high amount could not be.
- Crystallinity: generally, if polymers in a blend crystallize, they may form different crystalline phases, increasing the number of phases present in the molten state

During last decades, many studies have been conducted on fuel-based/bio-based thermoplastic blends, facing some important drawbacks [72], such as the incompatibility between different polymers, that can yield blends with poor properties. Generally, the compatibilization is

achieved through introduction of copolymers that have affinities for the polymers in the blend or with the use of nanoparticles. These ways of compatibilization are exposed below.

Because of their great importance and multitude of applications, PLA blends are deeply studied nowadays, in order to reduce PLA brittleness. Because of that, soft and tough polymers can be blended to PLA, improving their properties and their applications. At the same time, the production of biodegradable blends with traditional polyolefins is also possible.

Singh et al. [73] analysed linear low density polyethylene and PLLA blends in order to develop a film with good mechanical properties and biodegradability under specific conditions. Facing the problem of immiscible blends, they decided to introduce low-density polyethylene-graft-maleic anhydride as compatibilizer. Analysing different ratios of polymer amount and compatibilizer, they stated that 80 wt.% of LLPE, 20 wt.% of PLLA and 4 phr of compatibilizer was the best blend in terms of mechanical properties, thermal stability and biodegradability. An example of their results is given for thermal analysis in Figure 31.

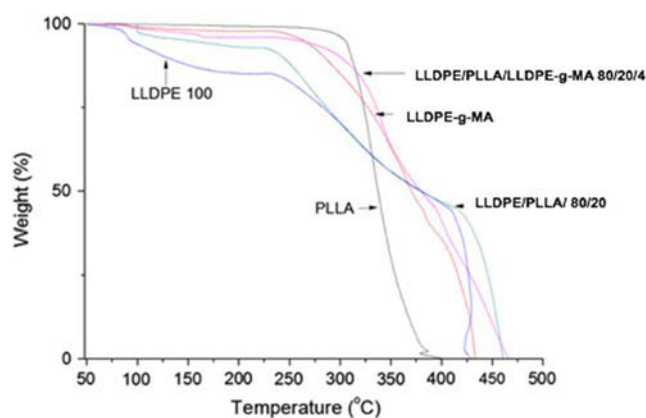


Figure 31: Thermal analysis results for low-density polyethylene/PLA blend with 4 phr of low-density polyethylene-graft-maleic anhydride [73]

Interesting studies for medical applications have been done by Polypetchara et al. [74] blending together different ratios of polypropylene and poly(lactic acid) with 3 wt.% of polypropylene-grafted-maleic anhydride as compatibilizer.

Important properties of water vapour permeability were observed: PLA increased water vapour permeability of the blend, indicating that PP biodegradability might be improved.

Another important compatibilizer, frequently used in polyolefin-PLA blend, is a random copolymer of polyolefin, such as ethylene, and glycidyl methacrylate. Kim et al. [75] prepared PLA-LLDPE blends through reactive compatibilization with random copolymer of ethylene and glycidyl methacrylate (PE-GMA). An evident effect of PE-GMA was displayed by SEM analysis, with a reduction of PLA domain size (Figure 32).

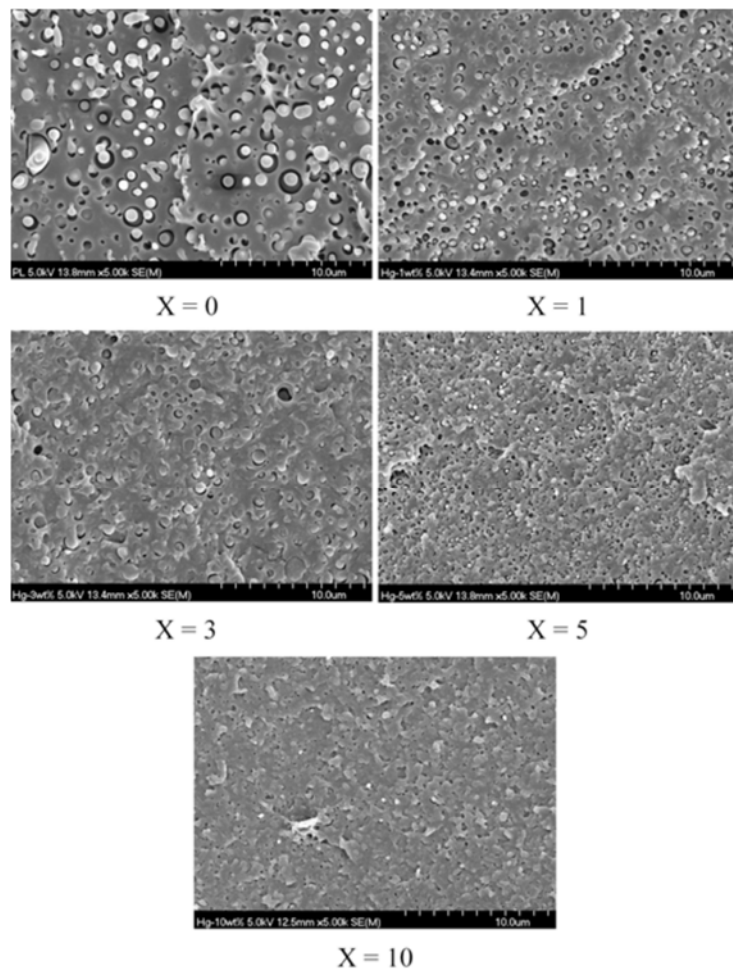


Figure 32: SEM micrographs of PLA80LDPE20 blends with different amounts of PE-GMA (0 to 10 wt.%) [75].

GMA presence in the compatibilizer allows a reaction, verified by H-NMR, with PLA, increasing compatibility between LDPE and PLA. In agreement with other literature results [76], the epoxide group in GMA can react with both carboxyl and hydroxyl groups located at the PLA chain ends during the process. Varying the amount of GMA in the compatibilizer influences the compatibility between LDPE and PLA. In fact, increasing GMA content facilitates the reaction with PLA, reducing the size of the dispersed phase. Otherwise, a higher GMA content makes harder the miscibility of PE-GMA with LDPE. An optimal amount of GMA must be chosen in

order to facilitate oil-based/bio-derived blend compatibility, keeping a good mixing between compatibilizer and polyolefin.

Ismail et al. [77] carried out interesting studies on LLDPE/Soy Protein Isolate (SPI) blends. Mechanical properties, such as tensile strength and elongation at break, decreased when increasing soy protein amount. In fact, despite the presence of some hydrophobic amino acids, SPI is characterized by hydrophilicity because of the presence of O-H groups on most amino acids. Conversely, LLDPE is composed of hydrophobic chains and the mix LLDPE/SPI resulted in the presence of two different phases. The addition of PE-g-MA as compatibilizer allowed an improved interfacial adhesion thanks to esterification reactions between O-H groups of SPI and anhydride group of MA. Higher elastic modulus and elongation at break (Figure 33) have been obtained, thanks to better interactions between LLDPE and SPI.

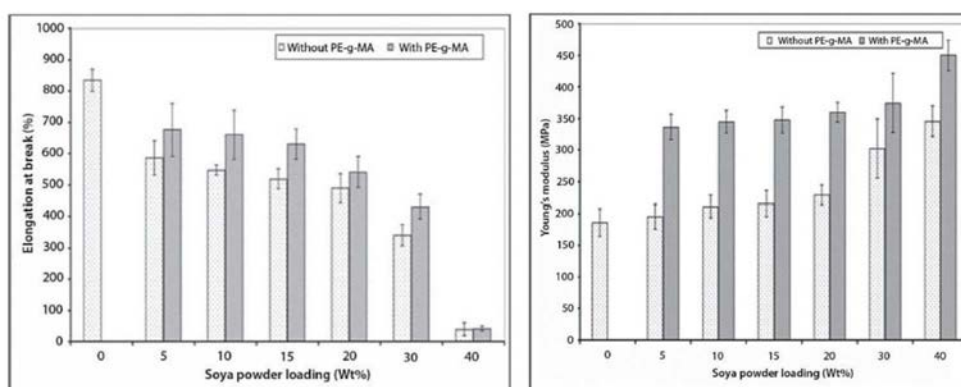


Figure 33: Effect on elongation at break and Young's modulus of PE-g-MA on LLDPE/SPI blends with different amounts of SPI [76].

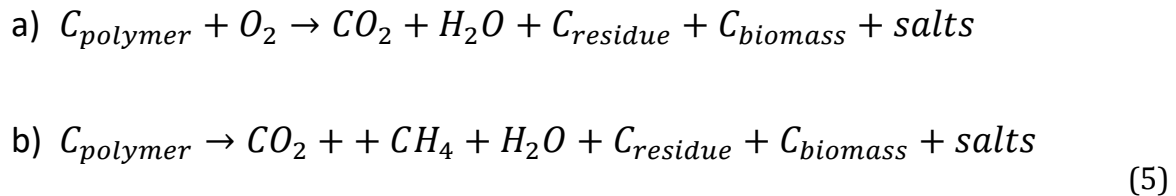
1.6 Biodegradability

As reported in the previous paragraph, the use oil-based/bio-derived blends is an effective way to reduce oil-based consumption, increasing, at the same time, bio-derived polymer properties. One of the main features of bio-derived polymers is their biodegradability. Many studies have been performed in order to analyse the biodegradability behaviour of blends composed of oil-based and bio-derived polymers.

Biodegradability can be evaluated through several standards, depending on the final application of the tested materials.

In general, biodegradation is a biological breakdown induced by aerobic or anaerobic bacteria. In particular, aerobic biodegradation mainly gives carbon dioxide as product, while anaerobic

biodegradation yields methane. The schemes a and b display the principle of aerobic and anaerobic biodegradation respectively.



Aerobic biodegradation (a) is characterized by two phases: firstly, a depolymerization occurs, reducing macromolecular chains lengths and increasing specific contact surface, secondly little oligomers can be assimilated by bacteria and microorganisms oxidizing these small molecules to obtain energy in cellular respiration.

Anaerobic biodegradation (b) is characterized by three main phases: firstly hydrolysis occurs, making available molecules for bacteria digestion, secondly acido and acetogenesis convert sugars and amino acids into CO₂, H₂, NH₃ and acetic acid. Finally, methanogenesis produces methane, CO₂ and water.

ASTM D6400-12 (Standard Specification for Labelling of Plastics Designed to be Aerobically Composted in Municipal or Industrial Facilities) provides more accurate definition of disintegration, biodegradation and compostability:

“

- Disintegration During Composting: A plastic product is considered to have demonstrated satisfactory disintegration if after twelve weeks (84 days) in a controlled composting test, no more than 10% of its original dry weight remains after sieving on a 2.0mm sieve. The test shall be carried out in accordance with ISO 1929 with a minimum vessel volume of 35L, or ISO 20200 under thermophilic aerobic composting conditions.
- Biodegradation: A plastic product must demonstrate a satisfactory rate of biodegradation by achieving the following ratio of conversion to carbon dioxide within 180 days using test method D5338, ISO 14855-1 or ISO 14855-2
 - Ninety percent (90%) of the organic carbon in the whole item or for each organic constituent, which is present in the material at a concentration of more than 1%

- (dry mass), shall be converted to carbon dioxide by the end of the test period when compared to the positive control or in the absolute.
- Organic constituents present at levels between 1 to 10% shall be tested individually for compliance to upper definition
 - Organic constituent which are present at concentration of less than 1% do not need to demonstrate biodegradability. However, the sum of such unproven constituents shall not exceed 5%.
 - Plastic product test samples shall not be subjected to conditions designed to accelerate biodegradation, prior to testing in biodegradation.
- Composting: a managed process that controls the biological decomposition and transformation of biodegradable materials into a humus-like substance called compost. The aerobic mesophilic and thermophilic degradation of organic matter yields compost through the transformation of biologically decomposable materials by controlled process of biooxidation. This latter proceeds through mesophilic or thermophilic phases and results in the production of carbon dioxide, water, minerals, and stabilized organic matter (compost or humus).”

Macroscopically, biodegradation appears as yellowing, fragmentation and breakage, as visible in Figure 34, in which biodegradation of a PLA film is displayed.



Figure 34: PLA macroscopical effects of soil burial testing (yellowing, breakage and fragmentation) [78]

Another qualitative method to evaluate bacteria attack on polymer surface is described by Massardier et al. [79]. ASTM G 21-90 and ASTM G 22-76 have been used to analyse material resistance to bacteria and fungi growth. Different materials were tested: Polyethylene, Eastar bio (poly(butadiene adipate-co-terephthalate), Mater-Bi (blend composed of starch and polycaprolactone), Polycaprolactone and Polylactic acid. Films were placed in Petri dishes with a mineral medium and microbial inoculum. Samples were incubated in a climatic chamber at 30°C and 90% relative humidity for 28 days. As visible from Figure 35, Polycaprolactone and Eastar bio displayed a sensitive colonization, making impossible sample extraction for further

analysis. Mater-Bi was also colonised, anyway allowing sample recovery for analyses. On the contrary, Polylactic acid did not display significant modification.

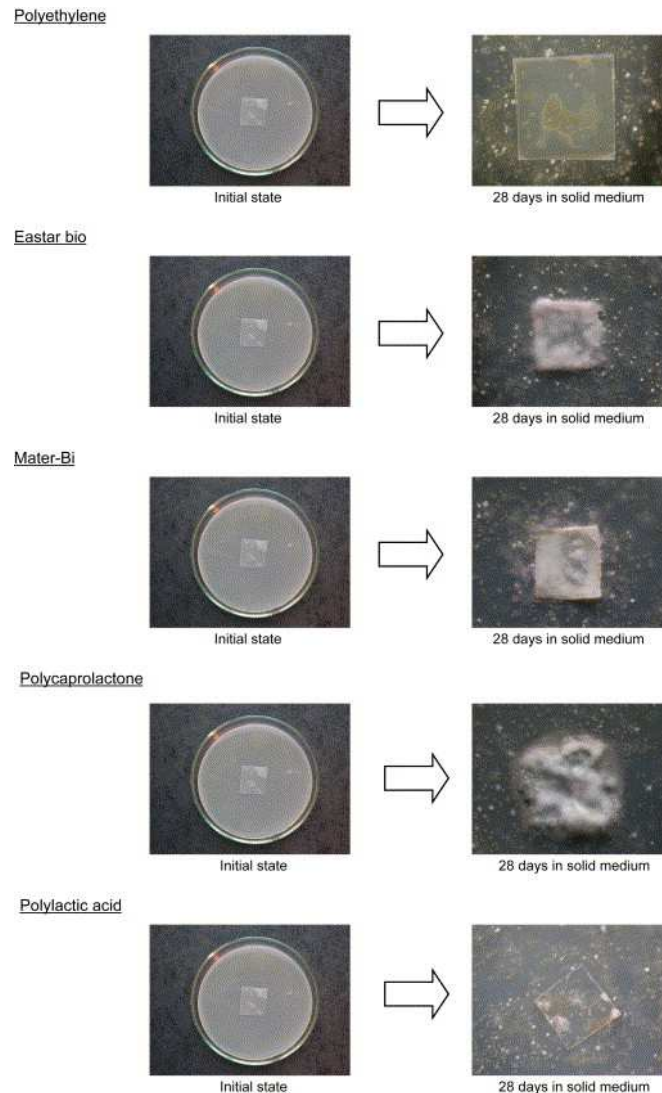


Figure 35: Evolution of different polymers after 28 days of incubation in solid medium [79].

Macroscopic effects of biodegradation are a useful tool in order to observe polymer degradation, although the only recommended and valuable test to detect biodegradation process is to analyse biodegradation products.

Several organizations, such as International Organization for Standardization ISO, American Society for Testing Materials ASTM, European Committee for Standardization CEN, provide standards to carry out biodegradation procedures in aerobic or anaerobic conditions.

Several studies have been performed in order to evaluate biodegradability behaviour of bio-derived polymers and composites, or to verify the effect of pro-oxidant on oil-based polymers. The purpose of this work is to evaluate the effect of oil-based polymers and natural fillers on biodegradability of bio-derived polymers.

In 1993 Sinclair et al. already [80] patented blends of polylactic acids with traditional oil-based polymers, aiming to produce blends with environmentally degradable features. They obtained partially degradable compositions, in which PLA rapidly decomposed compared to stable traditional polymers. The interesting aspect is the higher rapidity of degradation of these blends in comparison to conventional non-degradable plastics because of two simultaneous aspects: firstly, PLA degradation, secondly this degradation allows the formation of high specific surface area that is expected to accelerate the process.

More recently, other studies have been carried out in order to evaluate biodegradable influence of oil-based polymer processed with bio-derived polymers.

As'habi et al. [81] evaluated the influence of clays incorporated to PLA/LLDPE blends. In particular, despite the addition of a sensitive amount of LLDPE (25wt.%), their blends completely degrade in composting conditions after four months. They studied biodegradation of their samples in a homemade compost at 58°C for 5 months, recovering samples each week. Moreover, a catalytic effect of nanoclays on the biodegradation or hydrolytic degradation of PLA was displayed, thanks to the presence of terminal hydroxylated edge groups of the silicate layer. The degree of biodegradation was evaluated with both residual weight measurements and with CO₂ evolution (Figure 36).

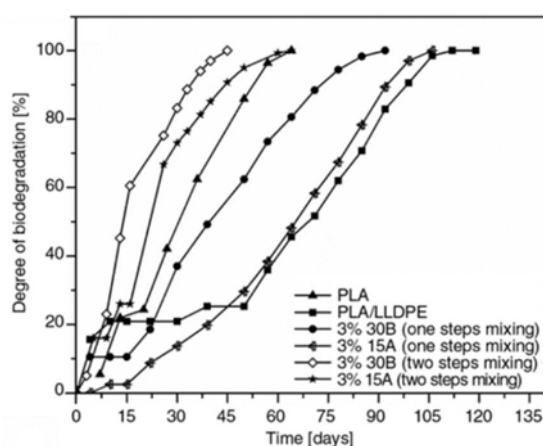


Figure 36: Degree of biodegradation (%) for pure PLA, PLA/LLDPE blend, PLA/LLDPE blends with nanoclay (Cloisite® 30B (30B), MMT-Na⁺ modified with bis-(2-hydroxyethyl) methyl tallow alkaly ammonium cations and Cloisite® 15A (15A), MMT-

Na⁺ modified with dimethyl, dehydrogenated tallow, quaternary ammonium cations) processed with one step or two steps mixing [81].

Typical two steps degradation behaviour of pure PLA was displayed, as a result of a first hydrolytic step and a second conversion of oligomers by microorganisms. PLA/LLDPE blend displayed a tendency very close to pure PLA, while the addition of clays sensibly reduces the time to obtain a complete degradation of the blend.

Medjdoub et al. [82], in agreement with results obtained from As'habi work, evaluated viscoelastic, thermal and environmental characteristics of a ternary blend composed of PLA, LLDPE and LDPE compatibilized with 5wt.% maleic anhydride grafted low density polyethylene (PE-g-MA). They produced a 50/50 PLA/LLDPE-LDPE blend, obtaining an intermediate biodegradation behaviour between pure PLA and pure LLDPE-LDPE. Compatibility problems between hydrophilic polymer (PLA) and hydrophobic polymer (LLDPE-LDPE) seem to be a positive aspect considering biodegradability as poor adhesion between two phases allow an easier access of microorganisms to polymer chains through pores and voids. Moreover, they evaluated the effect of 5wt.% of organophilic montmorillonite (Org-MMT), validating a catalytic effect of Org-MMT because of the presence of hydroxylated edge groups.

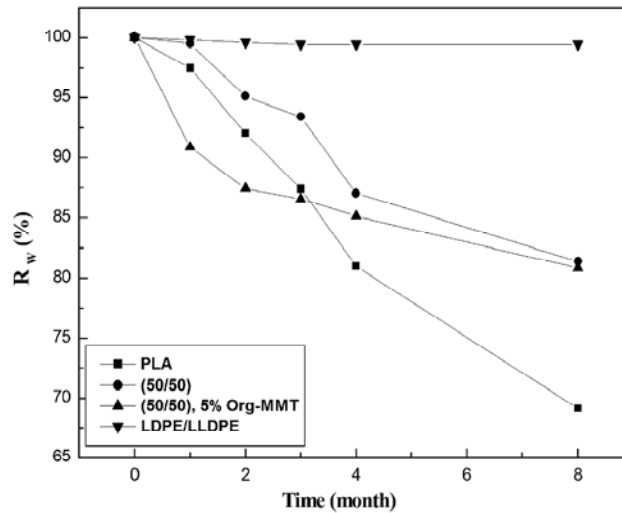


Figure 37: Time-dependence of residual weight R_w (%) for pure PLA, pure LLDPE-LDPE, PLA/(LLDPE-LDPE) 50/50 with and without 5% Organophilic montmorillonite (Org-MMT) [82].

Singh et al. [83] also evaluated the degradability of LLDPE blended with PLLA under composting conditions. Their experience suggest that PLLA addition to LLDPE allow a degradation of the blend around 12%, while compatibilizer addition in 4wt.% amount strongly reduces blend degradation. Moreover, in agreement with other studies, degradation firstly occurs in amorphous phase. In fact, DSC analyses display an increased crystallinity after burial composting.

Table 17: DSC results before and after composting for LLDPE, LLDPE 80wt.% and PLLA 20wt.%, and blend compatibilized with 4wt.% of low density polyethylene-graft-maleic anhydride [83].

Sample	ΔH (J/g)	
	Before Composting	After Composting
LLDPE100	61.63	62.30
LLDPE80	52.07	65.33
M-g-L 80/4	61.78	63.07

We analysed, in our study, the influence of natural fillers (such as wood flour and recycled waste paper fibres) on both PLA and HDPE degradation after three months buried in soil. Moreover, the end-of-life of a wood flour and recycled waste paper fibres mixed fillers in HDPE-PLA blend

matrix has been tested. Degradation of lignocellulosic fibres has attracted many interests during last years, in agreement with the increased environmental consciousness. Lignocellulosic fibres are characterized by a chemical composition influenced by genetic and environmental factors. In general, lignocellulosic fibres are mainly composed of three constituents [84-85]:

- Cellulose: linear macromolecules of glucose units. Hydroxyl groups can form hydrogen bonds giving rigidity and crystallinity to the structure. The higher the amount of cellulose, the higher the hydrophilicity of the fibres. Generally, around 50% of lignocellulosic fibres are composed of cellulose.
- Hemicellulose: composed of several polysaccharides. Hemicellulose is bounded to cellulose and lignin in the cell wall. Generally, around 30% of lignocellulosic fibres are composed of hemicellulose.
- Lignin: irregular and insoluble polymer, composed of aromatic units characterized by highly networked structures. No repeated subunits are present in lignin, making degradation more difficult. Generally, around 20% of lignocellulosic fibres are made of lignin.

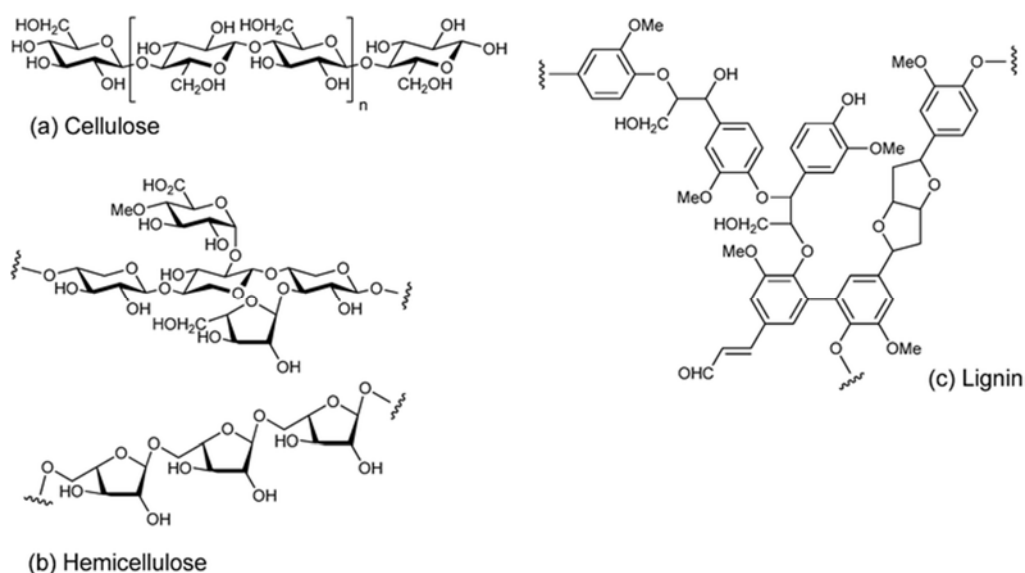


Figure 38: Chemical structure of the main constituents of natural fibres (cellulose, hemicellulose and lignin).

Chemical structure of lignocellulosic fibres directly affects not just mechanical properties, but also biodegradability. In fact, each constituent of lignocellulosic fibres can be more or less

susceptible to enzymatic hydrolysis, depending on the particular chemical structure [86]. Generally speaking, biological degradation occurs firstly for hemicellulose, then amorphous cellulose and lately for crystalline cellulose [87]. In fact, packed structures are less accessible for microorganisms, preventing macromolecules degradation. Biodegradation occurs through breakage of β 1,4-xylan bonds of hemicellulose by xylanase, β 1,4 glycosidic bonds of cellulose by cellulase and lignin biodegradation thanks to lignolytic fungi actions. The evaluation of single components degradation is difficult to isolate, because of interconnected structure (Figure 39).

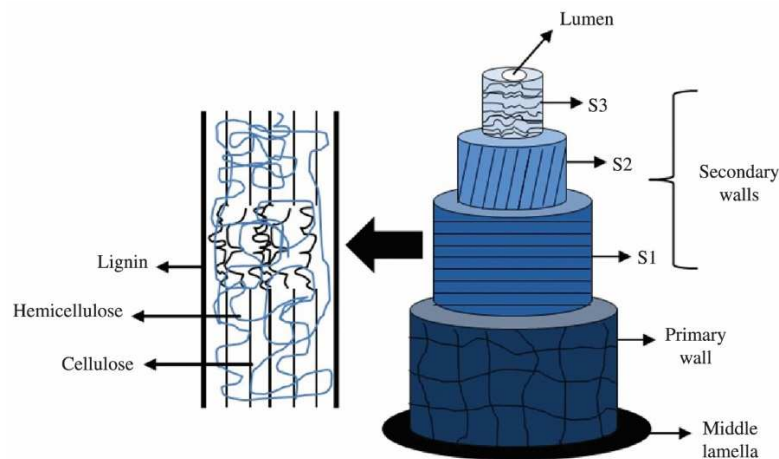


Figure 39: Hierarchical structure of lignocellulosic fibres [88].

Lignocellulosic fibres are characterized by a hierarchical structure composed of middle lamella, primary wall, secondary wall (S1, S2 and S3) and a central void lumen. Cells of primary and secondary walls are composed of cellulose, hemicellulose and lignin. Biodegradability of these fibres is severely dependent of their composition.

1.6.1 Conclusion

The importance achieved by thermoplastic polymers during last decades is undoubted. Unfortunately, thermoplastics diffusion did not correspond to an equal attention into end-of-life scenarios of these products. The consequence of this was an important pollution issue, significant on both earth and sea environment. In this context, two strategies appear particularly suitable to be pursued: diffusion of bio-derived polymers and production of composites with natural fillers. Polylactic acid (PLA) is one of the most diffused bio-derived polymers on market, thanks to its properties such as tensile strength, tensile modulus and flexural strength, comparable or higher than other traditional polyolefins. The main drawback of PLA is its high brittleness and limited toughness. Many solutions have been suggested, such

as the introduction of plasticizers e.g., glycerol, oligomeric lactic acid, poly (ethylene glycol) and citrates. These plasticizers are used in order to increase intermolecular space between polymer chains, thanks to the introduction of small molecules, a procedure that results in their increased plasticity and resistance to shear. Another strategy adopted in order to reduce PLA brittleness is producing blends with other thermoplastic polymers. During last decades, the production of polymer blends was recognised to play an important role in global markets as an easy method to tailor polymer properties for physical and mechanical requirements. However, an effective mutual compatibility between polymers is necessary to obtain blends with higher properties than the original polymers. The development of an oil-based/bio-derived thermoplastic blend is therefore the preliminary requirement of this work.

The second method, suggested to reduce plastic pollution, could be the development of thermoplastic matrix composites with natural fillers. Natural fillers gained great attention thanks to their appealing properties such as low density, low cost, renewability, recyclability and biodegradability. Among natural fillers, such as jute, flax, sisal, paper cellulose fibres, wood flour exhibits interesting properties as waste material used for composites production, obtaining the well-known class of material Wood Plastic Composites (WPC). It is widely recognised that a major issue with these composites is the poor miscibility between hydrophobic polyolefins and hydrophilic natural fillers. Many efforts have been done in order to face this problem and the use of compatibilizers is one of the most diffuse.

In agreement with plastic pollution, the evaluation of degradation of blends and composites with high amount of bio-derived charge seems to be interesting. Degradation of lignocellulosic fibres and composites filled with these fibres has attracted many interests during last years. Lignocellulosic fibres are characterized by a chemical composition influenced by genetic and environmental factors [89]. In general, lignocellulosic fibres are mainly composed of cellulose (linear macromolecules of glucose units, the higher the amount of cellulose, the higher the hydrophilicity of the fibres), hemicellulose (composed of several polysaccharides) and lignin (irregular and insoluble polymer, composed of aromatic units characterized by highly networked structures). Chemical structure of lignocellulosic fibres directly affects not just mechanical properties, but also biodegradability. In fact, each constituent of lignocellulosic fibres can be more or less susceptible to enzymatic hydrolysis, depending on the particular

chemical structure. As a consequence, the analyses of the degradation behaviour under composting conditions seem to be interesting for our samples.

1.6.2 References

- 1 R. Malkapuram, V. Kumar, and Y. S. Negi, "Recent Development in Natural Fibre," *J. Reinf. Plast.*, 2009.
- 2 P. Wambua, J. Ivens, and I. Verpoest, "Natural fibres: Can they replace glass in fibre reinforced plastics?," *Compos. Sci. Technol.*, vol. 63, no. 9, pp. 1259–1264, 2003.
- 3 H. Ku, H. Wang, N. Pattarachaiyakoop, and M. Trada, "A review on the tensile properties of natural fibre reinforced polymer composites," *Compos. Part B Eng.*, vol. 42, no. 4, pp. 856–873, 2011.
- 4 B. Suddell, "Industrial fibres: recent and current developments," *Symp. Nat. Fibres*, vol. 44, no. 0, pp. 71–82, 2008.
- 5 A. Ashori, "Wood-plastic composites as promising green-composites for automotive industries!," *Bioresour. Technol.*, vol. 99, no. 11, pp. 4661–4667, 2008.
- 6 D. N. Saheb, J. P. Jog, and others, "Natural fibre polymer composites: a review," *Adv. Polym. Technol.*, vol. 18, no. 4, pp. 351–363, 1999.
- 7 V. Mazzanti, F. Mollica, and N. El Kissi, "Rheological and Mechanical Characterization of Polypropylene-Based Wood Plastic Composites," *Wiley Online Libr.*, 2015.
- 8 A. L. Catto, B. V. Stefani, V. F. Ribeiro, R. Marlene, and C. Santana, "Influence of Coupling Agent in Compatibility of Post-consumer HDPE in Thermoplastic Composites Reinforced with Eucalyptus Fibre," *Mater. Res.*, vol. 17, no. 1, pp. 203–209, 2014.
- 9 Y. Lei, Q. Wu, F. Yao, and Y. Xu, "Preparation and properties of recycled HDPE/natural fibre composites," *Compos. Part A Appl. Sci. Manuf.*, vol. 38, no. 7, pp. 1664–1674, 2007.
- 10 T. J. Keener, R. K. Stuart, and T. K. Brown, "Maleated coupling agents for natural fibre composites," *Compos. Part A Appl. Sci. Manuf.*, vol. 35, no. 3, pp. 357–362, 2004.
- 11 J. R. Araùjo, W. R. Waldman, and M. A. De Paoli, "Thermal properties of high density polyethylene composites with natural fibres: Coupling agent effect," *Polym. Degrad. Stab.*, vol. 93, no. 10, pp. 1770–1775, 2008.
- 12 M. M. Kabir, H. Wang, K. T. Lau, and F. Cardona, "Chemical treatments on plant-based natural fibre reinforced polymer composites: An overview," *Compos. Part B Eng.*, vol. 43, no. 7, pp. 2883–2892, 2012.
- 13 X. Li, L. G. Tabil, and S. Panigrahi, "Chemical Treatments of Natural Fibre for Use in Natural Fibre-Reinforced Composites: A Review," *J. Polym. Environ.*, vol. 15, no. 1, pp. 25–33, 2007.

- 14 G. Pritchard, "Two technologies merge: wood plastic composites Geoff Pritchard describes how wood and resin are being," *Plast. Addit. Compd.*, vol. 48, no. 6, pp. 18–21, 2004.
- 15 N. M. Stark and L. M. Matuana, "Characterization of weathered wood-plastic composite surfaces using FTIR spectroscopy, contact angle, and XPS," *Polym. Degrad. Stab.*, vol. 92, no. 10, pp. 1883–1890, 2007.
- 16 M. P. Wolcott, "Wood-Plastic Composites," in *Encyclopedia of Materials - Science and Technology*, 2001, pp. 9759–9763.
- 17 C. Clemons, "Wood-Plastic Composites in the United States: the interfacing of two industries," *For. Prod. J.*, vol. 52, no. 6, pp. 10–18, 2002.
- 18 M. Hietala, J. Niinimäki, and K. Oksman, "Processing of wood chip–plastic composites: effect on wood particle size, microstructure and mechanical properties," *Plast. Rubber Compos.*, vol. 40, no. 2, pp. 49–56, 2011.
- 19 A. R. Sanadi and D. Caulfield, "Thermoplastic polyolefins as formaldehyde free binders in highly filled lignocellulosic panel boards: using glycerine as a processing aid in kenaf fibre polypropylene boards," *Mater. Res.*, vol. 11, no. 4, pp. 487–492, Dec. 2008.
- 20 M. Valente, J. Tirillò, A. Quitadamo, and C. Santulli, "Paper fibre filled polymer. Mechanical evaluation and interfaces modification," *Compos. Part B Eng.*, 2016.
- 21 M. Kazayawoko, J. J. Balatinecz, and L. M. Matuana, "Surface modification and adhesion mechanisms in woodfibre-polypropylene composites," *J. Mater. Sci.*, vol. 34, no. 24, pp. 6189–6199, 1999.
- 22 N. Sombatsompop, C. Yotinwattanakumtorn, and C. Thongpin, "Influence of type and concentration of maleic anhydride grafted polypropylene and impact modifiers on mechanical properties of PP/wood sawdust composites," *J. Appl. Polym. Sci.*, vol. 97, no. 2, pp. 475–484, 2005.
- 23 S. M. B. Nachtigall, G. S. Cerveira, and S. M. L. Rosa, "New polymeric-coupling agent for polypropylene/wood-flour composites," *Polym. Test.*, vol. 26, no. 5, pp. 619–628, Aug. 2007.
- 24 H. S. Kim, B. H. Lee, S. W. Choi, S. Kim, and H. J. Kim, "The effect of types of maleic anhydride-grafted polypropylene (MAPP) on the interfacial adhesion properties of bio-flour-filled polypropylene composites," *Compos. Part A Appl. Sci. Manuf.*, vol. 38, no. 6, pp. 1473–1482, 2007.
- 25 S. E. Selke and I. Wichman, "Wood fibre/polyolefin composites," *Compos. Part A Appl. Sci. Manuf.*, vol. 35, no. 3, pp. 321–326, 2004.
- 26 M. Tazi, F. Erchiqui, F. Godard, H. Kaddami, and A. Ajji, "Characterization of rheological and thermophysical properties of HDPE-wood composite," *J. Appl. Polym. Sci.*, vol. 131, no. 13, pp. 1–11, 2014.
- 27 S. Pilla, S. Gong, E. O'Neil, L. Yang and R. M. Rowell, "Polylactide-recycled wood fibre composites", *Journal of App. Polymer and Science*, vol. 111, pp. 37-47, 2009

- 28 P. Zierdt, T. Theumer, G. Kulkarni, V. Daumlich, J. Klehm, U. Hirsch, A. Weber, "Sustainable wood-plastic composites from bio-based polyamide 11 and chemically modified beech fibres", *Sustainable Materials and Technologies*, vol 6, pp. 6-14, 2015
- 29 M. S. Huda, A. K. Mohanty, L. T. Drzal, E. Schut, M. Misra, "'Green' composites from recycled cellulose and poly(lactic acid): Physico-mechanical and morphological properties evaluation", *Journal of Materials Science*, vol. 40, pp. 4221-4229, 2005
- 30 E. Pulp, "Key Statistics," 2012.
- 31 M. C. Flemings, B. Ilschner, E. J. Kramer, and S. Mahajan, "Paper: Recycling and Recycled Materials," *Encyclopedia of Materials - Science and Technology*, vol. 6, no. 3. pp. 6711-6720, 2001.
- 32 a. R. Sanadi, R. a. Young, C. Clemons, and R. M. Rowell, "Recycled Newspaper Fibres as Reinforcing Fillers in Thermoplastics: Part I-Analysis of Tensile and Impact Properties in Polypropylene," *J. Reinf. Plast. Compos.*, vol. 13, no. 1, pp. 54-67, 1994.
- 33 I. Baroulaki, O. Karakasi, G. Pappa, P. A. Tarantili, D. Economides, and K. Magoulas, "Preparation and study of plastic compounds containing polyolefins and post used newspaper fibres," *Compos. Part A Appl. Sci. Manuf.*, vol. 37, no. 10, pp. 1613-1625, 2006.
- 34 M. Prambauer, C. Paulik, and C. Burgstaller, "The influence of paper type on the properties of structural paper - Polypropylene composites," *Compos. Part A Appl. Sci. Manuf.*, vol. 74, pp. 107-113, 2015.
- 35 A. Serrano, F. X. Espinach, F. Julian, R. Del Rey, J. A. Mendez, and P. Mutje, "Estimation of the interfacial shears strength, orientation factor and mean equivalent intrinsic tensile strength in old newspaper fibre/polypropylene composites," *Compos. Part B Eng.*, vol. 50, pp. 232-238, 2013.
- 36 E. Franco-Marquès, J. A. Méndez, M. A. Pèlach, F. Vilaseca, J. Bayer, and P. Mutjé, "Influence of coupling agents in the preparation of polypropylene composites reinforced with recycled fibres," *Chem. Eng. J.*, vol. 166, no. 3, pp. 1170-1178, 2011.
- 37 A. Serrano, F. X. Espinach, J. Tresserras, R. del Rey, N. Pellicer, and P. Mutje, "Macro and micromechanics analysis of short fibre composites stiffness: The case of old newspaper fibres-polypropylene composites," *Mater. Des.*, vol. 55, pp. 319-324, 2014.
- 38 S. A. Balwaik and S. P. Raut, "Utilization of Waste Paper Pulp by Partial Replacement of Cement in Concrete," *Int. J. Eng. Res. Appl.*, vol. 1, no. 2, pp. 300-309, 2011.
- 39 T. Kuokkanen, H. Nurmesniemi, R. Pöykiö, K. Kujala, J. Kaakinen, and M. Kuokkanen, "Chemical and leaching properties of paper mill sludge," *Chem. Speciat. Bioavailab.*, vol. 20, no. 2, pp. 111-122, 2008.
- 40 Y. Hamzeh, A. Ashori, and B. Mirzaei, "Effects of Waste Paper Sludge on the Physico-Mechanical Properties of High Density Polyethylene/Wood Flour Composites," *J. Polym. Environ.*, vol. 19, no. 1, pp. 120-124, 2011.
- 41 J. Son, "Physico-mechanical Properties of Paper Sludge-Thermoplastic Polymer Composites," *J. Thermoplast. Compos. Mater.*, vol. 17, no. 6, pp. 509-522, 2004.

- 42 W. Carothers, G. . Dorough, and F. J. Van Natta, "Studies of Polymerization and ring formation. X. The reversible polymerization of six-membered cyclic esters," *J. Am. Chem. Soc.*, vol. 54, pp. 761–772, 1932.
- 43 K. Hamad, M. Kaseem, H. W. Yang, F. Deri, and Y. G. Ko, "Properties and medical applications of polylactic acid: A review," *Express Polym. Lett.*, vol. 9, no. 5, pp. 435–455, 2015.
- 44 M. Baiardo, G. Frisoni, M. Scandola, M. Rimelen, D. Lips, K. Ruffieux, and E. Wintermantel, "Thermal and Mechanical Properties of Plasticized Poly(L-lactic acid)," *J Appl Polym Sci*, vol. 90, pp. 1731–1738, 2003.
- 45 O. Martin and L. Avérous, "Poly(lactic acid): Plasticization and properties of biodegradable multiphase systems," *Polymer (Guildf)*, vol. 42, no. 14, pp. 6209–6219, 2001.
- 46 M. Maiza, M. T. Benaniba, and V. Massardier-Nageotte, "Plasticizing effects of citrate esters on properties of poly(lactic acid)," *J. Polym. Eng.*, vol. 36, no. 4, pp. 371–380, 2016.
- 47 B. K. Chen, T. Y. Wu, Y. M. Chang, and A. F. Chen, "Ductile polylactic acid prepared with ionic liquids," *Chem. Eng. J.*, vol. 215–216, pp. 886–893, 2013.
- 48 H. Tian, Y. Wang, L. Zhang, C. Quan, X. Zhang, "Improved flexibility and water resistance of soy protein thermoplastics containing waterborne polyurethane", *Ind. Crops and Prod.*, vol. 32, pp. 13-20, 2010.
- 49 Y. Han, K. Li, H. Chen, J. Li, "Properties of Soy Protein Isolate Biopolymer Film Modified by Graphene", *Polymers*, vol. 9, 312-323.
- 50 J.T. Kim and A.N. Netravali, "Soy and starch-based resins", in *Sustainable Composites: Fibres, Resins and Applications*, Ed. By A.N. Netravali and C.M. Pastore, DEStech Publication Inc. 2015.
- 51 K.M. Deepmala Chhavi, V.K. Singh, S. Chauhan, N. Jain, "Soy Protein Based Green Composites: A Review.", *J. Mat. Sci.*, vol. 5(2),
- 52 S.N. Swain, S.M. Biswal, P.K. Nanda, P.L. Nayak, "Biodegradable soy-based plastics: Opportunities and Challenges", *J. Poly. Env.*, vol 12(1), pp. 35-42, 2004.
- 53 P. Lodha, A. N. Netravali, "Thermal and mechanical properties of environment-friendly 'green' plastics from stearic acid modified-soy protein isolate", *Ind. Crops and Prod.*, vol. 21, pp. 49-64, 2005.
- 54 S. Scheiner, "Weak H-bonds. Comparisons of CH...O to NH...O in proteins and PH...N to direct P...N interactions" *Physical Chem Phys*, 31, 2011
- 55 M. Bozic, M. Majeric, M. Denac, V. Kokol, "Mechanical and barrier properties of soy protein isolate films plasticized with a mixture of glycerol and dendritic Polyglycerol", *J. App. Poly. Sci.*, vol. 132 (17), 2015.
- 56 M.G. Adeodato Vieira, M. Altenhofen da Silva, L. Oliveirados Santos, M. M. Beppu, "Natural-based plasticizers and biopolymer films: A review", *Eur. Poly. J.*, vol. 47(3), pp. 254-263,

2011.

- 57 C.J.R. Verbeek, L.E. Van Den Berg, "Extrusion Processing and Properties of Protein-Based Thermoplastics", *Macromol. J.*, vol. 295, pp.10-21, 2010.
- 58 T. Kurose, K. Urman, J. U. Otaigbe, R. Y. Lochhead, and S. F. Thames, "Effect of Uniaxial Drawing of Soy Protein Isolate Biopolymer Film on Structure and Mechanical Properties," *Polym. Eng. Sci.*, 2007.
- 59 P. Guerrero, A. Retegi, N. Gabilondo, K. De la Caba, "Mechanical and thermal properties of soy protein films processed by casting and compression", *J. Food Eng.*, vol. 100, pp.145-151, 2010.
- 60 V.M. Hernandez-Izquierdo, J.M. Krochta, "Thermoplastic Processing of Proteins for Film Formation- A review", *J. Food Sci.*, vol. 73 (2), pp. R30-R39, 2008.
- 61 P. Cunningham, A.A. Ogale, P.L. Dawson, J.C. Acton, "Tensile properties of Soy Protein Isolate films produced by a thermal compaction technique, *J Food Sci*, vol. 65 (4), pp. 668-671, 2000.
- 62 J.R.C. Verbeek, L.E. Van den Berg, "Extrusion Processing and Properties of Protein-based Thermoplastics", *Macromol Mater Eng*, vol. 295, pp. 10-21, 2010.
- 63 J. Parameswaranpillai, S. Thomas, and Y. Grohens, "Polymer Blends : State of the Art , New Challenges , and Opportunities," pp. 1–6, 2015.
- 64 J. S. Higgins, J. E. G. Lipson, and R. P. White, "A simple approach to polymer mixture miscibility.," *Philos. Trans. A. Math. Phys. Eng. Sci.*, vol. 368, no. 1914, pp. 1009–25, 2010.
- 65 B. A. Miller-Chou and J. L. Koenig, "A review of polymer dissolution," *Prog. Polym. Sci.*, vol. 28, no. 8, pp. 1223–1270, 2003.
- 66 J. Bicerano, *Prediction of polymer properties*. New York, 2009.
- 67 X. Chen, C. Yuan, C. K. Y. Wong, and G. Zhang, "Molecular modeling of temperature dependence of solubility parameters for amorphous polymers," *J. Mol. Model.*, vol. 18, no. 6, pp. 2333–2341, 2012.
- 68 J. H. Hildebrand, "Solubility," *J. Am. Chem. Soc.*, vol. 5, no. 1898, 1916.
- 69 J. H. Hildebrand, "Solubility. III. relative values of internal pressures and their practical application.," *J. Am. Chem. Soc.*, vol. 38, pp. 1067–1080, 1919.
- 70 C. M. Hansen, *Hansen solubility parameters, a user's handbook*, Second. New York, 2007.
- 71 L. a. Utracki, "Compatibilization of polymer blends," *Can. J. Chem. Eng.*, vol. 80, no. 6, pp. 1008–1016, 2002.
- 72 J. Hopewell, R. Dvorak, E. Kosior, "Plastics recycling: challenges and opportunities", *Phil. Trans. R. Soc. B*, vol. 364, pp. 2115–2126, 2009
- 73 G. Singh, H. Bhunia, A. Rajor, and V. Choudhary, "Thermal properties and degradation characteristics of polylactide, linear low density polyethylene, and their blends," *Polym. Bull.*, vol. 66, no. 7, pp. 939–953, 2011.

- 74 N. Ploypetchara, P. Suppakul, D. Atong, and C. Pechyen, "Blend of polypropylene/poly(lactic acid) for medical packaging application: Physicochemical, thermal, mechanical, and barrier properties," *Energy Procedia*, vol. 56, no. C, pp. 201–210, 2014.
- 75 Y.F. Kim, C.N. Choi, Y.D. Kim, K.Y.L, M.S. Lee, "Compatibilization of Immiscible Poly(l-lactide) and Low Density Polyethylene Blends", *Fib. Polym.*, vol.5 (4), pp. 270-274, 2004.
- 76 H.T. Oyama, "Super-tough poly(lactic acid) materials: Reactive blending with ethylene copolymer", *Polymer*, vol. 50, pp. 747-751, 2009.
- 77 H. Ismail, S.T. Sam, K.M. Chin, "Polyethylene/Soy Protein-based Biocomposites: Properties, Applications, Challenges and Opportunities", in *Polyethylene-Based Biocomposites and Bionanocomposites*, Ed. P.M. Visakh, S. Luftl, 2016.
- 78 C. Boonmee, C. Kositanont, T. Leejarkpai, "Degradation of Poly (Lactic Acid) under Simulated Landfill Conditions", *Env. Nat. Res. J.*, vol. 14(2), pp 1-9, 2016.
- 79 V. Massardier, C. Pestre, T. Cruard-Pradet, R. Bayard, "Aerobic and anaerobic biodegradability of polymer films and physico-chemical characterization", *Pol. Deg. St.*, vol.91, pp. 620-627, 2006.
- 80 R. G. Sinclair, "Blends of polyactic acid", Patent US5216050A, 1993.
- 81 L. As'habi, S.H. Jafari, H.A. Khonakdar, R. Boldt, U. Wagenknecht, G. Heinrich, "Tuning the processability, morphology and biodegradability of clay incorporated PLA/LLDPE blends via selective localization of nanoclay induced by melt mixing sequence", *Polym. Lett.*, vol. 7, pp. 21-39, 2013.
- 82 N. Medjdoub, M. Guessoum, M. Fois, "Viscoelastic, thermal and environmental characteristics of poly(lactic acid), linear low-density polyethylene and low-density polyethylene ternary blends and composites", *J. Adh. Sci. Tech.*, vol. 31(7), pp. 787-805, 2017.
- 83 G. Singh, N. Kaur, H. Bhunia, P. K. Bajpai, U. K. Mandal, "Degradation Behaviors of Linear Low-Density Polyethylene and Poly(L-lactic acid) Blends", *J. App. Poly. Sci.*, vol. 124(3), pp. 1993-1998, 2012.
- 84 A. K. Mohanty, M. Mishra, G. Hinrichsen, "Biofibres, biodegradable polymers and biocomposites: An overview", *Macromol. Mater. Eng.*, vol. 276, pp. 1-24, 2000.
- 85 T. Gurunathan, S. Mohanty, S.K. Nayak, "A review of the recent developments in biocomposites based on natural fibres and their application perspectives", *Comp. Part A*, vol. 77, pp. 1-25, 2015.
- 86 R.M. Rowell, H. P. Stout. 2007. Jute and Kenaf. In: *Handbook of fibre chemistry*, M. Lewin, 405–452, ed Vol. 3, Boca Raton, FL: CRC Press.

- 87 P. Saha, S. Manna, D. Roy, S. Chowdhury, K.G. Kim, S. Banik, B. Adhiikari, J.K. Kim, "Biodegradation of Chemically Modified Jute Fibres", *J. Nat. Fib.*, vol. 12(6), pp.542-551, 2015.
- 88 P. H. F. Pereira, M. de Freitas Rosa, M.O.H. Cioffi, K.C.C. de Carvalho Benini, A.C. Milanese, H. J. C. Voorwald, D.R. Mulinari, "Vegetal fibers in polymeric composites: a review", *Polym.*, vol. 25, 2015.
- 89 M. Sirueykm, A. Dickson, S.J. Hill, H. Pearson, "Plant Fibre: Molecular Structure and Biomechanical Properties, of a Complex Living Material, Influencing Its Deconstruction towards a Biobased Composite" *Materials*, 9(8), 2016.

2 Materials and Methods

The purpose of this study is to produce thermoplastic matrix composites at reduced environmental impact. In particular, oil-based/bio-derived thermoplastic blends have been chosen as matrices for wood flour and waste paper fibres. This chapter will focus on the choice of specific polymers and natural fillers, the production processes and the adopted techniques to characterize materials.

2.1 Materials

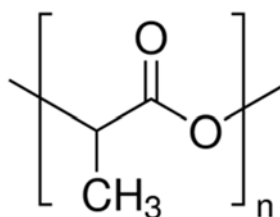
2.1.1 Polymers

Ingeo Biopolymer 3251D from Nature Works has been selected as Poly(lactic acid) (PLA). In fact, this PLA is designed for injection moulding applications, thanks to its higher melt flow index with respect to other PLA on the market. Some properties are displayed in Table 18. Tensile tests and Differential Scanning Calorimetry (DSC) properties have been obtained during the experimental part of the thesis. The specificities about the tests are described in paragraph 2.2.1 (tensile tests) and 2.2.5 (DSC).

Table 18: Ingeo Biopolymer 3251D technical properties.

Properties	Ingeo 3251D	Source
Specific Gravity	1.24	Technical data sheet
MFR, g/10' (190°C/2.16kg)	35	Technical data sheet
Melting Temperature (°C)	168	Differential Scanning Calorimetry (2.2.5)
Glass Transition Temperature (°C)	61	Differential Scanning Calorimetry (2.2.5)
Clarity	Transparent	Technical data sheet
Tensile Strength (MPa)	57	Tensile Test (2.2.1)

Elastic Modulus (MPa)	1490	Tensile Test (2.2.1)
Tensile Elongation (%)	7	Tensile Test (2.2.1)

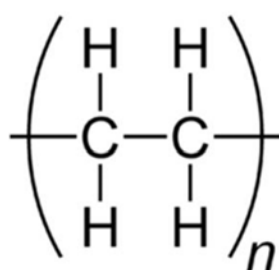


High-density polyethylene (HDPE), Eraclene MP90, was from ENI (Versalis). This polymer has low molecular weight distribution and high density, suitable for injection moulding processing. Some properties are displayed in Table 19. Tensile tests and Differential Scanning Calorimetry (DSC) properties have been obtained during the experimental part of the thesis. The specificities about the tests are described in paragraph 2.2.1 (tensile tests) and 2.2.5 (DSC).

Table 19: Eraclene MP90 properties.

Properties	Eraclene MO90	Source
Specific Gravity	0.96	Technical data sheet
MFR, g/10' (190°C/2.16kg)	7	Technical data sheet
Melting Temperature (°C)	134	Differential Scanning Calorimetry (obtained with conditions described in paragraph 2.2.5)
Glass Transition Temperature (°C)	<-60	Technical data sheet

Tensile Strength (MPa)	21	Tensile Test (obtained with conditions described in paragraph 2.2.1)
Elastic Modulus (MPa)	1160	Tensile Test (obtained with conditions described in paragraph 2.2.1)
Tensile Elongation (%)	>700	Tensile Test (obtained with conditions described in paragraph 2.2.1)



Soy Protein Isolate (SPI) Pro-Fam 974 has been provided by ADM. This SPI is characterized by 6% max moisture, 90% min protein, 4% max fat and 5% max ashes. Typical amino acids displayed in Pro-Fam 974 are listed in Table 20.

Table 20: Typical Amino Acids that are present in Pro-Fam 974 [Technical data sheet].

Amino acids	g/100g Protein
Aspartic Acid	11.5
Threonine	3.7
Serine	5.5
Glutamic Acid	19.2
Proline	5.2

Glycine	4.1
Alanine	4.3
Cystine	1.2
Valine	4.8
Methionine	1.4
Isoleucine	4.8
Leucine	8
Tyrosine	3.8
Phenylalanine	5.2
Histidine	2.7
Lysine	6.3
Arginine	7.5
Tryptophan	1.1

Amino acids structure is characterized by a side group R, which determines their specific properties. Figure 40 displays, separately by colour, the 20 universal amino acids in four different categories: non-polar (yellow), polar (blue), positive charge (green) and negative charge (fuchsia).

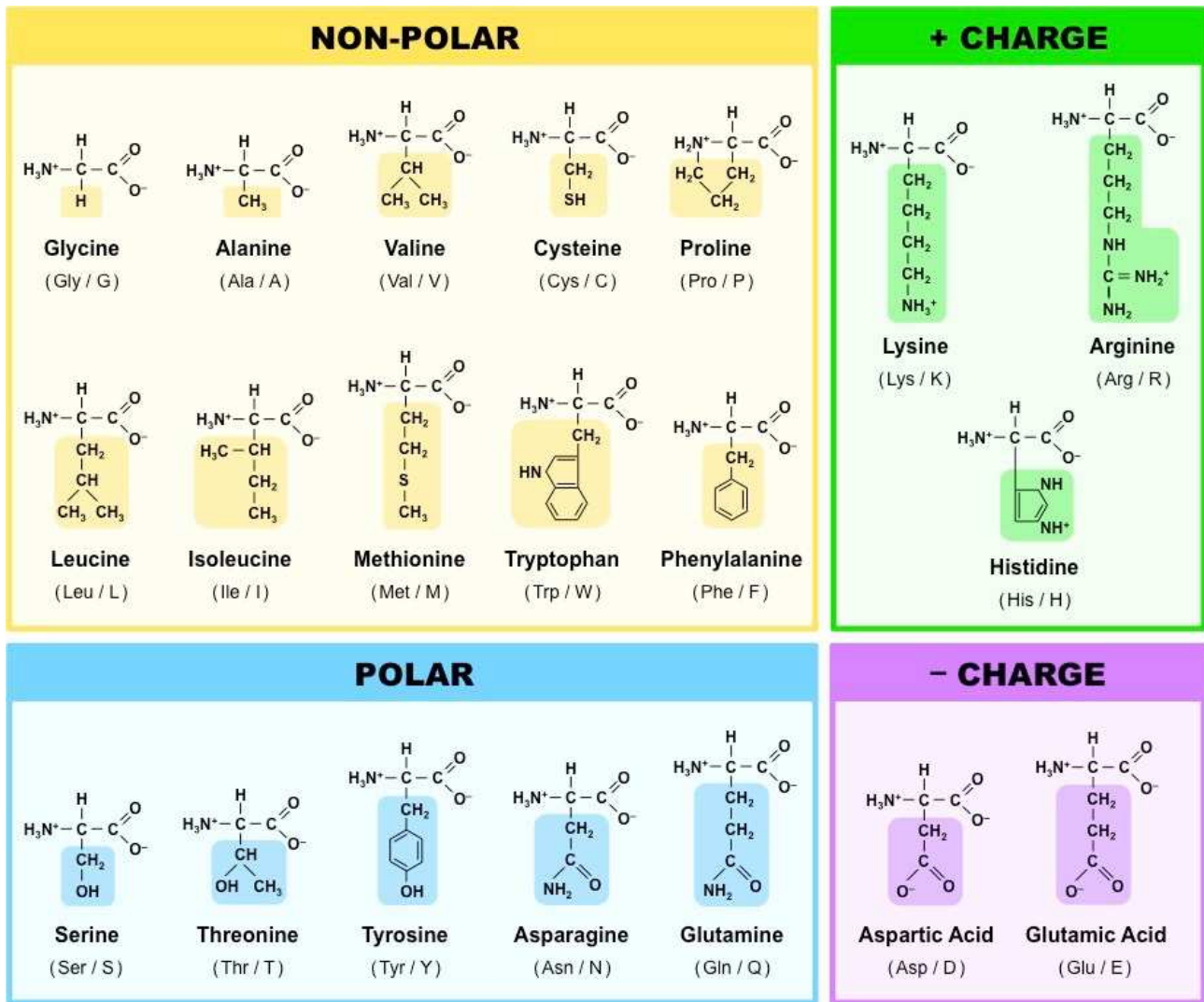
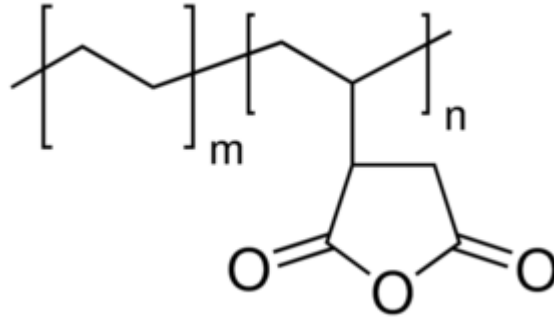


Figure 40: Chemical properties of different amino acids related to R side group presence [www. alevelbiology.co.uk, 18/07/2019].

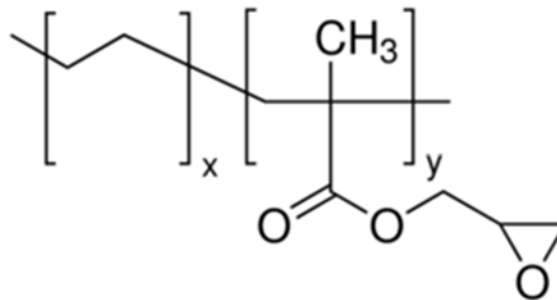
Glycerol has been used as plasticizer for SPI.

2.1.2 Additives

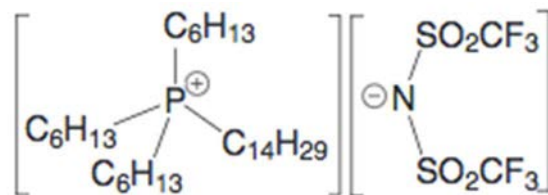
Polybond 3029 from Addivant: Maleic Anhydride (MA) content 1.5 to 1.7 wt.%, MFI 4 g/10 min (190°C/2.16 kg).



Copolymer of ethylene and glycidyl-methacrylate (PE-g-GMA), Lotader AX8840 from Arkema, is a random copolymer with 8 wt.% Glycidyl Methacrylate (GMA) content, MFI 5 g/10 min (190°C/2.16 kg).



IL trihexyl(tetradecyl)phosphonium bistriflamide from Cytec's Cyphos has been selected.



2.1.3 Natural Fibres

La.So.Le/est/Srl (Udine, Italy) provided the WF (European beech) with dimensions derived from datasheet:

>500 μm 0-5%

>300 μm 20-70%

>180 μm 20-80%

<180 μm 0-5%

Recycled waste paper, whose production process will deeply be described in chapter 3, have been observed with optical microscopy. Average length of $750\pm 300\ \mu\text{m}$ and diameter of $25\pm 10\ \mu\text{m}$ have been measured.

PLA, WF and recycled waste paper were dried one night at 80°C under vacuum, before processing.

2.1.4 Production processes

Extrusion and Injection Moulding

A Micro 15 Twin-screw DSM research extruder was used at 180°C , with screw speed of 75 rpm, N_2 atmosphere and 4 min residence time. The mould temperature was 55°C , and pressure parameters were depending on the formulation specificities because of different viscosities. Dog-bone samples have been obtained for each formulation, with a gauge length section $30\times 4\times 2\ \text{mm}^3$ (LxWxT).



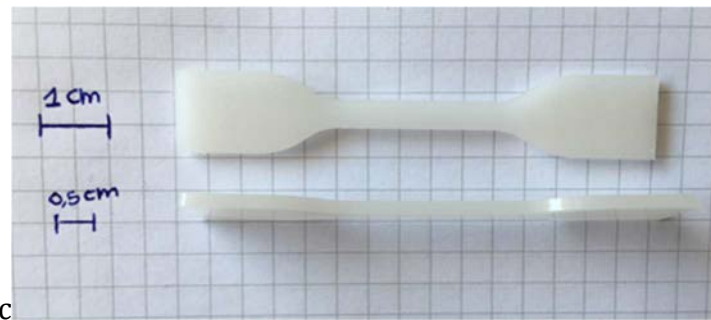


Figure 41: Extrusion equipment (a), Injection moulding equipment (b) and samples obtained from the production process.

Turbomixer and Compression Moulding

An equipment developed by our research group, turbomixer, has been used as alternative production process for composites. Turbomixer is composed of a cylindrical stator and a rotor with attached blades.



Figure 42: Cylindrical stator and rotor with blades of the turbomixer equipment.

Temperature recording is carried out through the application of three thermocouples, located on the cylinder wall, on the peripheral area and in the centre of the cylinder. Heat is produced through friction thanks to speeds of about 3000 rpm. This process allows the charge reaching the melting temperature (around 180°C in our study).

The turbomixer has a batch working: initially the material is charged, then the cylinder is closed, mixing is activated and finally the material is discharged by hand.

The melted charge is subjected to compression moulding, obtaining plates from which samples are derived.



Figure 43: General process to obtain samples with turbomixer processing: a) Introduction of polymer pellets, b) Introduction of natural fillers, c) Extraction of the melted charge after processing at melting temperature and high speed rotation, d) Introduction of melted charge in the compression moulding equipment, e) Extraction of samples.

2.2 Methods

2.2.1 Tensile tests

Tensile tests were performed in accordance with the ASTM D638 standard using Zwick/Roell Z010 and load cell of 10 kN. A crosshead speed of 5 mm/min has been used. The tensile tests were performed on five dog-bone samples per series with a gauge length section 30x4x2 mm³ (LxWxT).



Figure 44: Tensile test equipment used to evaluate mechanical properties.

2.2.2 Optical Microscopy

Samples have been observed with an Optical Microscope Zeiss, using also, if necessary, the temperature control equipment.

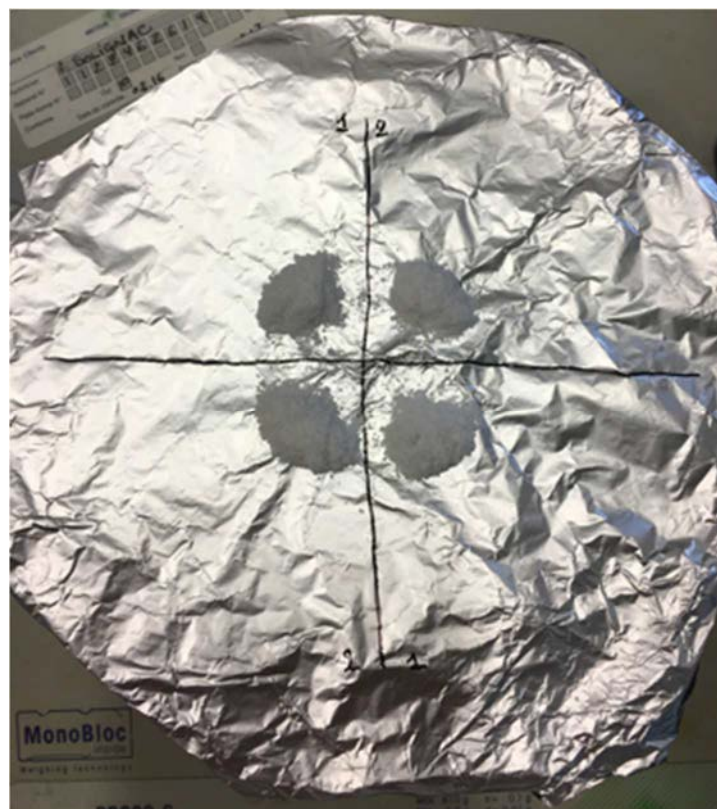
2.2.3 Scanning electron microscopy (SEM)

Samples have been observed with Hitachi S2500 and 25 kV in order to analyse blend and composite morphology and interfaces. Samples have been sputter-coated with gold particles before surfaces characterization. Software ImageJ has been used to evaluate blends

morphology. Phase separation is evident in blend with poor miscibility, allowing the evaluation of areas thanks to specific tools of the software. In fact, images can be treated enhancing chromatic contrast between phases and they can be binarized, keeping visible only the secondary phase.

2.2.4 Quartering

Samples produced, in the majority of cases, are characterized by high heterogeneity because of fibres dispersion and multiphase matrices. In order to obtain reliable results from thermal analysis, and analyse a representative amount of sample, a cryogenic mill was adopted to obtain samples in the form of powders. A subsequent statistical approach, quartering, was used to select an exemplary amount of samples used for chemical and thermal analysis. This method is based on the separation of the total amount of charge in four parts equal in weight. Then, two parts at the opposite side are mixed together and the two others are separated.



2.2.5 Differential Scanning Calorimetry (DSC)

Differential Scanning Calorimetry (DSC) tests were performed on a Q20 Thermal Analysis instrument with two cycles (with a 4 minutes interval between them) at 180°C to eliminate trace of thermal history. The first cycle is carried out from 25°C to 180°C at 10°C·min⁻¹ under a nitrogen flow of 50 mL·min⁻¹ followed by a cooling from 180°C to 25°C at 10°C·min⁻¹. T_c and ΔH_c were measured during this cooling phase. Then, a second heating from 25°C to 180°C at 10°C·min⁻¹ enables to determine T_{cc} , T_f and ΔH_f . The first cycle provides information about properties after injection moulding, while the second one gives materials properties. Melting and crystallization parameters (temperature and enthalpy) and glass transition temperatures were analysed. HDPE and PLA crystallinities have been evaluated as

$$X(\%) = \frac{\Delta H_m}{\Delta H_t} \times \frac{1}{w} \times 100 \quad (1)$$

where ΔH_m is the experimental enthalpy value from DSC analysis, ΔH_t is the theoretical melting enthalpy value of fully crystalline HDPE (293 J/g) [1] or fully crystalline PLA (93 J/g) [2], and w is the weight fraction of polymer in the composites. If cold crystallization phenomenon occurs, $X(\%)$ has to be evaluated as

$$X(\%) = \frac{\Delta H_m - \Delta H_{cc}}{\Delta H_t} \times \frac{1}{w} \times 100 \quad (2)$$



Figure 45: Differential Scanning Calorimetry equipment used to analyse thermo-chemical properties of samples.

2.2.6 Thermogravimetric Analysis (TGA)

Thermogravimetric Analysis (TGA) tests were carried out on a Q500 Thermal Analysis instrument, up to 600°C with a scanning temperature of 10°C·min⁻¹ under a nitrogen flow of 50mL·min⁻¹. From these analyses, we derived temperatures at which degradation started (Tonset), evaluated through the extrapolated onset temperature from TGA curve, and Δm , mass variation during the test.



Figure 46: Thermogravimetric analysis equipment used to analyse thermal stability of our samples.

2.2.7 Rheological measurements (ARES G2)

Rheological measurements were performed on a rotational rheometer model ARES-G2 with parallel plate geometry (40 mm diameter) manufactured by Thermal Instruments. Three different tests were performed at 120°C for HDPE and 180°C for PLA, temperatures to have melted polymers.

1) Amplitude sweep has been performed to detect a solicitation amplitude in which the module is independent of the deformation. This is a preliminary test to choose a suitable deformation for other tests. For this test, a scan between 0 and 10% of amplitude has been performed. Amplitude of 1% has been selected for frequency and time sweep.

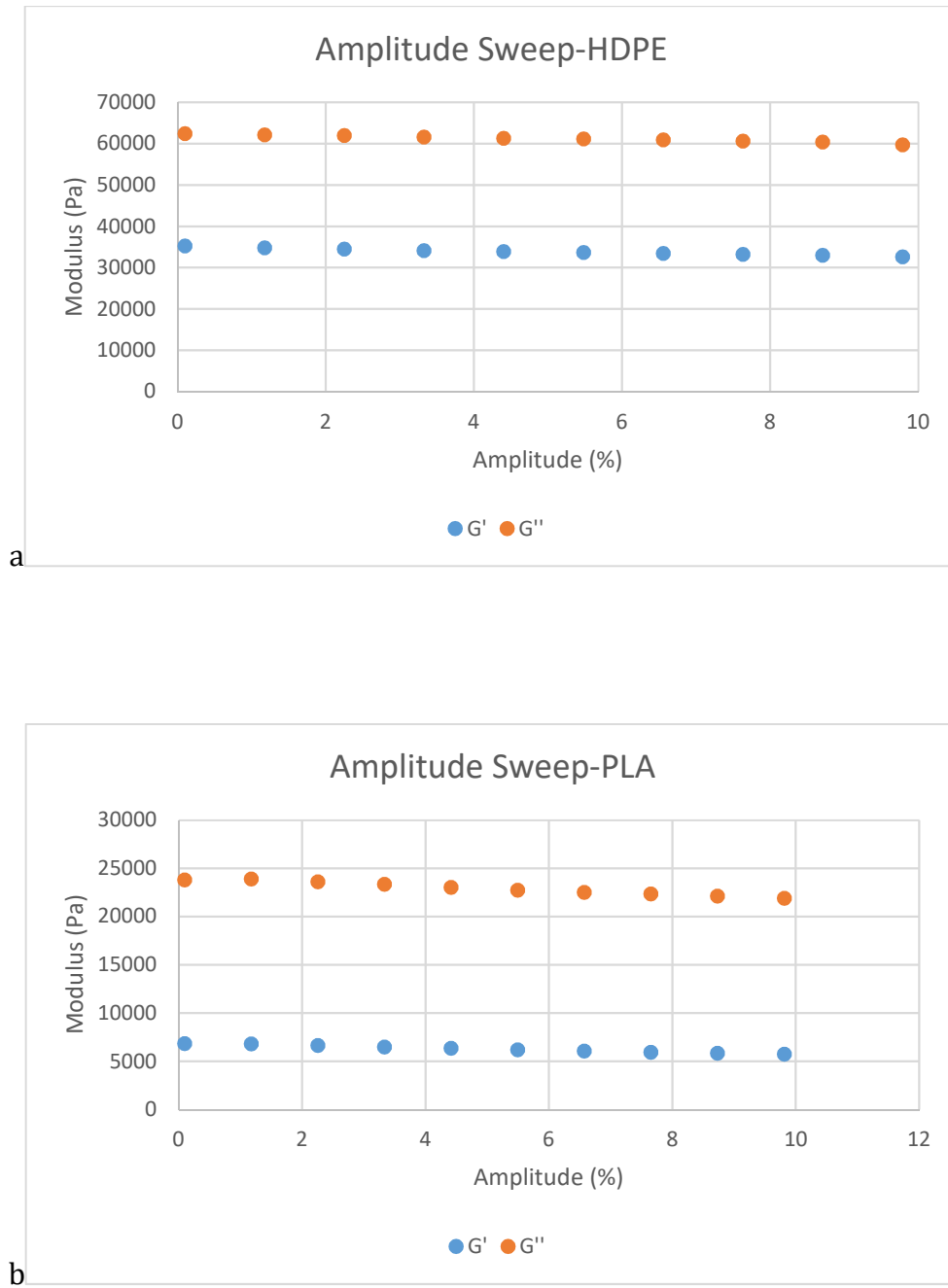


Figure 47: Amplitude sweep performed to detect a solicitation amplitude in which the module is independent of the deformation for both HDPE (a) and PLA (b)



Figure 48: Rheology equipment used to perform rheological measurements.

2) Time sweep has been performed to evaluate the stability of samples at fixed deformation (1% derived from amplitude sweep) and 10rad/s frequency for 1 hour. No sensitive variation for HDPE and PLA has been displayed during this test.

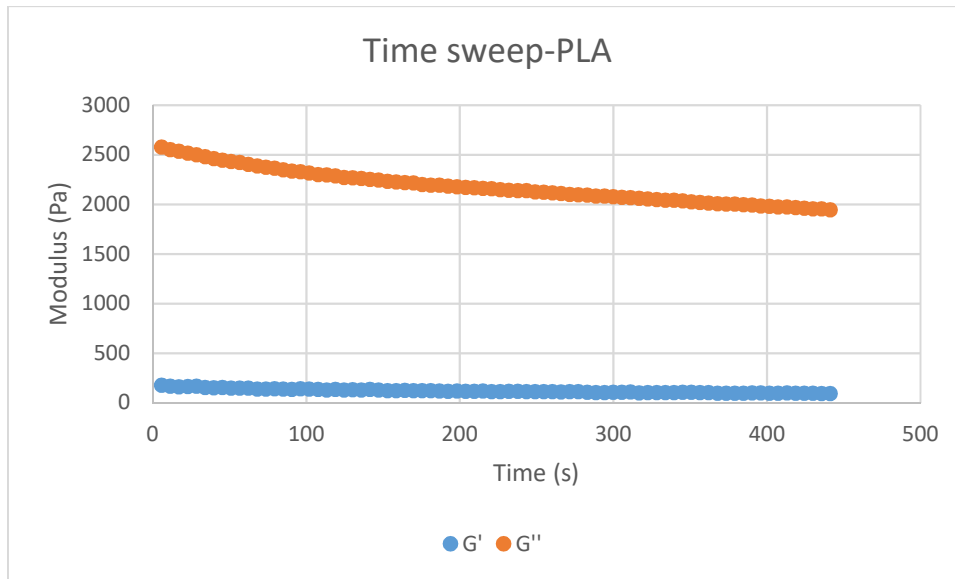


Figure 49: Time sweep performed to evaluate the stability of PLA at fixed deformation (1% derived from amplitude sweep) and 10rad/s frequency for 1 hour.

3) Frequency sweep has been performed between 0.01 and 100rad/s at 120°C and 5% deformation. This test allows the evaluation of storage and loss modulus, $\tan(\delta)$ and complex viscosity. Results about frequency sweep will be analysed in results section.

2.2.8 Infrared Analysis Attenuated Total Reflection (ATR-FTIR)

Infrared Analysis Attenuated Total Reflection (ATR-FTIR) tests were carried out with a thermo-scientific Nicolet IS10 spectrometer, with a spectral range 4000-400 cm^{-1} and 32 scans.



Figure 50: Infrared Analysis Attenuated Total Reflection (ATR-FTIR) equipment used to evaluate interactions or reactions between components.

2.2.9 Size Exclusion Chromatography (SEC)

SEC was performed using a Shimadzu apparatus equipped with a refractive index detector (RI) to determine polymer molar masses. The eluent is tetrahydrofuran (THF) with a flow rate of 1mL/min. Universal calibration was performed using polystyrene standards. Samples have been dissolved in THF eluent (around 15mg samples for 10mL eluent), and then filtered using PTFE filters of 0.45 μm .



Figure 51: Size Exclusion Chromatography equipment used to evaluate molecular weight of PLA-based samples.

2.2.10 Composting Tests

Tests were performed in order to analyse the effect of testing temperature, wood flour (WF) and cellulosic fibres (P) on PE and PLA, as well as the behaviour of soy protein isolate based formulations (with 30% of glycerol as plasticizer, blended with PE). We can also compare the behaviour of two bio-derived polymers (PLA and SPI).

Tests duration: 3 months (12weeks)

Two temperatures have been selected in order to understand the effect of temperature on these tests:

- Mesophilic condition (35°C)
- Thermophilic condition (58°C)

3 aquaria (1-2-3) at 35°C, 3 aquaria (4-5-6) at 58°C at 85% relative humidity.

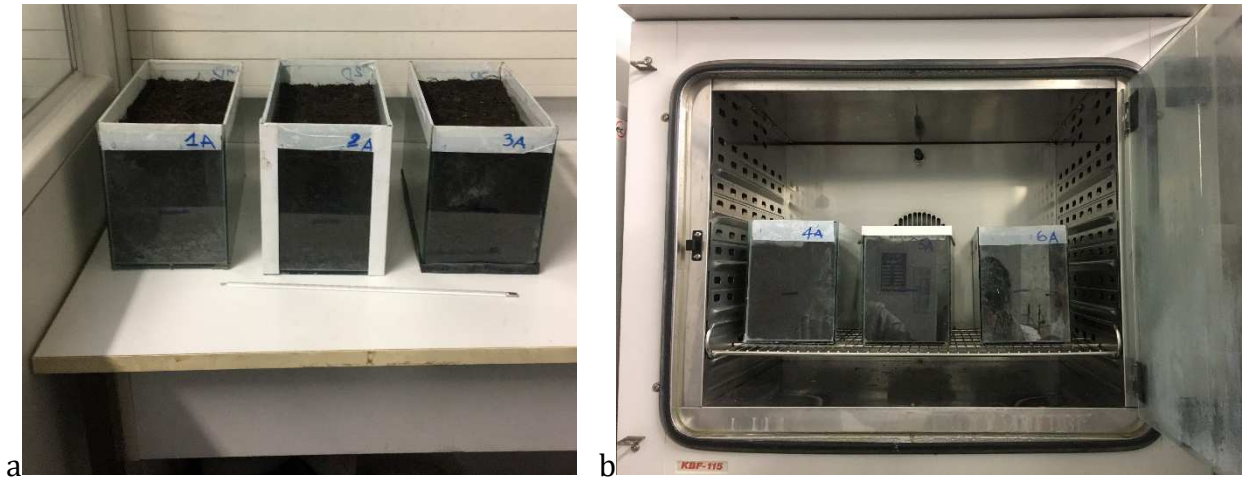


Figure 52: Aquaria used to perform composting tests at mesophilic (a) and thermophilic (b) conditions.

In each aquarium, 2kg of compost have been used: 1 kg has been put at the bottom, samples have been placed and then 1 kg of compost has been used to bury samples.

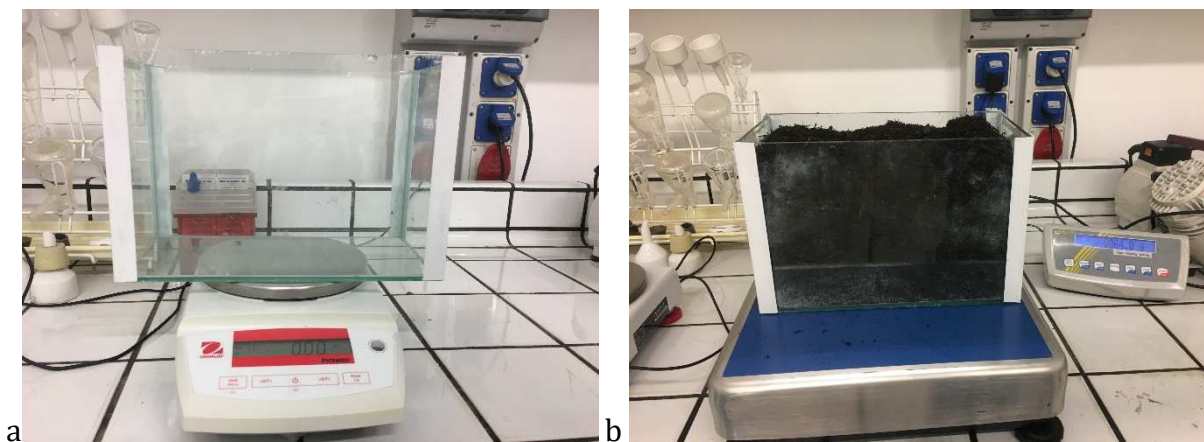


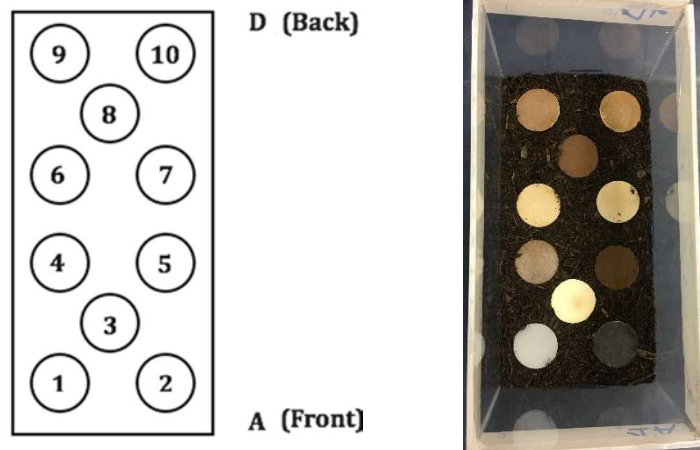
Figure 53: Aquaria weighted before (a) and after (b) the addition of soil and samples to evaluate the variation of weight under composting condition.

Before burying, all samples have been dried all night under vacuum at 50°C and weighted.

Samples to be tested

1. HDPE
2. PLA
3. SPI70Gly30
4. HDPE60WF40
5. PLA60WF40
6. HDPE60P40
7. PLA60P40
8. PLA60WF30P10
9. HDPE30PLA30WF30P10
10. HDPE50(SPI70Gly30)50

Scheme of samples' disposition in aquarium



t=1, 2, 3 months analyses (3 disks for each formulation + 1 disk for evaluation at t=0)

Each aquarium has been weighted empty and with 2kg of compost and samples. Every two days, aquarium weight is checked and eventually water is added to keep almost the same amount of humidity in each aquarium.

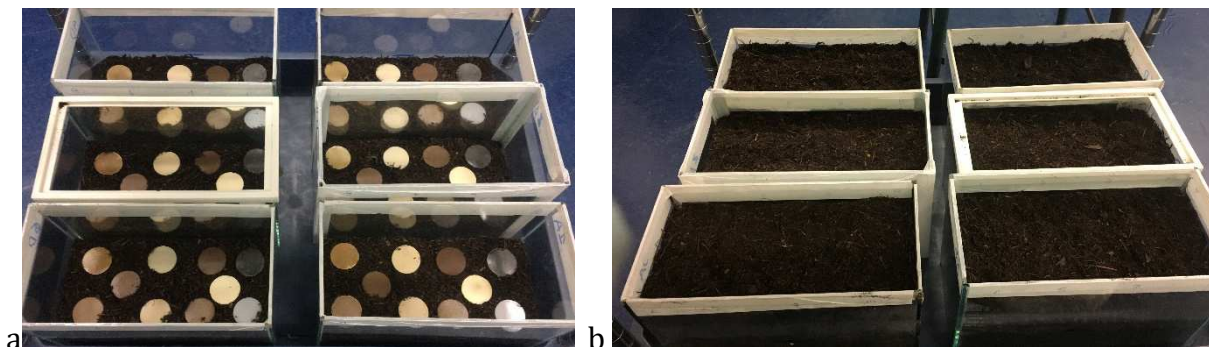


Figure 54: Samples have been placed over 1kg of soil (a) and then have been covered with another kg of soil to perform composting tests.

Each sample (disk d= 40mm, h=1.5mm) is sacrificed in order to perform different tests:

- Mass loss (after cleaning with water and drying)

All samples have first been subjected to visual observation after each month, as visible from Figure 109. Drying until constant weight has been reached, in order to be sure to eliminate absorbed water and humidity, in order to compare with samples' weight before testing (Figure 110). Mass variation is expressed as

$$\Delta M(\%) = ((M_{t0} - M_t) / M_{t0}) * 100 \quad (3)$$

In which $\Delta M(\%)$ is mass variation, M_{t0} is the mass value before composting and M_t is the mass value at time t (respectively 1,2 3 months at 35°C and 58°C).

- FTIR (to evaluate the variation of bond during degradation)
- Visual observation
- Thermogravimetric analysis (TGA)

2.3 References

- 1 Y. Lei, Q. Wu, C.M. Clemons, F. Yao, Y. Xu, "Influence of nanoclay on properties of HDPE/wood composites", *J App Polym Sci*, vol. 106, pp. 3958-3966, 2007.
- 2 D. Battezzore, S. Bocchini, A. Frache, "Crystallization kinetics of poly(lactic acid)-talc composites", *eXPRESS Polymer Letters*, vol. 5, 849-858, 2011.

3 Waste paper treatment and application in WPC

This chapter is derived and adapted from “Paper fiber filled polymer. Mechanical evaluation and interfaces modification” written by M. Valente, J. Tirillò, A. Quitadamo C. Santulli, “Industrial paper recycling process: suitable micronization for additive polymer application” written by M. Valente, J. Tirillò, A. Quitadamo, “Polymeric Matrix Composites at Reduced Environmental Impact”, written by M. Valente, A. Quitadamo.

The fibres’ origin directly affects the properties of the resulting composite [1]. In this project, we adopted a mechanical process to reduce waste paper in fibres.

The production of these composites is performed generally through injection moulding [2-4]. In this study we adopted turbomixing process, already used in other studies [5-6], which could allow to obtain better results. We developed our own equipment in order to improve the productive process. In this way, the production of a highly filled compounds was possible, using particles and/or short fibres at lower cost and with higher shearing compared to traditional processes.

3.1 From waste paper to useful fillers

Paper used in recycling processes or in thermovalorization is generally previously subjected to grinding by knife mill: in this way, fragments of few centimetres are obtained. This is a common process to obtain a useful shape for traditional waste paper processing. Therefore, in order to obtain paper suitable for incorporation in polymeric matrices, micronization treatment is needed: a far from trivial process due to paper fibrous nature. In our study, waste paper has been grinded with two different techniques: a superfine grinding mill, in order to obtain a suitable morphology to improve mechanical properties, and a knife mill, to obtain morphology more useful to improve damping and acoustic isolation properties.

3.1.1 Superfine grinding mill type SF

A pre-grinding process in hammer mill is previously adopted, to obtain paper fragments of 8-10 millimetres to realize a product suitable for the next step. The charge is then sent to micronization mill that exploits simultaneously the action of impact, shear and turbulence.

Superfine grinding mill SF is produced by Cimma, which works in the design and construction of machines and systems for powder technology.

Paper is introduced by a screw feeder or through a current of air sucked downwards into the grinding chamber. At the exit of the grinding chamber, the ground product, swept upwards by the airflow, is classified by the separator placed in the higher part of the mill. The refined material is discharged upwards and collected into a filter, while the reject of the separator is recycled into the mill.

Figure 55 represents the process scheme of the micronization plant.

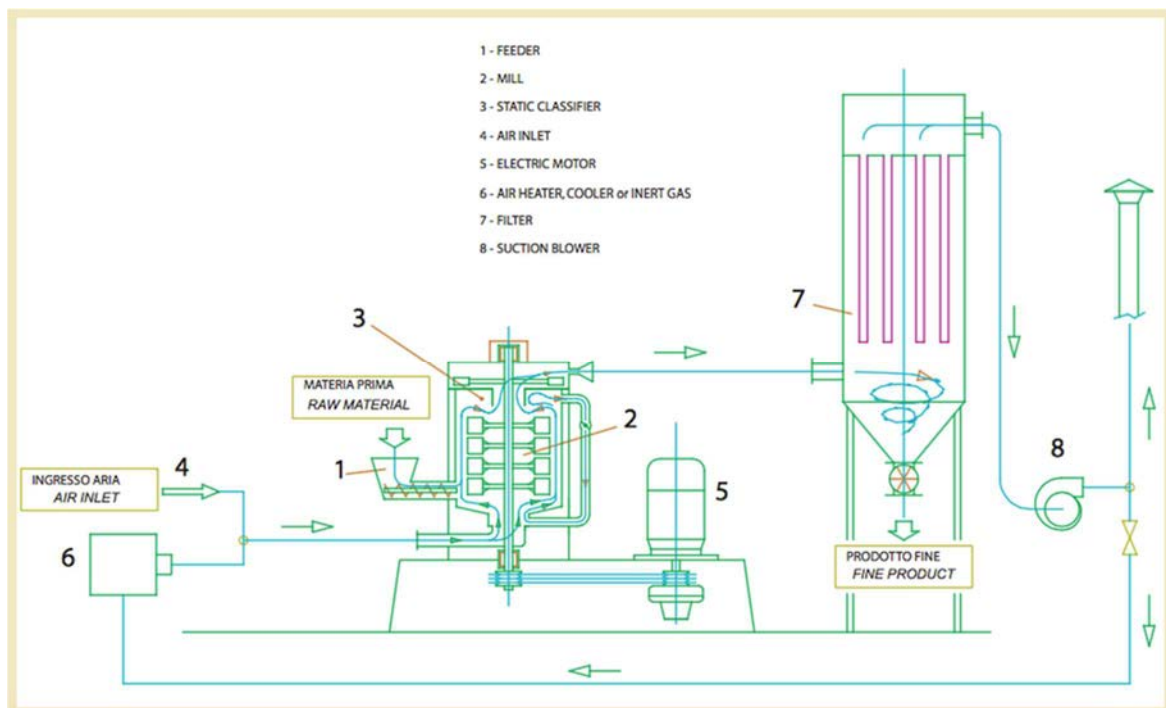


Figure 55: Process scheme of the micronization plant.

Figure 56 and Figure 57 represent the fibres obtained.

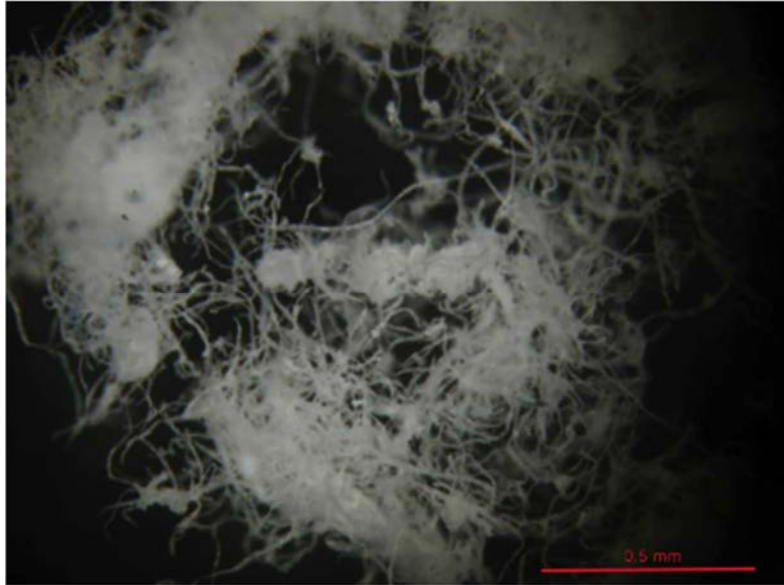


Figure 56: Stereomicroscopy image of micronized paper.

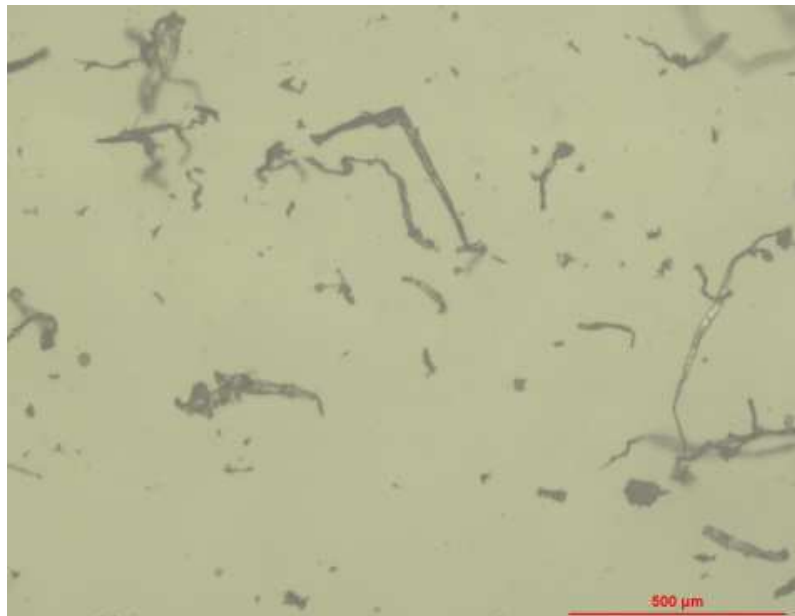


Figure 57: Optical microscopy image of micronized paper.

Figure 58 and Figure 59 represent the recycled paper before and after the micronizing process.



Figure 58: Recycled paper before micronizing process.



Figure 59: Recycled paper after micronizing process through Superfine grinding mill.

3.1.2 Knife mill SM 300

After a pre-grinding treatment, adopted also in the previous process, to obtain 8-10 mm fragments of paper, the charge is sent to a knife mill. The process adopted is a knife mill SM 300 from Retsch, a German company that is active in the fields of neutral-to-analysis sample preparation and characterization of solids [7]. Figure 60 represents the scheme of the adopted knife mill.

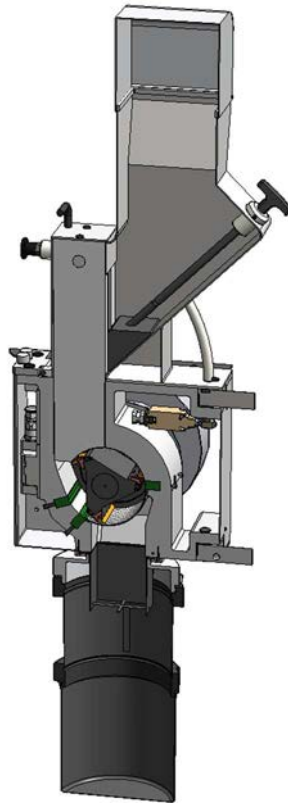


Figure 60: Scheme of the adopted knife mill SM300

Cutting bars of stainless steel are used in this mill.

Feeding charge is introduced through a hopper into the grinding chamber. Here it is in contact with the rotor and it is subjected to size reduction as a result of the cutting and friction action. The knife mill is equipped with double cutting effect to increase the number of the cutting during the grinding. The residence time of the charge in the chamber is generally short and depends on the type of sieve adopted: in this study, sieve from 1 mm and 0,5 mm are used. Once reached the size to pass through the sieve mesh, grinded paper is collected in a container. The speed of rotation varies between 700 and 3000 rotations/min: in this way, a rapid reduction in the size is possible. The product obtained from this process is very different from fibres obtained with the superfine grinding mill: in this case, paper is reduced in fragments from which some fibres are isolated.

Figure 61 represents the product obtained from the knife mill.



Figure 61: Stereomicroscopy image and visual observation of recycled paper after micronizing process through Knife mill.

Composites with grinded paper have been produced to analyse the mechanical and technological properties with waste paper addition.

The family samples tested are 10% of fibres derived from the superfine grinding mill (named as 10S) and 20% of fibres derived from both the superfine grinding mill (named as 20S) and the knife mill (named as 20K). The higher percentages of fibres have been chosen to compare the products from two different mills. Each family characterized by different fibres percentages is composed of five samples.

Tensile tests are commonly used to analyse mechanical properties of produced samples, suggesting hypothesis about the effectiveness of the production process in terms of filler dispersion and interface with matrix. Figure 62 and Table 21 display tensile test results for neat HDPE and HDPE with 10wt.% and 20wt.% of grinded paper with superfine grinding mill.

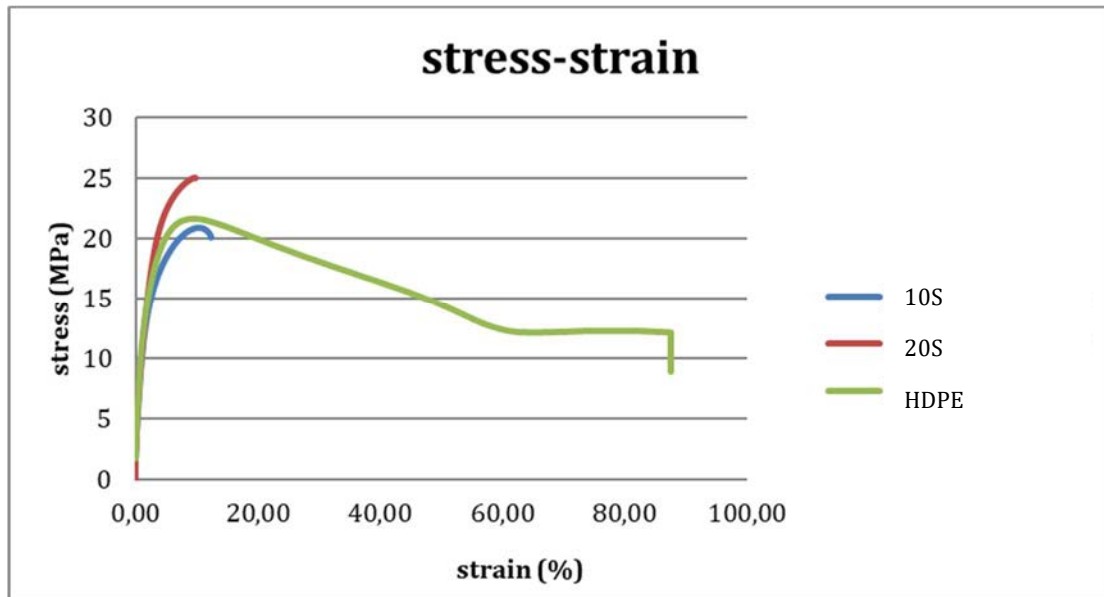


Figure 62: Stress-strain curves for neat HDPE and composites with 10 wt.% and 20 wt.% of waste paper processed with superfine grinding mill.

Table 21: Tensile test results for neat HDPE and composites with 10 wt.% and 20 wt.% of waste paper processed with superfine grinding mill (S).

Samples	Elastic modulus (MPa)	Breaking load (MPa)
HDPE	1160±87	21.6±0.2
10 S	1090±32	20.9±0.7
20 S	1250±18	24.6±1.2

The elastic modulus slightly increases or is constant with the introduction of fibres. The same behaviour is displayed by the breaking load, which is significantly improved with higher percentages of fibres, associated with a marked loss of material toughness.

Figure 63 represents the stress and strain curves of the specimens with 20% of fibres produced with the knife mill (20K) compared to polyethylene without fibres and the composite with 20% of fibres produced with the superfine grinding mill (20S).

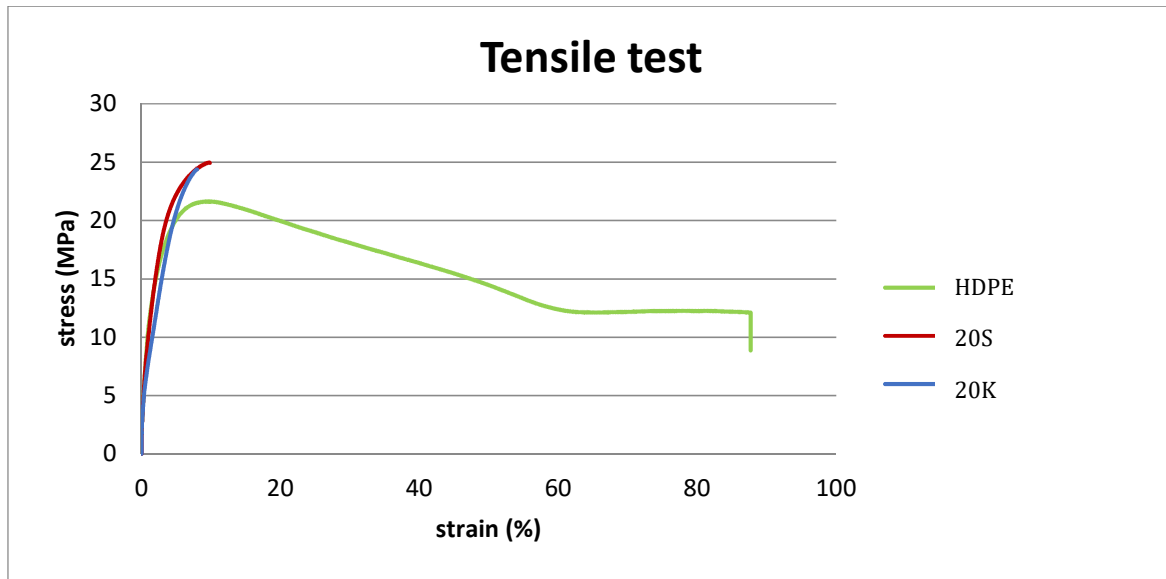


Figure 63: Stress-Strain curves for composites with 20wt.% of fillers from superfine grinding mill (20s) and knife mill(20k)

The “s” after paper in the graphic means the paper produced with the superfine grinding mill, while the “k” is for paper treated with the knife mill.

Grinded paper obtained with knife mill (paper k) is characterized by particle shape, which does not affect the elastic modulus while the mix of fibres and particles seems to contribute to the breaking load.

The elastic modulus of the composite produced with fibres from the knife mill is close to neat HDPE considering standard deviation, but the breaking load are higher and closer for composites produced with fibres from both the superfine grinding and knife mills, with the same amount of fibres. These results (Table 23), especially the higher elastic modulus for paper S, are in agreement with reinforcing behaviour of particles or fibres filler, suggesting a morphology influence.

Table 22: Main results of tensile tests for composites produced with 20wt.% of fibres from the superfine grinding (20S) and knife (20K) mill.

Samples	Elastic modulus (MPa)	Breaking load (MPa)	Elongation at break (%)
HDPE	1160±87	21.6±0.2	>700
20S	1250±18	24.6±1.2	9.7±1.4
20K	1067±78	24.7±1.7	7.9±0.8

Scanning Electron Microscopy (SEM) underlines the poor fibre matrix interface: a predictable result considering the hydrophilic nature of the fibre and the hydrophobic one of the matrix. This behaviour is shown with the specimens containing fibres both obtained with the superfine grinding and the knife mill. Figure 64 and Figure 65 display pictures of specimens with 10wt.% of fibres s and 20wt.% of fibres k, underlining in both cases a poor interface between fibres and HDPE.

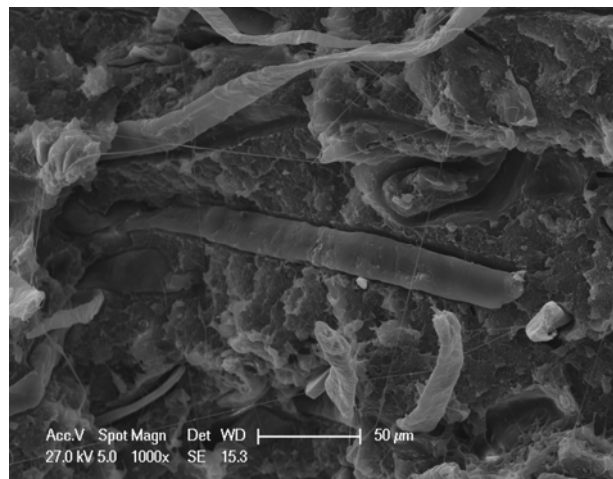


Figure 64: SEM picture of specimens with 10wt.% fibres s

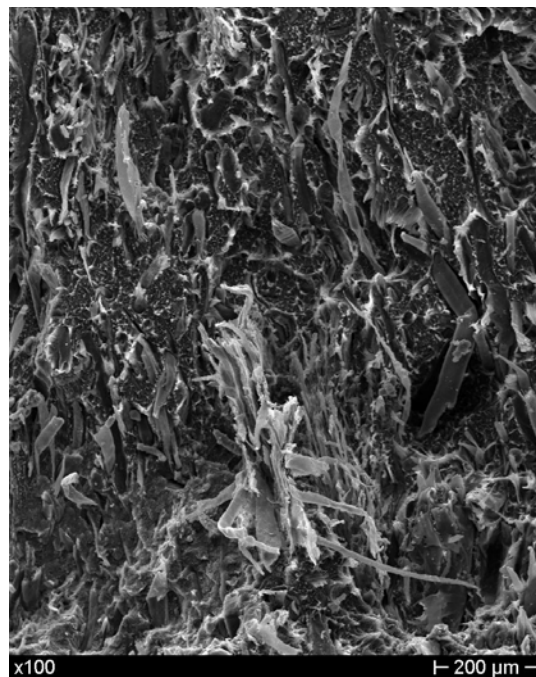


Figure 65: SEM picture of specimens with 20wt.% fibres k.

SEM analysis is also useful to study the fibres and particles dispersion.

A good dispersion of fibres is evident for the composite produced with fibres of superfine grinding mill with 10% and 20% of fibres. The composite with fibres derived from the knife mill is characterized by the presence of particles and isolated fibres. There are some agglomerates of fibres near the fragments. Figure 66 and Figure 67 display fibres dispersion in the matrix.

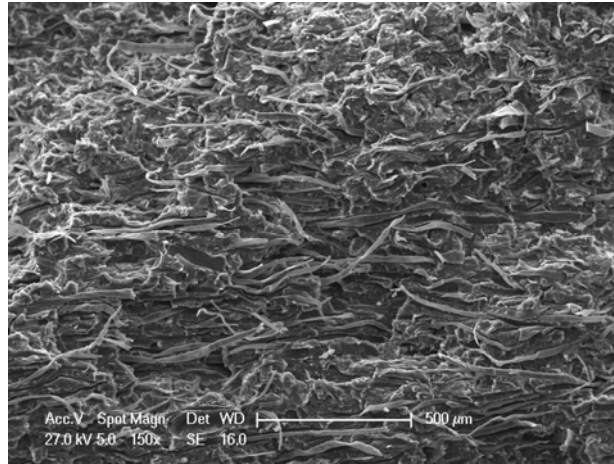


Figure 66: SEM of the composite produced with 20wt.% of fibres from the superfine grinding mill.

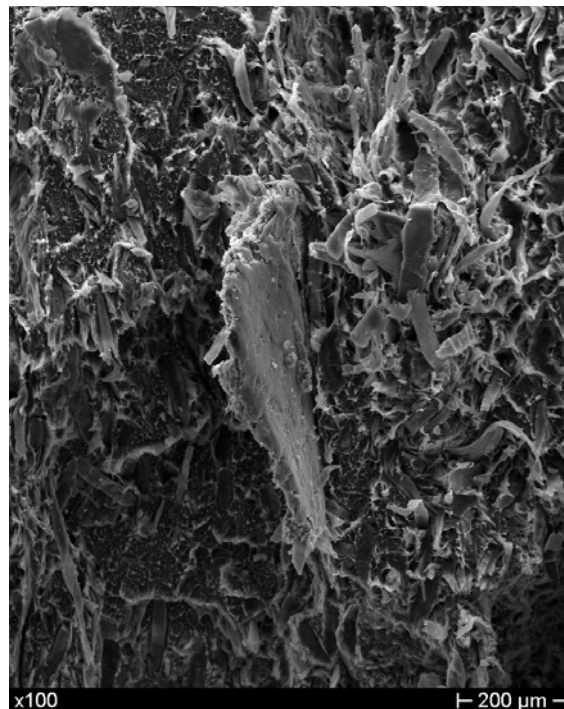


Figure 67: SEM of the composites produced with 20wt.% of fibres from the knife mill.

The analysis of the results, including encouraging tensile test data, shows that the paper can be used to reinforce composites with polymeric matrices.

3.2 Recycled waste paper fibres in HDPE and WPC

Recycled waste paper fibres produced with superfine grinding mill (described in the previous paragraph) have been selected and added in the amount of 10wt.% to HDPE matrix. In order to improve fibre-matrix interface, polyethylene grafted maleic anhydride MAPE, Polybond 3029, has been added in the amount of 1, 3 and 5 wt.% (Table 24)

Table 23: Samples produced with 10 wt.% of recycled waste paper fibres and three different percentages of MAPE (1, 3 and 5 wt.%)

Sample	HDPE (%)	Recycled waste fibre (%)	Polybond 3029 (MAPE) (%)
10F	90	10	
10F1A	89	10	1
10F3A	87	10	3
10F5A	85	10	5

Tensile test results are displayed in Figure 68 and Table 24.

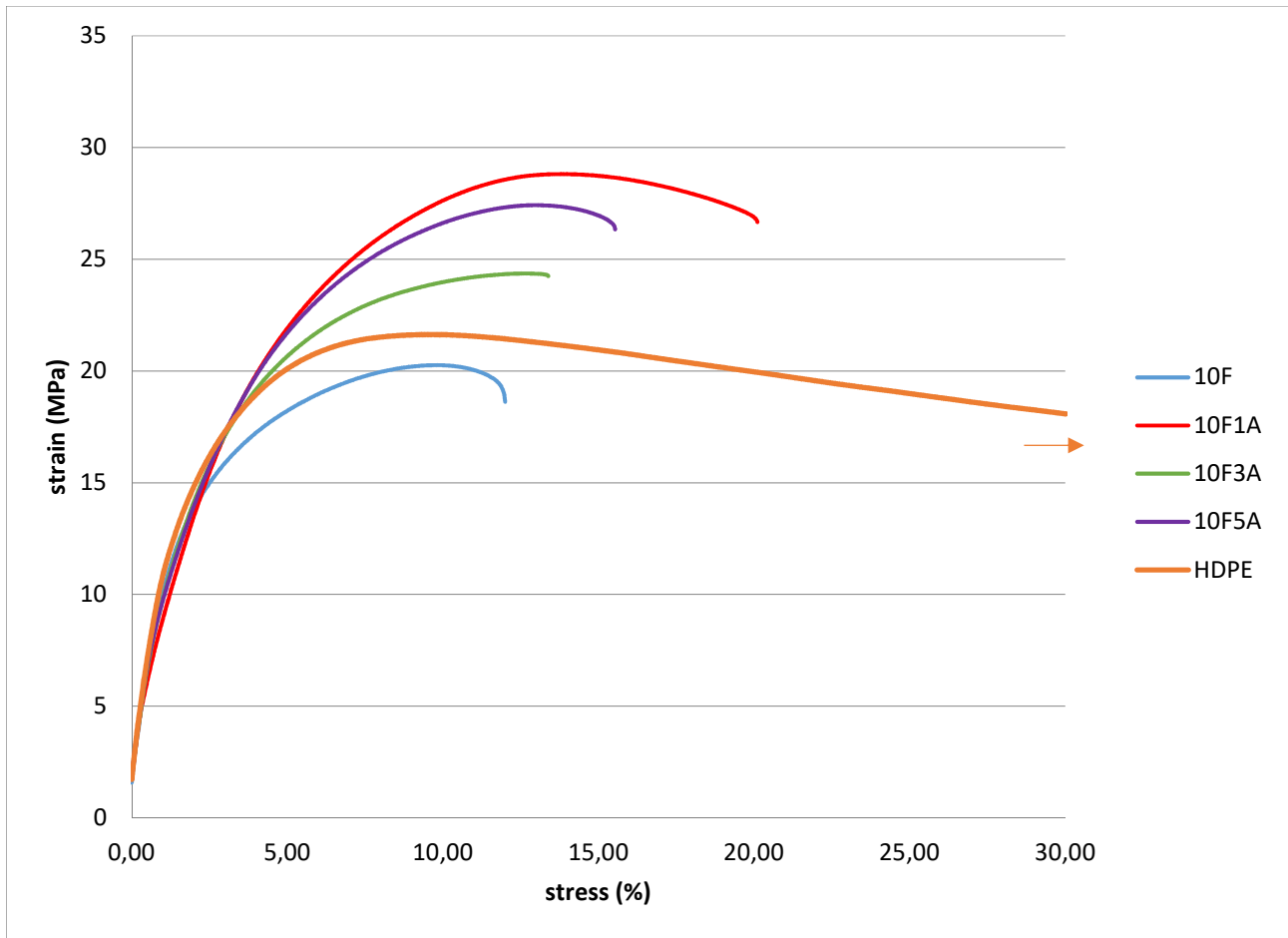


Figure 68: Stress-strain curve for composites with 10wt.% of fibres (F) from superfine grinding mill with 1-3-5 wt.% of MAPE(A).

The absence of interphase between hydrophilic recycled waste paper and hydrophobic HDPE seems to be responsible for poor mechanical properties when fibres are added in the amount of 10wt.%. Maleic anhydride of MAPE should allow it to act as a compatibilizer of HDPE and cellulosic matter. On the other side, the flowability of MAPE is substantially lower than those of HDPE: in particular, melt flow index (MFI), which is in the region of 7 g/ 10 min (190 C/2.16 kg) for HDPE, is only around 4 g/10 min (190 C/ 2.16 kg) for MAPE. The resulting polymer/cellulosic fibres blends seem to be influenced by the addition of small amounts of MAPE and a few % of this copolymer are probably sufficient.

Table 24: Main tensile tests results for composites produced with 10wt.% of fibres and three different percentages of Polybond 3029 (A).

Sample	Elastic modulus (MPa)	Ultimate stress (MPa)	Elongation at break (%)

10F	1090±32	20.9±0.7	12.6±2.1
10F1A	1062±26	27.5±1.5	12.5±2.3
10F3A	1032±109	24.6±1.2	15.3±1.2
10F5A	1080±21	27.0±0.9	13.8±1.5

Water absorption tests (Figure 69) were performed at two different temperatures, room temperature RT 21°C and 40°C, for samples with 10wt.% of fibres (F) and 1-3-5 wt.% of MAPE (A).

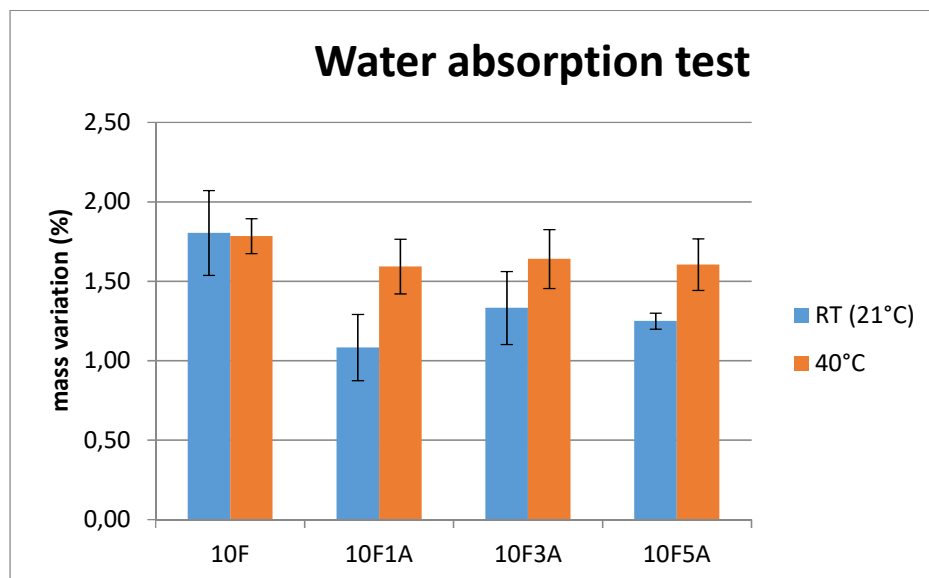


Figure 69: Comparison of water absorption tests at different temperatures.

Except for sample 10F, specimens reveal a higher percentage of mass variation at 40°C than at RT thanks to the acceleration of water diffusion through pores. Specimens of each family were characterized by a water uptake, rather close whatever the composition.

The positive results obtained for the use of recycled paper fibres promote the addition of this filler in traditional WPC, increasing the amount of natural fillers in the composite and allowing interactions between two different fillers morphology. In fact, wood flour has a particle morphology, while recycled paper fibres from superfine grinding mill have a fibrous morphology.

Samples with different composition have been tested and are listed in Table 25.

Table 25: Families of produced samples through turbo mixing. All samples have HDPE matrix.

Sample	Wood Flour W (%)	Fibres F (%)	MAPE A (%)
HDPE	-	-	-
10F	-	10	-
10F1A	-	10	1
30W	30	-	-
30W3A	30	-	3
30W5A	30	-	5
30W10F	30	10	-
30W10F3A	30	10	3
30W10F5A	30	10	5

Tensile test results display a positive effect in terms of elastic modulus for samples with both wood flour and recycled paper fibres. This result suggests a good interaction between two different morphologies (Figure 70).

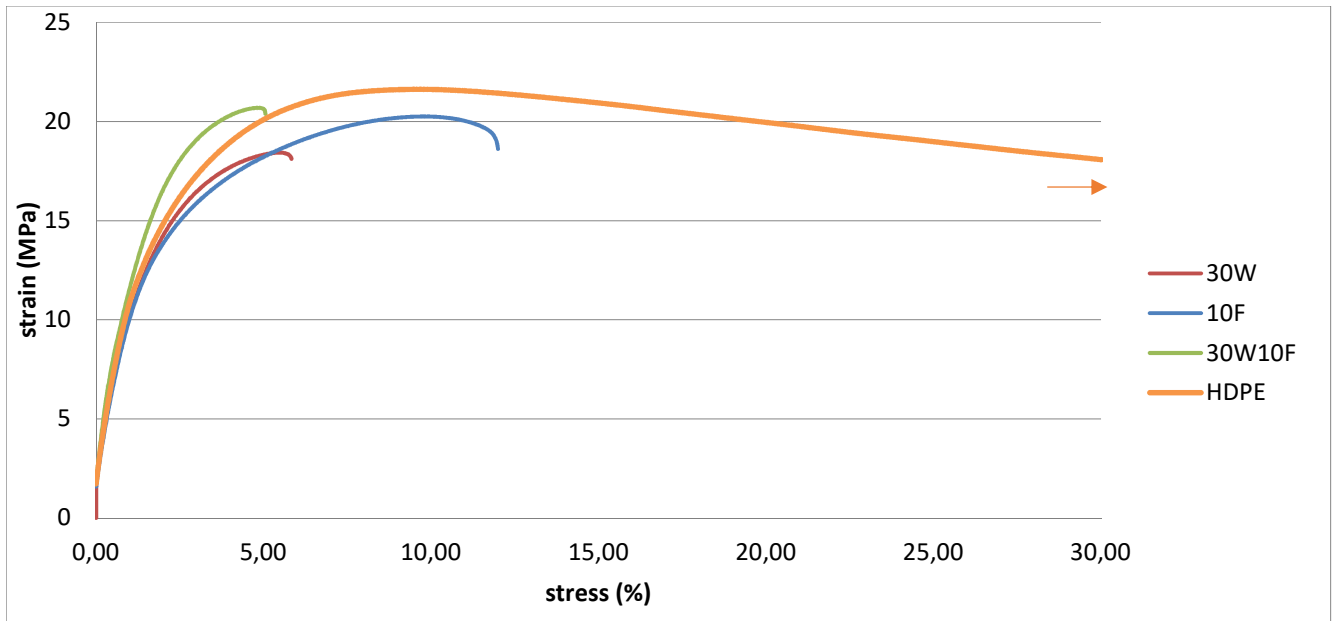


Figure 70: Tensile test results for HDPE based composites with 30wt.% of wood flour, 10wt.% of recycled paper fibres and a mix of two morphologies.

Because of poor interface between natural fillers and HDPE matrix, MAPE (A), Polybond 3029, has been added. In particular, we selected polyethylene grafted maleic anhydride in 3wt.% and 5wt.%. Tensile tests results are displayed in Figure 71 and Table 26.

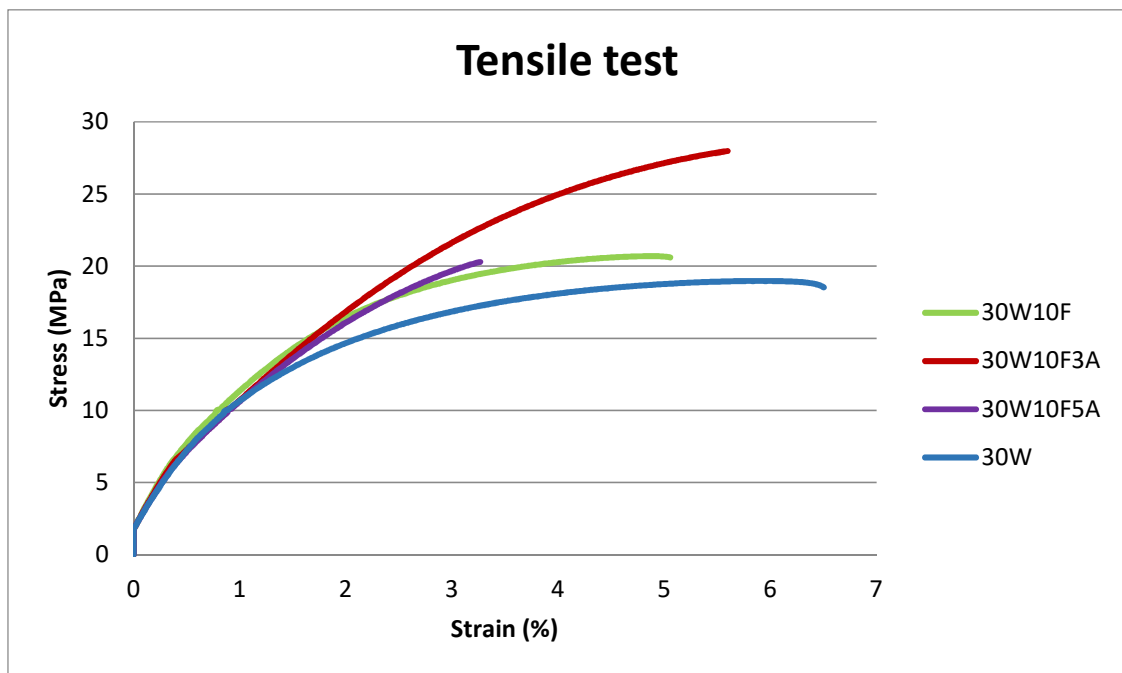


Figure 71: Tensile test results for HDPE based composites with 30wt.% of wood flour, 30wt.% of wood flour and 10wt.% of recycled paper fibres with and without MAPE.

Table 26: Tensile test results for neat HDPE based composite with 30wt.% of wood flour, 10wt.% of recycled paper fibres and with 3wt.% and 5wt.% of MAPE compatibilizer.

Samples	Elastic Modulus (MPa)	Tensile Strength (MPa)
30W10F	1387±78	19 ±1
30W10F3A	1417±100	28±1
30W10F5A	1350±57	20±1

As experienced for HDPE filled with recycled paper fibres, the amount of compatibilizer must be optimized in order to improve its performance. In particular, the addition of 3wt.% of polyethylene grafted with maleic anhydride to HDPE with 30wt.% of wood flour and 10wt.% of fibres allows a small improvement in tensile strength and elongation at break. It does not seem necessary to add more than 3wt.% of MAPE.

In agreement with tensile test results, water absorption (Figure 72) reveals a positive effect of MAPE addition. The same test as for composite with only recycled paper fibres has been performed.

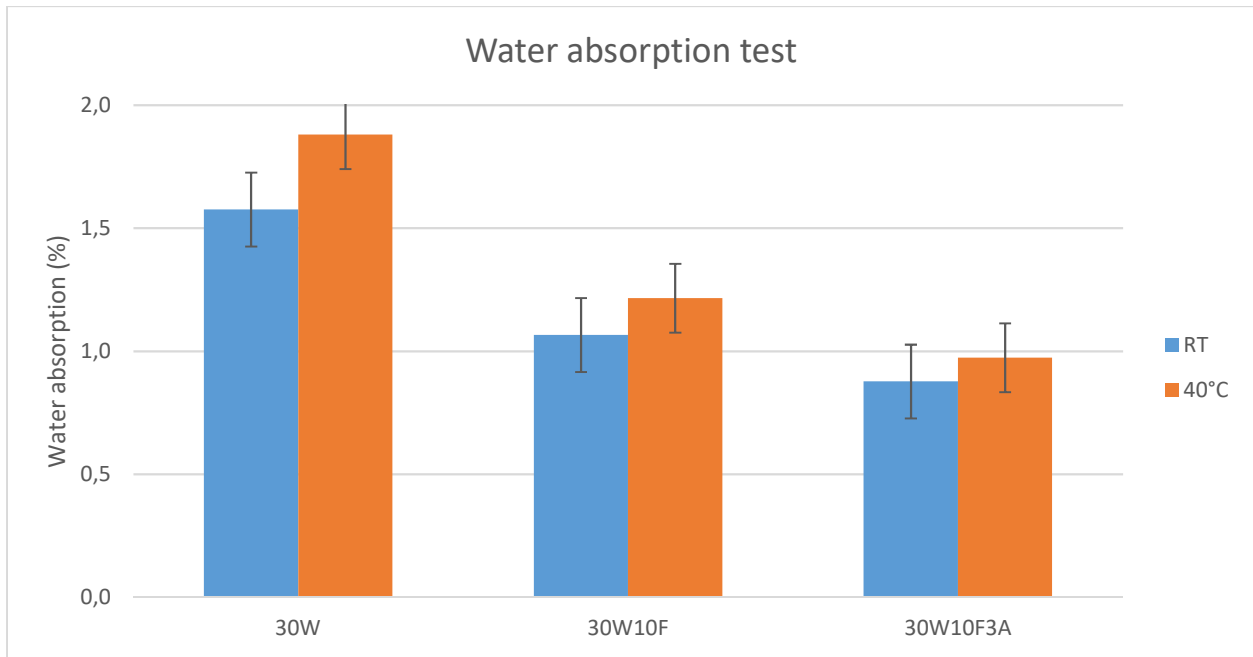


Figure 72: Water absorption tests for HDPE based composites with 30wt.% of wood flour (W),30wt.% of wood flour (W) and 10wt.% of recycled paper fibres (F) with and without MAPE compatibilizer (A).

Despite the addition of almost one third more by volume of cellulosic filler for 30W10F, a lower water absorption was displayed by this composite when compared with 30W. This result suggests a higher homogeneity of the matrix and a good interaction between fillers. The addition of MAPE may allow a reduction of absorbed water, which can be considered as a positive effect of MAPE addition for this amount.

3.3 Conclusions

The analysis of the results obtained shows that the paper can be used as reinforcement in composite with a thermoplastic matrix. In order to introduce paper, a micronization process is needed that has to be optimized to produce fine fibres. The SEM analysis shows the absence of interphase if no MAPE is added. The presence of the right percentage of MAPE seems to improve interactions between fibres and polymer chains .

Recycled paper fibres could also be interesting fillers for WPC.

The best sample was 30W10F3A, provides good balance of properties between different additive percentages tested. MAPE should improve interactions between different fillers (wood flour and recycled paper fibres).

We propose the possibility to use recycled waste paper fibres as filler in thermoplastic matrix composites. Moreover, the mix 30wt.% wood flour and 10wt.% recycled waste paper fibres seems to be interesting for addition in HDPE-PLA blends.

3.4 References

- 1 J. Soucy, A. Koubaa, S. Migneault, B. Riedl, The potential of paper mill sludge for wood plastic composites, *Industrial crops and products*, vol. 54, pp. 248-256, 2014.
- 2 M. Prambauer, C. Paulik, C. Burgstaller, The influence of paper type on the properties of structural paper-polypropylene composites, *Composites: Part A*, vol. 74, pp.107-113, 2014.
- 3 X. Qiao, Y. Zhang, Y. Zhang, Maleic anhydride grafted polypropylene as coupling agent for polypropylene composites filled with ink-eliminated waste paper sludge flour, *Journal of applied polymer science*, vol.91, pp. 2320-2325, 2004.
- 4 C. Burgstaller, W. Ruf, W. Stadlbauer, G. Pilz, R.W. Lang, Utilizing unbleached cellulosic fibres in polypropylene matrix composites for injection moulding, *Journal of biobased materials and bioenergy*, vol. 3, pp. 226-231, 2003.
- 5 A.R. Sanadi, D. Caulfield, Thermoplastic polyolefins as formaldehyde free binders in highly filled lignocellulosic panel boards: using glycerine as a processing aid in kenaf fiber polypropylene boards, *Material Research*, vol 11, pp. 487-492, 2008.
- 6 A.R. Sanadi, highly filled kenaf fiber (85%) thermoplastic composites using a novel process, *Electronic proceeding of: 5th International Conference on Innovative Natural Fibre Composites for Industrial Applications* ISBN 9788890924002.
- 7 M.R. Doshi, J.M. Dyer, *Paper: Recycling and Recycled Materials*, *Encyclopedia of Materials: Science and Technology (Second Edition)*, pp. 6711-6720, 2001.

4 Polymer Blends

A part of this chapter is derived and adapted from “Interactions between PLA, PE and Wood flour: effects of compatibilizing agents and ionic liquids.” By A. Quitadamo, V. Massardier and M. Valente and “Optimization of thermoplastic blend matrix HDPE PLA with different nature and level of coupling agent”, written by A. Quitadamo, V. Massardier, C. Santulli and M. Valente.

Elaboration of PLA based blend

Among bio-derived polymers, PLA achieved great importance as one of the most representative biodegradable polymers on market. The first part of this chapter is focused on the use of PLA as bio-derived polymer in oil-based/bio-derived blends with or without use of compatibilizer. In fact, the interest is to have interaction or even chemical reaction between acid or alcohol groups of PLA and functional groups of Lotader AX8840 (the epoxy group of glycidyl methacrylate) or Polybond 3029 (the anhydride of maleic anhydride). Under specific condition, a possible reaction between the end hydroxyl and/or carboxyl groups of PLA and epoxy groups can occur via nucleophilic substitution [1].

4.1 Effect of functional PE on PLA

Accurate analyses have been first performed in order to evaluate the influence of compatibilizer on PLA. In fact, samples composed of either Lotader AX8840 or Polybond 3029 have been produced and tested (Table 27).

Table 27: Formulations of PLA and PLA-functional Polyethylene blends to evaluate the influence of Lotader AX8840 and Polybond 3029 on PLA.

Sample	PLA (%)	Lotader AX8840 (%)	Polybond 3029 (%)
PLA	100		
PLA75-Lot25	75	25	
PLA75-Poly25	75		25

4.1.1 Tensile tests

Table 28 displays main tensile tests results for PLA, PLA75-Lot25 and PLA75-Poly25. Lotader AX8840 seems to be more efficient in toughness improvement than Polybond 3029: the highest elongation at break was achieved for PLA75-Lot25 at the expense of elastic modulus and tensile

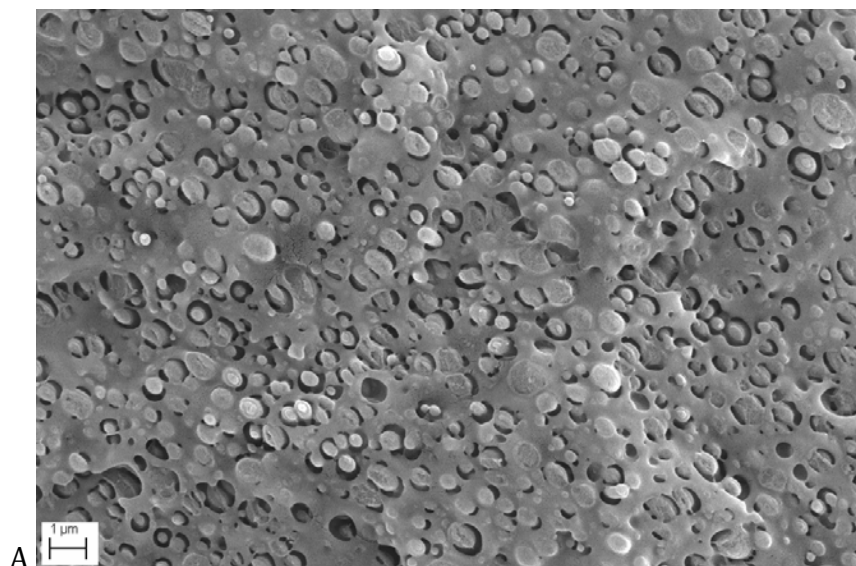
strength. The higher content of glycidyl methacrylate (about 8 wt.%) in comparison to maleic anhydride (about 1.5 to 1.7) can explain the higher efficiency of glycidyl methacrylate-based copolymer.

Table 28: Tensile tests results for neat PLA, PLA75-Lot25 and PLA75-Poly25.

Samples	E (MPa)	σ_{\max} (MPa)	ϵ_{break} (%)
PLA	1490±20	57±1	7.5±0.7
PLA75-Lot25	956±25	39±1	193±47
PLA75-Poly25	1042±94	46±1	28.9±13

4.1.2 Scanning electron microscopy (SEM)

PLA75-Lot25 and PLA75-Poly25 have different surface morphologies. A better dispersion and miscibility is evident for PLA75-Lot25 (Figure 73A) in comparison to PLA75-Poly25 (Figure 73B). Fewer defects are visible for PLA75-Lot25 than in case of PLA75-Poly25. Image analysis was performed by means of the Image J software. PLA75-Lot25 and PLA75-Poly25 have medium particle diameters of $0.51\pm 0.17 \mu\text{m}$ and $1.28\pm 0.62 \mu\text{m}$, respectively. The homogeneity of the former seems better than the one of the latter, in agreement with the higher compatibility between PLA and Lotader AX8840.



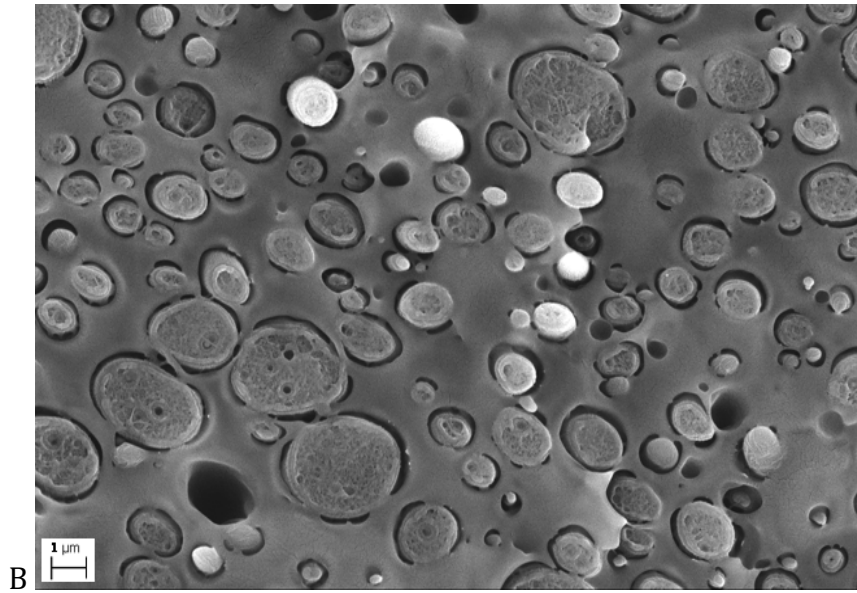


Figure 73: Scanning Electron Microscopy images of PLA75-Lot25 (A) and PLA75-Poly25 (B).

4.1.3 Size Exclusion Chromatography (SEC)

PLA has been analysed through SEC in order to know if there are i) degradation during extrusion and injection moulding processes and ii) thermo chemical degradation when melt blending in presence of functional PE.

PLA, before extrusion and injection moulding processes, is characterized by a molecular weight \overline{M}_w of 63 kDa.

Processing condition seems to be well adapted as PLA \overline{M}_w is maintained at 61kDa. Moreover, \overline{M}_w of 62 kDa have been obtained for PLA when mixed with PE additives, confirming the absence of PLA degradation. In all cases, the PolyDispersity Index (PDI) was close to 1.2. As a consequence, we can suppose that the increased elongation at break is due to PE additives, excluding PLA degradation (verified by PLA) during the production process.

4.1.4 Differential scanning calorimetry (DSC)

DSC evidences the typical cold crystallization peak of PLA (Table 29). This peak refers to the slow crystallization capacity of PLA during the 1st cooling cycle. As a consequence, an additional crystallization occurs during the 2nd heating cycle (cold crystallization) [2]. Both Lotader AX8840 and Polybond 3029 also increase cold crystallisation temperatures and enthalpies. PLA75-Lot25 displays melting ranges and Tg close to neat PLA, but the crystallisation

temperature is higher. Lotader AX8840 seems to inhibit the crystal formation to a certain degree and to increase the ductility of the composites.

PLA75-Poly25 is characterised by higher T_c and enthalpy (as a sum of both Polybond 3029 and PLA crystallization) with respect to both PLA and PLA75-Lot25. Moreover, PLA75-Poly25 has a slightly higher crystallinity than PLA75-Lot25. This result is in agreement with data of TS and SEM images. The two melting peaks at 125.9°C seem to refer to Polybond 3029, while the peak at 167.9°C refers to PLA melting.

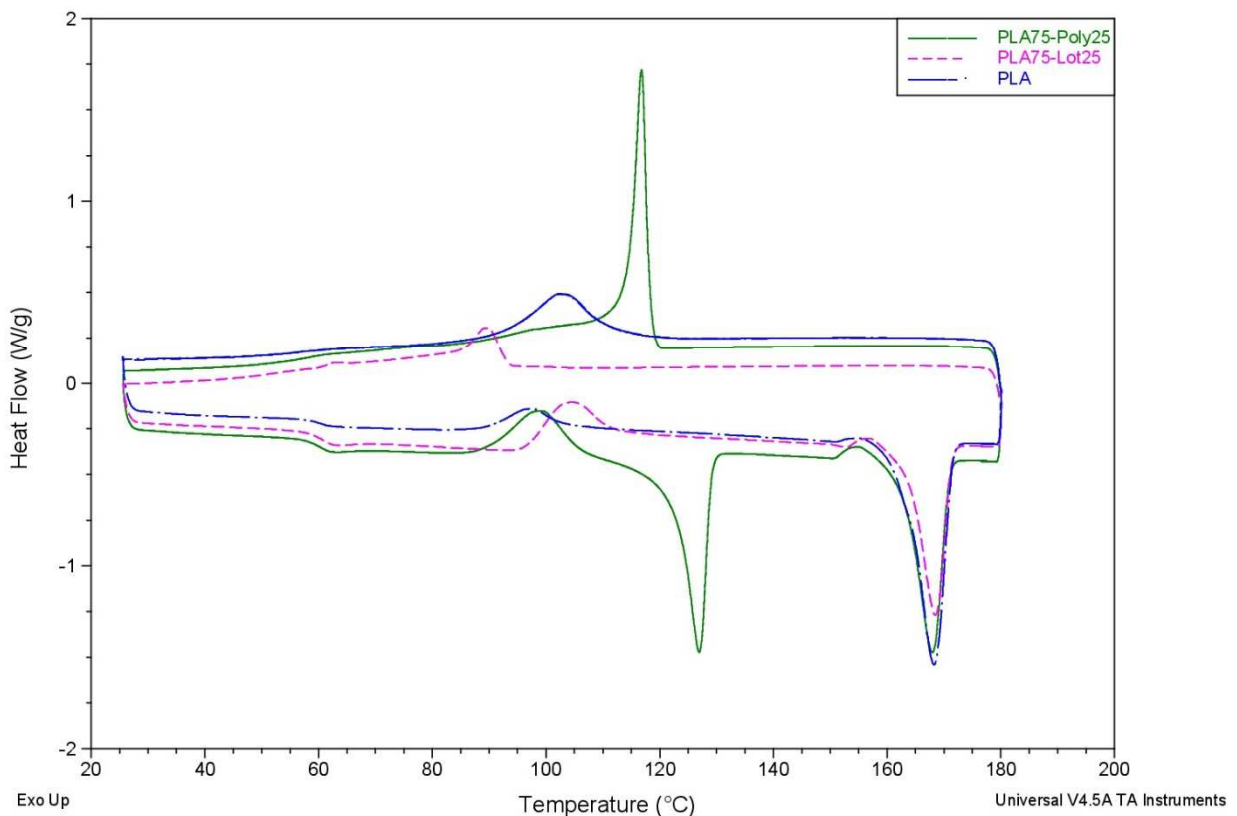


Figure 74: DSC curves of neat PLA (blue), PLA75-Lot25 (fuchsia) and PLA74-Poly25 (green).

Table 29: Differential Scanning Calorimetry results for neat PLA, Lotader AX8840 and Polybond 3029, PLA75-Lot25 and PLA75-Poly 25 blends.

Sample	T_{cc} ($^\circ\text{C}$)	ΔH_{cc} (J/g PLA)	T_m ($^\circ\text{C}$)	ΔH_m (J/g Poly or Lot)	ΔH_m (J/g PLA)	T_g ($^\circ\text{C}$)	T_c ($^\circ\text{C}$)	ΔH_c (J/g PLA)	X_c %(PLA)
--------	----------------------------------	------------------------------	-------------------------------	--------------------------------------	---------------------------	-------------------------------	-------------------------------	---------------------------	-----------------

PLA	98.1	7.6	168.4	-	41.0	60.7	102.5	33.4	36
Lot	-	-	95.3	75.3	-	-	89.5	75.3	
Poly	-	-	120.5	160.4	-	-	112.8	160.4	
PLA75-Lot25	103.5	14.4	168.5	-	30.4	60.7	89.7	16.0	17
PLA75-Poly25	99.0	13.0	126.9/167.9	37.5	37.2	60.4	116.8	61.7	26

4.1.5 ATR-FTIR

ATR-FTIR analyses display absorbance peaks at typical wavenumbers for each bond.

PLA main peaks are:

- 2800-3000 cm^{-1} symmetric stretching vibration of CH groups in saturated hydrocarbons.
- 1749 cm^{-1} stretching vibration of C=O.
- 1630 cm^{-1} bending vibration of H-O-H.
- 1300-1500 cm^{-1} vibration of C-H CH₃.
- 1250-1050 cm^{-1} stretching vibration of C-O and C-O-C.

[3]

Lotader AX8840 main peaks are:

- 2915-2847 cm^{-1} symmetric stretching vibration of CH groups in saturated hydrocarbons.
- 1733 cm^{-1} carbonyl stretching of C=O in glycidyl methacrylate.
- 900 cm^{-1} epoxide rings stretching of C-O in glycidyl methacrylate.

[4]

Polybond 3029 main peaks are:

- 2914-2847 cm^{-1} symmetric stretching vibration of CH groups in saturated hydrocarbons.
- 1700-1800 cm^{-1} stretching vibration of C=O group in maleic anhydride.

[5]

No sensible peaks variation has been detected with this technique, suggesting the absence of reactions between PLA and functional PE. (Figure 75), Because of dilution, it seems difficult to study variation of epoxy peak in the region 850 cm^{-1} .

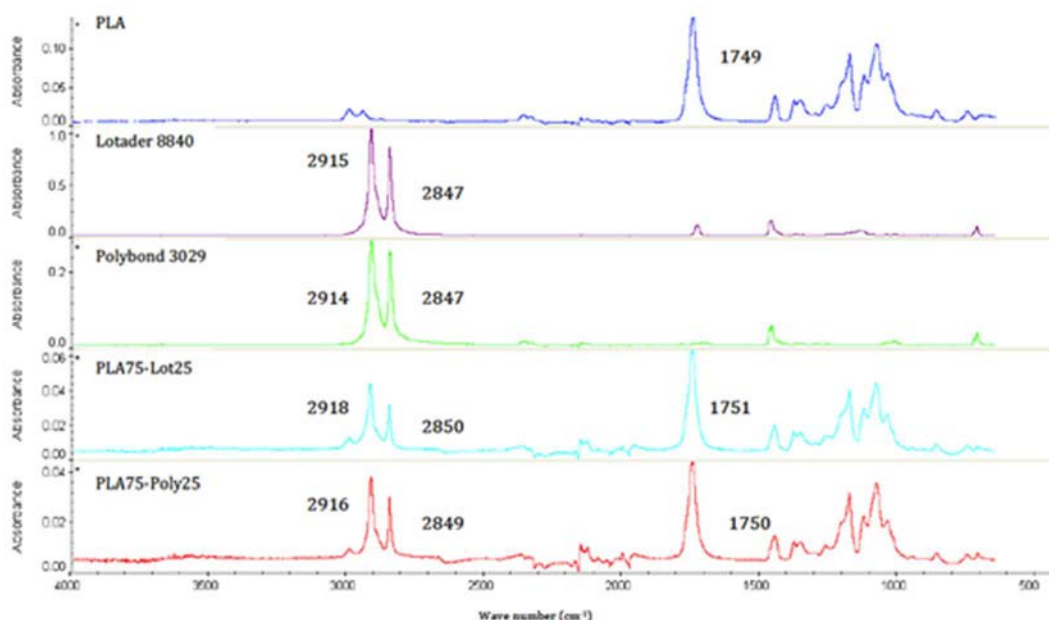


Figure 75: ATR-FTIR spectra of PLA, Lotader AX8840, Polybond 3029, PLA75-Lot25 and PLA75-Poly25.

4.1.6 NMR

NMR analyses (1D ^1H and 1D ^{13}C) were recorded using a Bruker Avance III 400 MHz spectrometer, equipped with a 5mm multinuclear broad band probe (BBFO+) with z-gradient coil. The samples (XX mg) were dissolved in DMSO- d_6 (1 ml), in which PLA only is soluble, and the spectra were recorded at 90°C (363K) and with 256 scans for 1D ^1H and with 10240 scans for 1D ^{13}C . Chemical shifts (in ppm) were expressed relative to the resonance of solvent ($\delta = 2.5$ ppm in ^1H , 39.5 ppm in ^{13}C). This analysis has been performed on PLA75Lot25 in order to validate the absence or low amount of chemical reaction between functional PE and PLA. Figure 76, in fact, displays no variation of NMR spectrum of PLA75Lot25 (red) with respect to neat PLA (blue).

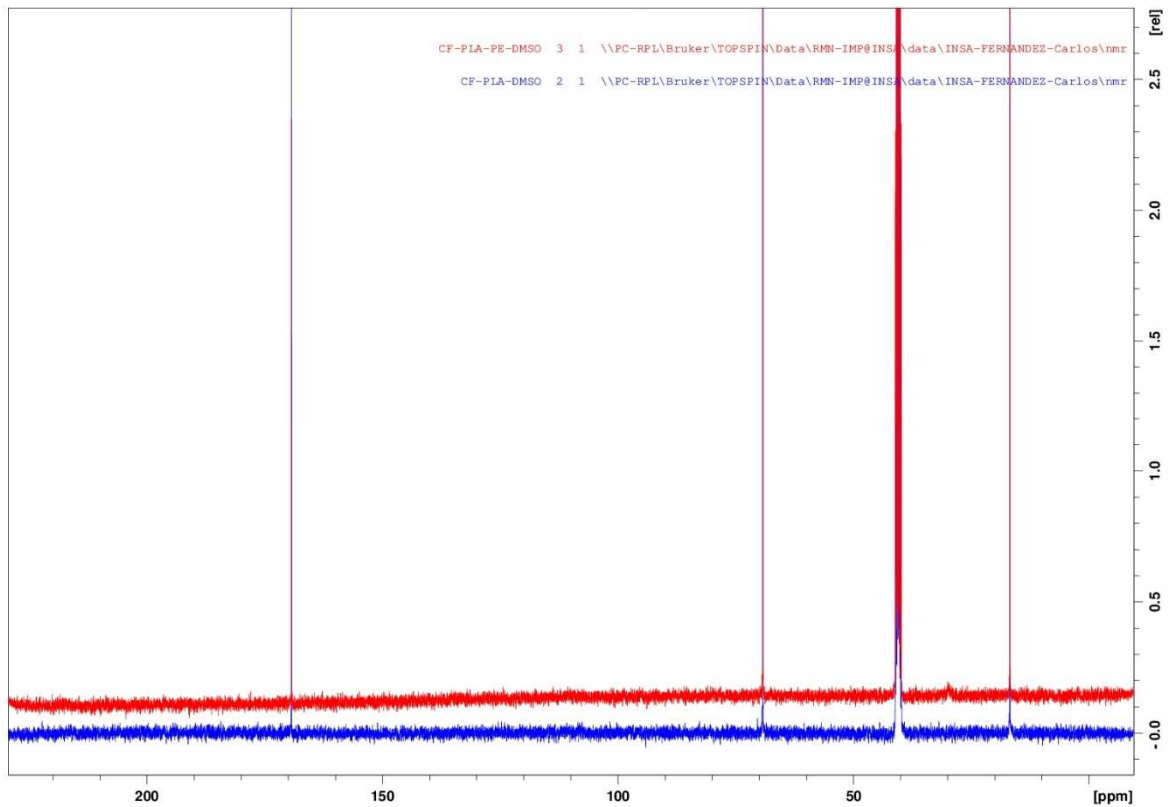


Figure 76: NMR spectra of neat PLA (blue) and PLA75Lot25 (red).

4.2 HDPE-PLA blend

4.2.1 Tensile Test

HDPE-PLA blends properties were first analysed through tensile tests of HDPE70-PLA30, HDPE50-PLA50 and HDPE30-PLA70 to evaluate mechanical performances and to identify the influence on polymer blends. Table 30 and Figure 77 sum up results of these three blends.

Table 30: Tensile tests results of HDPE-PLA blends without compatibilizers.

Samples	E (GPa)	σ (MPa)	ϵ (%)
HDPE	1.2±0.1	21.6±0.2	>400
PLA	3.0±0.1	57.3±1.0	7.1±0.3
HDPE70-PLA30	1.5±0.1	30.8±0.7	>400
HDPE50-PLA50	1.9±0.1	38.7±0.2	99.4±2.1

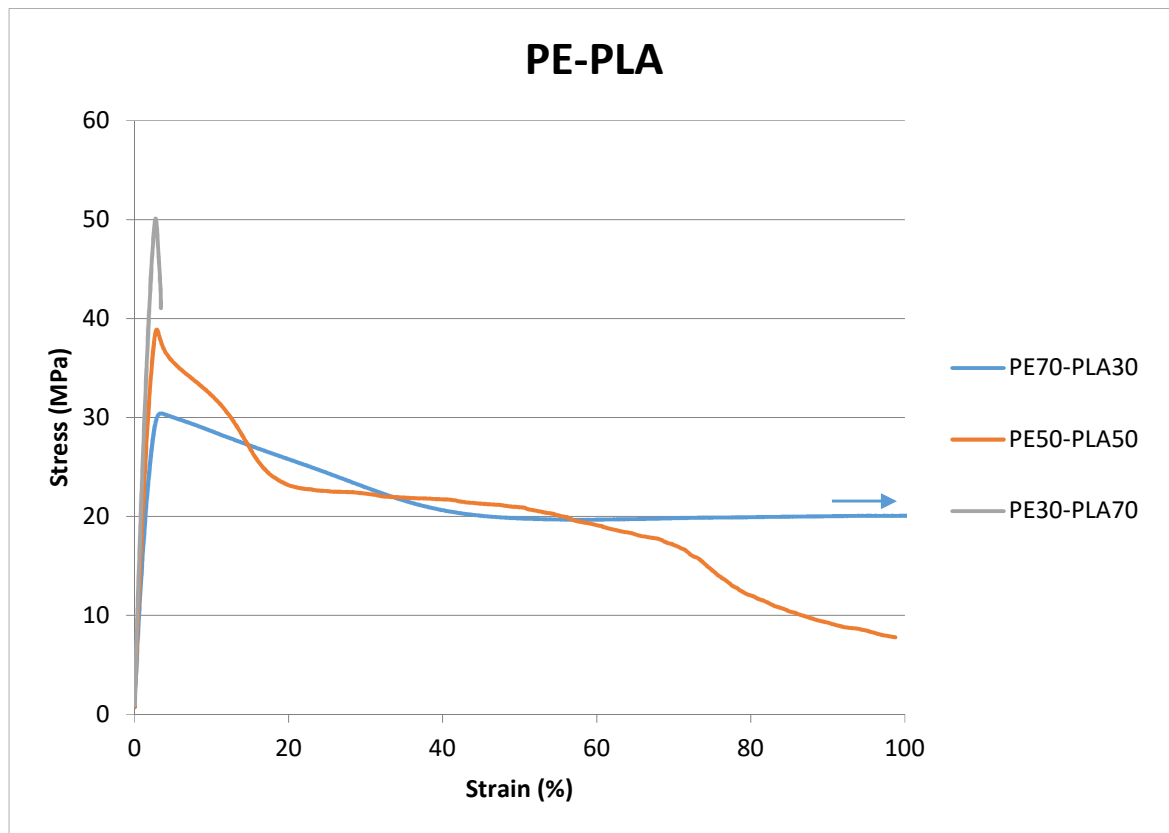


Figure 77: Tensile tests results of HDPE-PLA blends with different ratios (blue HDPE70-PLA30, orange HDPE50-PLA50 and grey HDPE30-PLA70).

The presence of 30 and 50wt.% of PLA allows to obtain good modulus and tensile strength, with respect to neat HDPE, keeping at the same time good elongation at break: which are significant results regarding the considerable amount of a brittle polymer (PLA) blended with HDPE. In contrast, increasing the amount of PLA up to 70wt.% strongly reduces the elongation at break, reaching elastic modulus and tensile strength near to neat PLA. A visible double step fracture has been detected with the blend PE50-PLA50: probably firstly a fracture related to PLA domains fails, with a reduction of stress from the plateaux (around 22 MPa) to lower values, then a failure related to HDPE domains is detected until the complete break of samples at around 100% of deformation. The aim of this work is the possible introduction of the highest amount of bio-derived charge, in agreement with acceptable properties. As a consequence, HDPE50-PLA50 was selected as a promising blend as it offers a satisfying compromise between mechanical properties and amount of bio-based material. Analyses on blends with 50 wt.% PLA

have been considered for deeper analyses. The application of three different percentages of compatibilizers was investigated to elucidate their effects on HDPE50-PLA50 and to identify the most suitable compatibilizer and related amount. In particular, Lotader AX8840 and Polybond 3029 were investigated as compatibilizing agents in the amount of 1, 3 and 5 wt.% (Table 31 and Figure 78).

Table 31: Tensile tests results for HDPE-PLA blend with Lotader AX8840 and Polybond 3029 in different amounts (1, 3, 5wt.%).

Samples	E (GPa)	σ (MPa)	ϵ (%)
HDPE50-PLA50	1.8±0.1	38.7±0.2	99.4±2.1
HDPE50-PLA50-Poly1	2.2±0.1	43.3±2.8	86.2±17.3
HDPE50-PLA50-Poly3	2.3±0.1	42.8±2.6	71.9±46.9
HDPE50-PLA50-Poly5	1.9±0.0	39.7±0.4	34.1±13.1
HDPE50-PLA50-Lot1	2.2±0.2	40.7±4.0	175.3±84.2
HDPE50-PLA50-Lot3	2.1±0.1	41.7±1.9	193.0±59.1
HDPE50-PLA50-Lot5	1.7±0.1	34.3±1.5	173.2±56.2

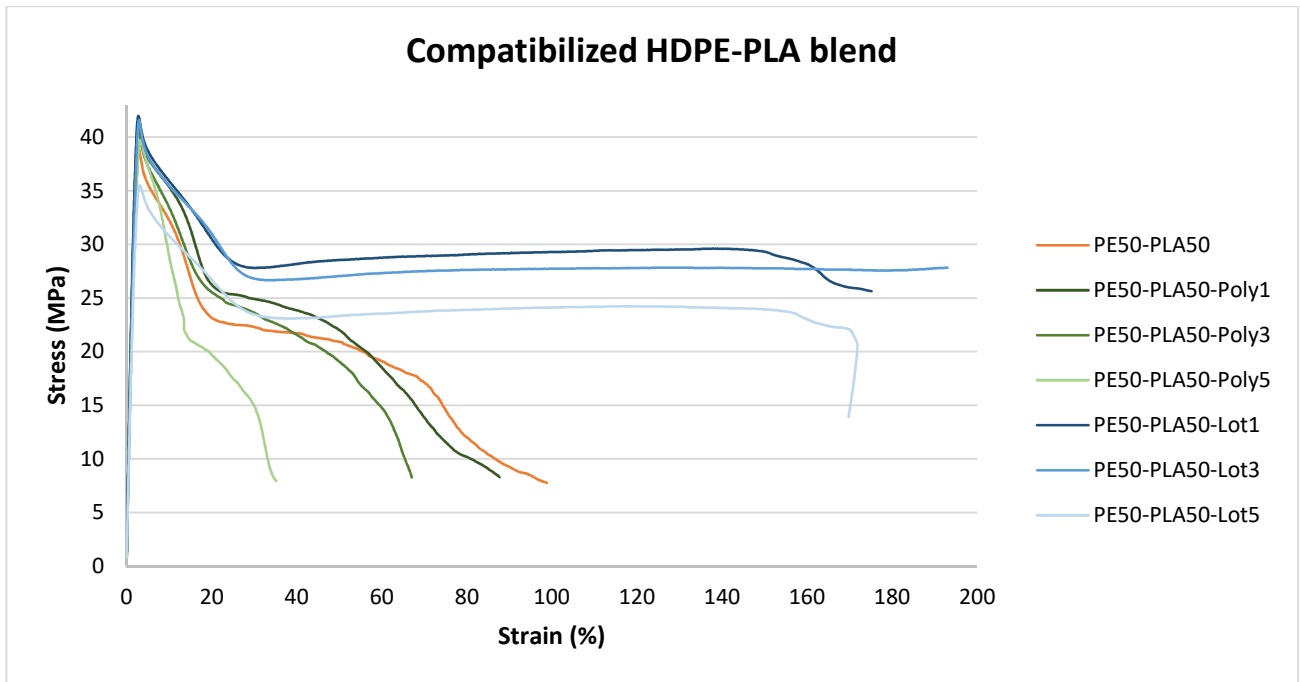


Figure 78: Tensile tests results of compatibilized HDPE50-PLA50 blends with 1, 3 and 5wt.% of Lotader AX8840 and Polybond 3029.

Lotader AX8840 and Polybond 3029 were selected because of their ability to interact with both polyethylene and polymers with polar groups. Moreover, Lotader AX8840 and Polybond 3029 could react with natural fillers, such as wood flour. The addition of Lotader AX8840 seems to be very effective in order to improve compatibility between HDPE and PLA. In fact, a sensitive improvement in elongation at break was displayed for all compatibilizer percentages. At the same time, slight reductions in elastic modulus and tensile strength have been displayed for the highest compatibilizer percentage. Polybond 3029 seems to have a lower compatibility effect with respect to Lotader AX8840, as visible also from tensile tests curves. In fact, despite the absence of a visible double step fracture, a similar trend of curves is visible for PE50-PLA50 with and without Polybond 3029 as compatibilizer. Moreover, the higher the amount of Polybond 3029, the lower the elongation at break. However, the standard deviation related to elongation at break with 3wt.% of Polybond is the higher of the series and interesting elastic modulus and tensile strength have been obtained with this amount of compatibilizer. As a consequence, 3wt.% of Polybond 3029 has been selected as optimal amount.”To conclude, both Lotader AX8840 and Polybond 3029 require an optimal percentage of compatibilizer: and 3 wt % seems to correspond to a good compromise..

4.2.2 Scanning Electron Microscopy (SEM)

Scanning electron microscopy (SEM) analyses aim at investigating both HDPE-PLA compatibility and the influence of compatibilizers on the blends. HDPE-PLA SEM images display typical immiscible blend morphology between hydrophobic (polyethylene) and hydrophilic (poly (lactic) acid) (Figure 79). A visible phase separation of HDPE and PLA is displayed: in fact, as expected for polymer with different hydrophilicities, a weak interface between HDPE and PLA is evident. The problem of compatibilization between polyethylene and poly(lactic) acid polymers is of paramount importance in recent resin manufacturing, and has been partially addressed with interfacially localised catalysts, based for example on stannous octoate [6]. However, the problem appears generally far from being totally resolved.

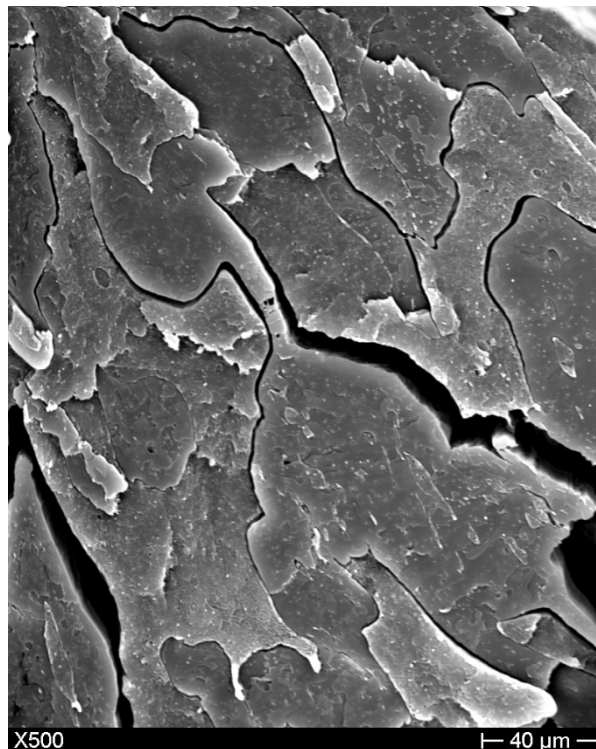


Figure 79: HDPE50-PLA50 blend morphology of cryo-fractured surface.

The addition of compatibilizers to HDPE50-PLA50 blend allows a reduction in the dimension of the different phases, suggesting a higher compatibility between HDPE and PLA (Figure 80). This result is more evident for Lotader AX8840 than for Polybond 3029: in fact, a higher phase separation and easier distinction between polymers was displayed for samples compatibilized with Polybond 3029. The higher affinity of PLA for Lotader AX8840 is in agreement with results

obtained from PLA-compatibilizer analysis, revealing the presence of a smaller spherical secondary phase for Lotader AX8840 than for Polybond 3029 when blended with PLA. Reactive groups of compatibilizers can interact with hydroxyl and/or carboxyl groups of PLA, while ethylene chain of compatibilizers can easily be mixed with HDPE. These results are in agreement with FTIR analyses.

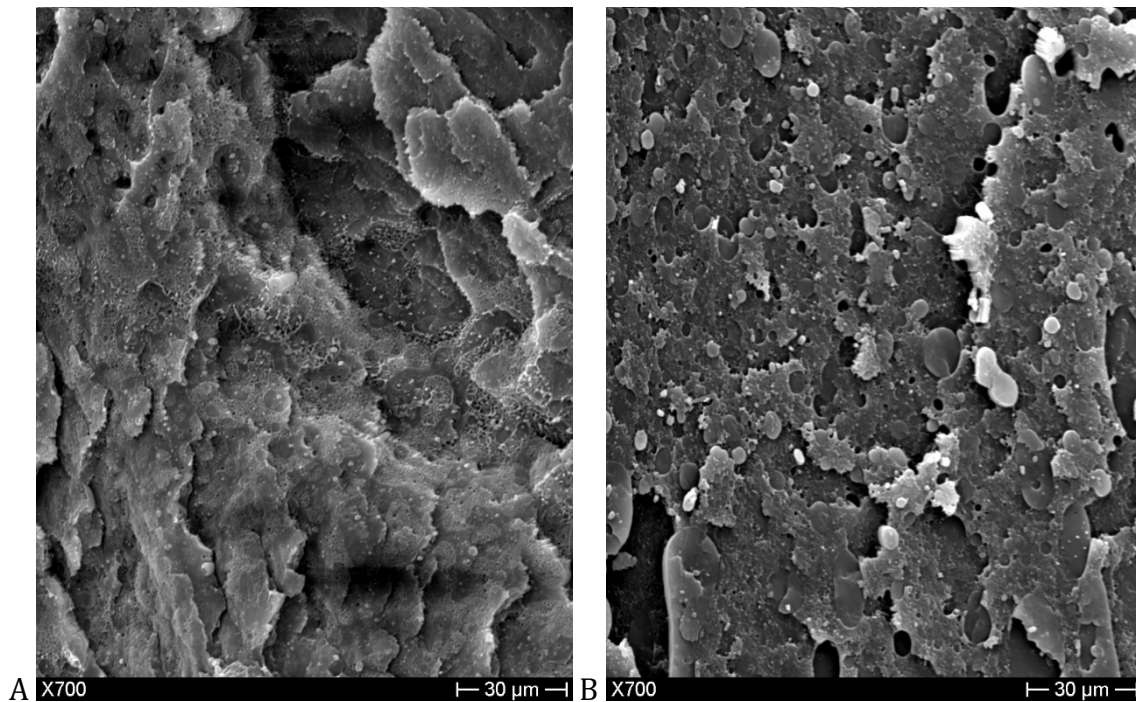


Figure 80: HDPE50-PLA50 blend with 3wt.% of Lotader AX8840 (A) and Polybond 3029 (B) of cryo-fractured surface.

4.2.3 Differential Scanning Calorimetry (DSC)

Differential Scanning Calorimetry was useful for analysing the combined effects of blending HDPE with PLA, and the effects of adding compatibilizers and wood flour. ΔH_{mPE} (J/gPE) and ΔH_{mPLA} (J/gPLA) refers to enthalpies value to the exact amount of polyethylene and poly(lactic acid) in the samples. For example, HDPE50-PLA50 displayed ΔH_{mPE} of 113.2 J/g but we have to divide by 0.5 to obtain the real amount of enthalpy referred to HDPE; as a consequence, the effective ΔH_{mPE} is 226.4 J/gPE. Table 32 and Figure 81 sum up DSC results for HDPE, PLA and HDPE50-PLA50.

Table 32: DSC results for HDPE, PLA and HDPE50-PLA50.

Samples	ΔH_{CCPLA} (J/gPLA)	TCC (°C)	ΔH_{mPE} (J/gPE)	T _{mPE} (°C)	ΔH_{mPLA} (J/gPLA)	T _{mPLA} (°C)	T _{gPLA} (°C)
HDPE	-	-	215	134	-	-	-
PLA	7	98	-	-	41	168	61

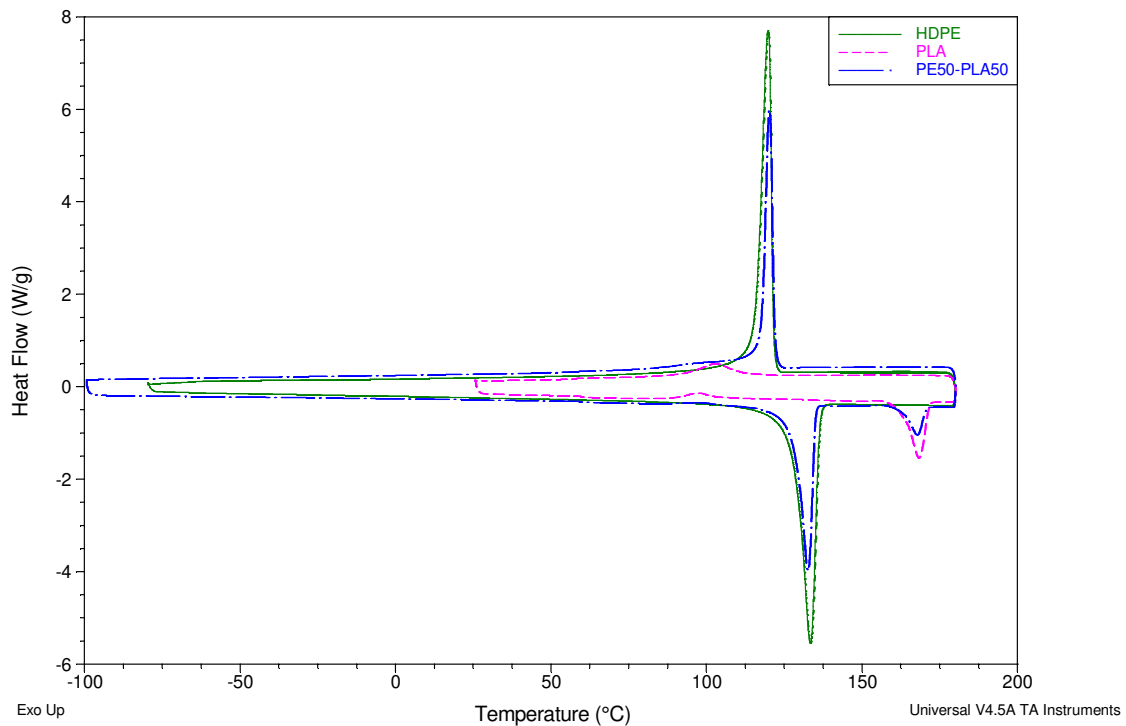


Figure 81: Differential Scanning Calorimetry thermograms of neat PLA, HDPE and HDPE50-PLA50.

Interesting results have been displayed for HDPE50-PLA50 blends. The typical PLA cold crystallization process [2] is still revealed by HDPE50-PLA50. Moreover, slightly higher crystallinity of HDPE phase is demonstrated, in agreement with both higher mechanical properties of the blend and with a phase separation because of the presence of crystals [7]. The effect of Lotader AX8840 and Polybond 3029 on HDPE50-PLA50 properties was also analysed (Table 33). Both Polybond 3029 and Lotader AX8840 addition reveal the presence of cold crystallization. Higher cold crystallization enthalpies values were measured for Lotader AX8840 addition with respect to Polybond 3029, but in both cases, the influence of adding different amounts of compatibilizers is not evident. A possible interpretation for higher cold crystallization enthalpies is that the addition of compatibilizers possibly reduced PLA chain mobility from molten state, increasing the possible organization of crystals from solid state.

A more evident effect of compatibilizer addition is displayed with Lotader AX8840, displaying lower melting enthalpy for HDPE phase. This result suggests an interaction between HDPE and PLA through Lotader AX8840, hindering HDPE macromolecules mobility [8].

Table 33: DSC results of HDPE50-PLA50 with 1-3-5 wt.% of Lotader AX8840 or Polybond 3029.

Sample	ΔH_{CCPLA} (J/g _{PLA})	T _{CC} (°C)	ΔH_{mPE} (J/g _{PE})	T _{mPE} (°C)	ΔH_{mPLA} (J/g _{PLA})	T _{mPLA} (°C)	T _{gPLA} (°C)
HDPE50-PLA50	16	97	236	132	40	168	62
HDPE50-PLA50-Poly1	15	94	195	132	40	168	61
HDPE50-PLA50-Poly3	15	100	190	132	41	168	61
HDPE50-PLA50-Poly5	16	101	198	132	41	168	61
HDPE50-PLA50-Lot1	20	103	192	132	40	168	61
HDPE50-PLA50-Lot3	21	103	182	132	41	168	61
HDPE50-PLA50-Lot5	20	104	192	132	36	168	61

4.2.4 Thermogravimetric Analysis (TGA)

In order to evaluate thermal stability of our blends, analyses are focused on onset Temperature (Tonset) of degradation (Table 34). PLA reveals a lower thermal stability compared to HDPE: in fact, Tonset is around 319°C for PLA and 458°C for HDPE. Blending HDPE and PLA (HDPE50-PLA50) results in a Tonset near to neat PLA, confirming a reduced thermal stability of the blend (322°C) with respect to neat HDPE (458°C). All formulations display a complete degradation of polymers, without formation of a residual char (100% of mass variation Δm between the total amount of sample before the test and the residual mass after the test). The addition of Lotader AX8840 increases blend thermal stability, with higher Tonset when increasing Lotader AX8840 amount. Blend formulations, either compatibilized or not, display two separated thermal degradations, the first refers to poly(lactic)acid and the second to polyethylene. A maximum rate of weight loss corresponds to each degradation step. Blend formulations exhibit two separated temperatures of the peak value for the first derivative of the TGA curve (TDTG).

Table 34: TGA results for HDPE-PLA blends with different compatibilizer percentages, HDPE50-PLA50 matrix composites with 3 wt.% of compatibilizer and 20, 30 or 40 wt.% of wood flour. T_{onset} ($^{\circ}\text{C}$) are evaluated with the extrapolated onset temperature from TGA curve. T_{DTG} ($^{\circ}\text{C}$) are the temperatures of maximum DTG curves peaks. Δm (%) are the mass variation percentages between the total amount of sample before the test and the residual mass after the test.

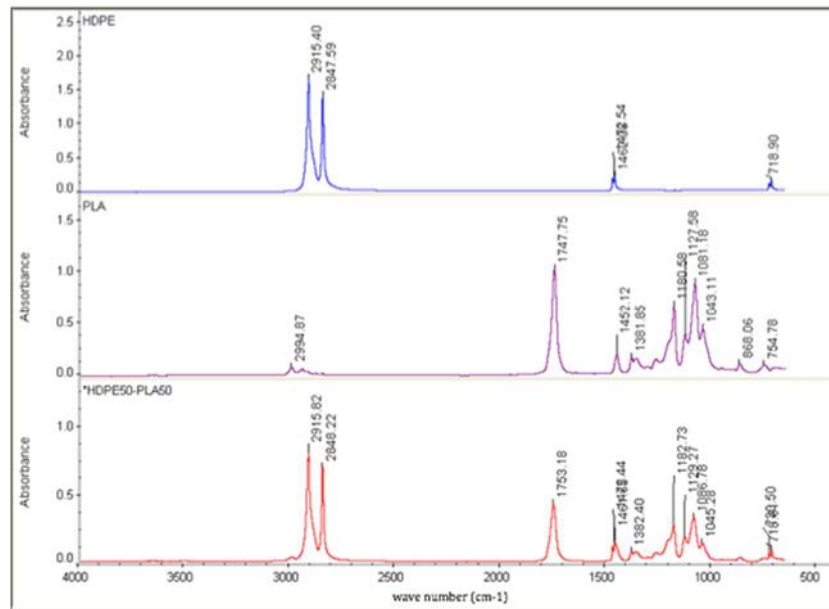
Samples	T_{onset} ($^{\circ}\text{C}$)	T_{DTG} ($^{\circ}\text{C}$)	Δm (%)
HDPE	458	474	100
PLA	319	351	100
Poly	459	480	100
Lot	434	464	100
HDPE50-PLA50	322	345/471	100
HDPE50-PLA50-Poly1	316	351/444	100
HDPE50-PLA50-Poly3	322	358/438	100
HDPE50-PLA50-Poly5	313	342/432	100
HDPE50-PLA50-Lot1	325	350/470	100
HDPE50-PLA50-Lot3	325	350/468	100
HDPE50-PLA50-Lot5	334	351/474	100

4.2.5 Infrared Analysis Attenuated Total Reflection (ATR-FTIR)

Infrared spectroscopy has been done to evaluate interactions between polymers, and the main results are displayed in figure 68. As expected, HDPE50PLA50 does not display peaks variation confirming the presence of an immiscible blend without interactions between HDPE and PLA

(Figure 82A). The addition of Lotader AX8840 and Polybond 3029 do not display variation of HDPE50-PLA50 peaks(Figure 82B).

A



B

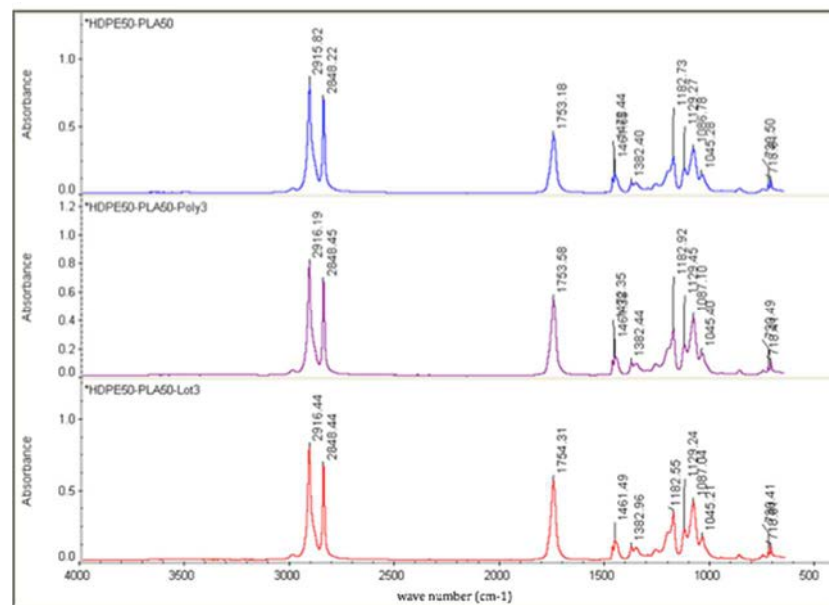


Figure 82: Infrared spectra (ATR-FTIR) of A) HDPE, PLA and HDPE50-PLA50 and B) HDPE50-PLA50, HDPE50-PLA50-Poly3 and HDPE50-PLA50-Lot3.

4.3 Elaboration of SPI based blends

SPI achieved great importance in eco-friendly materials, displaying good biocompatibility, biodegradability and compostability. SPI has been used as bio-derived polymer as a possible alternative to PLA. Similarly to PLA paragraph, first the effect of compatibilizer on SPI is exposed, and then HDPE-SPI properties are displayed.

4.4 Effect of compatibilizer on SPI

We have analysed different blend ratios of random copolymer of ethylene glycidyl methacrylate (Lotader AX8840, named as Lot), soy protein isolate (SPI), and plasticizer effect (Glycerol named as Gly) on the optimal blend obtained in terms of high amount of biodegradable polymer as well as mechanical properties. SPI was dried one night at 80°C, before processing. A Micro 15 Twin-screw DSM research extruder was used at 120°C, with screw speed of 100 rpm, N₂ atmosphere (Ljungberg 2002), and 3 min residence time. The injection moulding temperature was 55°C, and pressure parameters were depending on the polymer viscosity. Injection moulding has been performed in order to obtain both dog-bone specimens of 4x2x30 mm³ (TxWxL), as well as disks of 40mm diameter and 1.5mm width for rheology tests. SPI disks have been obtained by compression moulding at 120°C because of impossibility to extrude SPI alone. Table 35 displays compositions and processing conditions of Lotader AX8840-Soy Protein Isolate (SPI) blend.

Table 35: Composition and processing conditions for Soy Protein Isolate (SPI) based blend.

Sample	Process	Lotader AX8840 (%)	Soy Protein Isolate (%)	Glycerol (%)
Lotader AX8840	Injection moulding	100		
SPI (presse)	Compression moulding		100	
SPI70-Gly30 (presse)	Compression moulding		100	
Lot75-SPI25	Injection moulding	75	25	
Lot75-(SPI90-Gly10)25	Injection moulding	75	22.5	2.5

Lot75-(SPI70-Gly30)25	Injection moulding	75	17.5	7.5
Lot65-(SPI70-Gly30)35	Injection moulding	65	24.5	10.5
Lot50-(SPI70-Gly30)50	Injection moulding	50	35	15
Lot35-(SPI70-Gly30)65	Injection moulding	35	45.5	19.5

4.4.1 Tensile tests

Tensile tests have been performed in order to evaluate mechanical properties of blends as well as the influence of individual components. Figure 69 displays glycerol influence on Lotader AX8840-SPI blends.

Keeping a ratio Lotader AX8840-SPI of 75-25, SPI have been plasticized with 10 and 30 wt.% of glycerol.

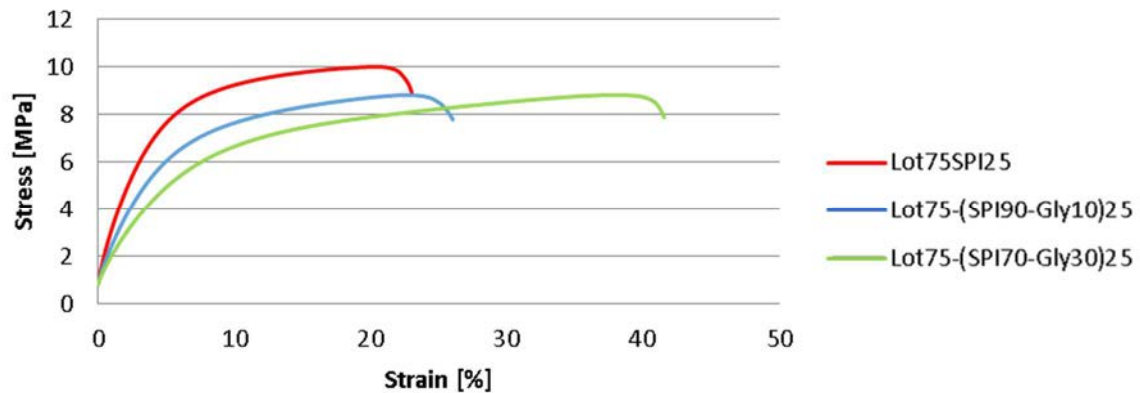


Figure 83: Tensile tests results of Lotader AX8840-Soy Protein Isolate (SPI) blend with 10 and 30 wt.% of plasticizer (Glycerol).

Table 36: Tensile tests results for Lotader Ax8840 SPI blend with different amount of glycerol.

	E_{mod} GPa	F_{max} MPa	dL at break %
Lot75SPI25	0.16±0.01	9.8±0.4	22.9±1.2
Lot75-(SPI90Gly10)SPI	0.10±0.01	8.2±0.6	26.7±2.2
Lot75-(SPI70Gly30)SPI	0.07±0.01	8.9±0.5	42.4±1.8

The addition of glycerol allows an improvement in blend toughness, at the expense of elastic modulus, while tensile strength remains approximately constant. As reported in literature [8-9], 30 wt.% of glycerol allows a good balance of mechanical properties. Starting from these results, samples with different Lotader AX8840-SPI ratios have been tested (Table 37), increasing SPI amount from 0.7 x 25wt.% to 0.7 x 65wt.%.

Table 37: Tensile tests results of 30.wt% glycerol plasticized SPI blended with different ratios of Lotader AX8840.

Samples	E (MPa)	σ (MPa)	ε (%)
Lot75-SPI25	185±6	9±1	22±2
Lot75-(SPI70-Gly30)25	86±4	9±1	37±1
Lot65-(SPI70-Gly30)35	169±8	8±1	12±1
Lot50-(SPI70-Gly30)50	122±13	7±1	20±4
Lot35-(SPI70-Gly30)65	117±5	9±1	26±1

The introduction of SPI in blend with Lotader AX8840 requires also the addition of glycerol to obtain better performances, in agreement with previous results. We keep constant the ratio between SPI and glycerol at 70wt.%-30wt.% respectively. Results of Table 37 shows that our process enables to obtain materials with acceptable properties even with about half of the mass corresponding to SPI.

4.4.2 Rheological measurements

Production process seems to be more complicated when SPI is added in the extruder. Rheological behaviour analyses, as a consequence, have been carried out to study SPI influence, especially on viscosity variation.

Dynamic viscosity η^* has been evaluated through a frequency sweep between 0.1 and 100 rad/s at 120°C (processing temperature of Lotader AX8840-SPI blends) and 5% of deformation (selected to perform analyses in linear elasticity range of our blends). Section Rheological measurements (ARES G2) of Chapter 2 “Materials and Methods” explains how preliminary studies have validated the selected parameters. In this paragraph, only results related to frequency sweep tests will be described.

As expected, the addition of SPI to Lotader AX8840 increases dynamic viscosity with respect to neat Lotader AX8840. In fact, the highest SPI amount, the highest η^* , especially at low frequencies. Figure 84 displays dynamic viscosity as a consequence of angular frequency for neat Lotader AX8840 and blend with SPI in four different ratios (75-25, 65-35, 50-50 and 35-65).

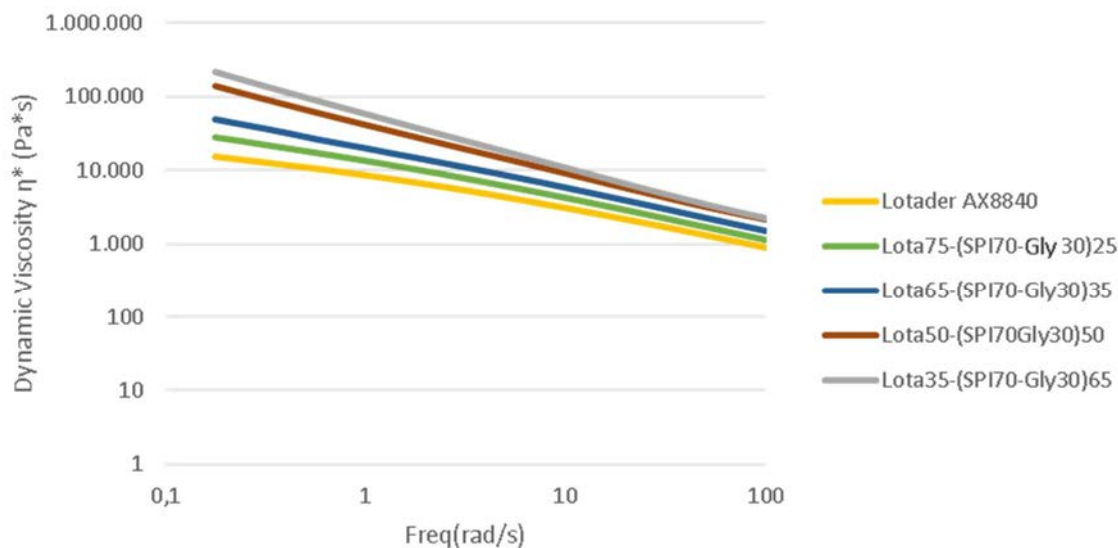


Figure 84: Dynamic viscosity of Lotader AX8840 and its blends with SPI.

Lotader AX8840, as polymer melts, is a non-Newtonian liquid, characterized by viscosity reduction with increasing shear rate. This phenomenon is known as Shear Thinning behaviour,

representative of polymer processing. In fact, lower viscosity is detected near injection, helping polymer processing during the injection phase. On the contrary, polymer viscosity increases once the polymer is into the reservoir because of lower shear rate, providing the mobility control desired [11].

A certain linearity between viscosity and Lotader AX8840 concentration in the blends has been obtained, as suggested in Figure 71. The higher the Lotader AX8840 percentage in the blend, the lower the dynamic viscosity. This trend can be useful in order to predict blends viscosity before processing in the analysed range.

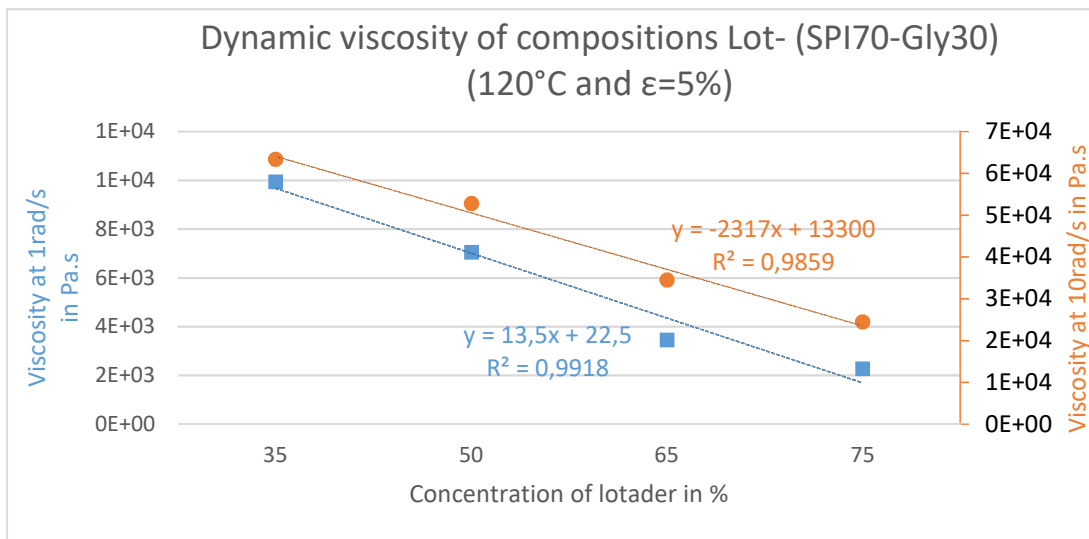
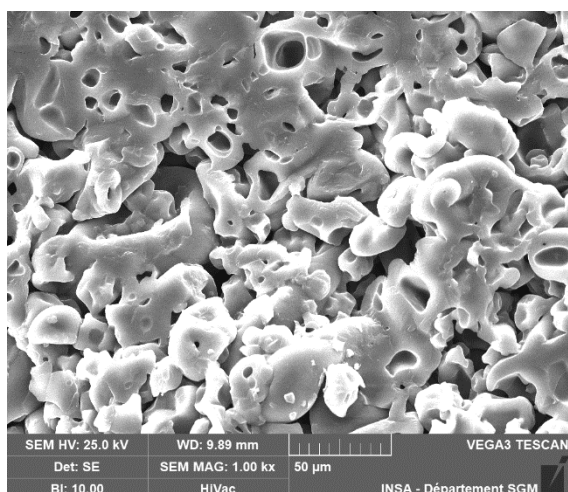


Figure 85: Dynamic viscosity of Lot-(SPI70-Gly30) for different blend ratios.

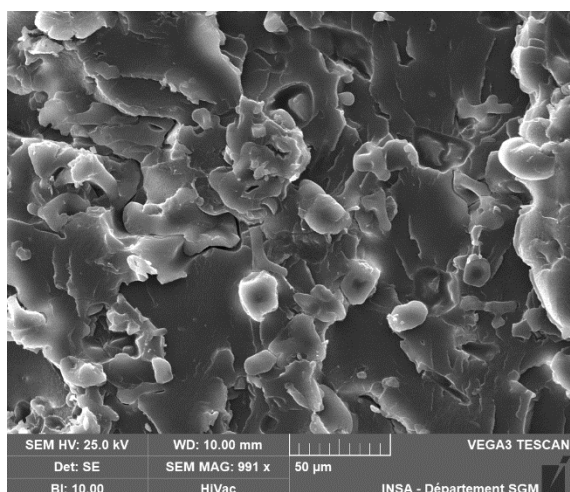
4.4.3 Scanning Electron Microscopy (SEM)

First investigations have been done on the influence of Glycerol on Lotader AX8840-SPI blends. Figure 86 displays different morphologies for SPI-Glycerol (A) and Lotader AX8840-SPI blend without glycerol addition to SPI (B), with 10 and 30wt.% of glycerol (C and D respectively).

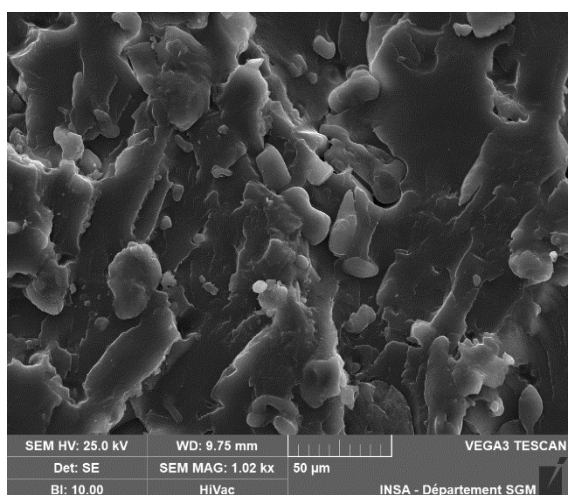
A



B



C



D

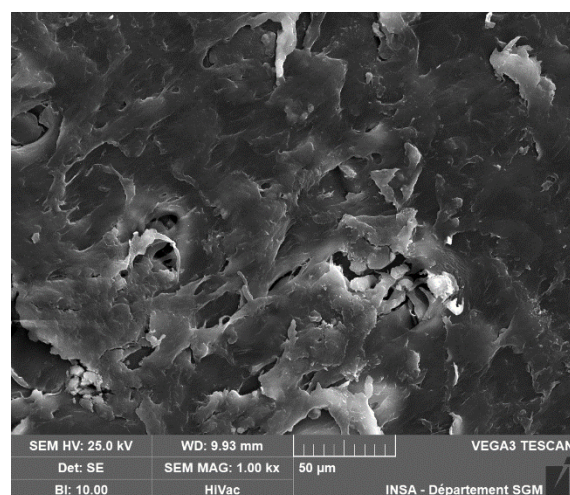


Figure 86: SEM images of A) SPI70-Gly30, B) Lot75-SPI25, C) Lot75-(SPI90-Gly10)25, D) Lot75-(SPI70-Gly30)25.

Nodular shape of SPI, visible in SPI70-Gly30 image, is still present when SPI is blended with Lotader AX8840. Moreover, a phase separation is observable between SPI and Lotader AX8840, in agreement with moderate elongation at break and higher Young modulus.

Higher homogeneity is displayed when glycerol is added to SPI, in coherence with mechanical properties. In fact, the higher the glycerol content, the higher the deformation.

Another investigation has been performed, analysing the influence of different blend ratios.

Figure 74 displays samples with increasing Lotader AX8840 percentage from 35 wt.% (figure A) to 75wt.% (figure D).

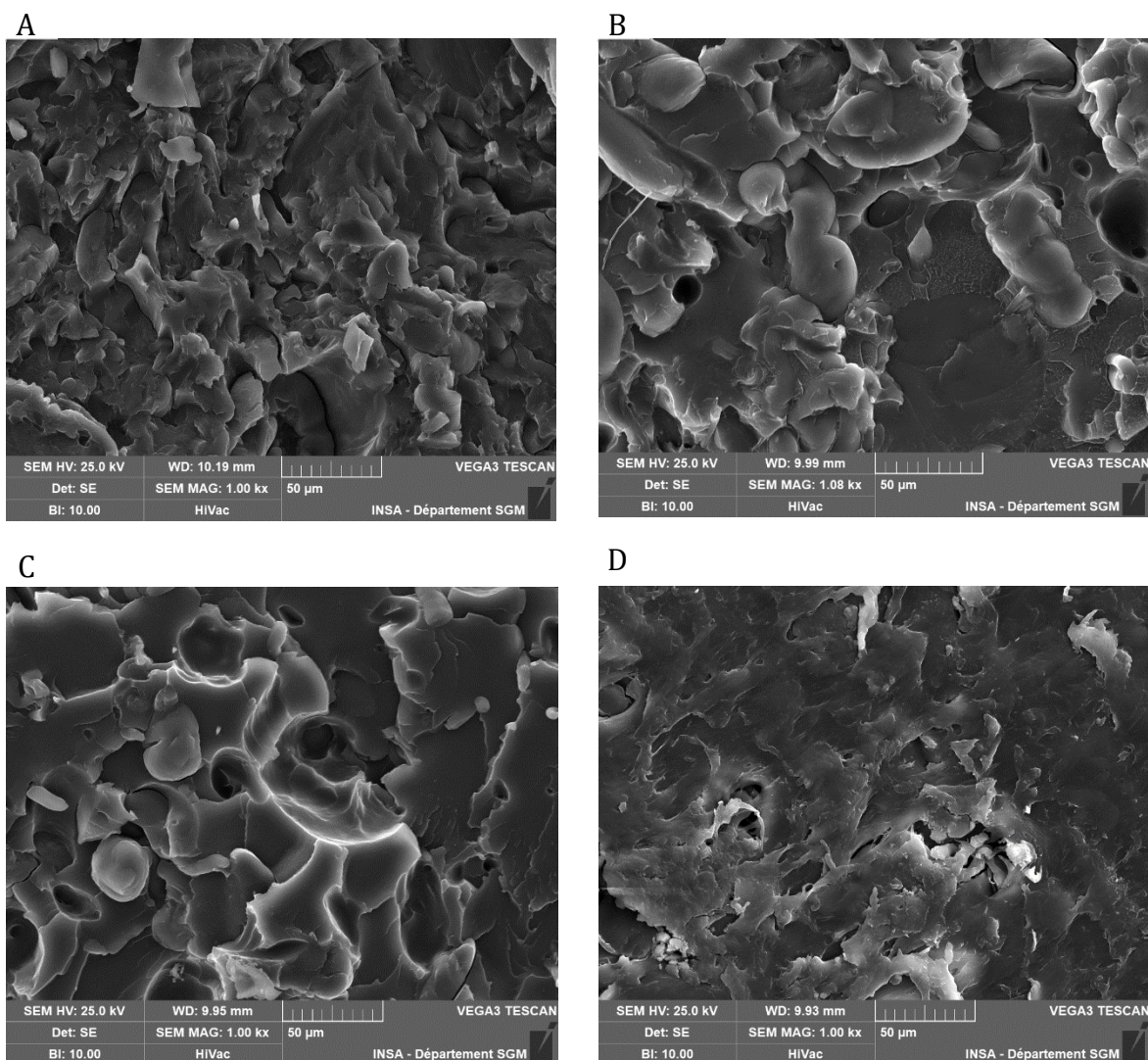


Figure 87 : SEM images of a) Lot35-(SPI70-Gly30)65 , b) Lot50-(SPI70-Gly30)50, c) lot65-(SPI70-Gly30)35 , d) lot75-(SPI70-Gly30)25 at 120°C with secondary electrons SE

As expected, the higher the Lotader AX8840 content the lower the area of the SPI nodular phase. As a consequence, nodules in images are supposed to be SPI phase. Using ImageJ as software for image analysis, SPI area of about $865 \pm 519 \mu\text{m}^2$ have been observed in Lot50-(SPI70-Gly30)50, while SPI area extension is about $379 \pm 142 \mu\text{m}^2$ in Lot75-(SPI70-Gly30)25. As a consequence, a lower homogeneity is displayed with high SPI content. In fact, the lower the SPI content, the smaller both SPI area and standard deviation, suggesting a better homogeneity and distribution of SPI in Lotader AX8840.

4.4.4 Thermogravimetric Analysis (TGA)

Samples thermal stability has been evaluated through thermogravimetric analysis, studying the influence of different elements on blends properties in order to investigate the accuracy of selected processing parameters.

First, the influence of glycerol on SPI degradation is displayed in Figure 88.

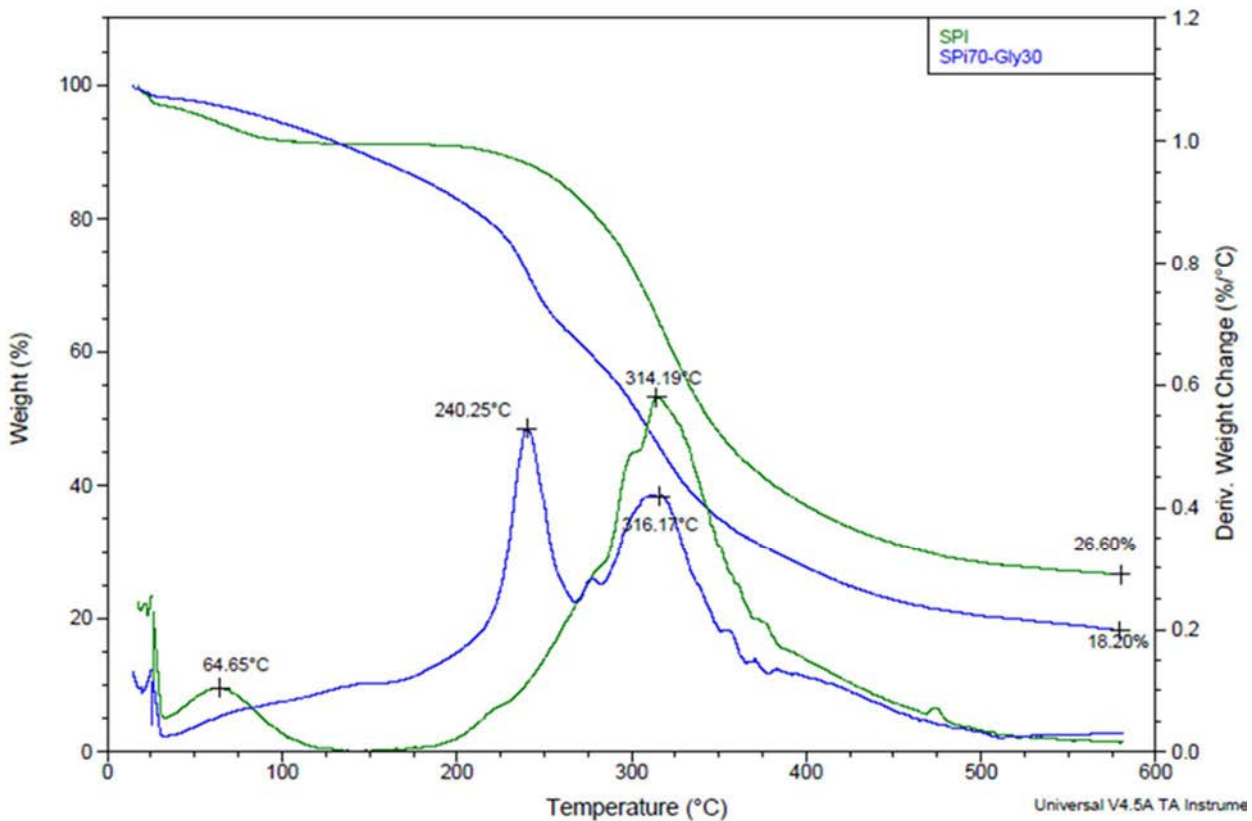


Figure 88: Influence of Glycerol on SPI degradation.

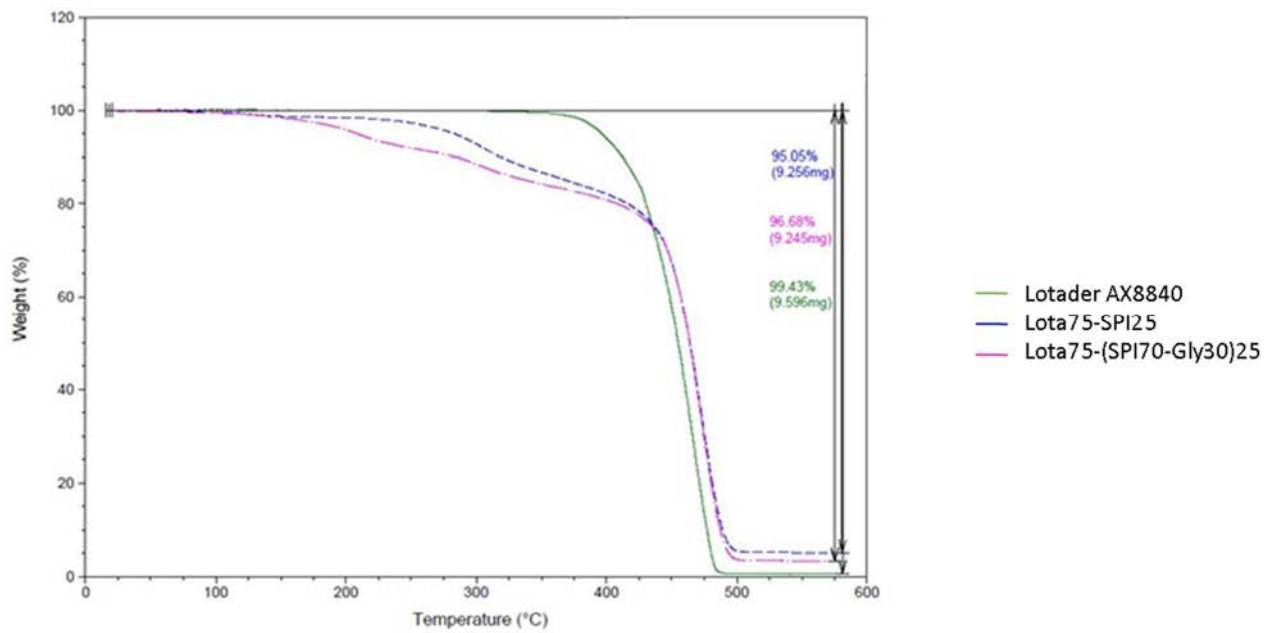
Results obtained from thermogravimetric analysis for SPI and SPI70-Gly30 are similar to those obtained in literature [12]. Soy protein isolate displays a first peak around 65°C, related to loss of moisture, and a second peak around 314°C, related to protein degradation. Glycerol addition reveals the presence of another peak, around 240°C, suggesting glycerol degradation because of the absence of this peak in the previous thermogram. These analyses display no sensitive degradation of SPI for temperatures around 120°C, suggesting a good choice of processing parameters.

SPI and SPI70-Gly30 display a residual mass after analysis until 600°C. Glycerol is normally completely degraded before 600°C. As a consequence, the residual mass is related to SPI. Considering the amount of SPI in each sample (100% in SPI and 70% in SPI70-Gly30), the residual mass is approximately the same (around 26% in both cases). In agreement with FTIR

spectra of SPI based blends, these results suggest that no chemical reaction occurs between SPI and glycerol. As a consequence, the same thermal behaviour is displayed for the thermogram related to SPI degradation.

On the contrary, no mass residue has been observed for Lotader AX8840 degradation, as usually expected for polyolefins. Figure 89A displays mass variation during the test: Lotader AX8840 displays a single step degradation while blends (both with or without glycerol) display a first step related to SPI (and glycerol when mixed in the blend) and a second step at higher temperature related to Lotader AX8840. In agreement with a single or multiple step degradation, Figure 89B displays only one peak for Lotader AX8840 degradation at 466°C, while Lot75-SPI25 reveals two peaks (the first at 301°C related to SPI and the second at 473°C to Lotader AX8840).

A



B

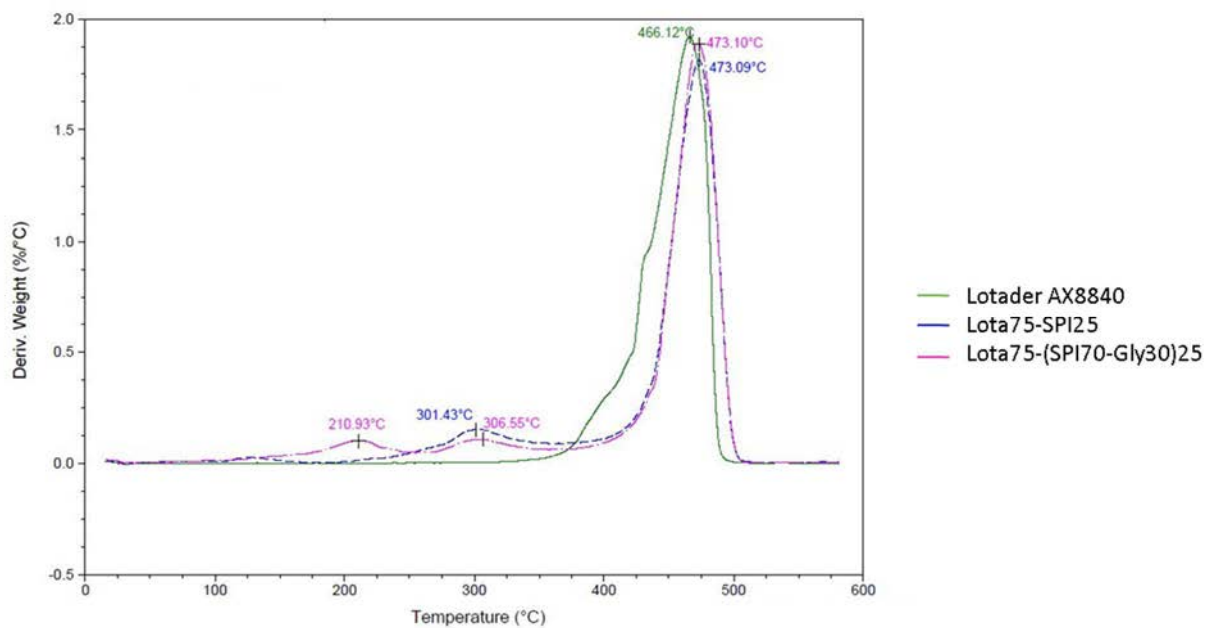


Figure 89: a) Mass variation during degradation of Lotader AX8840 (green), Lot75-SPI25 (blue) and Lot75-(SPI70-Gly30)25 (fuchsia), b) Derivative weight curve for Lotader AX8840 (green), Lot75-SPI25 (blue) and Lot75-(SPI70-Gly30)25 (fuchsia).

SPI addition to Lotader AX8840 reduces thermal stability of the blend, because of a first SPI degradation with a maximum peak around 301°C and a second Lotader AX8840 degradation around 473°C. The presence of glycerol seems to further reduce thermal stability of the blend,

lowering the degradation onset point. In fact, glycerol flashpoint and onset temperature are respectively around 180°C and 199°C under nitrogen atmosphere [12-13].

4.4.5 Attenuated Total Reflection Infrared Spectroscopy

ATR-FTIR has been performed to evaluate interactions between SPI, glycerol and Lotader AX8840.

Figure 76 displays results for SPI and Glycerol.

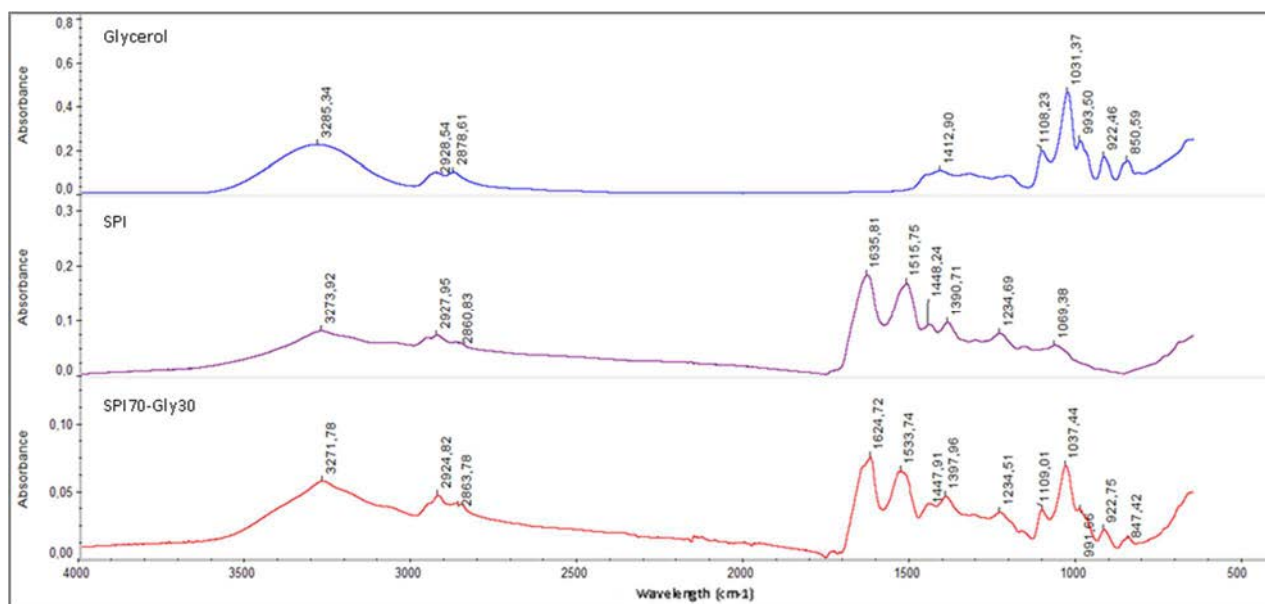


Figure 90 : FTIR spectra of glycerol, SPI and SPI70-Gly30

In agreement with literature results [14], SPI displays a spectrum composed of several peaks:

- -OH stretching groups characteristic of 3274 cm⁻¹
- -CH and -NH₃ groups vibration characteristic of 2927 and 2860 cm⁻¹
- -C=O (amide I) stretching characteristic of 1636 cm⁻¹
- -NH (amide II) group characteristic of 1516 cm⁻¹
- -COH deformation characteristic of 1450 cm⁻¹
- -CH₃ deformation characteristic of 1390 cm⁻¹
- -CN (amide III) group characteristic of 1235 cm⁻¹
- -OC stretching group characteristic of 1069 cm⁻¹

Similarly, the same analysis has been done for glycerol spectrum, obtaining the following peaks [15-16]:

- -OH stretching groups characteristic of 3285 cm⁻¹
- -CH and -NH₃ groups vibration characteristic of 2927 and 2878 cm⁻¹

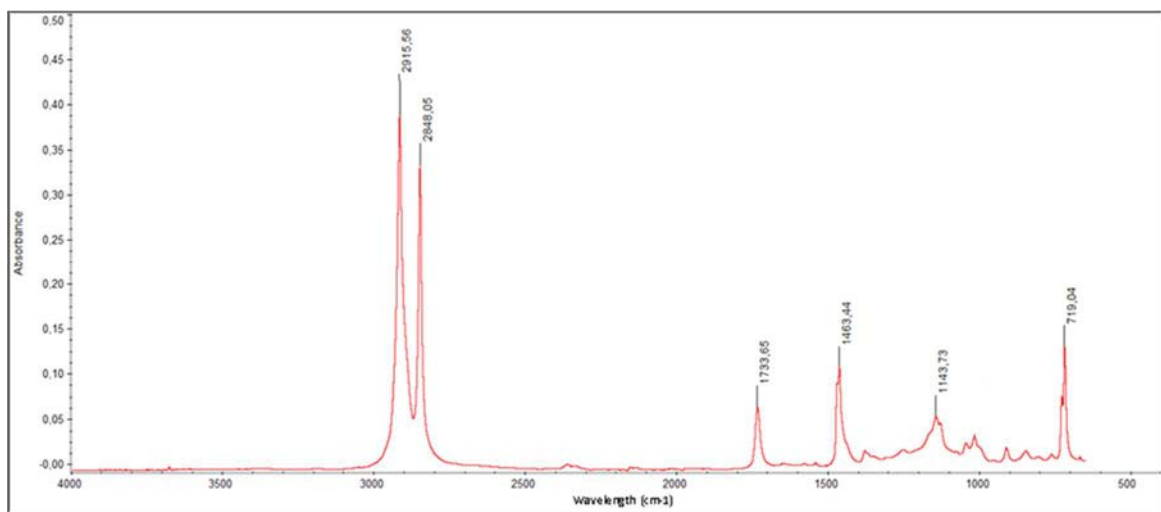
- -CO stretching in CH₂OH characteristic of 1413 cm⁻¹
- -COH stretching in secondary alcohol of glycerol characteristic of 1108 cm⁻¹
- -COH stretching in primary alcohol of glycerol characteristic of 1031 cm⁻¹

Analysing SPI70Gly30 spectrum, any relevance is displayed for peaks between 3274 cm⁻¹ and 2861 cm⁻¹, as well as for peaks below 1235 cm⁻¹. As a consequence, we can only suppose a physical interaction between SPI and glycerol, avoiding chemical reactions.

Polymer chemical reactions with proteins are difficult to occur because the carboxylic acids are in the carboxylate form and the amines in the NH₃⁺ form. pH variation could lead to reactions, but in the solid state this processing is not possible. Consequently, the absence of grafting reaction can be expected.

Figure 91 displays ATR-FTIR spectra of Lotader AX8840, Lot75-SPI25 and Lot75-(SPI70Gly30)25.

A



B

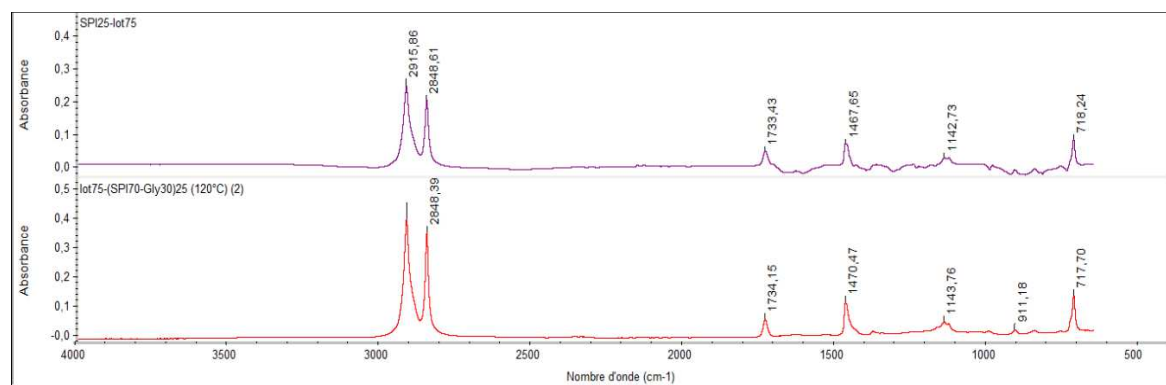


Figure 91: ATR-FTIR spectra of Lotader AX8840 (a), Lot75-SPI25(b) and Lot75-(SPI70Gly30)25 (b).

Lotader AX8840 displays peaks:

- -CH₂ symmetric and asymmetric stretch, characteristic of 2915 cm⁻¹ and 2848cm⁻¹
- -C=O stretch characteristic of 1734 cm⁻¹
- -CH₂ and -CH₃ deformation characteristic of 1465 cm⁻¹

ATR-FTIR has also been performed to investigate which interaction could occur between SPI and Lotader AX8840. Peaks seem to be generally unchanged, suggesting the absence of chemical reaction between SPI and Lotader AX8840. Indeed, it is unlikely to have reaction between the polymer chains and the proteins containing -COO⁻ and NH₃⁺. To have reaction, it would be necessary to adjust pH, which is not possible in the melt state.

4.5 HDPE-SPI blends

Results have also been obtained for HDPE-SPI blends. These are preliminary results, suggesting future studies on this field in terms of production processes, ratio and analysis to complete the characterization.

4.5.1 Tensile tests

The main problem related to HDPE and SPI blend is their different hydrophilicity, as expected for oil-based/bio-derived blends. As a consequence, immiscible blends have been produced, displaying poor mechanical properties.

In fact, brittle blend has been obtained with 50wt.% of HDPE and 50wt.% of SPI, as displayed in Figure 92 and Table 38. 30wt.% of glycerol and Lotader AX8840 have been introduced to modify HDPE-SPI interface, aiming for a better miscibility between polymers. An improvement in mechanical properties has been displayed with the addition of glycerol and Lotader AX8840, as also confirmed by SEM analysis. Further analyses can be performed to analyse blend properties, such as Charpy tests. In fact, impact test can improve scientific comprehension of blend miscibility and interactions between polymers.

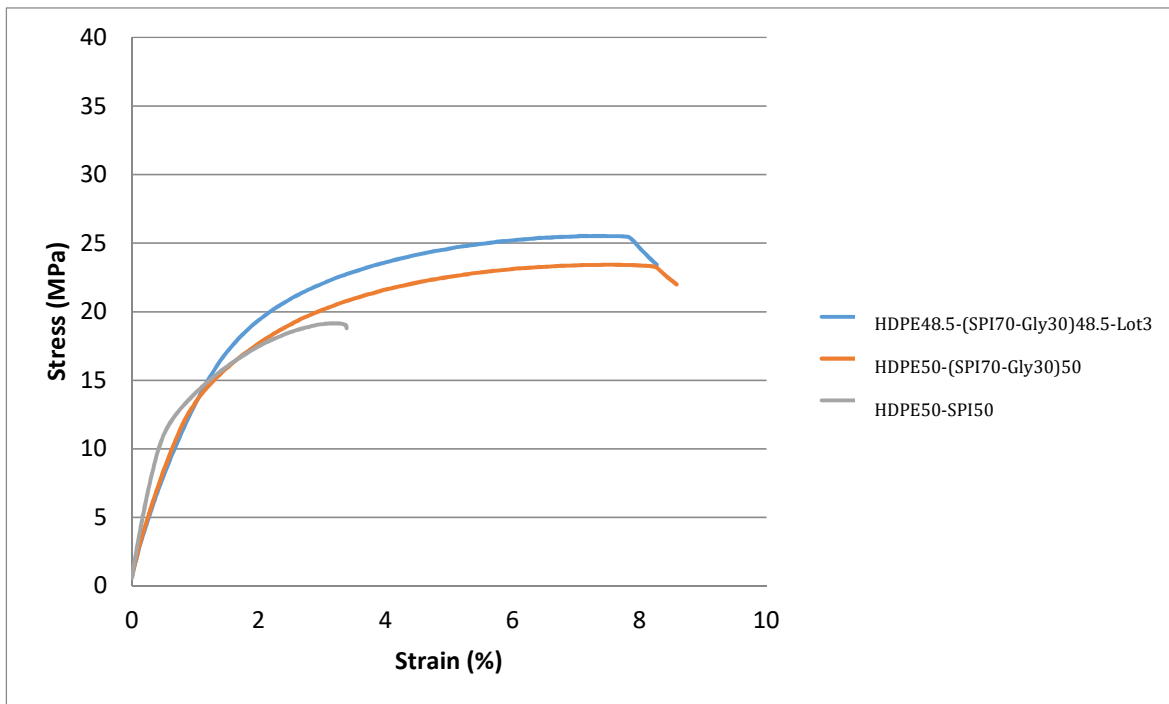


Figure 92: Tensile tests results for HDPE50-SPI50 (grey), HDPE50-(SPI70-Gly30)50 (orange) and HDPE48.5-(SPI70-Gly30)-48.5-Lot3(blue).

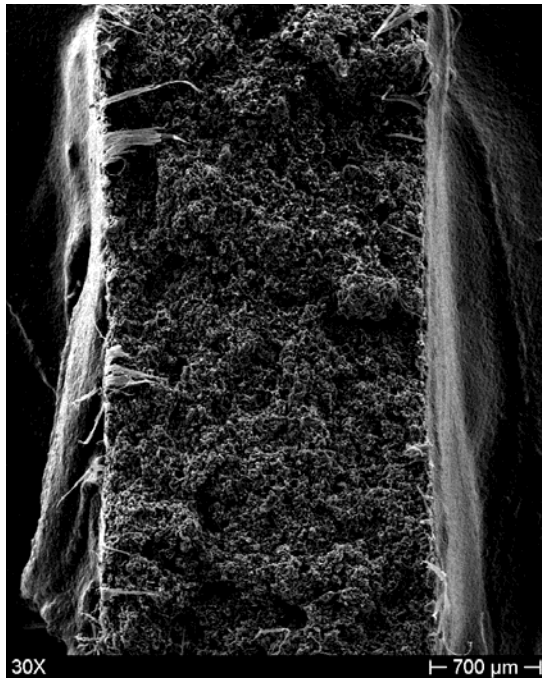
Table 38: Tensile tests results for HDPE-SPI blend, analysing the influence of Glycerol addition as plasticizer and Lotader AX8840 as compatibilizer.

Samples	E (GPa)	σ (MPa)	E (%)
HDPE50-SPI50	2.7±0.1	18.1±4.1	2.8±0.5
HDPE50-(SPI70Gly30)50	1.7±0.1	22.7±0.8	9.2±2.7
HDPE48.5-(SPI70Gly30)48.5-Lot3	1.6±0.2	24.7±2.5	6.2±2.0

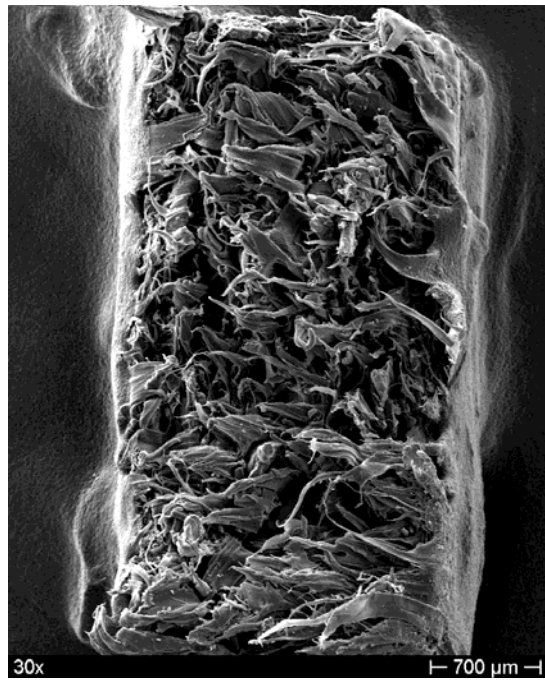
4.5.2 Scanning Electron Microscopy

Scanning Electron Microscopy on both fracture surfaces, obtained after tensile tests (Figure 93 A and B), and cryo-fractured surfaces, obtained after cooling in liquid nitrogen (Figure 93 C and D), has been performed. HDPE50-SPI50 already displays a brittle surface from fracture surface analysis, while glycerol addition reveals a positive effect in terms of material ductility. The addition of Lotader AX8840 seems to partially improve HDPE50-(SPI70Gly30)50 compatibility (Figure 93E), obtaining a slightly better homogeneity.

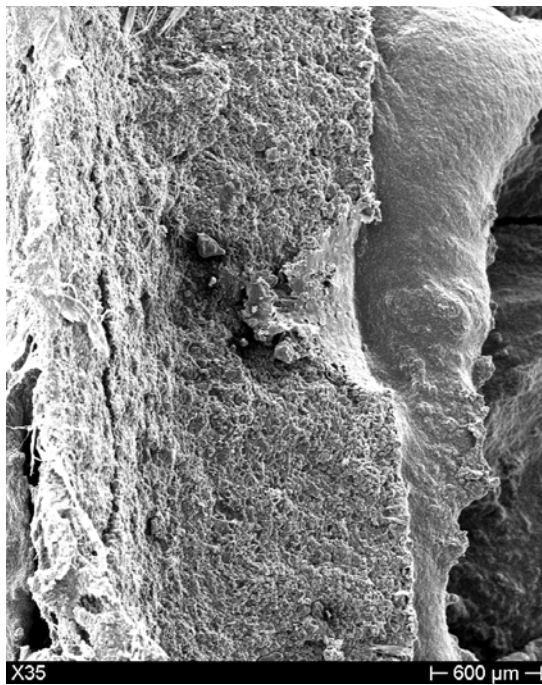
A



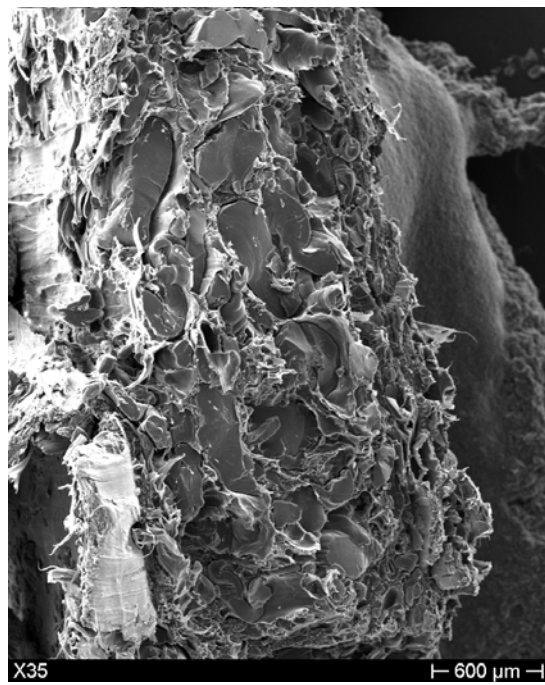
B



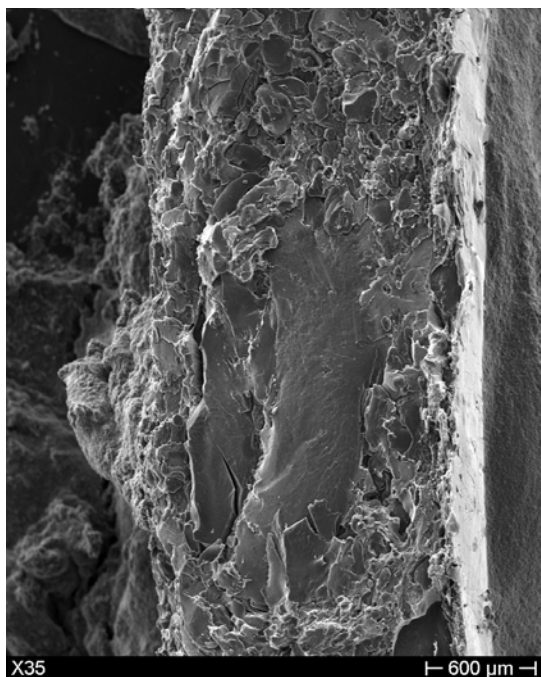
C



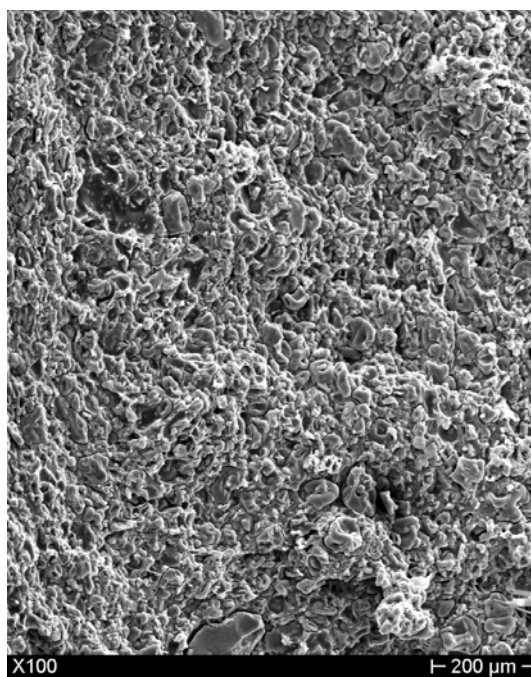
D



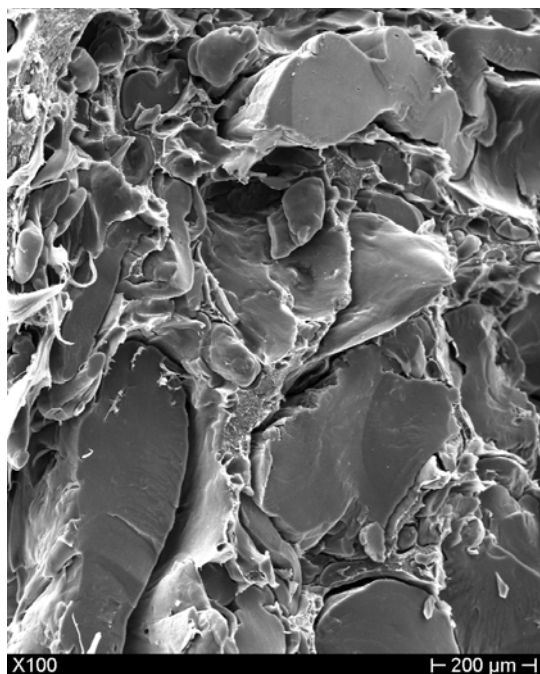
E



F



G



H

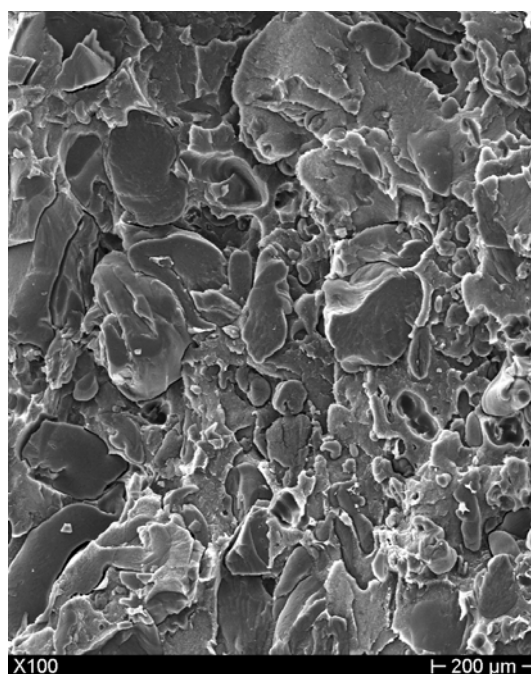


Figure 93: : SEM images of a) HDPE50-SPI50 fracture surface from tensile test 30X, b) HDPE50-(SPI70-Gly30)50 fracture surface from tensile test 30X, c) HDPE50-SPI50 cryo-fractured surface 35X, d) HDPE50-(SPI70-Gly30)50 cryo-fractured surface 35X, e) HDPE50-(SPI70-Gly30)50-Lot3 cryo-fractured 35X, f) HDPE50-SPI50 Cryo-fractured 100X, g) HDPE50-(SPI70-Gly30)50 cryo-fractured 100X, h) HDPE50-(SPI70-Gly30)50-Lot3 cryo-fractured 100X.

Cryo-fractured surfaces (Figure 93 F, G and H) have been analysed in order to evaluate blend morphology variation with glycerol and Lotader AX8840 addition to HDPE-SPI.

HDPE-SPI reveals the presence of SPI nodule in HDPE matrix, as experienced for Lotader AX8840-SPI blends.

SEM observations remain very subjective and, in some cases, an objective evaluation with this technique is difficult to obtain. Tensile tests under SEM would be interesting to carry out, in order to correlate the phenomena of interfacial decohesion and the mechanisms of rupture (ductile, fragile) to an image, understanding the relations structure-properties and micro-macro approach.

4.5.3 Composting tests

Polymers can undergo biodegradation or composting if microorganisms can interact with their surface. As a consequence, hydrophilic surfaces are needed to promote the process. HDPE is characterized by long macromolecular chains composed of only CH₂ groups, making it not susceptible to microorganism attack [17].

HDPE has been tested in order to both verify its resistance to microorganism attack, as reported in literature [18], and to have a negative reference during the test. In fact, no visual modification (Figure 94) has been observed for HDPE during the tested period (three months) for both mesophilic and thermophilic conditions (35°C and 58°C respectively).

Mass variation measurements confirm the absence of HDPE variation (Figure 95), as well as ATR-FTIR analyses (Figure 96a and Figure 96b).

SPI, on the contrary, displays rapid composting degradation. In fact, after already one month of test, a complete disintegration of sample was evident. As a consequence, SPI can be considered as a positive reference. Otherwise, unfortunately, no residual material could be extracted for other analysis, in order to study in detail how degradation evolves over time.

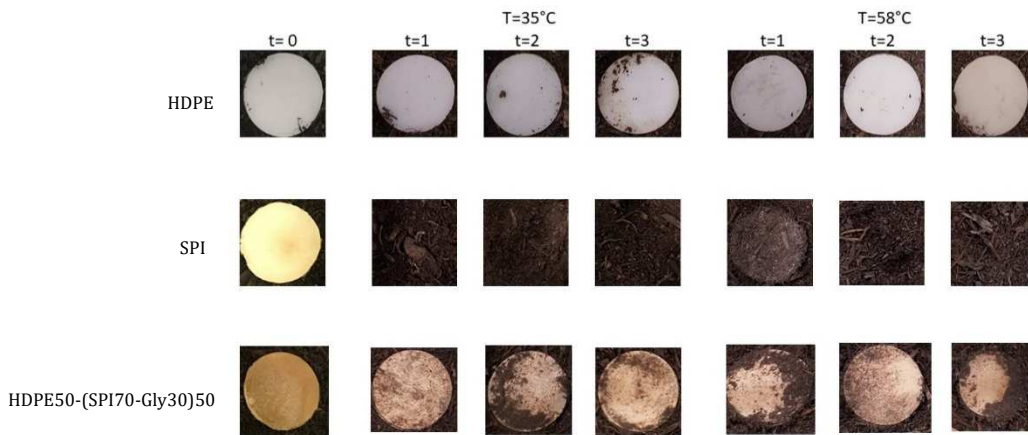


Figure 94: Visual observation of HDPE, Soy Protein Isolate (SPI) and HDPE50-SPI50 during three months testing in soil at 35°C and 58°C.

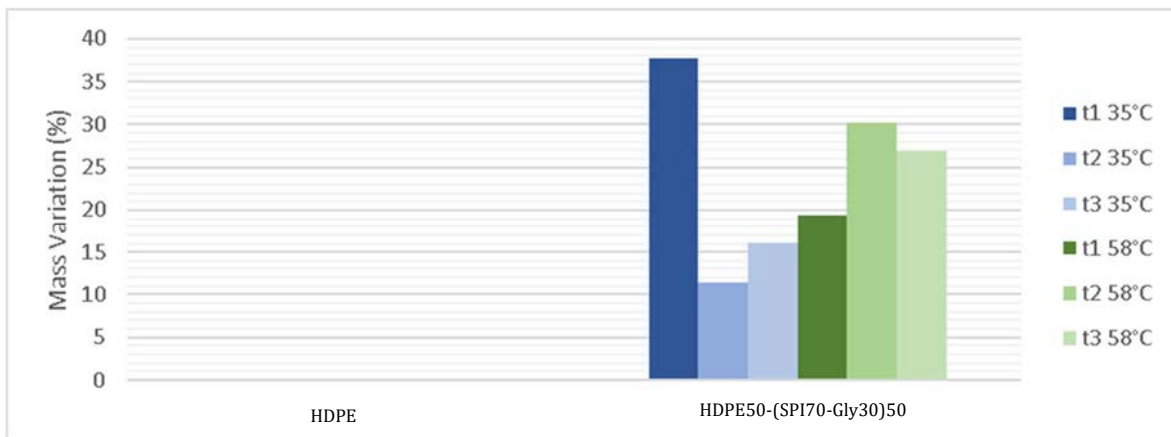
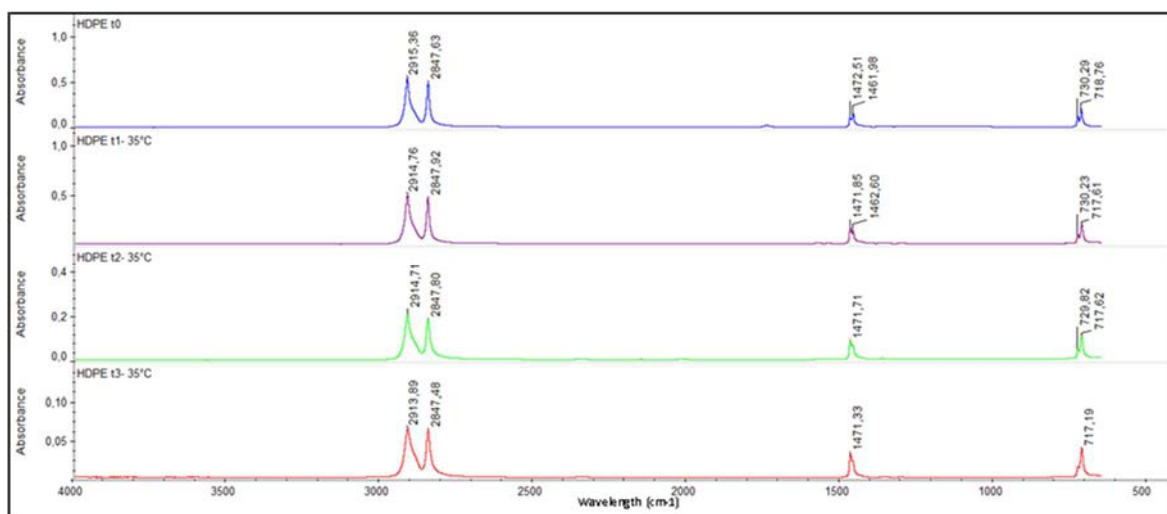


Figure 95: Mass variation measurements of HDPE and HDPE50-(SPI70-Gly30)50 during three months testing in soil at 35°C (blue-scale) and 58°C (green-scale).

A



B

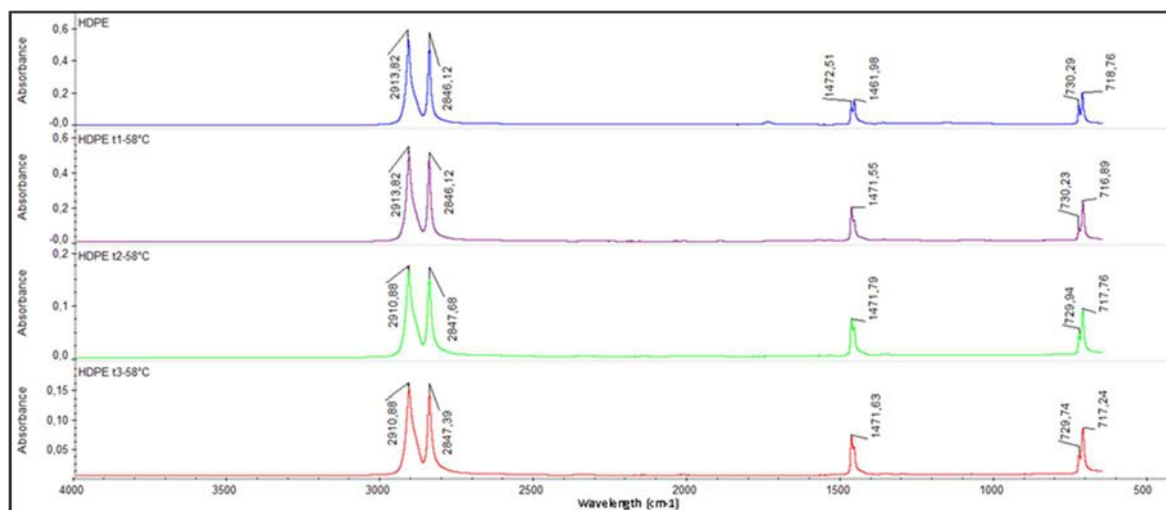
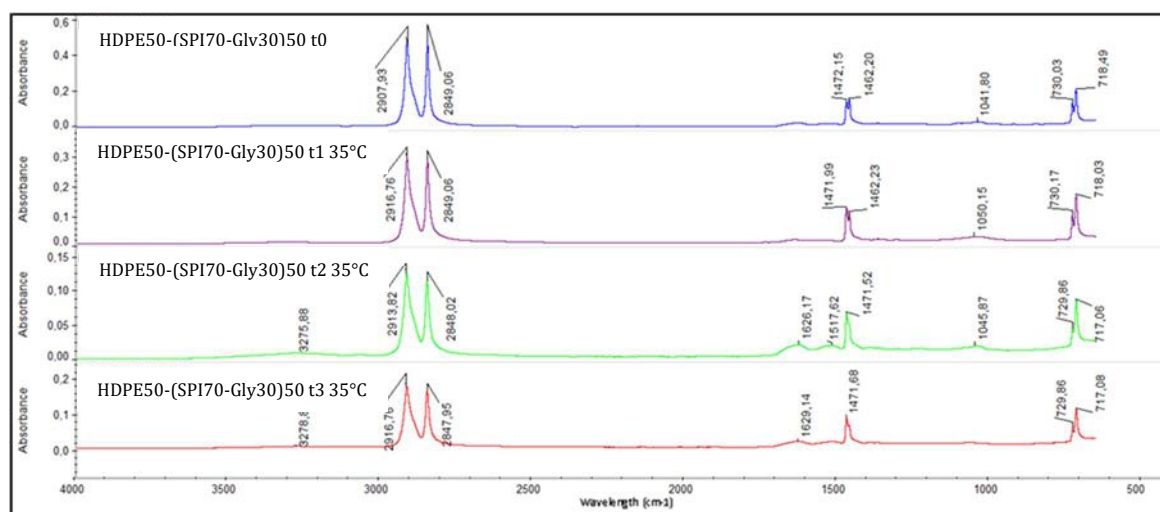


Figure 96: ATR-FTIR results for HDPE during three months testing in soil at 35°C (a) and 58°C (b).

HDPE50-(SPI70-Gly30)50 displays modification of spectra during composting (Figure 97 a and Figure 97b). In fact, peaks related to CH and NH₃ stretch around 2907 cm⁻¹ and 2849 cm⁻¹ slightly shift to values typical of neat HDPE (2915 cm⁻¹ and 2847 cm⁻¹). Moreover, OH, amide I and amide II stretch are not displayed in HDPE50-SPI50 before composting, while their peaks appear with composting process. All these data, in agreement with the other results, suggest a progression of composting tests of HDPE50-(SPI70-Gly30)50.

A



B

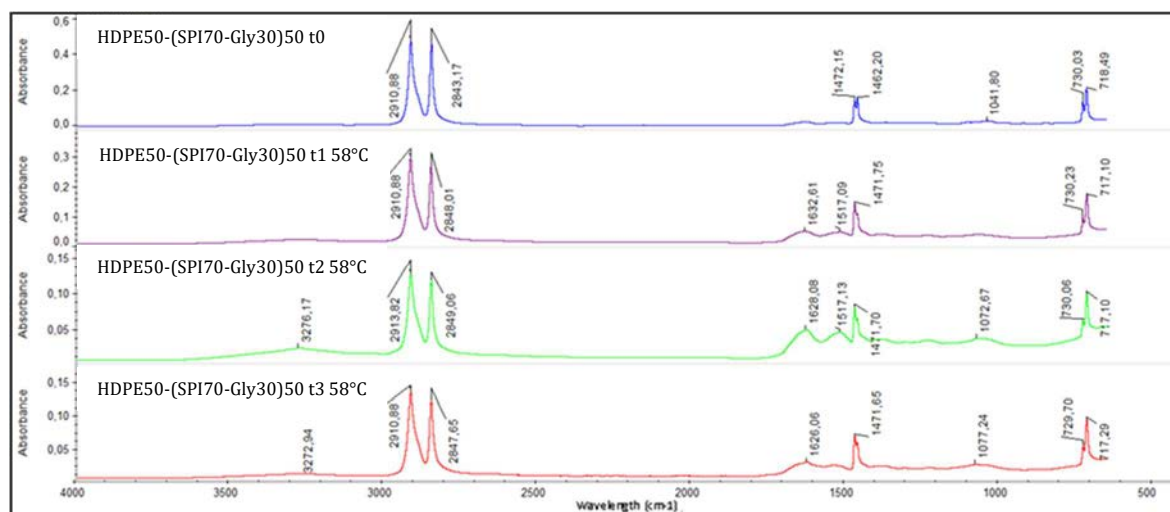


Figure 97: ATR-FTIR results during three months of composting in soil for HDPE50-(SPI70-Gly30)50 at 35°C (A) and 58°C (B).

4.6 Conclusion

After a preliminary study on HDPE-PLA blends, the one containing equal amounts of HDPE and PLA appears to be the most suitable towards keeping good mechanical properties and a significant reduction of non bio-derived charge. The addition of compatibilizer, such as Lotader AX8840 and Polybond 3029, seems to increase homogeneity of the blend. In fact, functional PE with either 1.5 to 1.7 wt.% of maleic anhydride (Polybond 3029) or 8 wt.% of glycidyl methacrylate (Lotader AX8840) have proved to be efficient to improve mechanical properties of PLA based blends. Lotader AX8840 seems to be more efficient in toughness improvement

than Polybond 3029: the higher content of glycidyl methacrylate in comparison to maleic anhydride can explain the higher efficiency of glycidyl methacrylate-based copolymer. In agreement, SEM images display a better dispersion and miscibility for PLA75-Lot25 than for PLA75-Poly25.

An appropriate percentage of compatibilizer in HDPE50-PLA50 has to be selected in order to optimize blend properties. In fact, 3wt.% of compatibilizer seem to optimize (considering strength and plasticity) mechanical properties and affinity between HDPE and PLA. SEM images reveal a typical immiscible morphology between HDPE and PLA when blended without compatibilizer. Both Lotader AX8840 and Polybond 3029, more moderately, seem to increase homogeneity of the blend thanks to functional groups interaction with PLA, in agreement with FTIR results.

SPI has been selected as bio-derived polymer as a possible alternative to PLA. A positive influence of glycerol addition (especially 30 wt.%) as plasticizer for SPI-Lotader AX8840 blends have been displayed, revealing higher samples deformation analysed by tensile test and higher homogeneity analysed by SEM. Glycerol seems to interact physically with SPI, without a chemical reaction, as suggested from TGA and ATR-FTIR analyses. Different Lot-(SPI70-Gly30) blends have been tested, selecting lot50-(SPI70-Gly30)50 as a good compromise between amount of bio-derived polymer and mechanical properties. Production process seems to be more complicated when SPI is added in the extruder: the higher the SPI amount, the higher η^* , especially at low frequencies. Moreover, linearity between viscosity and Lotader AX8840 amount in the blends has been obtained, useful trend to estimate blends viscosity.

HDPE-SPI blends have been tested, similarly to HDPE-PLA blend, after the preliminary evaluation of Lotader AX8840-Soy Protein Isolate blends. An improvement in mechanical properties has been displayed with the addition of glycerol and Lotader AX8840, as also confirmed by SEM analysis. Composting tests have been performed and mass variation measurements confirm the absence of HDPE degradation, as well as ATR-FTIR analyses. SPI, on the contrary, displays rapid composting degradation. In fact, after already one month of test a complete disintegration of sample was evident. HDPE50-(SPI70-Gly30)50 displays modification of ATR-FTIR spectra during composting, suggesting, in agreement with the other results, a progression of composting test of HDPE50-(SPI70-Gly30)50.

4.7 References

- 1 S. Zhizhong, L. Qiuying, L. Yongjun, H. Guo-Hua, W. Chifei, "Compatibility and phase structure of binary blends of poly(lactic acid)and glycidyl methacrylate grafted poly(ethylene octane)", *European Polymer Journal*, vol. 45, pp. 2428–2433, 2009.
- 2 A. Gregorova, "Application of Differential Scanning Calorimetry to the characterization of Biopolymers". In: World ' s largest Science , Technology & Medicine Open Access book publisher A Study of the Porosity of Activated Carbons Using the Scanning Electron Microscope. InTech; p. 3–20
- 3 R. Al-Itry, K. Lamnawar, A. Maazouz, A, "Improvement of thermal stability, rheological and mechanical properties of PLA, PBAT and their blends by reactive extrusion with functionalized epoxy", *Polym Degrad Stabil*, vol.97, pp.1898-1914, 2012.
- 4 M. Mohammadalipour, M. Masoomi, M. Ahmadi, S. Safi, "Interfacial shear strength characterization of GMA-grafted UHMWPE fiber/epoxy/nano clay hybrid nanocomposite materials", *RSC Adv*, vol. 6, pp. 41793-41799, 2016.
- 5 S. Nandi, S. Bose, S. Mitra, A.K. Ghosh, "Effect of maleic anhydride grafted polyethylene on engineering properties and morphology of fumed silica filled polyethylene blown films", *J Plast Film Sheet*, vol. 28, pp. 207-227, 2012.
- 6 C.M. Thurber, Y. Xu, J.C. Myers, T.P. Lodge, C.W. W. Macosko, "Accelerating reactive compatibilization of PE/PLA blends by an interfacially localized catalyst", *ACS Macro Lett.*, vol.4 (1), pp.30–33, 2015.
- 7 L.A. Utracki, "Compatibilization of polymer blends", *Can J Chem Eng*, vol. 80(6), pp. 1008-1016, 2002.
- 8 M.K.A. Wahab, H. Ismail, N. Othman, "Compatibilization effects of PE-g-MA on mechanical thermal and swelling properties of high density polyethylene/natural rubber/thermoplastic tapioca starch blends, *Polym Plastics Tech Engi*, vol.51, pp. 298-303, 2012.
- 9 Chhavi; K.N. Deepmala, V.K. Singh, S. Chauhan, N. Jain, "Soy Protein Based Green Composites: A review", *J Mater Sci*, vol.5, pp.66-77, 2017.
- 10 R.R. Koshy, S.K. Mary, S. Thomas, L.A. Pothan, "Environment friendly green composites based on soy protein isolate-A review", *Food Hydrocolloid*, vol. 50, pp. 174-192, 2015.
- 11 K.S. Lee, "The Effects of the Shear-thinning Property of Injection Fluid on the Performance of Polymer Flood", *Energ Source*, vol.35, pp. 1550-1559, 2013.

- 12 P. Guerrero, A. Retegi, N. Gabilondo, K. De la Caba, "Mechanical and thermal properties of soy protein films processed by casting and compression", *J. Food Eng.*, vol. 100, pp.145-151, 2010.
- 13 S. Liang, L. Wang, "A Natural antibacterial-antioxidant film from soy protein isolate incorporated with cortex phellodendron extract", *Polymers*, vol. 10(1), pp. 71-84, 2018.
- 14 M.L. Castello, J. Dweck, D.A.G. Aranda, "Thermal stability and water content determination of glycerol by thermogravimetry", *J Therm Anal Calorim*, vol. 97, pp.627-630, 2009.
- 15 Y. Kataoka, N. Kitadai, O. Hisatomi, A. Nakashima, "Nature of hydrogen bonding of water molecules in aqueous solutions of glycerol by attenuated total reflection (ATR) infrared spectroscopy", *Appl Spectrosc*, vol. 65(4), pp. 436-441, 2011.
- 16 Z. Yan, Q. Li, P. Zhang, "Soy Protein Isolate and Glycerol Hydrogen Bonding Using Two Dimensional Correlation (2D-COS) Attenuated Total Reflection Fourier Transform Infrared (ATR FT-IR) Spectroscopy", *Appl Spectrosc*, vol. 71(11), pp. 2437-2445, 2017
- 17 J. Arutchelvi, M. Sudhakar, M. Doble, S. Bhaduri, P.V. Uppara, "Biodegradation of polyethylene and polypropylene", *Indian J Biotech*, 7, pp. 9-22, 2008.
- 18 V. Massardier-Nageotte, C. Pestre, T. Cruard-Pradet, R. Bayard, "Aerobic and anaerobic biodegradability of polymer films and physico-chemical characterization", *Polym Degrad Stabil*, vol.91, pp. 620-627, 2006.

5 Composites with Natural Fillers

A part of this chapter is derived and adapted from "Ecofriendly approach and potentially biodegradable polymer matrix for WPC composite materials in outdoor application" by A. Quitadamo, V. Massardier and M. Valente

Wood Flour (WF)

The idea is to develop oil-based/bio-derived thermoplastic polymers blends as matrices for composites filled with natural fillers. We developed composites with wood flour in blended matrix composed of PLA and Lotader AX8840 or Polybond 3029, in order to previously analyse the effect of compatibilizers.

5.1 Effect of compatibilizers on PLA-WF composites

Samples PLA-based have been produced to analyse the effect of compatibilizers (Lotader AX8840 and Polybond 3029) and the effect of an innovative surface treatment with ionic liquid (IL). ILs as molten salts with melting points below 100°C are attractive because of their high thermal stability, low vapor pressure, recyclability and non-flammability [1]. Therefore, ILs are also called "green solvents" [2-4]. Some of the recent IL applications include mediums for chemical reactions, batteries, lubricants, plasticizers and catalysts [5]. Our group studied the possible applications of IL as a compatibility agent between polymer matrix and natural fillers, which have different hydrophilicities [6-7]. ILs are characterized by polar and nonpolar sections, making them suitable to interact with hydrophobic polymers and hydrophilic fillers.

Table 39 displays samples produced through injection moulding.

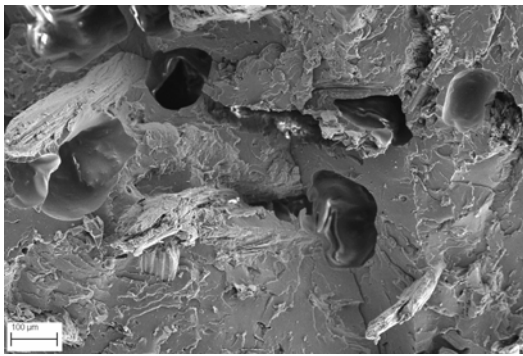
Table 39: Produced formulations of PLA, PLA composites (PLA70-WF30) and modification with compatibilizing agents (Polybond 3029 and Lotader AX8840) and Ionic Liquid (IL).

Samples	PLA (%)	Polybond 3029 (%)	Lotader AX8840 (%)	Wood Flour (%)	IL (%)
PLA	100				
PLA70-WF30	70			30	
PLA70-WFIL30	70			30	1
PLA52.5-Poly17.5-WF30	52.5	17.5		30	
PLA52.5-Lot17.5-WF30	52.5		17.5	30	

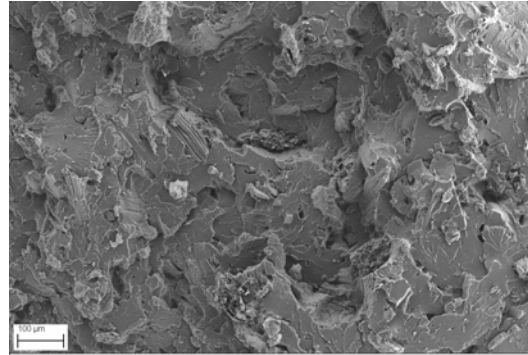
Scanning Electron Microscopy (SEM)

PLA70-WF30, more defects are seen, probably due to limited interactions between PLA and WF, in the course of which cavity formation occurs on the weak interface (Figure 98A). IL treatment seems to be effective, because less cavities are seen in Figure 4B, as a result of higher compatibility between PLA and WF. The addition of both Lotader AX8840 and Polybond 3029 to PLA70-WF30 are beneficial. Lotader AX8840 introduction entails good matrix homogeneity and interactions between PLA and WF (Figure 98C). Otherwise, Polybond 3029 leads to a higher phase separation also in PLA52.5-Poly17.5-WF30, (Figure 98D) with respect to Lotader AX8840 addition. The reason can be related to different graft nature of two compatibilizers, and their different grafting amount, higher for Lotader AX8840.

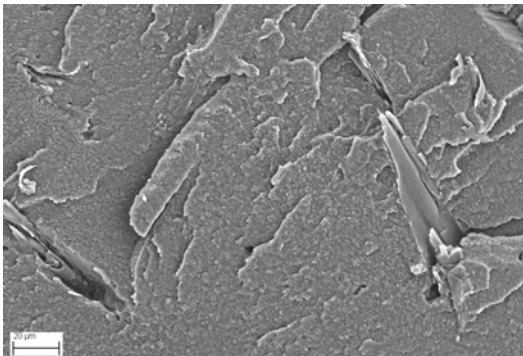
A



B



C



D

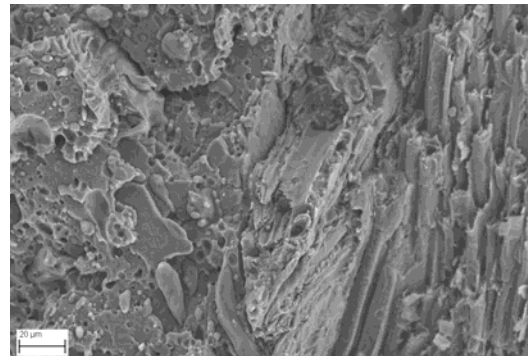


Figure 98: Scanning Electron Microscopy images of A) PLA70-WF30, B) PLA70WF30IL, C) PLA52.5-Lot17.5-WF30 and D) PLA52.5-Poly17.5-WF30

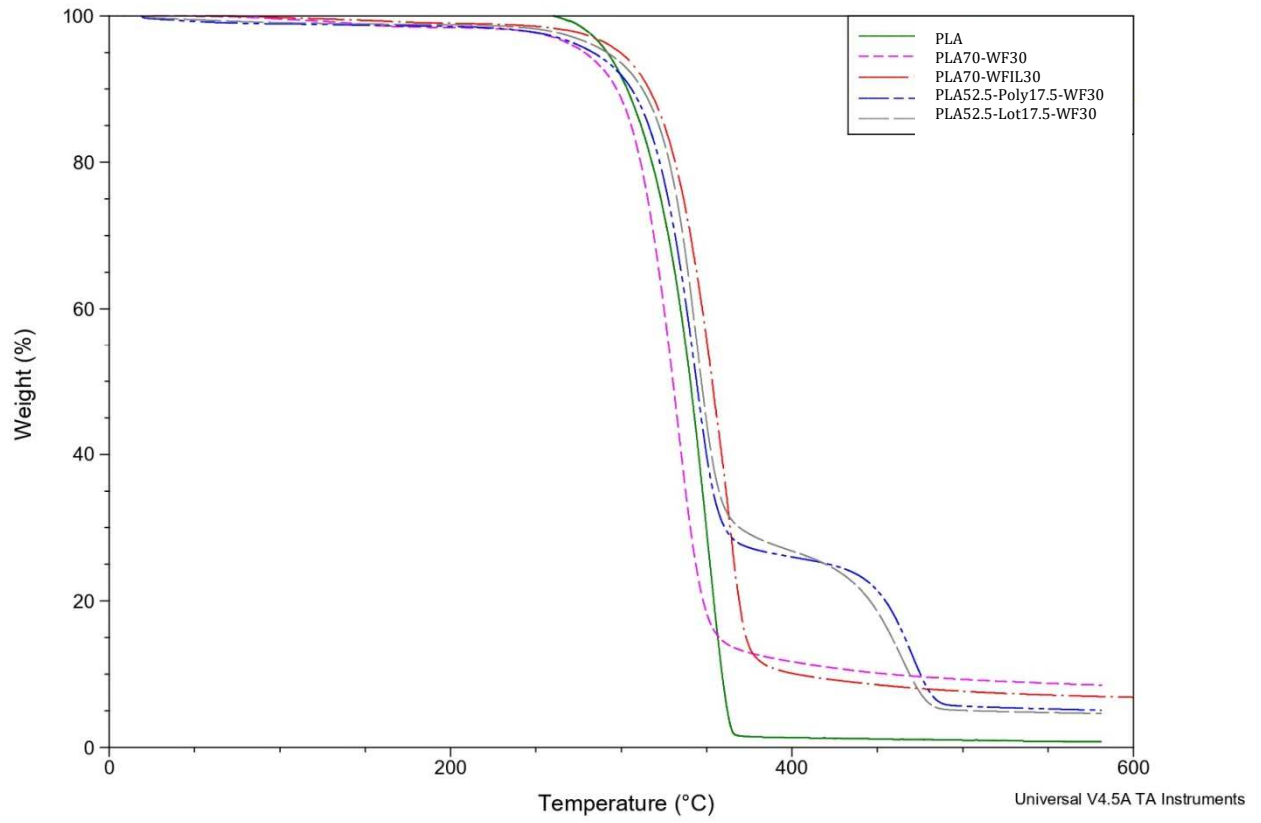
Thermogravimetric analysis (TGA)

DTG profiles from wood display two maxima: the first one (292°C) refers to hemicellulose degradation and the second one (349°C) mainly to lignin degradation (Table 40) [9]. Tonset of WF is around 212°C, while IL-treated WFs shifted up to 240°C, confirming increased thermal stability with IL treatment, in agreement with similar results obtained by Livi et al [9] with montmorillonites treated with phosphonium IL. We analysed the influence of IL on PLA thermal stability, increasing the amount of IL from 1wt.% to 10wt.%. A slight improvement in TDTG has been displayed with the addition of IL, independently from the specific amount of IL. The interactions between IL and PLA and the OH groups of wood may be responsible for the higher thermal stability that facilitates melt processing. As expected, IL increases the thermal stability of PLA filled with WF plus IL.. WF as well as Lotader and Polybond also increase thermal stability. In further work, it would be interesting to study the influence of the ionic liquid on each neat component.

Table 40:TGA results for PLA, PLA70WF30 and compatibilized composites with Lotader AX8840, Polybond 3029 and IL. T_{onset} (°C) is evaluated with the extrapolated onset temperature from TGA curve. T_{DTG} (°C) Temperature of maximum DTG curves peaks. Δm (%) is the mass variation percentage between the total amount of sample before the test and the residual mass after the test.

Samples	T_{onset} (°C)	T_{DTG} (°C)	Δm (%)
PLA	319	351	100
WF	212	292/349	74
IL 109	240	292/350/400	86
Polybond 3029	459	480	100
Lotader AX8840	434	464	100
PLA95-IL5	316	359	99
PLA90-IL10	316	359	99
PLA70-WF30	278	340	90
PLA70-WFIL30	299	362	92
PLA52.5-Poly17.5-WF30	284	343/470	94
PLA52.5-Lot17.5-WF30	291	344/470	94

A



B

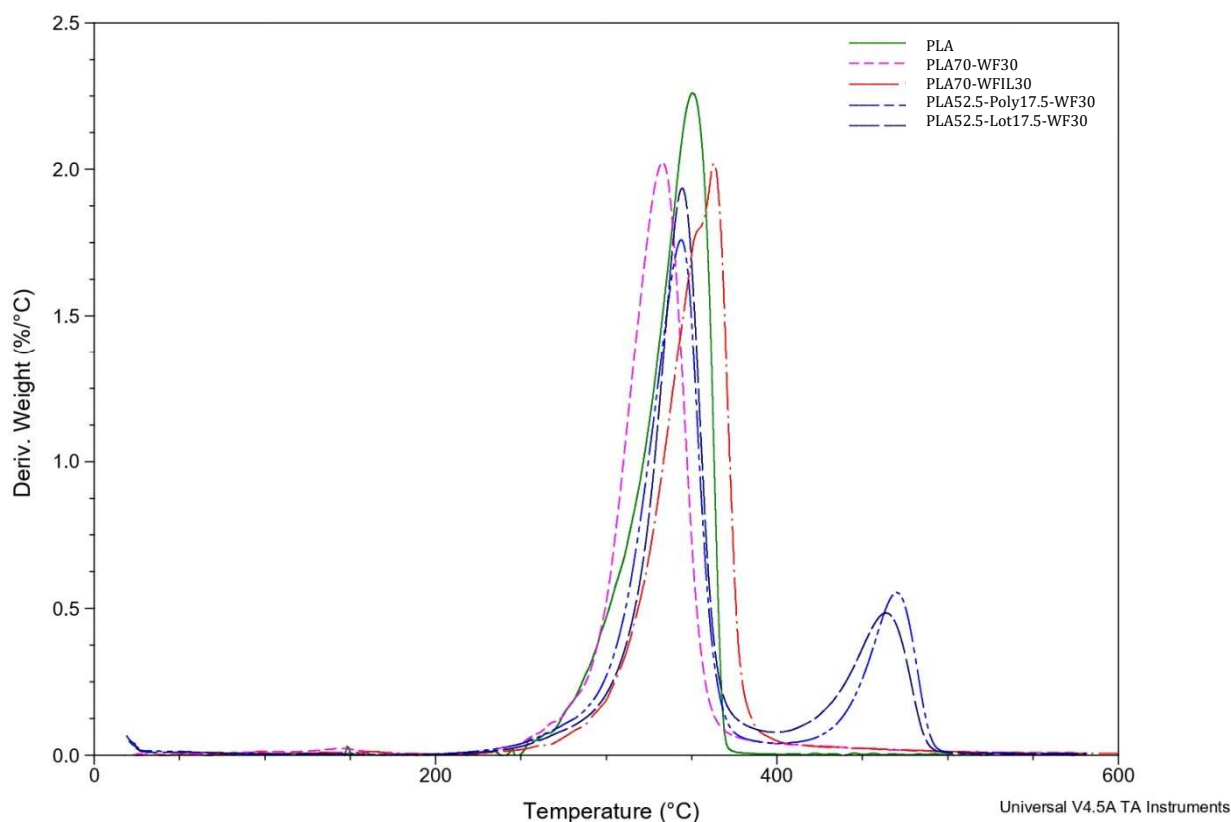


Figure 99:A) Mass variation during degradation of PLA (green), PLA70WF30 (purple), PLA70WFIL30 (red), PLA52.5Poly17.5WF30 (blue, one dashed line) and PLA52.5Lot17.5WF30 (dashed line) B) Derivative weight curve for PLA (green), PLA70WF30 (purple), PLA70WFIL30 (red), PLA52.5Poly17.5WF30 (blue, one dashed line) and PLA52.5Lot17.5WF30 (dashed line).

Conclusion

Functional PE with either 1.7% of maleic anhydride (Polybond 3029) or 8% of glycidyl methacrylate (Lotader AX8840) has proved to be efficient in improving the mechanical properties of PLA-based blends. Phase separation is still observable because of the differences in hydrophilicity between PLA and functional PE. Addition of phosphonium-based IL is efficient in improving the thermal stability of WF. The interactions between phosphonium-based IL and PLA and the OH groups of wood may be responsible for the higher thermal stability that facilitates melt processing. As expected, WF addition to PLA improve Young's modulus. Moreover, the random PE-g-GMA (Lotader AX8840) improve the PE-PLA miscibility and increase the filler matrix interfaces. In this context, PE-g-GMA with 8% GMA and IL seem to be

promising for reducing the environmental impact of WPCs. Further analysis should be performed to evaluate the effects of ionic liquids on the various components of the mixture considered separately.

These results have been used in order to analyse in more details the effect of compatibilizers on composites properties. The other tests in this project have been done considering lower amount of compatibilizers, in agreement with literature.

HDPE-PLA composites

We selected high density polyethylene and poly(lactic acid) as respectively oil-based and bio-derived polymers.

Table 41 displays formulations produced and analysed in agreement with the purpose of this project. Starting from results obtained in chapter 4, HDPE50-PLA50 has been selected as matrix for composites production. Lotader AX8840 and Polybond 3029 have been added as compatibilizers in the amount of 3wt.%. Moreover, an important purpose of this work is the valorisation of a natural waste, such as wood flour. As a consequence, the highest possible amount of wood flour has been added, compatibly with technological process limits. As a consequence, 20, 30 and 40wt.% of wood flour have been added.

Table 41: Produced formulations of HDPE50-PLA50 composites with 20, 30 and 40wt.% of wood flour and 3 wt.% of compatibilizing agent.

Samples	HDPE (%)	PLA (%)	Polybond 3029 (%)	Lotader AX8840 (%)	Wood Flour (%)
HDPE50-PLA50	50	50			
HDPE50-PLA50-WF20	40	40			20
HDPE50-PLA50-WF30	35	35			30
HDPE50-PLA50-WF40	30	30			40
HDPE50-PLA50-Poly3-WF20	38.8	38.5	3		20
HDPE50-PLA50-Poly3-WF30	33.5	33.5	3		30
HDPE50-PLA50-Poly3-WF40	28.5	28.5	3		40
HDPE50-PLA50-Lot3-WF20	38.8	38.5		3	20
HDPE50-PLA50-Lot3-WF30	33.5	33.5		3	30
HDPE50-PLA50-Lot3-WF40	28.5	28.5		3	40

5.2 Tensile tests

Mechanical properties of these composites have been evaluated to detect the influence of wood flour on blend properties. In another study we analysed the influence of compatibilizers on HDPE-PLA blends. In particular, we studied the effect of 1,3 and 5 wt.% of Lotader AX8840 and Polybond 3029 on HDPE-PLA compatibility. The compatibilizer percentage has been selected as 3wt.% in both cases. We evaluated, as a consequence, the effect of 3wt.% of both Lotader AX8840 and Polybond 3029 on HDPE50-PLA50-WF composites.

Lotader AX8840 and Polybond 3029 were selected because of their ability to interact with both polyethylene and polymers with polar groups. Moreover, Lotader AX8840 and Polybond 3029 could interact with natural fillers, such as wood flour. Wood flour was only added in HDPE50-PLA50-Poly3 and HDPE50-PLA50-Lot3 samples in three different percentages (20, 30 and 40 wt.%). In fact, higher wood flour percentages have not been added because of processing technological limits. Table 42 sums up tensile tests results for these families of samples.

Table 42: Tensile tests results of samples filled with wood flour. Blue colour is for wood flour, purple for Polybond 3029 and red is for Lotader AX8840 addition.

Samples	E (GPa)	σ (MPa)	ϵ (%)
HDPE50-PLA50	1.8±0.1	38.7±0.2	99.4±2.1
HDPE50-PLA50-WF20	3.4±0.1	34.6±2.8	1.6±0.1
HDPE50-PLA50-WF30	4.1±0.1	34.0±1.3	1.2±0.2
HDPE50-PLA50-WF40	5.0±0.2	33.5±1.5	1.9±0.0
HDPE50-PLA50-Poly3-WF20	3.3±0.1	36.0±0.8	1.8±0.1
HDPE50-PLA50-Poly3-WF30	4.1±0.2	35.9±1.4	1.4±0.1
HDPE50-PLA50-Poly3-WF40	4.9±0.1	33.6±1.7	0.9±0.2
HDPE50-PLA50-Lot3-WF20	3.3±0.1	37.8±1.5	2.0±0.1
HDPE50-PLA50-Lot3-WF30	4.1±0.1	35.0±1.2	1.4±0.1
HDPE50-PLA50-Lot3-WF40	5.0±0.1	34.1±3.3	1.0±0.1

Wood flour addition improves elastic modulus at the strong expense of elongation at break: increased wood flour percentages resulted in higher values of the elastic modulus, yet tensile strength does not experience the same growth. The latter result is attributed to poor interface between HDPE50-PLA50 matrix and wood flour (Figure 100).

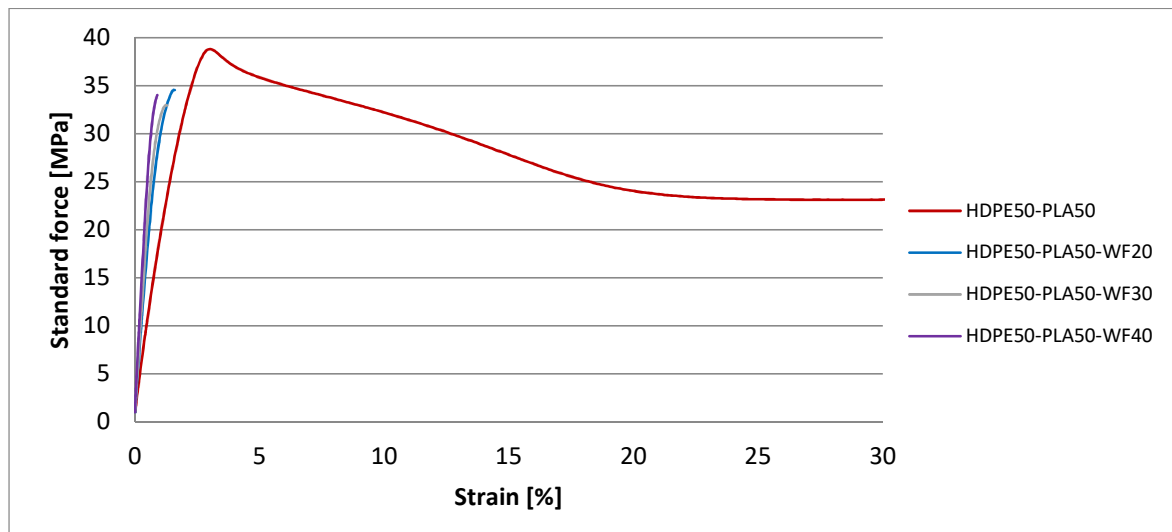


Figure 100: Tensile tests results for HDPE50-PLA50 (red), HDPE50-PLA50-WF20 (blue), HDPE50-PLA50-WF30 (grey) and HDPE50-PLA50-WF40 (purple).

The addition of Polybond 3029 and Lotader AX8840 in the amount of 3wt.% does not strongly affect mechanical properties of the composite (Figure 101); all the results are comparable to HDPE50-PLA50 WF for all three wood flour percentages. Probably, the presence of 3 wt.% does not prove sufficient to have a significant effect on the strength of both HDPE-PLA and polymer blend-wood flour interfaces. One can suppose that compatibilizers amount of 3wt.% slightly acts on blend matrix-wood flour interfaces, but it was not sufficient to satisfy the total improvement of the composites.

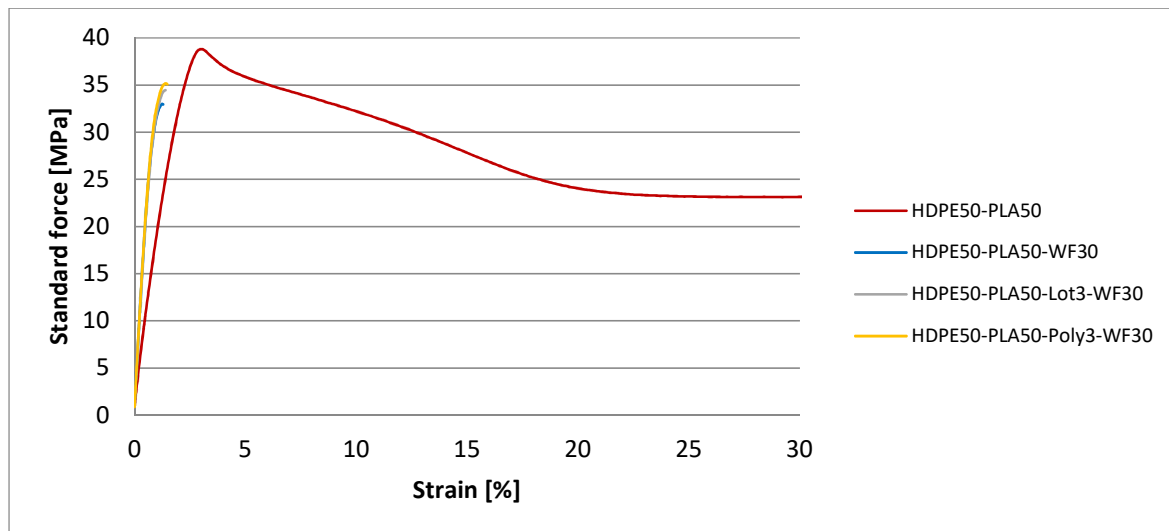


Figure 101: Tensile test results for HDPE50-PLA50 (red), HDPE50-PLA50-WF30 (blue), HDPE50-PLA50-Lot3-WF30 (grey) and HDPE50-PLA50-Poly3-WF30 (yellow).

Future studies will focus on optimizing the amount of compatibilizers, and the analysis of chemical treatments on wood flour that could improve blend matrix-wood flour interfaces.

5.3 Scanning Electron Microscopy (SEM)

Scanning electron microscopy (SEM) analyses aim at investigating the soundness of interfaces between blended matrix and wood flour.

Wood flour addition increases morphology complexity, in agreement with mechanical properties, especially low elongation at break. Wood particles seem to be partially related to polymer matrix, but not completely compatibilized. In particular, as suggested from other tests, we can suppose that PLA has more affinity for wood flour than HDPE. However, a high inhomogeneity of the blended matrix is displayed (Figure 102).

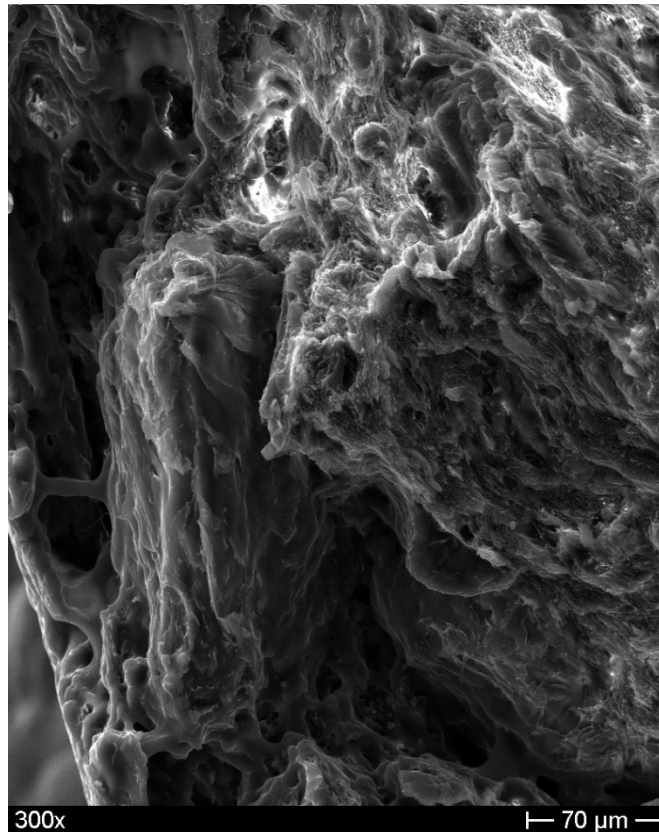
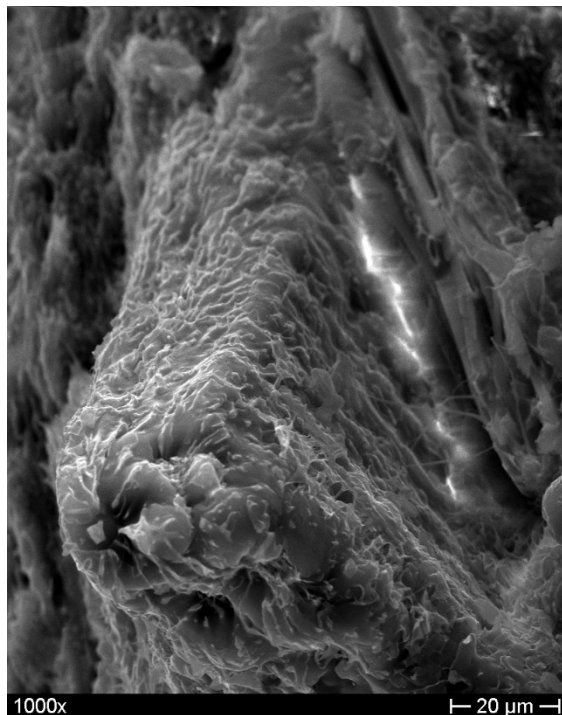


Figure 102: HDPE50-PLA50-WF30 composite

The presence of Lotader AX8840, thanks to glycidyl methacrylate groups, seems to increase matrix homogeneity, improving at the same time interface with wood flour (Figure 103A). The presence of Polybond 3029 does not allow obtaining a sensitive reduction in matrix defectiveness and there seems to be phase separation (Figure 103B). In fact, in chapter 4, we analysed blends of PLA with both Lotader AX8840 and Polybond 3029. Higher homogeneity has been displayed by PLA-Lotader AX8840 blend, probably because of higher glycidyl methacrylate content (about 8wt.%) compared to maleic anhydride content in Polybond 3029 (1.5-1.7 wt.%).

A



B

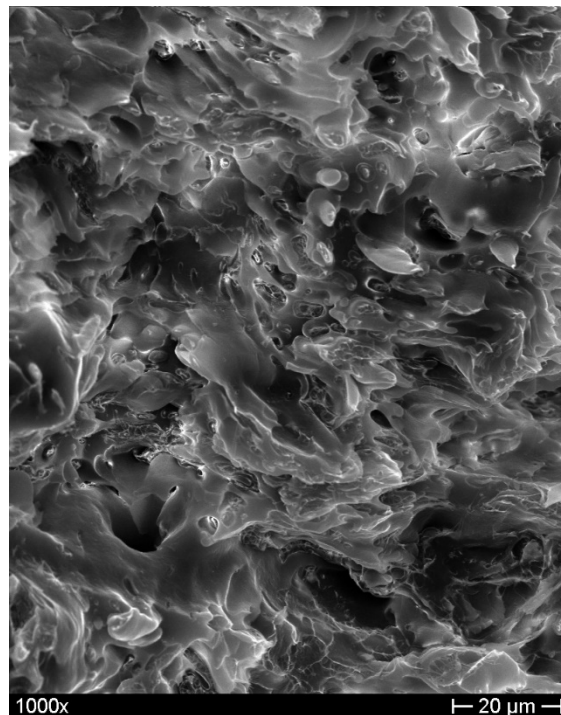


Figure 103: HDPE50-PLA50-Lot3-WF30 (a) HDPE50-PLA50-Poly3-WF30 (b)

5.4 Differential Scanning Calorimetry (DSC)

Differential Scanning Calorimetry aims at evaluating the influence of compatibilizers and wood flour on HDPE and PLA.

In order to assess wood flour effect on HDPE-PLA blends (compatibilized or not), Table 43 displays DSC results. PLA particles dispersed in HDPE matrix seems to act as nucleating agent on HDPE, increasing its crystallinity in HDPE50-PLA50 [10]. The typical PLA cold crystallization phenomena are not revealed with wood flour addition, suggesting a higher difficulty of PLA macromolecules to arrange during cooling from molten state. In fact, we can suppose a nucleating effect of wood flour on PLA phase, increasing its crystallinity. Moreover, the higher wood flour amount in HDPE50-PLA50-WF composites the lower the crystallinity for both HDPE and PLA phases. This result is probably related to competitive nucleating effect of PLA on HDPE and WF on both HDPE and PLA, revealing higher difficulties in macromolecules organization. Both Polybond 3029 and Lotader AX8840 added to HDPE-PLA-WF composites displays a positive effect in terms of compatibility. In particular, Polybond 3029 seems to be more effective in compatibilizing PLA with WF, displaying a slight reduction lower crystallinity of PLA and, as a consequence, higher cold crystallization enthalpy. In fact, generally speaking, the

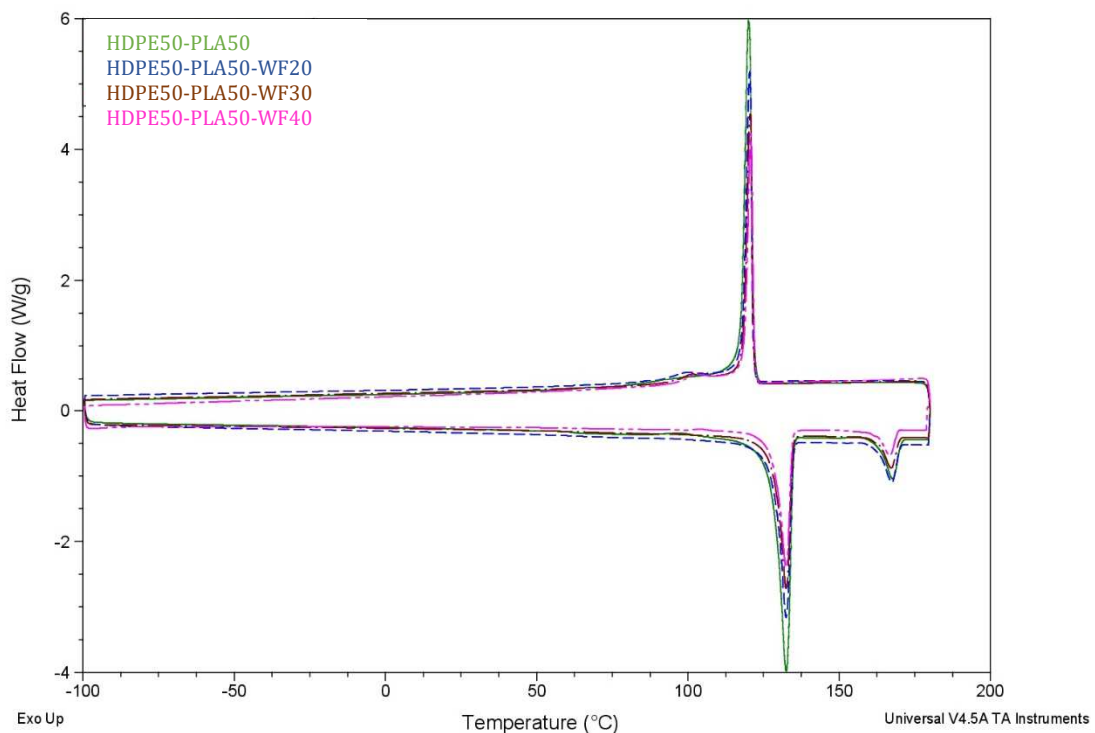
higher the compatibility the lower the nucleating effect [10]. On the contrary, Lotader AX8840 seems to have higher influence on HDPE-PLA compatibility, obtaining lower HDPE crystallinity.

Table 43: DSC results for HDPE50-PLA50 composites with 20, 30 and 40 wt.% of wood flour and 3 wt.% of compatibilizer Polybond 3029 or Lotader AX8840.

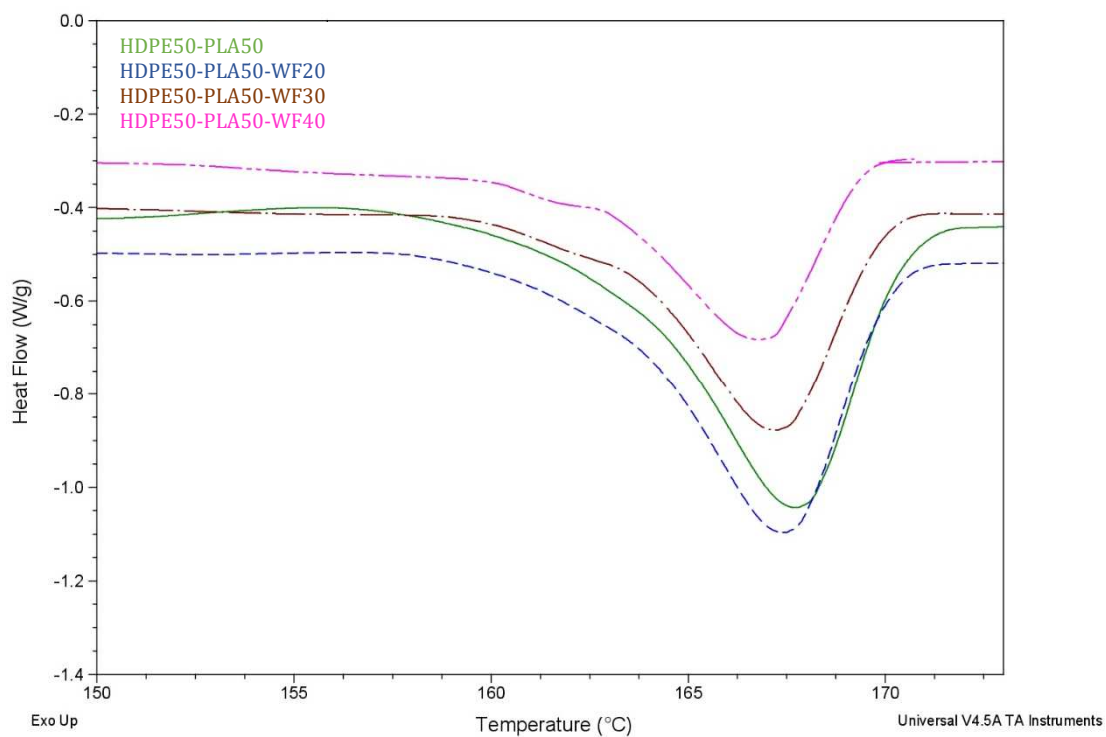
Samples	ΔH_{CCPLA} (J/g _{PLA})	T _{CC} (°C)	ΔH_{mPE} (J/g _{PE})	T _{mPE} (°C)	ΔH_{mPLA} (J/g _{PLA})	T _{mPLA} (°C)	T _{gPLA} (°C)	X _{HDPE} (%)	X _{PLA} (%)
HDPE50-PLA50	16	97	226	132	40	168	62	81	43
HDPE50-50PLA50-WF20	-	-	190	132	35	167	61	65	38
HDPE50-50PLA50-WF30	-	-	200	132	37	167	62	68	40
HDPE50-50PLA50-WF40	-	-	193	132	40	167	63	66	43
HDPE50-PLA50-Poly3-WF20	15	99	202	132	44	167	61	69	31
HDPE50-PLA50-Poly3-WF30	12	99	186	132	43	167	61	63	33
HDPE50-PLA50-Poly3-WF40	11	97	187	132	42	165	59	64	33
HDPE50-PLA50-Lot3-WF20	11	100	185	132	44	167	61	63	35
HDPE50-PLA50-Lot3-WF30	6	99	189	132	45	166	60	65	42
HDPE50-PLA50-Lot3-WF40	3	98	184	132	42	166	61	63	42

For HDPE50-PLA50-WF composites DSC thermograms (Figure 104) also reveal the presence of shoulder for PLA melting peak for HDPE50-PLA50-WF composites, suggesting the presence of two different crystalline phases (more accurate analysis about WF influence on HDPE and PLA crystallinity will be described in the paragraph “Influence of Wood flour and Recycled waste paper on HDPE and PLA” of this chapter) in agreement with an effect of WF on PLA crystallinity. Compatibilizers’ addition seems to influence also crystals morphology, displaying in DSC thermograms only one PLA melting peak.

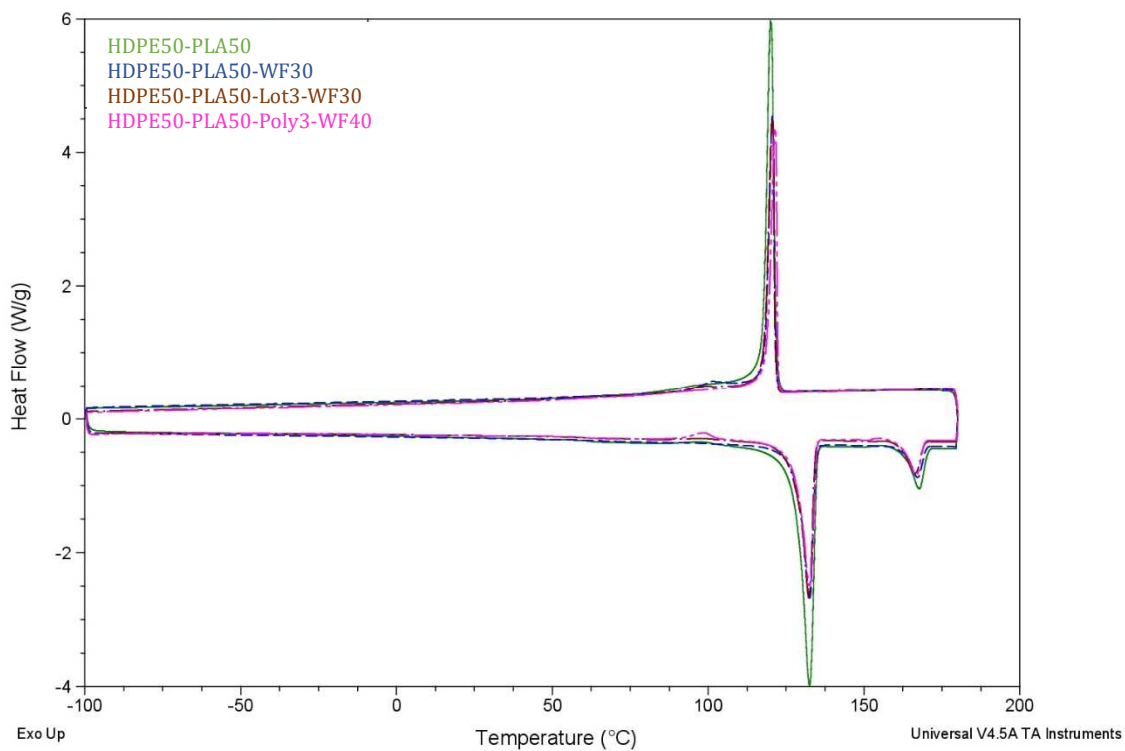
A



B



C



D

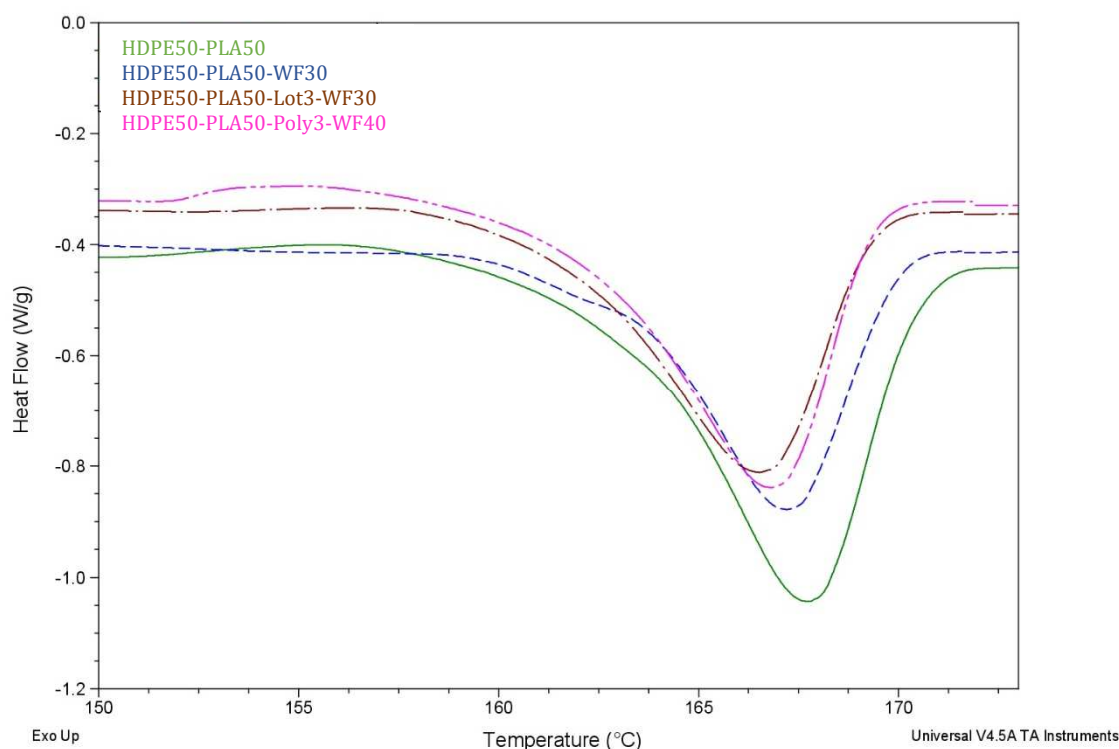


Figure 104: DSC thermograms of A) HDPE50-PLA50, HDPE50-PLA50-WF20, HDPE50-PLA50-WF30, HDPE50-PLA50-WF40, B) PLA melting peak magnification of HDPE50-PLA50, HDPE50-PLA50-WF20, HDPE50-PLA50-WF30, HDPE50-PLA50-WF40, C) HDPE50-PLA50, HDPE50-PLA50-WF30, HDPE50-PLA50-Lot3-WF30, HDPE50-PLA50-Poly3-WF40, D) PLA melting peak magnification of HDPE50-PLA50, HDPE50-PLA50-WF30, HDPE50-PLA50-Lot3-WF30, HDPE50-PLA50-Poly3-WF40.

5.5 Thermogravimetric Analysis (TGA)

Studying the mass variation of samples Δm (%), only samples filled with wood flour displays a residual char after the test (Table 44), as a result of wood pyrolysis. As a consequence, the higher the amounts of wood flour the higher the residual mass. In general, firstly evaporation of adsorbed moisture occurs from room temperature to 100°C. Secondly, degradation of hemicellulose occurs around 295°C, while cellulose pyrolysis occurs at higher temperature (315-400°C) [11]. PLA onset degradation temperature is around 319°C, near to degradation of WF. In fact, HDPE50-PLA50-WF composites display a unique degradation peak for PLA and WF degradation [12], while a second peak, at higher temperatures, is displayed for HDPE degradation around 470°C.

The addition of Lotader AX8840 seems to increase thermal stability of blended matrix composites. A possible hypothesis would be that PE based compatibilizers interact with PLA and wood flour: maleated groups seem to be more efficient with the presence of wood flour, increasing thermal stability of blended matrix composites, while the presence of glycidyl methacrylate seems to be more efficient with PLA, increasing thermal stability of HDPE-PLA blends. In fact, maleated groups react easily with OH groups of wood, which is not the case of glycidyl groups. Indeed, the OH group of cellulose reacts with more difficulty with glycidyl functions. On the contrary, CO₂H at the ends of PLA chains are very reactive with glycidyl groups. We already assume a higher affinity between PLA and Lotader AX8840 in the paragraph “Effect of compatibilizer on PLA” in chapter 4, displaying smaller secondary phase for Lotader AX8840 than for Polybond 3029 when blended with PLA. In fact, as visible from figure 4, a shift of PLA and WF degradation step is displayed when compatibilizers are added, in agreement with interaction between bio-based products and compatibilizers.

Table 44: TGA results for HDPE-PLA blends with different compatibilizer percentages and HDPE50-PLA50 matrix composites with 3 wt.% of compatibilizer and 20, 30, 40 wt.% of wood flour. T_{onset} (°C) is evaluated with the extrapolated onset temperature from TGA curves. T_{DTG} (°C) Temperature of maximum DTG curves peaks. Δm (%) is the mass variation percentage between the total amount of sample before the test and the residual mass after the test.

Samples	T _{onset} (°C)	T _{DTG} (°C)	Δm (%)
HDPE	458	474	100
PLA	319	351	100
Poly	459	480	100
Lot	434	464	100
WF	289	292/349	74
HDPE50-PLA50	322	345/471	100
HDPE50-50PLA50WF20	294	315/465	95
HDPE50-50PLA50WF30	287	313/469	93
HDPE50-50PLA50WF40	284	314/469	91
HDPE50-PLA50-Poly3-WF20	309	347/472	95
HDPE50-PLA50-Poly3-WF30	302	335/472	93
HDPE50-PLA50-Poly3-WF40	291	332/470	91

HDPE50-PLA50-Lot3-WF20	296	324/472	95
HDPE50-PLA50-Lot3-WF30	286	320/470	93
HDPE50-PLA50-Lot3-WF40	285	322/472	91

5.6 Infrared Analysis Attenuated Total Reflection (ATR-FTIR)

Infrared spectroscopy has been done to evaluate interactions between polymers and wood flour, and the main results are displayed in Figure 105. No visible variation of peaks seems to be evident from these spectra. The only variation is displayed by OH- peak variation of WF, however this peak is a broad peak, complicating the effective analysis of the variation of this peak.

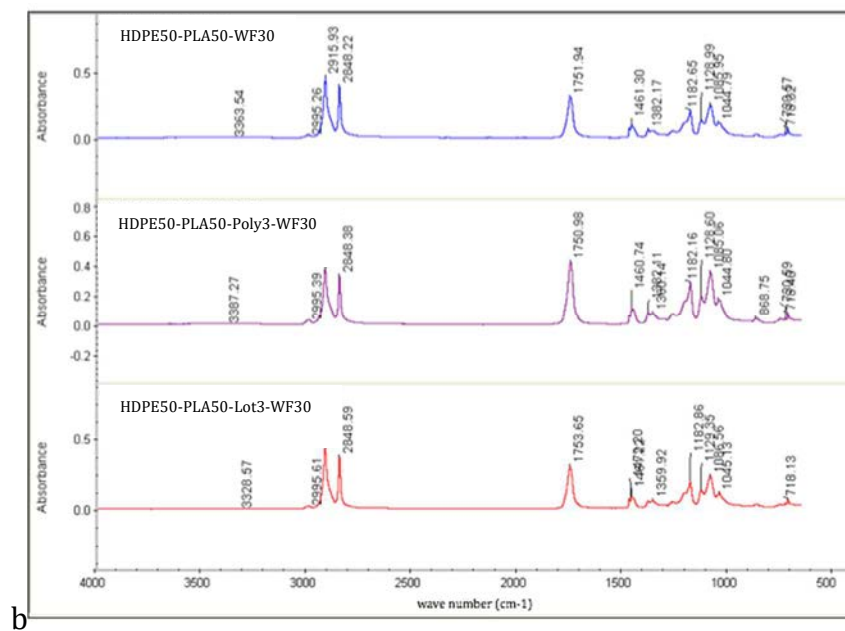


Figure 105:ATR-FTIR results for HDPE-PLA blends HDPE50-PLA50 matrix composites with 3 wt.% of compatibilizer and 30 wt.% of wood flour.

Recycled waste paper (P) and mix WF-P

The valorisation of natural waste as filler in thermoplastic matrix composites is one of the main goal of this project. In agreement with procedures followed for wood flour, we also analysed the effects of recycled waste paper (named as P in this chapter) as filler in HDPE50-PLA50 matrix. The highest possible amount of recycled waste paper has been tried to be added,

compatibly with technological process limits. In fact, using extrusion and injection moulding techniques, a maximum of 40wt.% of recycled P has been added. Moreover, previous studies reveal interesting results when mixing fillers with different morphologies in terms of amount of filler and obtained properties [13]. In fact, WPC composites with HDPE matrix and 30wt.% of wood flour and a mix of 30wt.% of wood flour and 10wt.% of recycled waste paper have been produced. Tensile and hardness tests (Shore D) reveal increased properties for wood flour and recycled waste paper mix compared to only wood flour composites. Moreover, water absorption of samples with 30wt.% of wood flour and 10wt.% recycled waste paper displays lower absorption compared to only 30wt.% of wood flour. As a consequence, studies have also been carried out on composites with both wood flour and recycled waste paper. In particular, 30wt.% of wood flour and 10wt.% of recycled paper have been selected as an optimal mix. Table 45 displays formulations produced and tested.

Table 45: Produced formulations of HDPE50-PLA50 composites with 10, 20, 30 and 40wt.% of recycled waste paper, mix of 30wt.% of wood flour and 10wt.% of recycled waste paper with and without 3 wt.% of compatibilizing agent.

Samples	HDPE (%)	PLA (%)	Polybond 3029 (%)	Lotader AX8840 (%)	Recycled Waste Paper (P) (%)	Wood Flour (WF) (%)
HDPE50-PLA50	50	50				
HDPE50-PLA50-P10	45	45			10	
HDPE50-PLA50-P20	40	40			20	
HDPE50-PLA50-P30	35	35			30	
HDPE50-PLA50-P40	30	30			40	
HDPE50-PLA50-WF30P10	30	30			10	30
HDPE50-PLA50-Poly3-WF30-P10	28.5	28.5	3		10	30
HDPE50-PLA50-Lot3-WF30-P10	28.5	28.5		3	10	30

5.7 Tensile tests

Tensile tests have been performed on composites with increasing amount of recycled waste paper (from 10 to 40 wt.%) and compared with results obtained when wood flour is added. Main results are displayed in Table 46.

Table 46: Tensile tests results for recycled waste paper composites (from 10 to 40wt.%) and mix of 30wt.% of wood flour and 10wt.% of recycled waste paper, compared with neat HDPE50-PLA50 matrix and composites with wood flour.

Samples	E (GPa)	σ (MPa)	ϵ (%)
HDPE50-PLA50	1.88±0.05	38.73±0.18	99.38±2.08
HDPE50-PLA50-WF20	3.37±0.14	34.60±2.79	1.61±0.01
HDPE50-PLA50-WF30	4.12±0.11	34.00±1.27	1.20±0.20
HDPE50-PLA50-WF40	5.04±0.17	33.50±1.46	1.92±0.03
HDPE50-PLA50-P10	2.97±0.05	31.72±0.34	2.02±0.13
HDPE50-PLA50-P20	3.67±0.04	30.2±0.97	1.5±0.19
HDPE50-PLA50-P30	4.95±0.17	31.4±0.35	1.01±0.05
HDPE50-PLA50-P40	5.91±0.56	34.06±4.41	0.94±0.22
HDPE50-PLA50-WF30P10	5.5±0.1	39.2±1.15	1.05±0.03
HDPE50-PLA50-Poly3-WF30-P10	5.19±0.12	31.74±3.74	1.64±1
HDPE50-PLA50-Lot3-WF30-P10	5.49±0.18	32±4.29	1.02±0.08

Recycled waste paper addition sensibly reduces elongation at break of HDPE50-PLA50 (Figure 106) already in the amount of 10wt.%, increasing at the same time elastic modulus.

As expected, the higher the amount of recycled waste paper the higher the elastic modulus (Figure 107), as experienced also with wood flour addition.

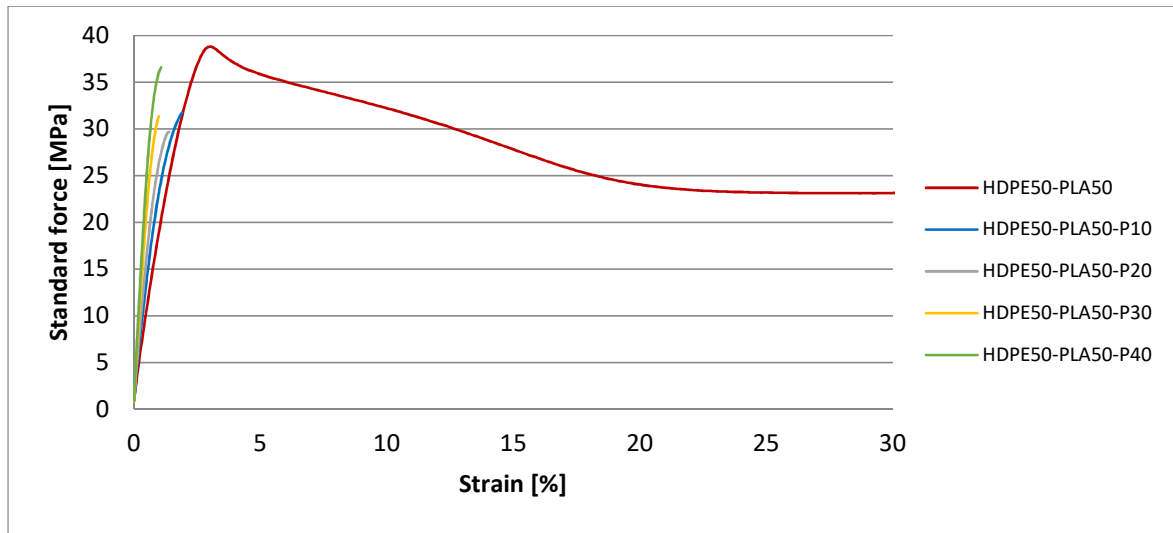


Figure 106: Tensile tests curves of HDPE50-PLA50 (red), HDPE50-PLA50-P10 (blue), HDPE50-PLA50-P20 (grey), HDPE50-PLA50-P30 (yellow), HDPE50-PLA50-P40 (green).

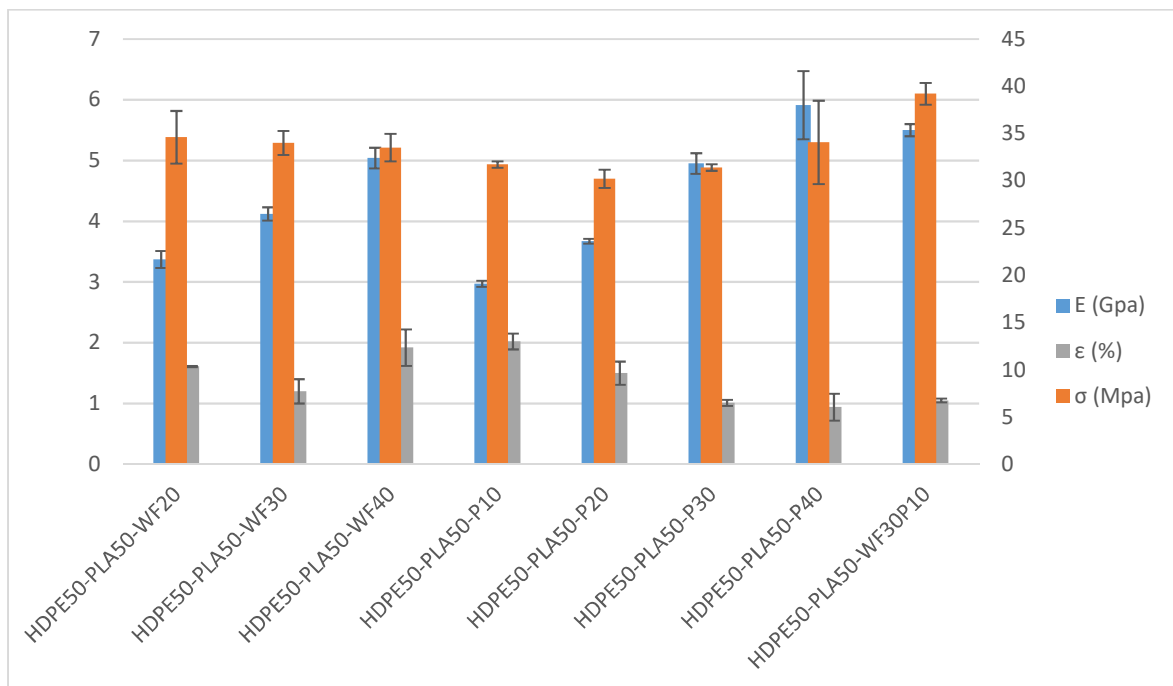


Figure 107: Elastic modulus (blue), elongation at break (grey) and tensile strength (orange) trend for composites with wood flour and recycled waste paper.

Mix of recycled waste paper (10wt.%) and wood flour (30wt.%) seems to increase both elastic modulus and tensile strength comparing results with the same filler amount (40wt.%) of only recycled waste paper or wood flour (Figure 108).

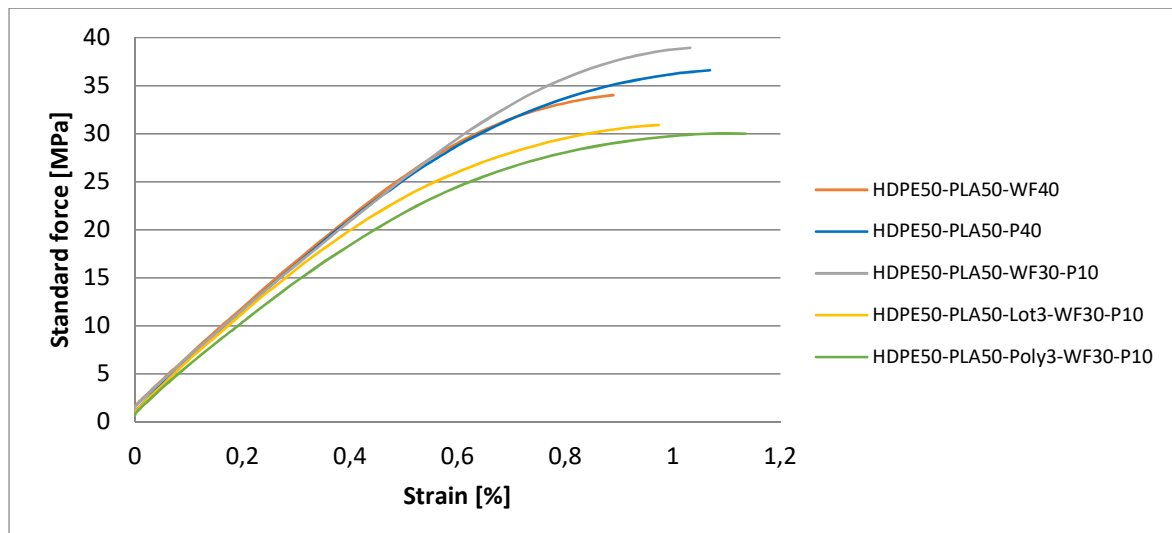


Figure 108: Tensile test curves of HDPE50-PLA50-WF40 (red), HDPE50-PLA50-P40 (blue), HDPE50-PLA50-WF30-P10 (green), HDPE50-PLA50-Lot3-WF30-P10 (purple) and HDPE50-PLA50-Poly3-WF30-P10 (orange).

As reported in literature [14], fillers' aspect ratio is an important parameter to characterize its effectiveness. The aspect ratio is the ratio between the two most representative dimensions of the filler. In order to act as reinforcement, this ratio must be as high as possible. Wood flour displays a lower aspect ratio compared to recycled waste paper because of their different morphologies (the first is particulate and the second fibrous). The main problem related to recycled waste paper fibres is their tendency to form agglomerates when mixed with polymers, as visible in the next SEM paragraph. As a consequence, a mix of wood flour, exempt from agglomerates formation, and recycled waste paper fibres, more effective in increasing elastic modulus, can optimize composite properties.

5.8 Scanning Electron Microscopy (SEM)

Scanning Electron Microscopy has been performed to analyse both fibres distribution and interface with blended matrix.

One of the main problem with recycled waste paper fibres is the possibility to form agglomerates in polymer matrix. Agglomerates formation is derived from two main factors:

1. Different hydrophilicity between recycled waste paper fibres (hydrophilic) and polymer matrix (hydrophobic). In fact, fibres dispersion is hampered by inter-fibre hydrogen bonding [15].
2. Fibre morphology also facilitates mechanical agglomerates formation, as already visible from recycled waste paper fibres visual observation before processing (Chapter 2).

Figure 109A displays good fibres distribution for HDPE50-PLA50-P10. Unfortunately, already with 20wt.% of P, agglomerates formation is visible (Figure 109B). This is one of the reasons to select 10wt.% of recycled waste paper in the mix with wood flour.

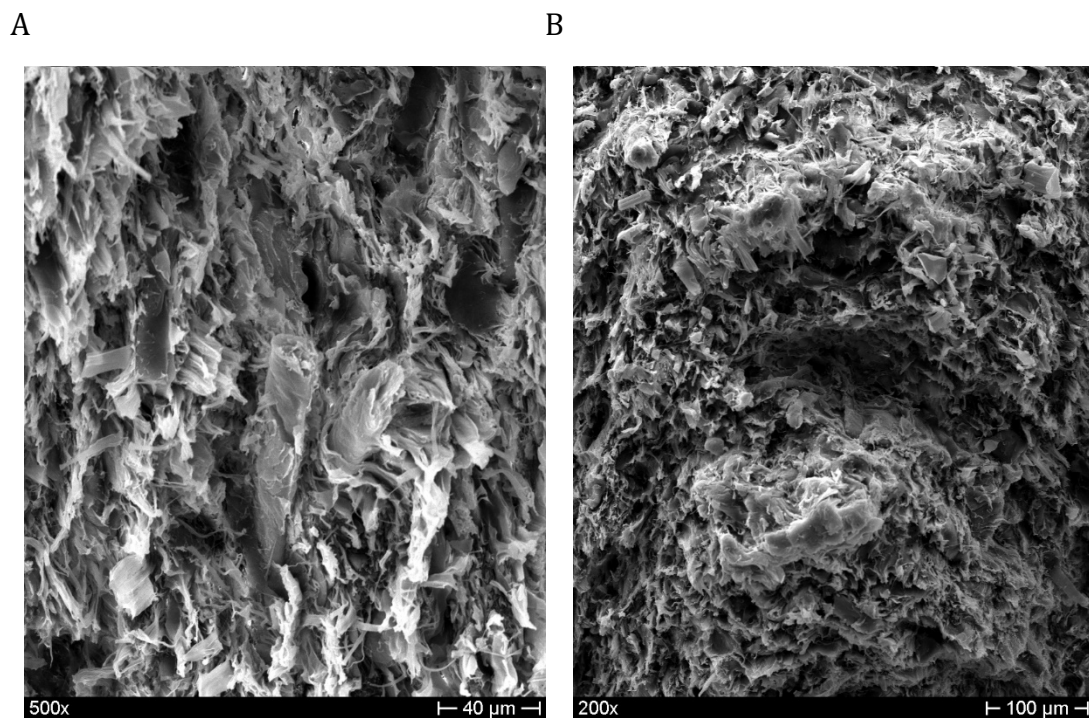


Figure 109: SEM images of A)HDPE50-PLA50-P10 and B)HDPE50-PLA50-P20.

Good fillers distribution, both wood flour and recycled waste paper, was displayed by HDPE50-PLA50-WF30-P10 (Figure 110). Fillers' mix, likewise wood flour addition, already displays an increased morphology complexity, in agreement with mechanical properties, especially low

elongation at break. Both wood particles and recycled waste paper seem to be partially related to polymer matrix, but not completely compatibilized.

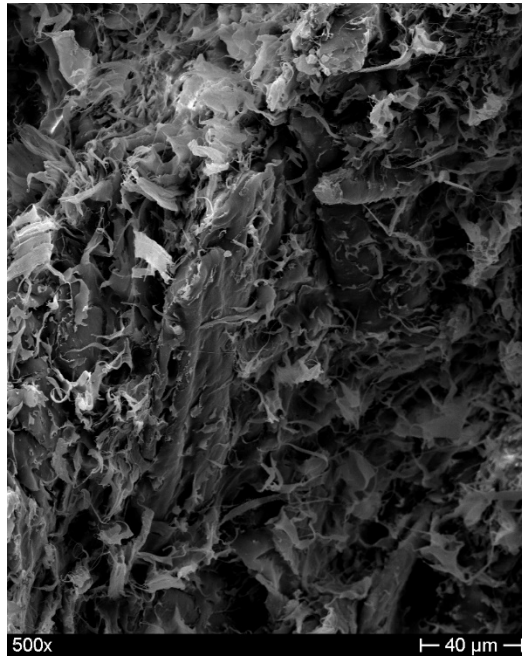
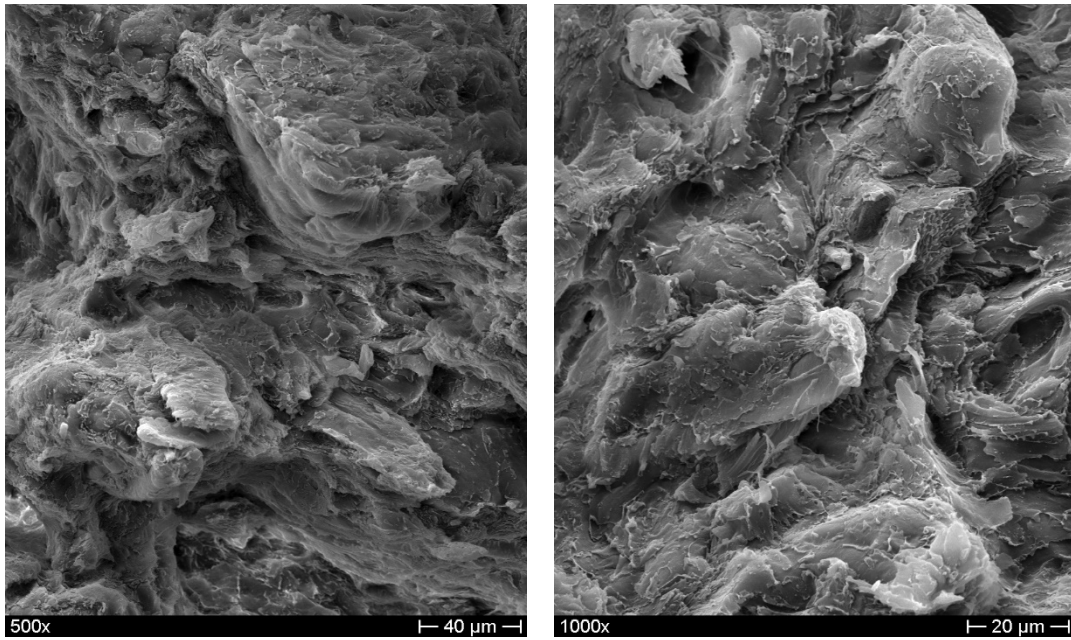


Figure 110: SEM images of HDPE50-PLA50-WF30-P10

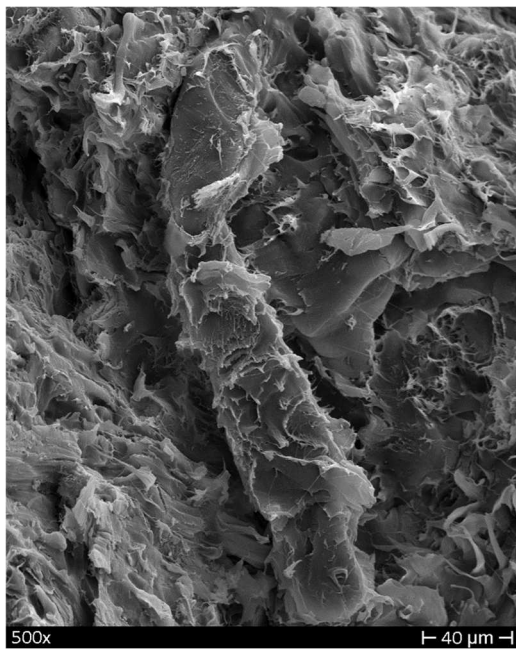
The presence of Lotader AX8840, thanks to glycidyl methacrylate groups, seems to reduce matrix defectiveness, increasing at the same time interface with wood flour and recycled waste paper (Figure 111A and B). The presence of Polybond 3029 seems to have a lower effect on matrix homogeneity and improvement of fillers-matrix interfaces: in fact, phase separation is more visible compared to Lotader AX8840 addition and fillers are less covered by the polymer (Figure 111C and D).

A

B



C



D

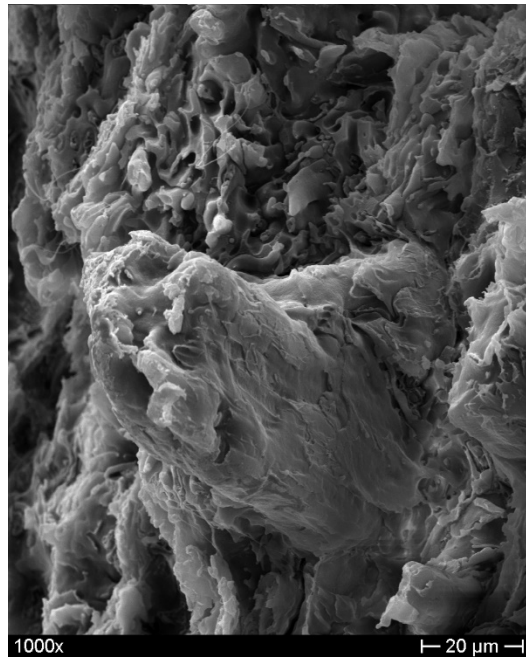


Figure 111: SEM images of A) HDPE50-PLA50-Lot3-WF30-P10 (500X), B) HDPE50-PLA50-Lot3-WF30-P10 (1000X), C) HDPE50-PLA50-Poly3-WF30-P10 (500X) and D) HDPE50-PLA50-Poly3-WF30-P10 (1000X).

5.9 Differential Scanning Calorimetry (DSC)

PLA cold crystallization is still absent with both recycled waste paper and wood flour addition, suggesting again a higher difficulty of PLA macromolecules to arrange themselves.

Recycled waste paper seems to increase both HDPE and PLA crystallinity. In particular, HDPE crystallinity is still lower than neat HDPE, while PLA crystallinity is higher than the one of neat PLA or wood flour composites. This result can be in agreement with the influence of wood flour and recycled waste paper described in more detail in the paragraph “Influence of Wood flour and Recycled waste paper on HDPE and PLA” of this chapter. Mixing 30wt.% of wood flour and 10wt.% of recycled waste paper seems to decrease crystallinity of both HDPE (62% crystallinity is the lowest value obtained in this study) and PLA. A possible explanation is the higher difficulty of macromolecules to arrange themselves when both fillers are present in the blend.

The addition of both Lotader AX8840 and Polybond 3029 seems to increase more effectively HDPE crystallinity, but a slight influence is also displayed on PLA crystallinity. These results can be in agreement with a higher compatibility in composites with coupling agent addition.

Table 47: DSC results for HDPE50-PLA50, HDPE50-PLA50-P composites and HDPE50-PLA50-WF-P composites with and without coupling agents.

	$\Delta H_{cc}PLA$ (J/gPLA)	T_{cc} (°C)	ΔH_{mPE} (J/gPE)	T_{mPE} (°C)	ΔH_{mPLA} (J/gPLA)	T_{mPLA} (°C)	T_{gPLA} (°C)	X (%) HDPE	X (%) PLA
HDPE50-PLA50	16	97	226	132	40	168	62	81	43
HDPE50-PLA50-P10	-	-	200	134	38	169	61	68	41
HDPE50-PLA50-P20	-	-	202	133	42	169	61	69	45
HDPE50-PLA50-P30	-	-	203	134	46	169	62	69	49
HDPE50-PLA50-P40	-	-	216	133	44	169	61	74	47
HDPE50-PLA50-WF30	-	-	200	132	37	167	62	68	40
HDPE50-PLA50-WF30P10	-	-	183	133	40	168	61	62	43
HDPE50-PLA50-Lot3-WF30P10	-	-	197	133	42	167	59	67	45
HDPE50-PLA50-Poly3-WF30P10	-	-	197	133	42	167	61	67	45

5.10 Influence of Wood flour and Recycled waste paper on HDPE and PLA

More accurate analyses have been performed on the effect of wood flour and recycled waste paper on HDPE and PLA separately.

Mechanical properties of composites with only HDPE or PLA matrix have been evaluated to understand the effect of wood flour and recycled waste paper on both polymers. Main results are displayed in Table 48.

Table 48: Tensile tests results of HDPE and PLA composites with wood flour and recycled waste paper fibres.

Samples	E (GPa)	σ (MPa)	ϵ (%)
PLA	3.0±0.1	57±1	7.5±0.7
HDPE	1.1±0.1	21±1	>400
PLA60-WF40	7.5±0.2	54.0±14.1	0.9±0.3
PLA60-P40	7.8±0.1	66.8±5.6	1.0±0.1
HDPE60-WF40	4.4±0.1	28.3±1.7	2.5±0.2
HDPE60-P40	4.5±0.1	28.1±0.5	2.6±0.8

Both wood flour and recycled waste paper fibres allow an improvement in elastic modulus and tensile strength, at the expense of elongation at break.

Literature reports a nucleating effect of natural fillers on HDPE and PLA [16-17]. As a consequence, we analysed the influence of wood flour and recycled waste paper fibres on HDPE and PLA crystallinity.

A thermo-optical microscope from Zeiss has been used to study crystals growth in both neat HDPE or PLA and polymers with wood flour or recycled waste paper.

In any case, samples have been heated until the melting point and kept at this temperature for PLA and 125°C for HDPE to perform isothermal crystallization [19]. Approximately, each snap has been done every 3 second.

Figure 112 displays development of Malta cross in PLA at 500X magnification.

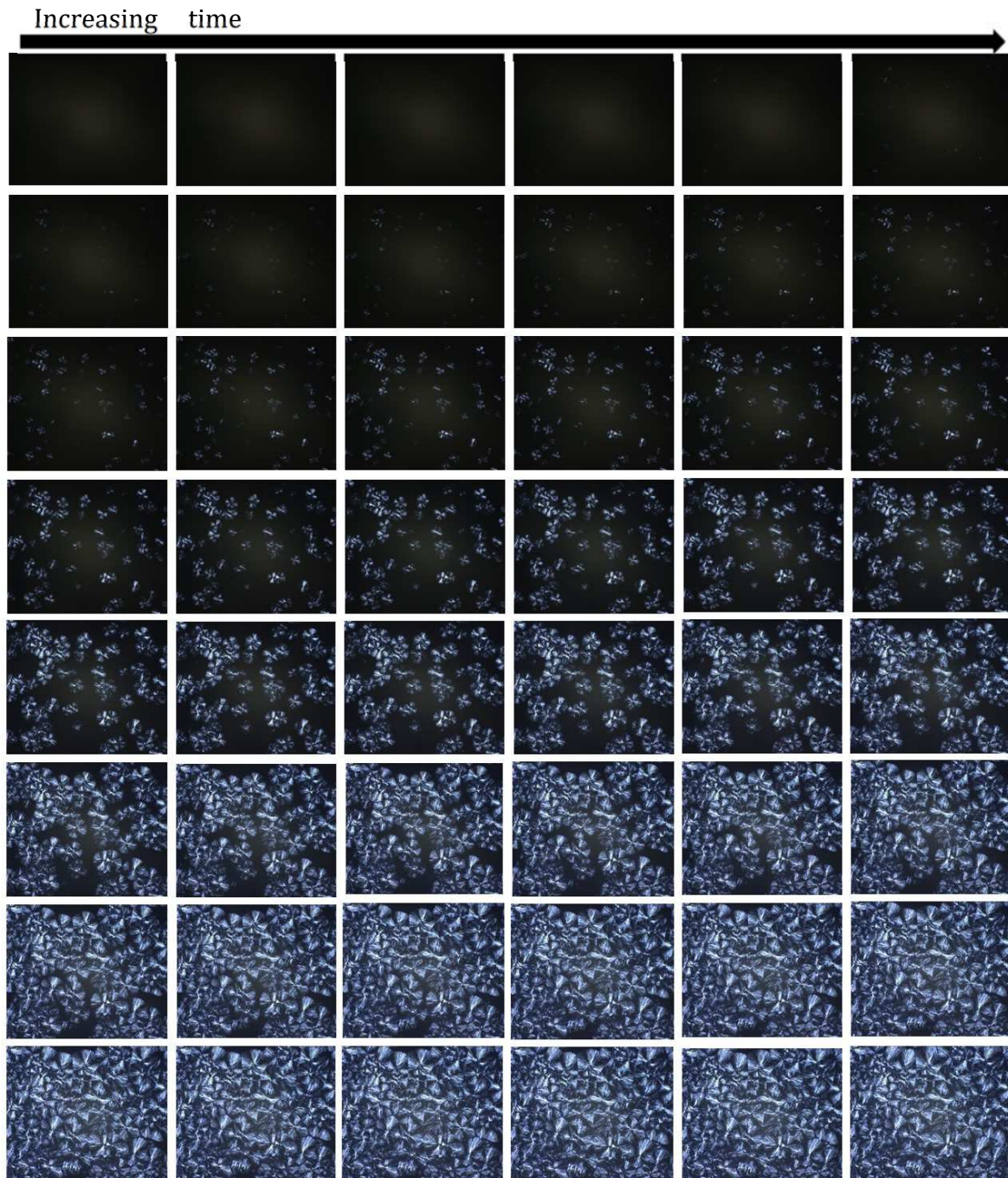


Figure 112: Malta cross evolution in PLA studied with a thermo-optical microscope at 500X magnification with polarized light.

Homogeneous crystals growth is displayed, with uniform crystals development all over PLA.

Figure 113 displays PLA crystals growth when recycled waste paper fibres are added.

Increasing time

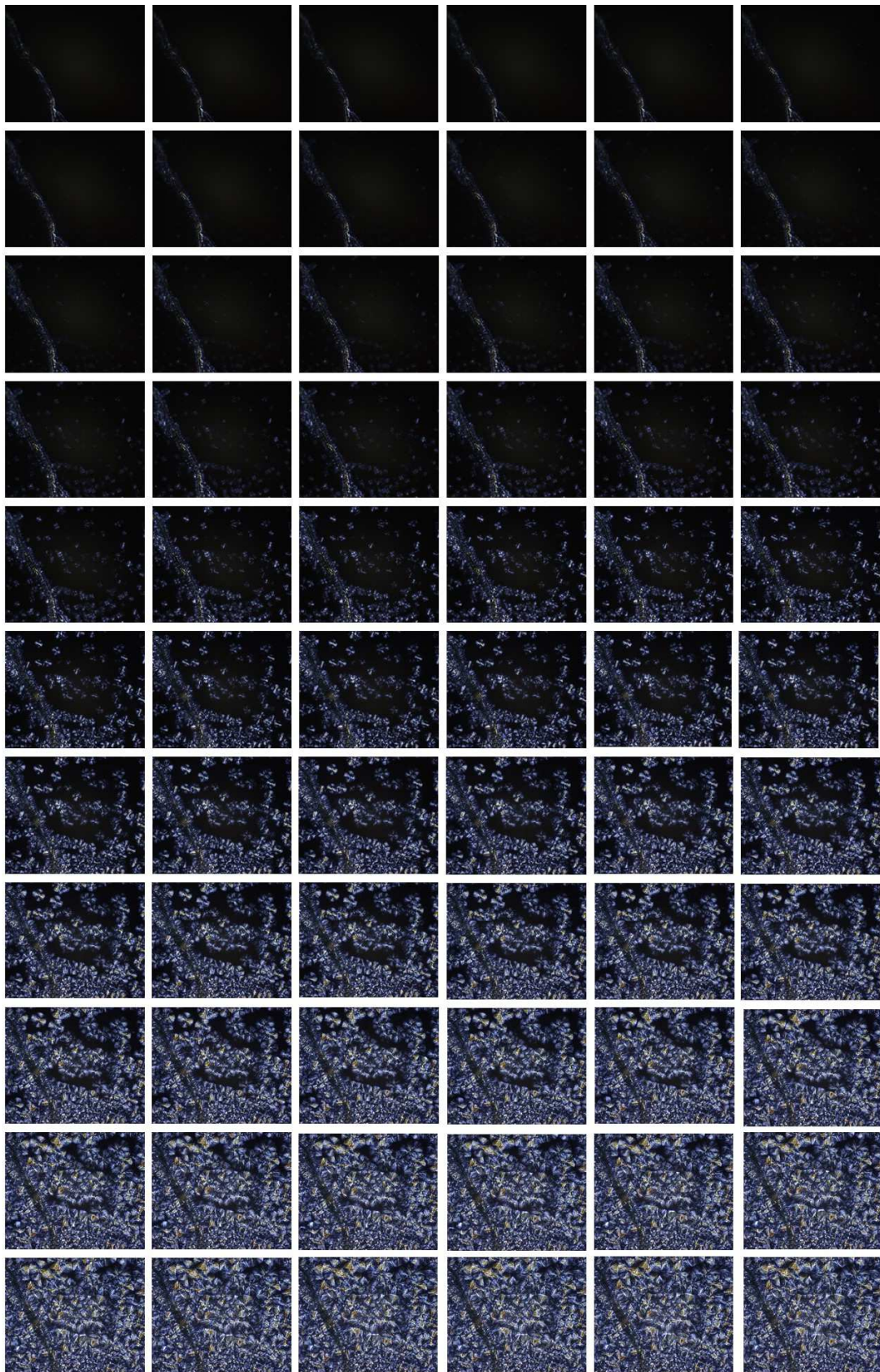


Figure 113: Crystals growth in PLA with recycled waste paper (PLA60-P40), studied with a thermo-optical microscope at 500X magnification with polarized light.

PLA crystals growth first develop near recycled waste paper fibre, and then in bulk PLA. Images suggest the formation of an individual spherulites row on the surface of the fibres, typical of fibres with moderate nucleating ability, as reported in literature [20]. Wood flour seems to have an influence on PLA crystals growth, but deeper analyses have to be done (Figure 114).



Figure 114: Crystals growth in PLA with wood flour (PLA60-WF40), studied with a thermo-optical microscope at 100X magnification with polarized light.

Differential Scanning Calorimetry is one of the technique to analyse the influence of fillers on polymer matrix crystallinity. In particular, sample is heated up to the melting point and stabilized at this temperature to erase thermal history. Sample is then quenched to crystallization temperature and it is kept at this temperature until complete crystallization

occurs. Figure 115 displays crystallinity rate vs time for neat PLA (blue), PLA60-P40 (orange) and PLA60-WF40 (grey), at $T_c=105^\circ\text{C}$.

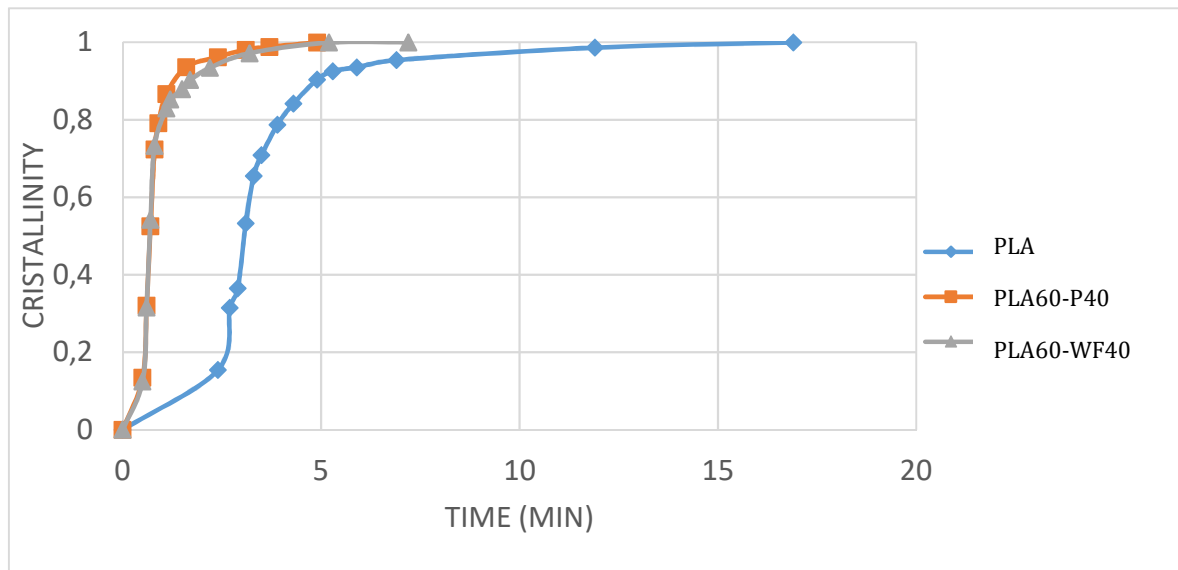


Figure 115: Crystallinity rate vs time for neat PLA (blue), PLA60-P40 (orange) and PLA60-WF40 (grey).

Both wood flour and recycled waste paper seem to act as nucleating agents, reducing the half time crystallization $t_{1/2}$. $t_{1/2}$ is the time required to reach 50% of the final crystallinity [21]. Neat PLA displays a $t_{1/2}$ of 3,1 min, while PLA with both wood flour and recycled waste paper fibres have $t_{1/2}$ of 0,7 min.

Same analyses have been performed on HDPE, HDPE filled with recycled waste paper and HDPE filled with wood flour (Figure 116, 103 and 104).

Increasing time

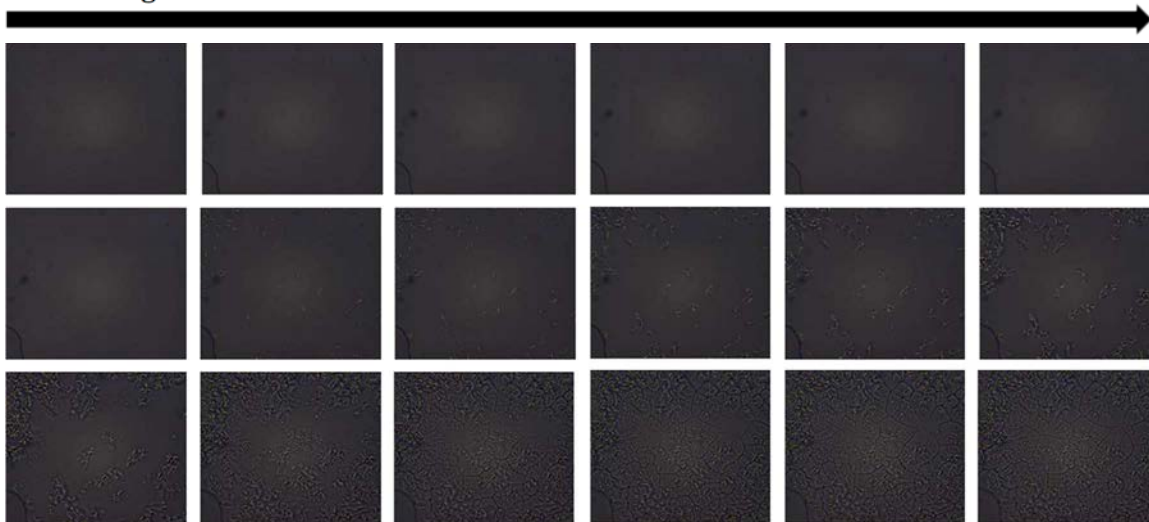


Figure 116: Crystals' growth in HDPE studied with a thermo-optical microscope at 500X magnification

Increasing time

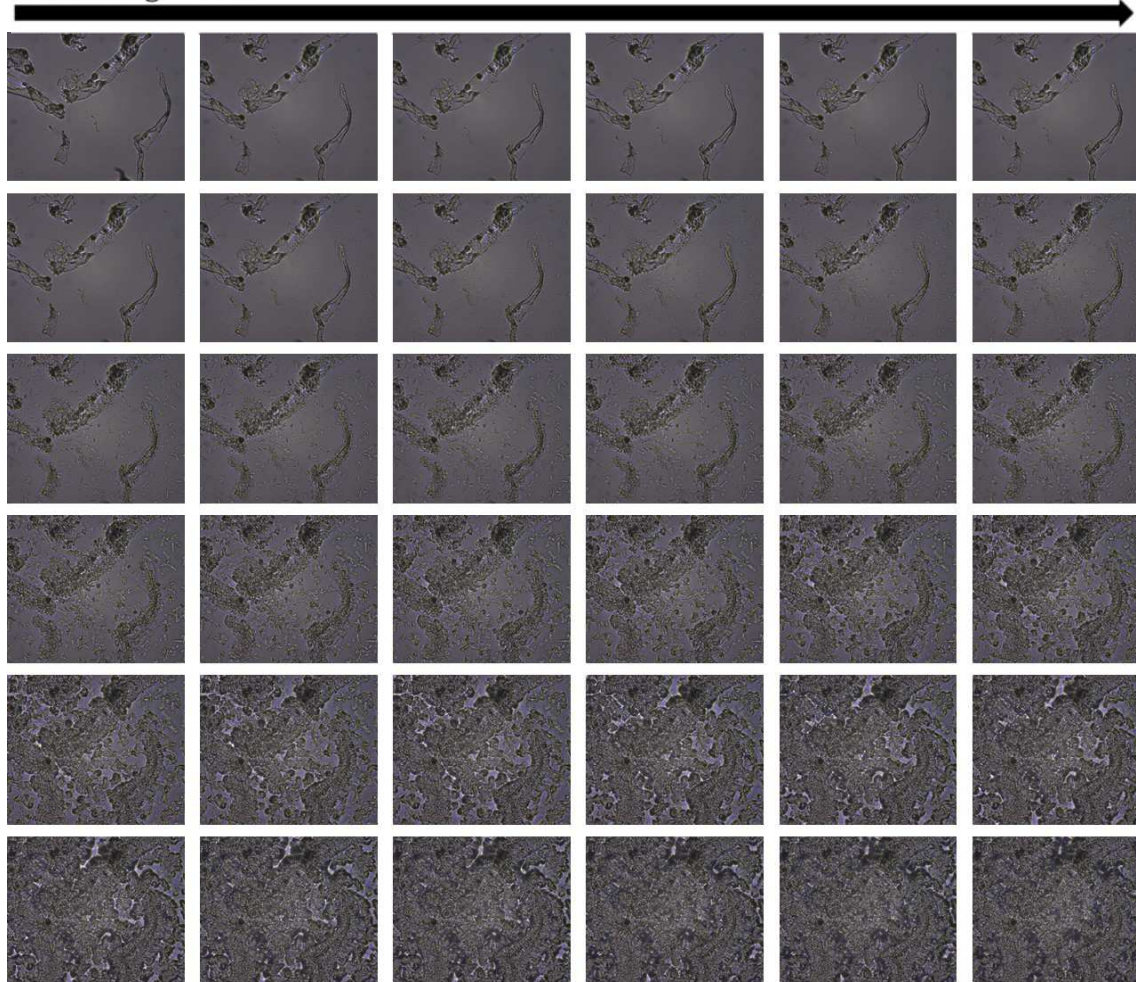


Figure 117: Crystals' growth in HDPE with recycled waste paper (HDPE60-P40), studied with a thermo-optical microscope at 500X magnification.

Increasing time



Figure 118: Crystals' growth in HDPE with wood flour (HDPE60-WF40), studied with a thermo-optical microscope at 500X magnification.

Thermo-Optical Microscope images display the same tendency revealed from PLA based samples. In fact, HDPE also reveals the formation of a unique row of spherulites around fibres and a nucleating effect of wood flour.

DSC analyses have been performed and Figure 105 displays crystallinity rate vs time for neat HDPE (blue), HDPE60-P40 (orange) and HDPE60-WF40 (grey), at $T_c=125^\circ\text{C}$. Results reveal a $t_{1/2}$ of 4,4 min for neat HDPE, 2,9 min for HDPE with wood flour and 1,9 min for HDPE with recycled waste paper. A lower $t_{1/2}$ for recycled waste paper fibres is probably related to different fibres morphology and composition with respect to wood flour.

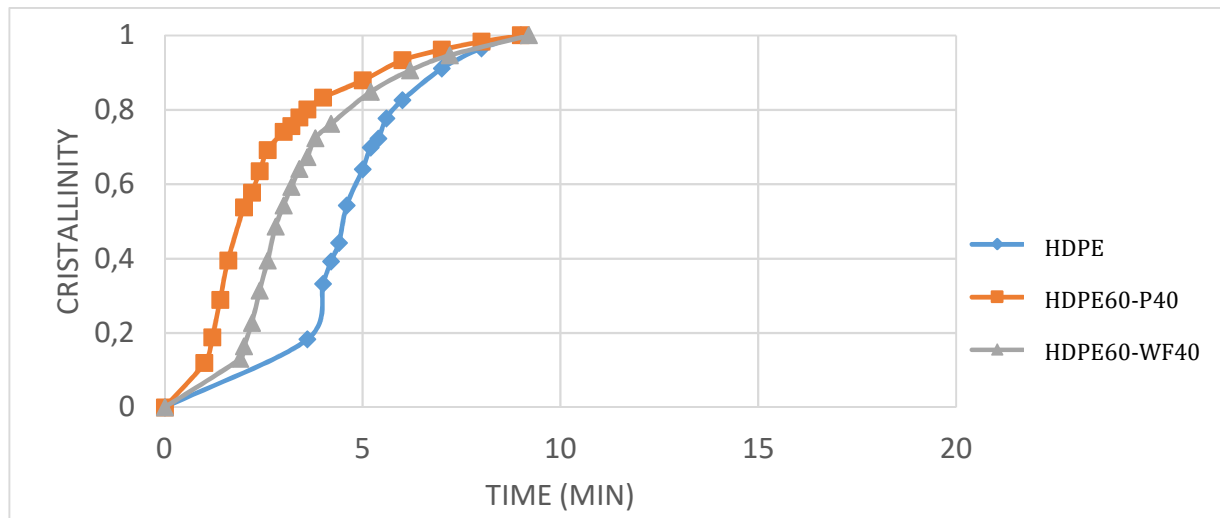


Figure 119: Crystallinity rate vs time for neat HDPE (blue), HDPE60-P40 (orange) and HDPE60-WF40 (grey).

5.11 Turbomixer processing

Turbomixer processing has been tested in order to compare this innovative technique with the traditional extrusion and injection moulding processing. In this first analysis, samples with the same amount of fillers obtained with extrusion have been produced, but future improvement involves the introduction of higher amount of fillers, overcoming extrusion limits. Table 49 displays formulation of samples produced with this technique and Figure 120, 107 and 108 display turbomixer and compression moulding equipment.



Figure 120: Tubromixer processing of samples with HDPE, PLA, wood flour and recycled waste paper.



Figure 121: Compression moulding technique (plates at 90°C) performed on samples produced with turbomixer processing.



Figure 122: Samples obtained with compression moulding technique.

Table 49: Samples produced with turbomixer processing.

Samples	HDPE (%)	PLA (%)	Polybond 3029 (%)	Lotader AX8840 (%)	Recycled Waste Paper (P) (%)	Wood Flour (WF) (%)
HDPE50-PLA50-WF30	35	35				30
HDPE50-PLA50-WF40	30	30				40
HDPE50-PLA50-WF30-P10	30	30			10	30
HDPE50-PLA50-Poly3-WF30-P10	28.5	28.5	3		10	30
HDPE50-PLA50-Lot3-WF30-P10	28.5	28.5		3	10	30

Firstly, tensile tests have been performed in order to evaluate mechanical properties (Table 50). Unfortunately, results seem to be lower compared to samples obtained with extrusion and injection moulding. A possible explanation is related to a low specific power of this equipment, not optimized for natural filler composites. In fact, they are characterized by low thermal

conductivity. However, future studies will be done to optimize equipment dimensions in order to increase specific power, and also the amount of fillers.

Table 50: Tensile tests results for samples produced with turbomixer processing.

Samples	E (GPa)	σ (MPa)	ϵ (%)
HDPE50-PLA50-WF30	3.3±0.8	18.21±2.19	0.59±0.11
HDPE50-PLA50-WF40	4.0±0.5	11.74±3.85	0.32±0.03
HDPE50-PLA50-WF30-P10	3.5±0.8	10.35±3.26	0.42±0.34
HDPE50-PLA50-Poly3-WF30-P10	3.3±0.4	12.52±0.82	0.71±0.31
HDPE50-PLA50-Lot3-WF30-P10	3.3±0.5	13.19±3.85	0.51±0.03

5.12 Composting tests

Samples have been subjected to composting in soil for three months at 35°C and 58°C, in order to evaluate their degradation. In particular, HDPE-based and PLA-based composites have been tested to analyse the effect of natural fillers (wood flour, recycled waste paper and a mix of both fillers) on polymer degradation. Moreover, a sample with HDPE-PLA blend composite and a mix of two fillers has also been tested. Table 51 displays all formulations subjected to this test.

Table 51: Formulations of samples for composting test in soil.

Samples	HDPE (%)	PLA (%)	Wood Flour (WF) (%)	Recycled Waste Paper (P) (%)
---------	-------------	------------	------------------------------	---------------------------------------

HDPE	100			
PLA		100		
HDPE60-WF40	60		40	
HDPE60-P40	60			40
PLA60-WF40		60	40	
PLA60-P40		60		40
PLA60-WF30-P10		60	30	10
HDPE50-PLA50-WF30-P10	30	30	30	10

5.12.1 Mass Variation and Visual Observation

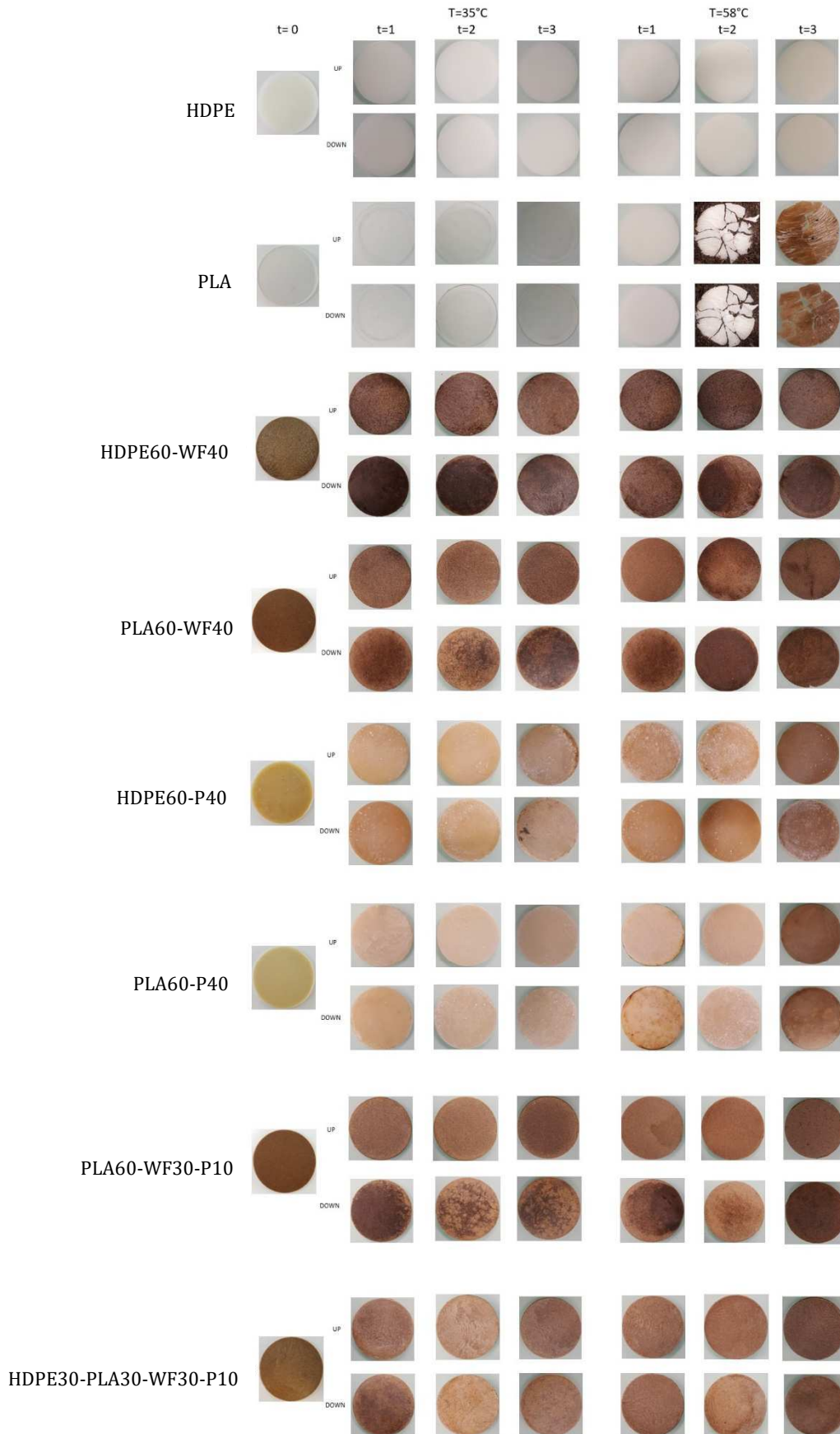


Figure 123: Visual observation of HDPE, PLA, HDPE60-WF40, PLA60-WF40, HDPE60-P40, PLA60-P40, PLA60-WF30-P10 and HDPE30-PLA30-WF30-P10 for three months testing in soil at 35°C and 58°C.

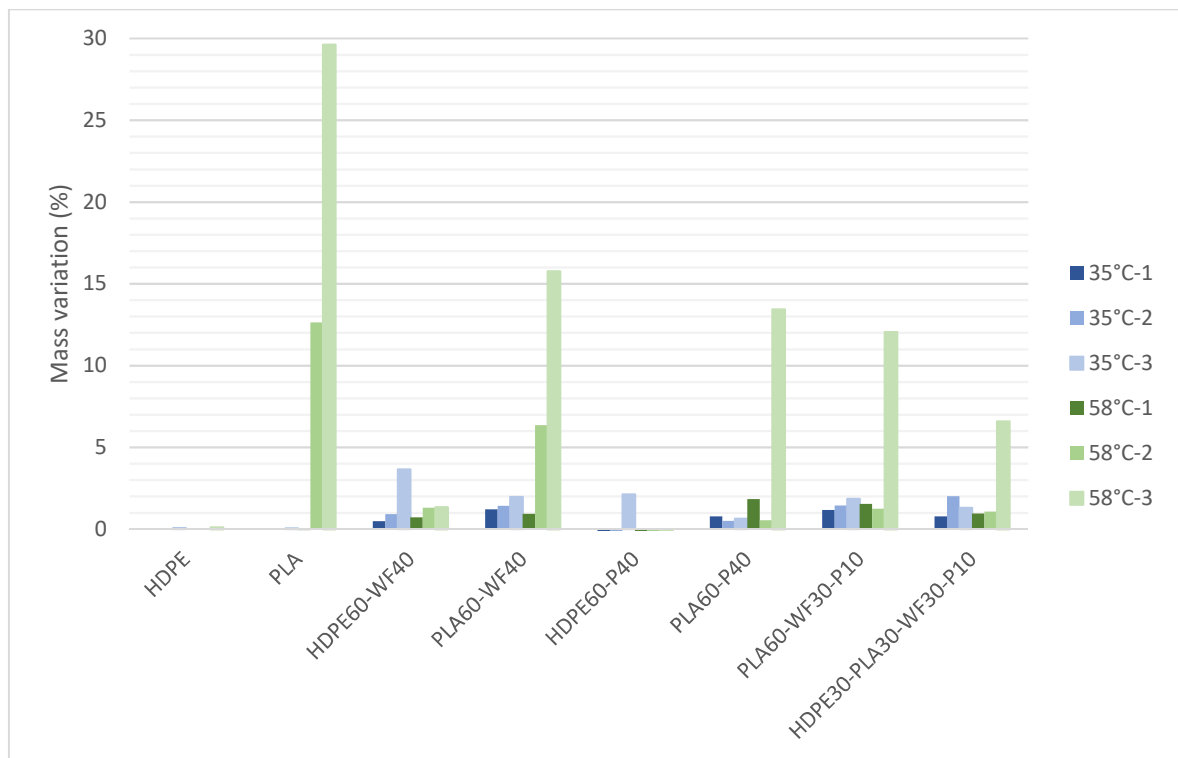


Figure 124: Mass variation measurements of HDPE, PLA, HDPE60-WF40, PLA60-WF40, HDPE60-P40, PLA60-P40, PLA60-WF30-P10 and HDPE30-PLA30-WF30-P10 for three months testing in soil at 35°C and 58°C.

As expected, HDPE displays no mass variation at both 35°C and 58°C, as visible from Figure 124, in agreement with visual observation (Figure 123), from which no colour changing is displayed except for a little yellowing for time 3 at 58°C. In fact, in agreement with literature [22], HDPE samples display a very slow degradation process in soil. The addition of wood flour and recycled waste paper influenced mass variation.

PLA-based samples, thanks to PLA biodegradability, display mass variation, especially after three months at 58°C.

PLA degradation is due to breakage of ester bonds. Water hydrolyses polymeric chain randomly, as a consequence, polymer molecular weight is reduced, and oligomers are obtained. In fact, degradation can be evaluated through mass variation [23]. A visible effect of temperature is displayed for neat PLA degradation process. In fact, samples at 58°C are characterized by a higher degradation rate and higher mass variation with respect to samples at 35°C.

Mass variation results are in agreement with visual observations: PLA at 35°C appears to be stable, without visible variation, while PLA at 58°C becomes opaque after one month, breaking in smaller pieces during the second and third month [24].

Wood flour and recycled waste paper addition seems to increase mass variation for PLA-based samples at 35°C. This can be related to humidity absorbed by wood flour and recycled waste paper [21]. Moreover, a degradation of natural filler can also occur, reducing sample's mass. PLA-based composites at 58°C are characterized by a lower mass variation with respect to neat PLA.

In agreement with literature results [25], PLA is normally characterized by a first lag phase, in which diffusion of water occurs and macromolecules are still too long to be degraded by microorganisms. As a consequence, mass variation displays a higher difference for time 3 with respect to time 1 and 2.

HDPE30PLA30WF30P10 is characterized by the lowest mass variation, probably due to HDPE presence. In fact, HDPE is hydrophobic and can obstacle water diffusion in wood flour, recycled waste paper and PLA [26].

To conclude, HDPE-based samples experienced no sensitive mass variation, however an influence of WF and P addition seemed to be evident. Neat PLA displayed higher mass variation when buried under thermophilic condition, while di addition of natural fillers increased mass variation under mesophilic condition.

5.12.2 SEC

PLA-based samples have also been analysed by SEC in tetrahydrofuran, in order to evaluate average molecular weight variation during composting at 35°C (Figure 125) and 58°C (Figure 126).

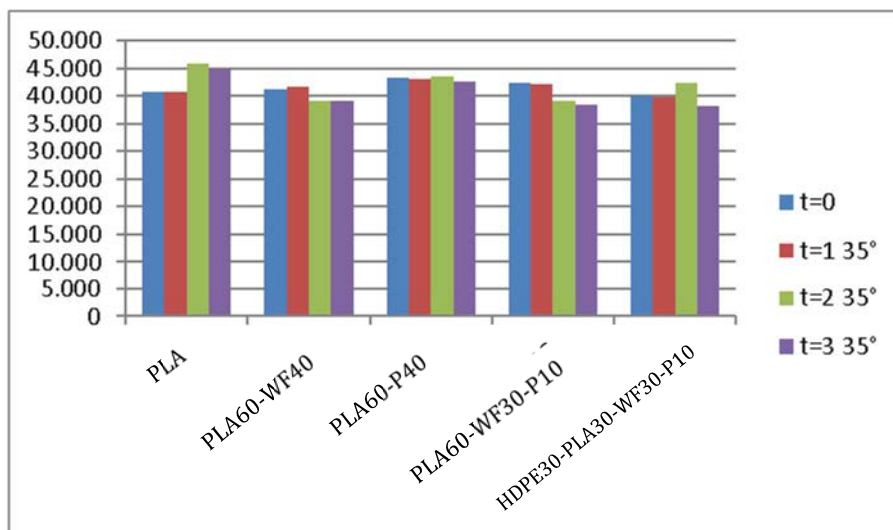


Figure 125: Mass average molecular weight of PLA-based samples before burying in soil (t=0) and after one, two or three months burying (t=1, t=2 and t=3 respectively) at 35°C.

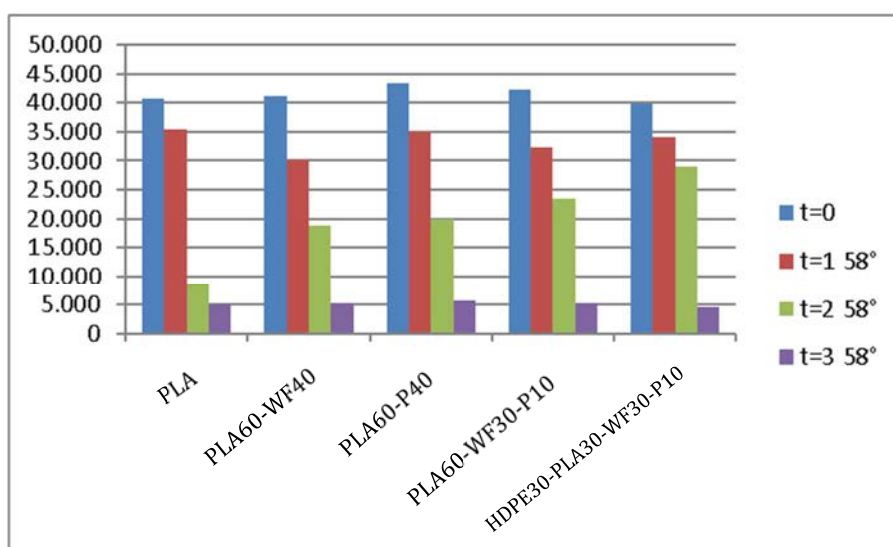


Figure 126: Mass average molecular weight of PLA-based samples before burying in soil (t=0) and after one, two or three months burying (t=1, t=2 and t=3 respectively) at 58°C.

Mass-average molecular weight (Mw) in mesophilic conditions (35°C) did not display sensitive variations, suggesting a slow PLA degradation. PLA-based composites, both with wood flour and recycled waste paper, still display small Mw variations.

PLA-based samples tested in thermophilic conditions (58°C), conversely, displayed Mw sensitive reduction by time: in fact, Mw decreased from about 40kDa to about 5kDa after three months. PLA degradation hydrolytic step, in agreement with literature results, is temperature

sensitive, displaying optimal kinetic condition around 58°C. However, recycled waste paper seems to partially hinder PLA degradation with respect to wood flour, keeping Mw at slightly higher values.

To conclude, Mw reduction have been displayed for PLA-based composites after composting tests at 58°C especially for time 3, because hydrolytic process is favoured at higher temperature.

5.12.3 Infrared Spectroscopy

Infrared spectroscopy allows following of biodegradation development, analysing peaks shifting and intensity variations. Table 52 displays characteristic peaks of HDPE, cellulose, hemicellulose and lignin. Figure 127 and Figure 128 display ATR-FTIR spectra of recycled waste paper and wood flour.

Table 52: Characteristic peaks of HDPE, cellulose, hemicellulose and lignin

HDPE	
Wavenumber (cm ⁻¹)	Vibrational type
2915	C–H stretching asimmetric CH ₂
2848	stretching simmetric CH ₂
1474	CH ₂ scissoring (crystallised)
1464	CH ₂ scissoring (amorphous)
730	Rocking of the ethylene group CH ₂ (crystallised)
720	Rocking of the ethylene group CH ₂ (amorphous)
Hemicellulose and Lignin	
1735	C=O stretching in unconjugated ketones aldehydes and carboxyl (xylan and hemicellulose)
1595	C=C stretching of the aromatic ring (lignin)
1512	C=C stretching of the aromatic ring (lignin)
1463	Asymmetric bending in CH ₃ (lignin)

1269	CO stretching (lignin and hemicellulose)
1125	C-H aromatic, bending lignin
1032	C-O in cellulose and primary alcol (lignin)
Cellulose	
3200-3400	OH stretching
2890	CH stretching
1600-1650	H ₂ O bending
1425	CH ₂ bending (crystallised I)
1375	CH bending Cellulose
1317	CH ₂ wagging (crystallised)
1335	OH in plane bending (amorphous)
1163	COC asym. bridge oxygen stretching
1150	COC stretching
896	asym. out of phase ring stretching

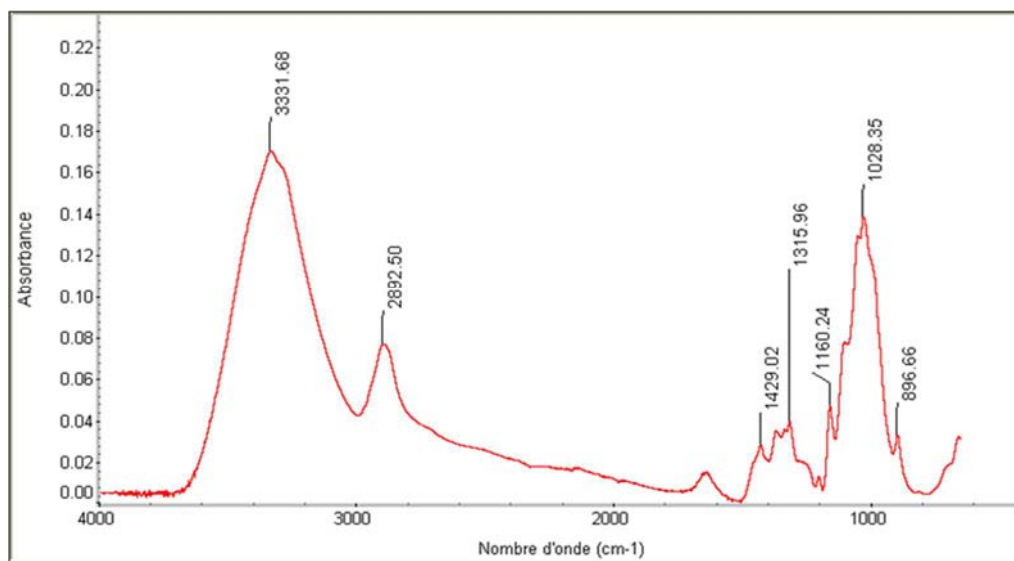


Figure 127: ATR-FTIR spectrum of recycled wastepaper

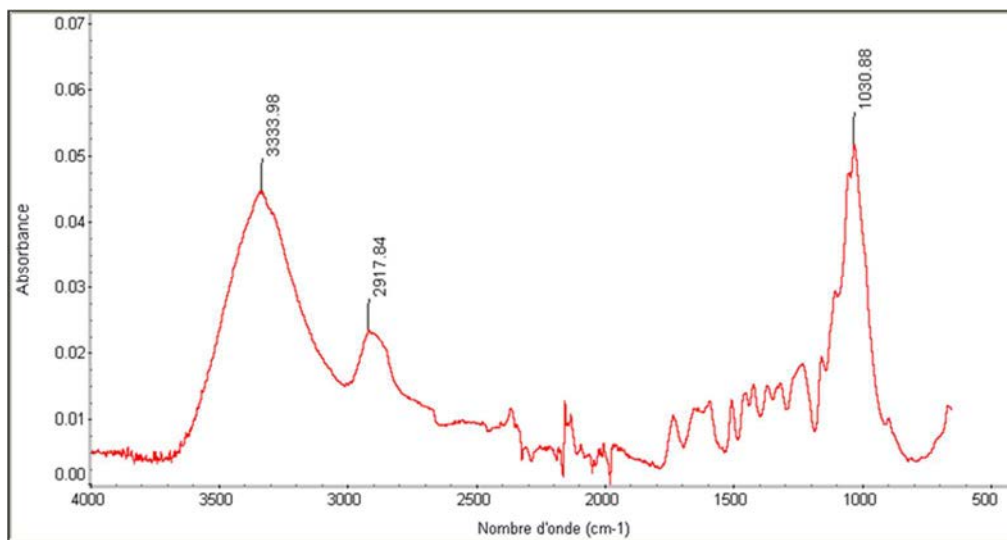


Figure 128: ATR-FTIR spectrum of wood flour

HDPE

HDPE did not display any modification of its spectra after three months buried in soil at both 35°C (Figure 129) and 58°C (Figure 130).

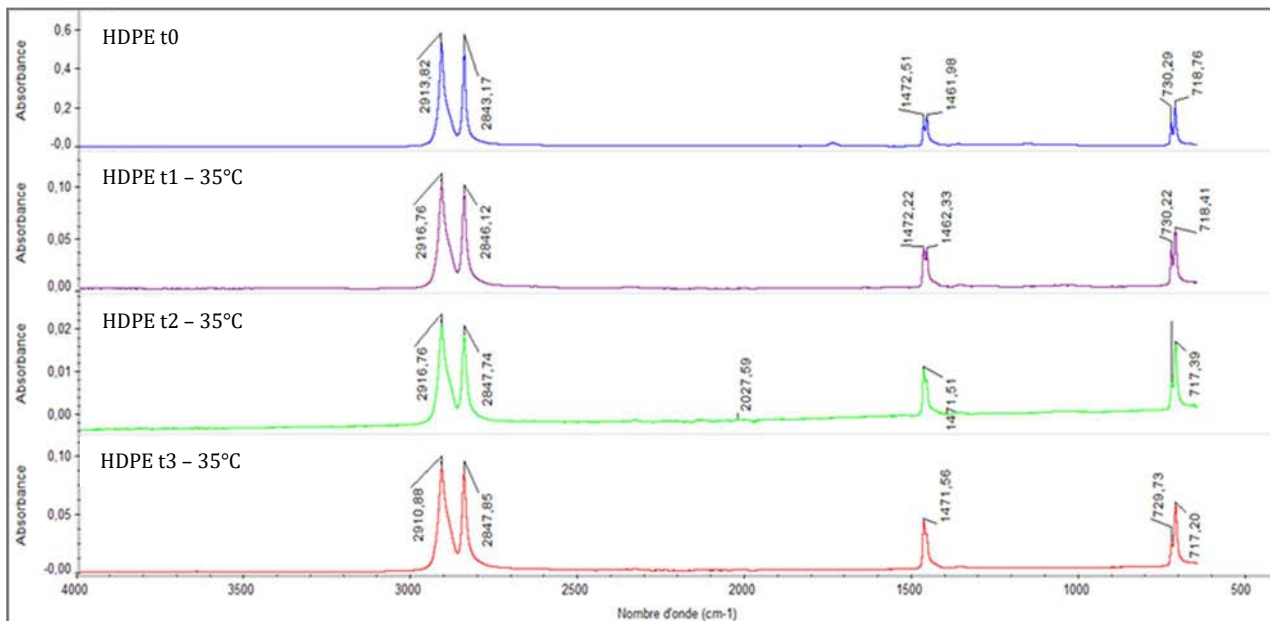


Figure 129: ATR-FTIR spectra of HDPE from time 0 to time 3 for buried samples at 35°C.

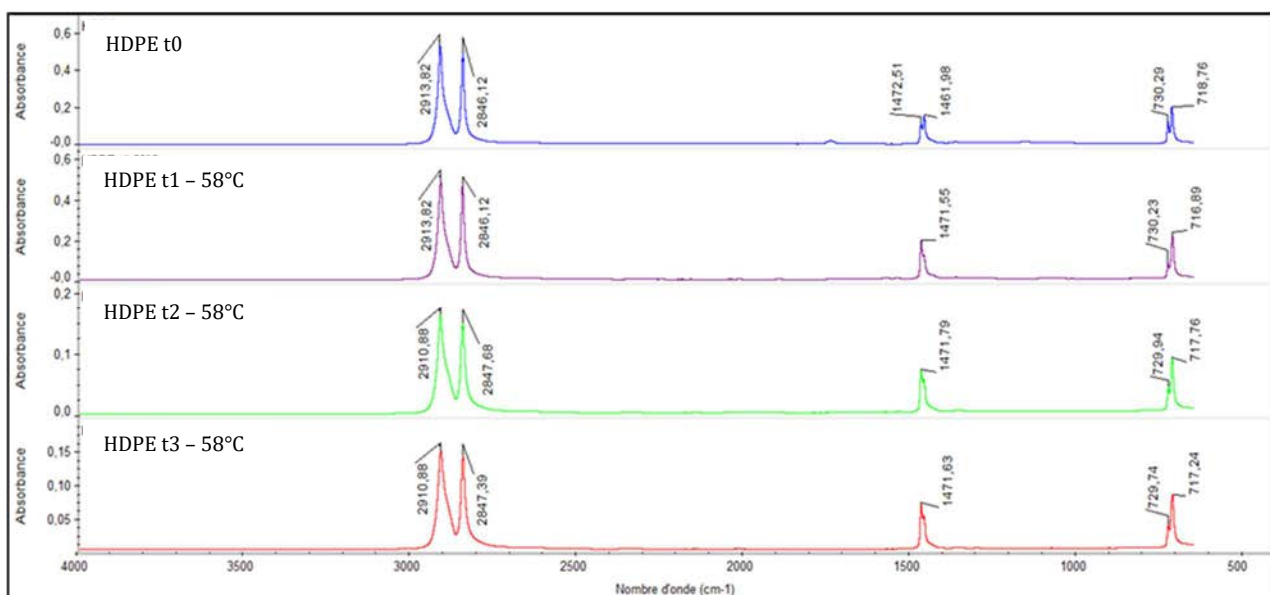


Figure 130: ATR-FTIR spectra of HDPE from time 0 to time 3 for buried samples at 58°C

HDPE60-P40

Spectra of HDPE60-P40 combine the absorption bands of HDPE matrix and characteristic absorption peaks of cellulose (Figure 131 samples buried at 35°C and Figure 132 samples buried at 58°C). Paper consists mainly of cellulose fibres but also contains hemicellulose and lignin [27]. Cellulose is characterized by:

- peak at 1425 cm^{-1} , known as the crystalline band, caused by the vibrations of the aromatic skeleton combined with the bending of the C-H (a lowering of its intensity reflects the decrease in the degree of crystallinity of samples) [28];
- peak at 1032 cm^{-1} , associated both with the symmetrical CO stretching of the cellulose and with the CO deformation of the primary alcohols in the lignin;
- peaks between $3400\text{-}3300\text{ cm}^{-1}$ and 1593 cm^{-1} attributed to the stretching and bending, respectively, of OH groups of cellulose [29]. This modification, together with the shift of peak at 1316 cm^{-1} towards higher values, denotes the development of new inter- and intramolecular hydrogen bonds [30].

The predominant degradation phenomenon that characterizes the filler is oxidative, especially for hemicellulose and lignin. [31] The oxidative process is detected by increasing intensity of the small peaks generated by the functional carbonyl group in the absorption range between $1800\text{-}1600\text{ cm}^{-1}$ [32]. In particular, small signals revealed in the area $1740\text{-}1709\text{ cm}^{-1}$ are an expression of the carbonyl groups related to C = O stretching of hemicellulose groups or to the ester bond of the carboxylic group in the ferulic and coumarinic acids of the lignin and hemicellulose [31]. This also makes this zone a good "marker" of oxidative processes, the intensity of the band around 1735 cm^{-1} is usually proportional to the oxidation of hemicellulose (C = O in xylan). The peak at 1035 cm^{-1} assigned to the stretching vibration CO of the cellulose ring and the primary alcohols in lignin, shows an increase at t3, both at 35 and at 58 ° C over time, probably due to a relative increase in cellulose due to the degradation of hemicellulose and lignin [33-34].

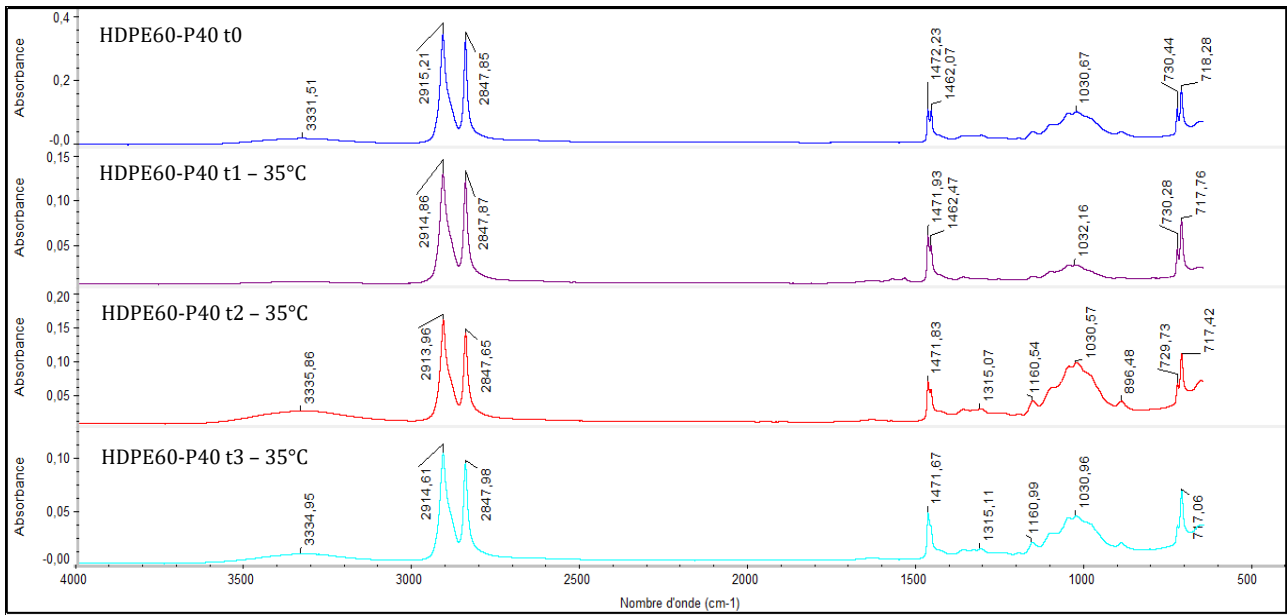


Figure 131: ATR-FTIR spectra of HDPE60-P40 at time 0,1,2,3 of the samples placed at 35 ° C.

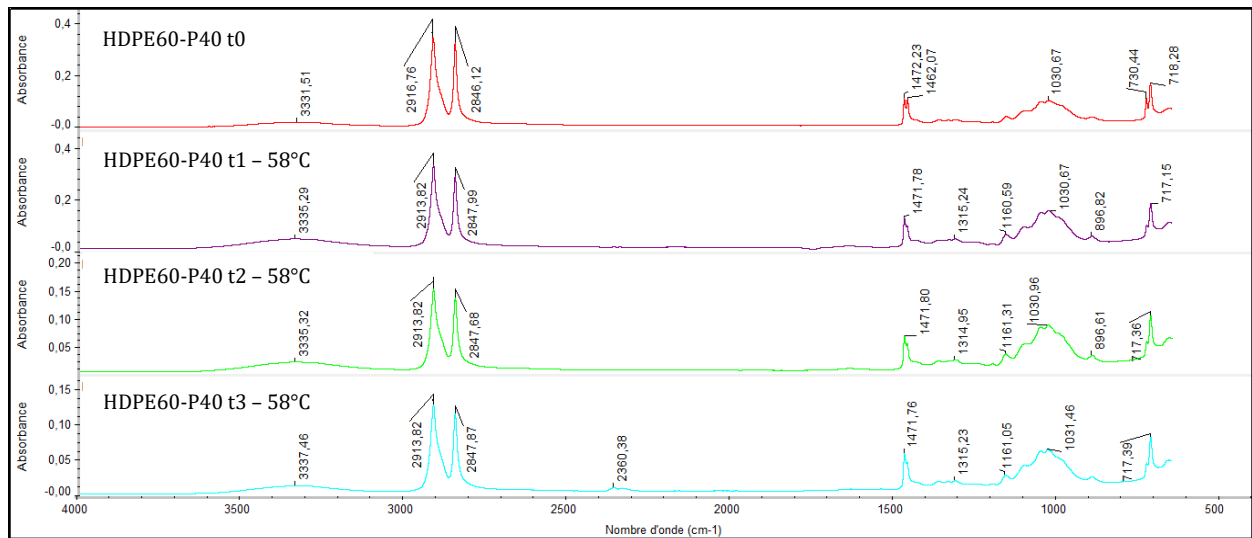


Figure 132: ATR-FTIR spectra of HDPE60-P40 at time 0, 1, 2, 3 of samples placed at 58 ° C.

Shifts are evident throughout the hydrogen bonding zone considering bands between 3100 cm⁻¹ and 3700 cm⁻¹ generated both by the vibration stretching of the O-H bonds and by the C-OH groups. Cellulose is characterized by a large number of hydroxyl side groups (-OH); these groups allow the formation of intra- and intermolecular hydrogen bonds [36-37].

In almost all samples from time 1, no degradation of the HDPE fraction is observed.

HDPE60-WF40

FTIR analysis of the HDPE60-WF40 composite shows the characteristic HDPE peaks added to the wood flour peaks, richer in lignin and hemicellulose compared to paper (Figure 133 samples buried at 35°C and Figure 134 samples buried at 58°C).

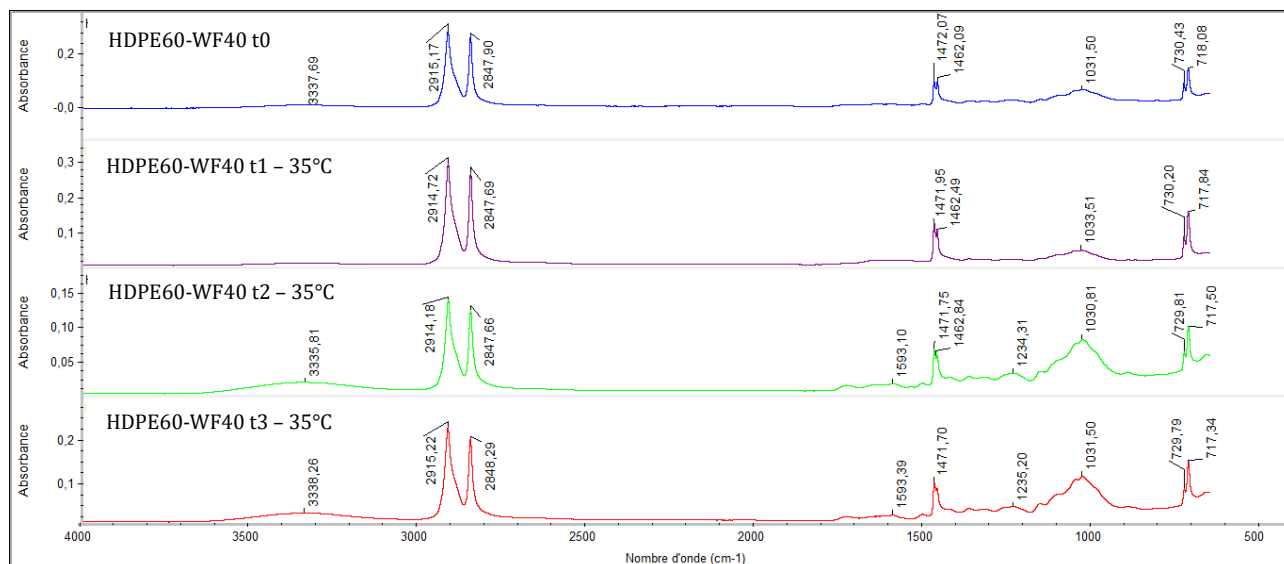


Figure 133: ATR-FTIR spectra of HDPE60-WF40 at time 0,1,2,3 of the samples placed at 35° C.

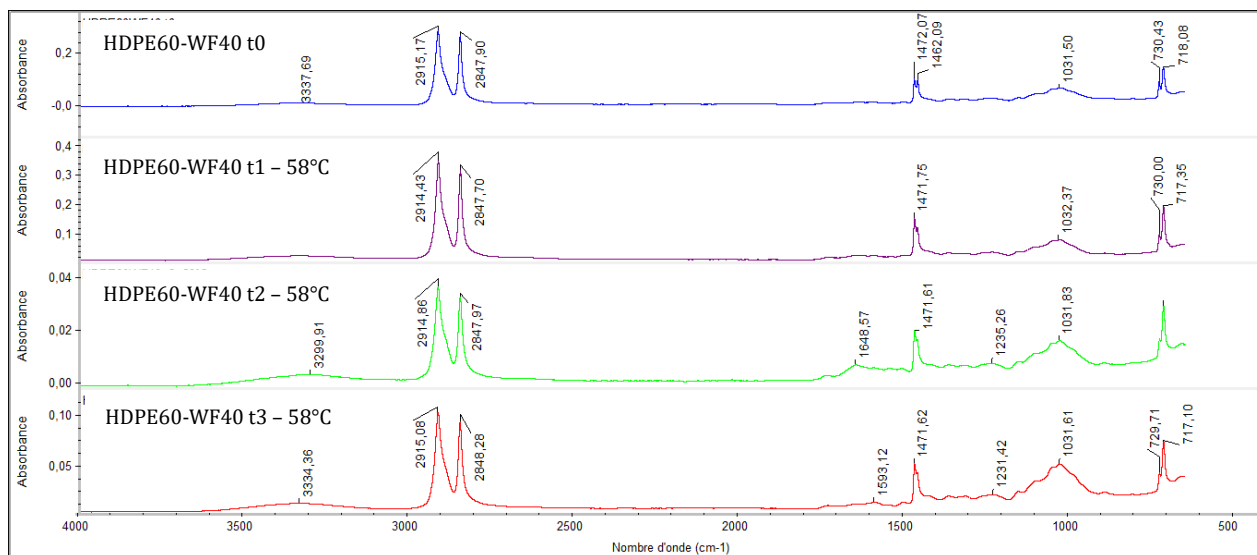


Figure 134: ATR-FTIR spectra of HDPE60-WF40 at time 0, 1, 2, 3 of samples placed at 58 ° C.

Comparing the spectra of samples both at 35 and at 58 ° C, with respect to t0, the presence of more marked degradation processes is highlighted with respect to the HDPE60-P40 composite. 1500-1700 cm^{-1} range displays peaks variation, increasing over time both in mesophilic and thermophilic conditions, mainly due to the stretching of carbonyl group because of oxidative degradation of hemicellulose and lignin [38-39].

In this composite, as for HDPE60-P40, no significant degradation of the HDPE fraction [32] is observed.

PLA

The areas of interest for PLA at about 1750 and 1180 cm^{-1} are clearly visible, which belong to the stretching C-O and to the stretching C-O-C of PLA. 1080 cm^{-1} is associated to the C-C stretching [40].

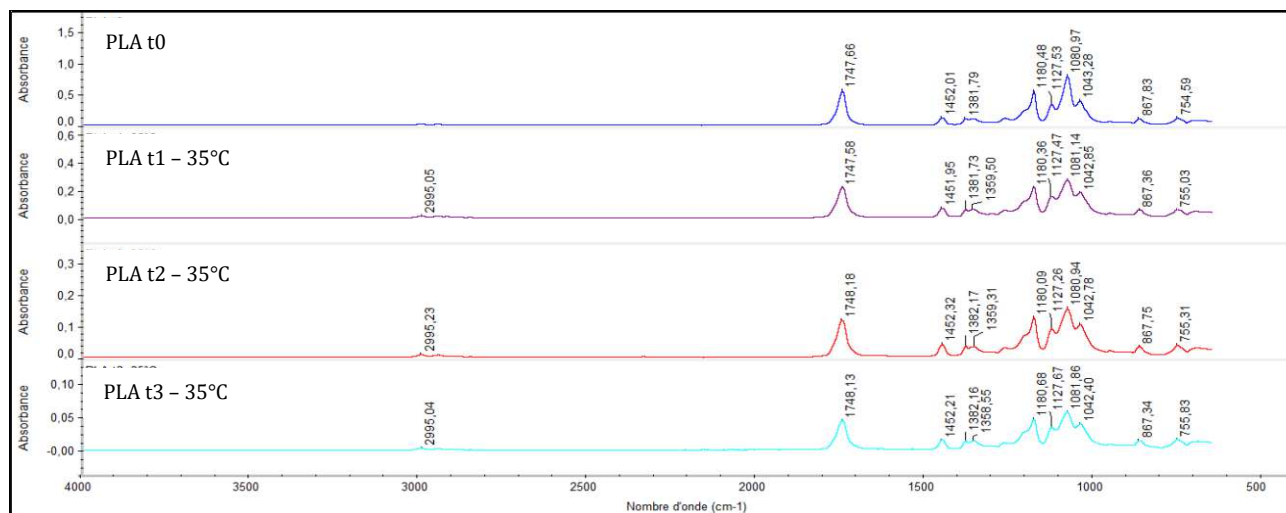


Figure 135: ATR-FTIR spectra of PLA at time 0, 1, 2, 3 of samples placed at 35 ° C.

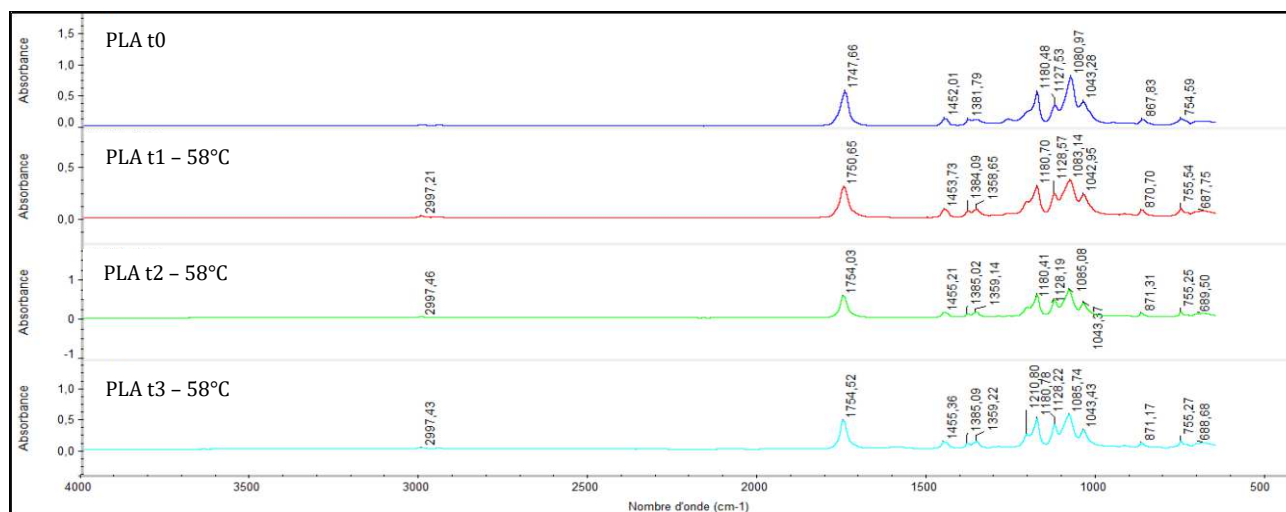


Figure 136: ATR-FTIR spectra of PLA at time 0, 1, 2, 3 of samples placed at 58 ° C.

The observation of significant peaks highlights the correspondence between the spectra obtained at time 1, 2, and 3, both at 35 ° C (Figure 135) and at 58 ° C (Figure 136), and at time 0. The biodegradation of polylactic acid should determine an increase of carboxylic and alcoholic groups. Over time, at 35 ° C, there are no evident peaks variation, while at 58 ° C, as

the biodegradation process proceeds, PLA displays a variation related to the peak at 1750cm⁻¹ due to the stretching of the C = O group. PLA biodegradation is highly sensitive to moisture, obtaining a degradation process characterized by water absorption, ester cleavage forming oligomers, solubilization of oligomer fractions and diffusion of bacteria into soluble oligomers [40].

PLA60-WF40

PLA60-WF40 displays peaks variation for both mesophilic (Figure 137) and thermophilic (Figure 138) conditions.

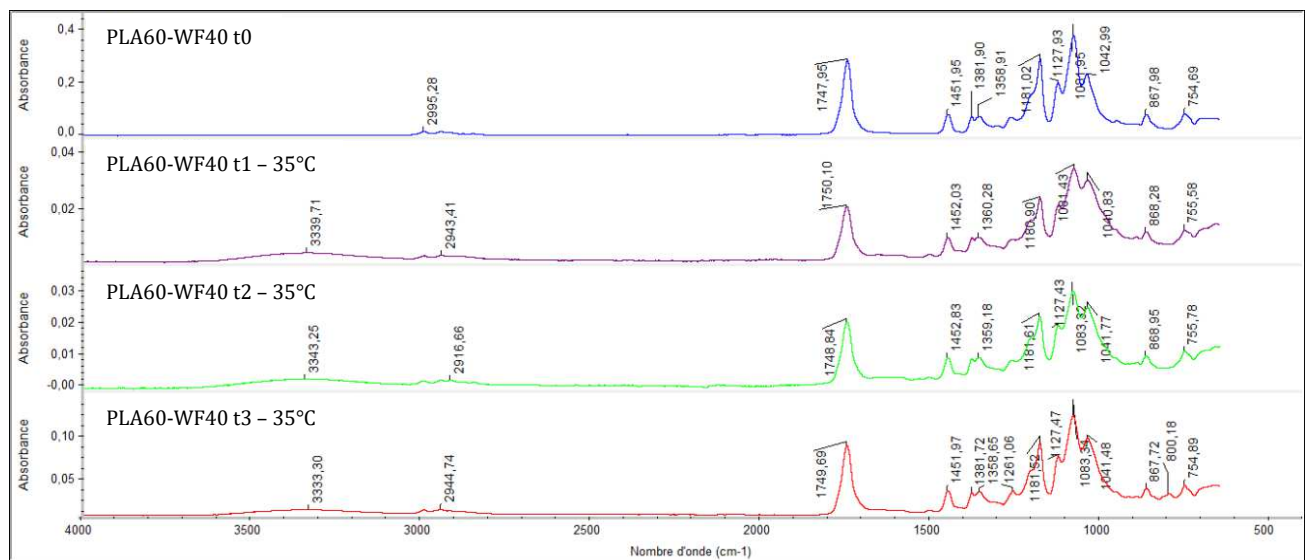


Figure 137: ATR-FTIR spectra of PLA60-WF40 at time 0, 1, 2, 3 of samples placed at 35 ° C.

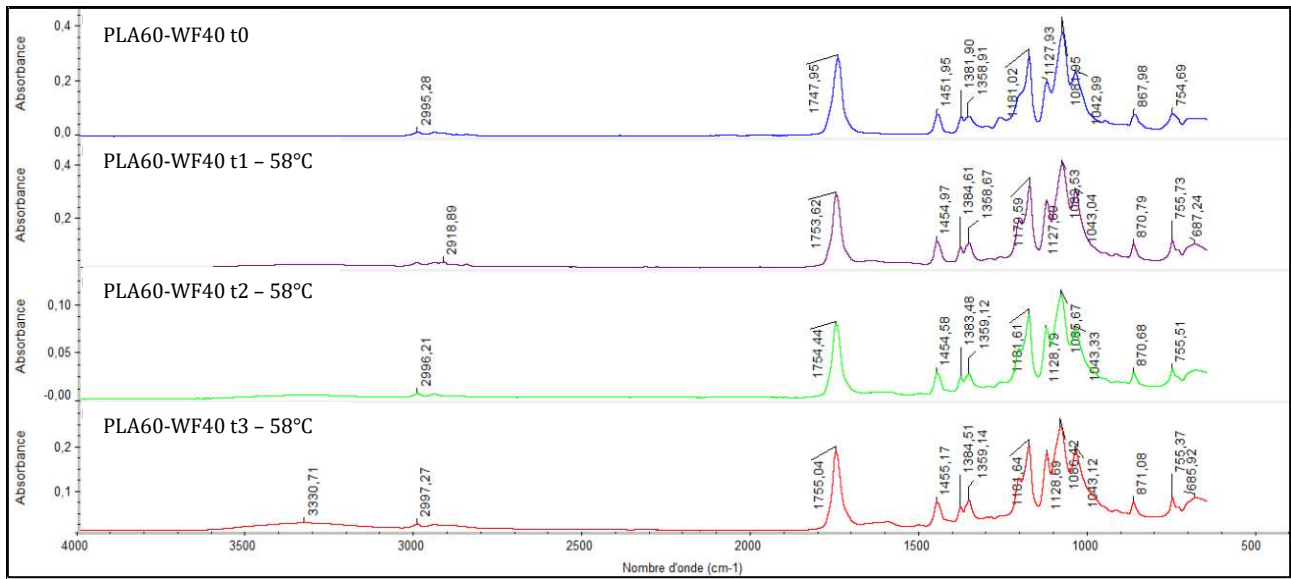


Figure 138: ATR-FTIR spectra of PLA60-WF40 at time 0, 1, 2, 3 of samples placed at 58 ° C.

Biodegradation of PLA should lead to an increase in carboxylic and alcoholic groups. In fact, a shift of the peak at 1750 cm^{-1} , assigned to the stretching of the carbonyl, confirms a successful degradation. According to Ru Liu et al. [41], at 35°C, WF probably accelerated the degradation of composite, over time enriched in WF [37;41]. The explanation would be attributed to a greater degradation by hydrolysis of PLA due to the presence of moisture in the wood [28;37].

PLA60-P40

The analysis of the spectra of PLA60-P40 reveals the same characteristics of PLA60-WF40 spectra.

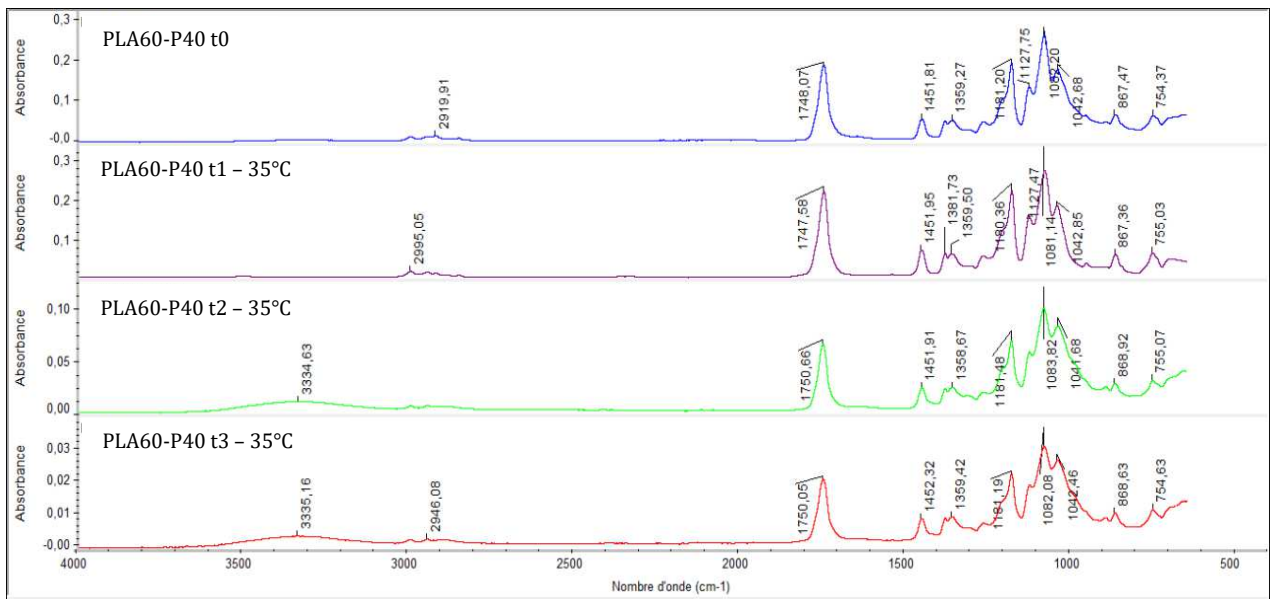


Figure 139: ATR-FTIR spectra of PLA60-P40 at time 0, 1, 2, 3 of samples placed at 35 ° C.

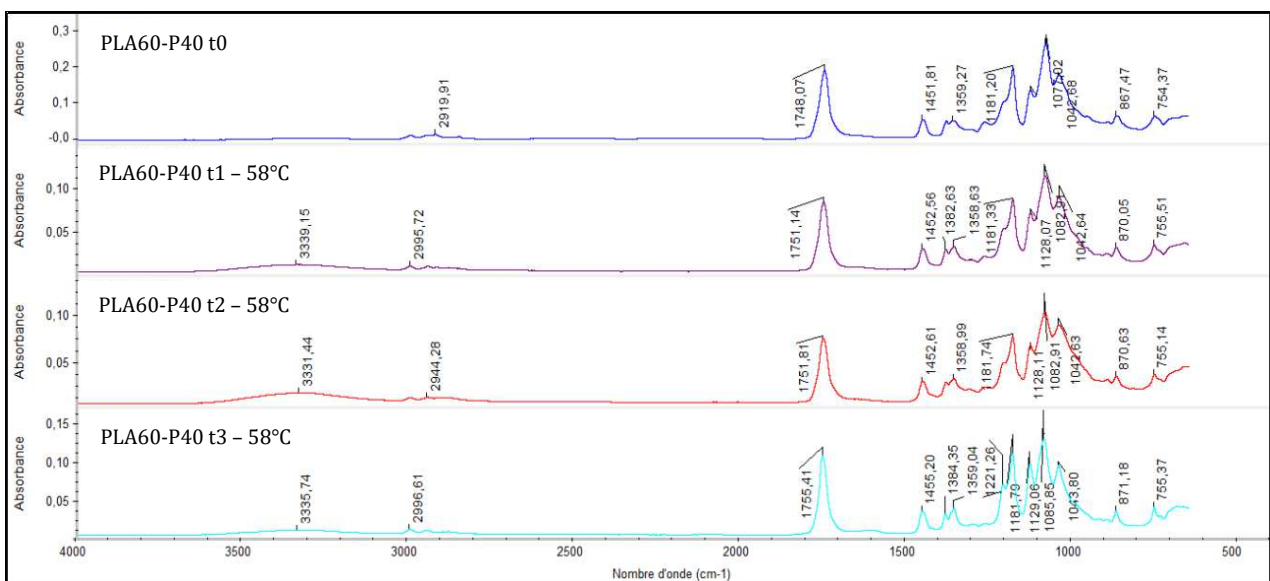


Figure 140: ATR-FTIR spectra of PLA60-P40 at time 0, 1, 2, 3 of samples placed at 58 ° C.

The variations that are highlighted concern the wide peak between 3300 cm⁻¹ and 3500 cm⁻¹ that appears at t₂ at 35 ° C (Figure 139) and already from t₁ to 58 ° C (Figure 140). The O-H band becomes more broader over time and may be associated with the hydroxyl groups of cellulose [29]. Degradation of PLA, also for PLA60-P40, can be associated with the increase of the terminal hydroxyl peak and the variation of the peak in the area between 1730 and 1750 cm⁻¹, characteristic of carbonyl groups related to C = O stretching [37].

PLA60-WF30-P10

The appearance of the peak related to the stretching of OH group (Figure 141 for samples buried at 35°C and Figure 142 for samples buried at 58°C), probably associated with an enrichment of the hydroxyl groups of cellulose, [29] suggests a development of degradation in these samples. As for PLA60-WF40 and PLA60-P40, we could suppose that paper and wood flour accelerated the degradation of composite, especially at 35 ° C, and the composite during the composting process was enriched with fillers [37].

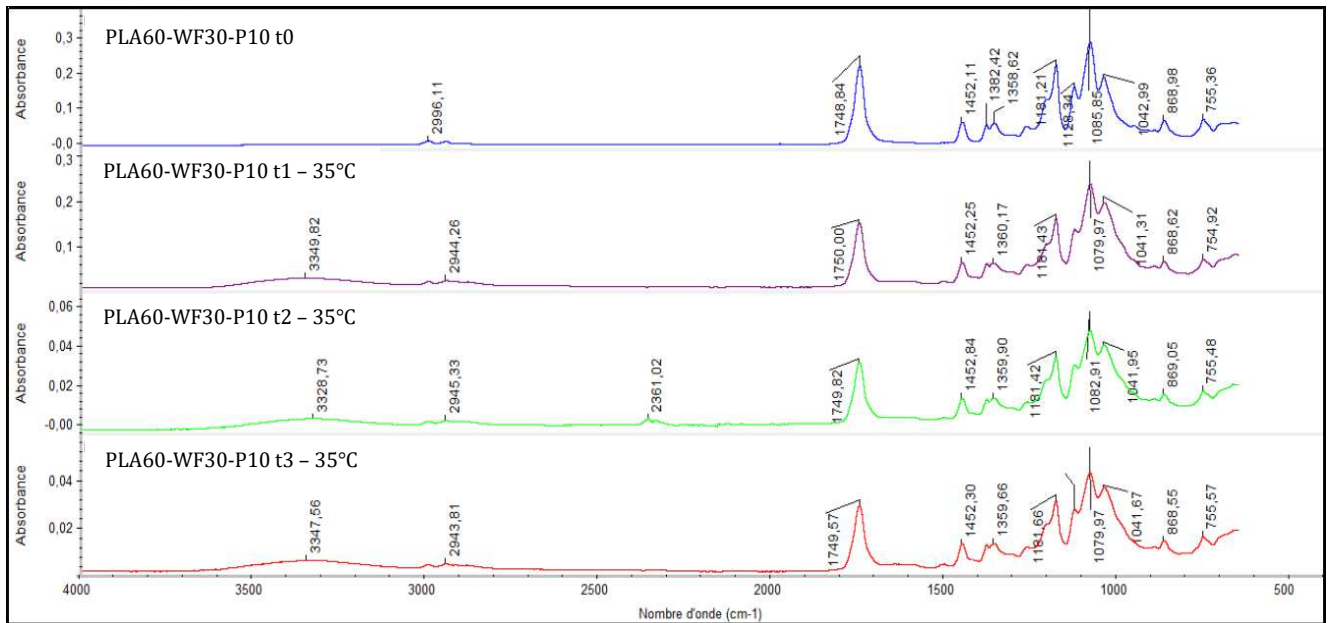


Figure 141: ATR-FTIR spectra of PLA60-WF30-P10 at time 0, 1, 2, 3 of samples placed at 35 ° C.

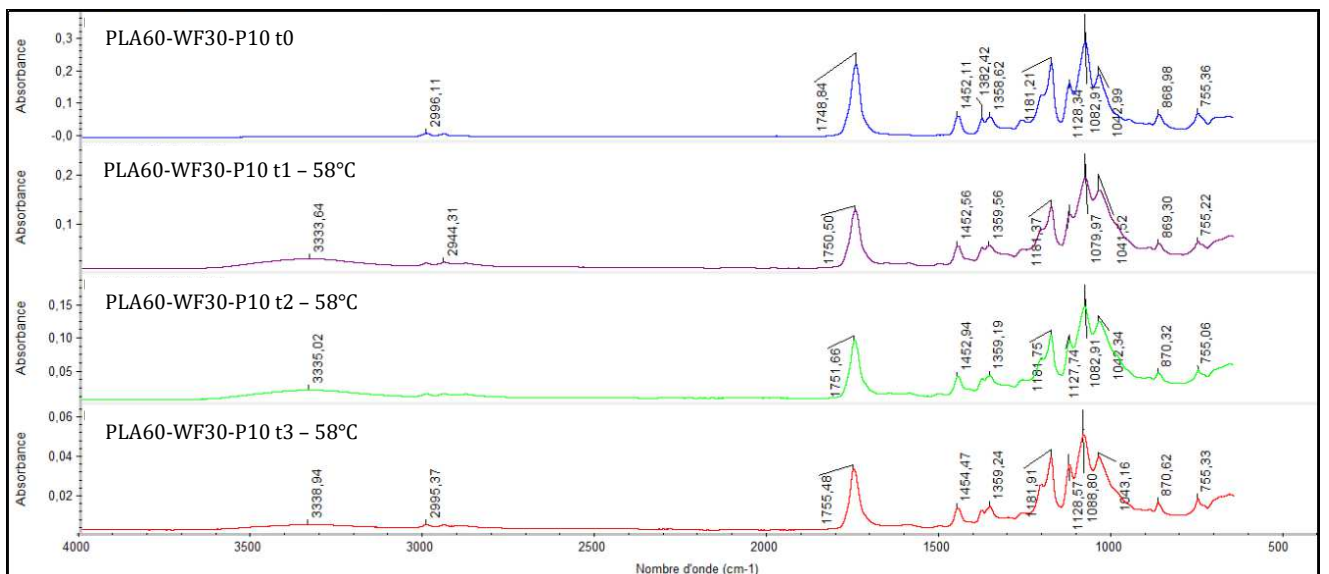


Figure 142: ATR-FTIR spectra of PLA60-WF30-P10 at time 0, 1, 2, 3 of samples placed at 58 ° C.

HDPE30-PLA30-WF30-P10

With respect to time 0, spectra of HDPE30PLA30WF30P10, both in mesophilic (Figure 143) and thermophilic (Figure 144) conditions, display the appearance of a peak between 3330 cm⁻¹ and 3500 cm⁻¹ related to the vibrations of the hydroxyl group. As a consequence, samples can be enriched in cellulose [25].

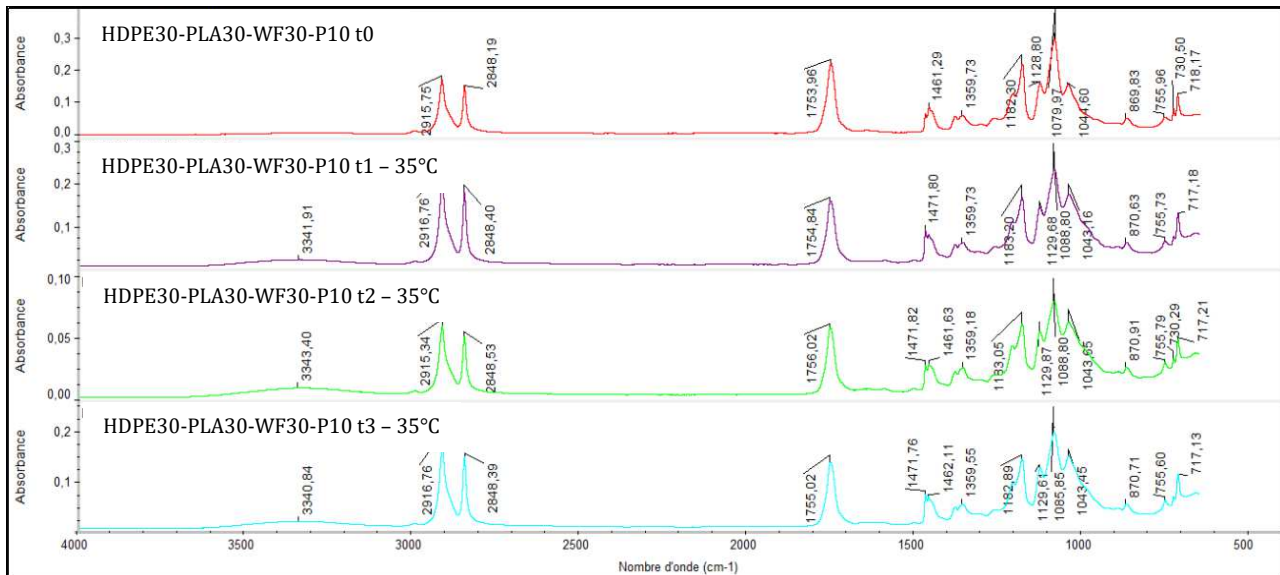


Figure 143: ATR-FTIR spectra of HDPE30-PLA30-WF30P-10 at time 0, 1, 2, 3 of samples placed at 35 °C.

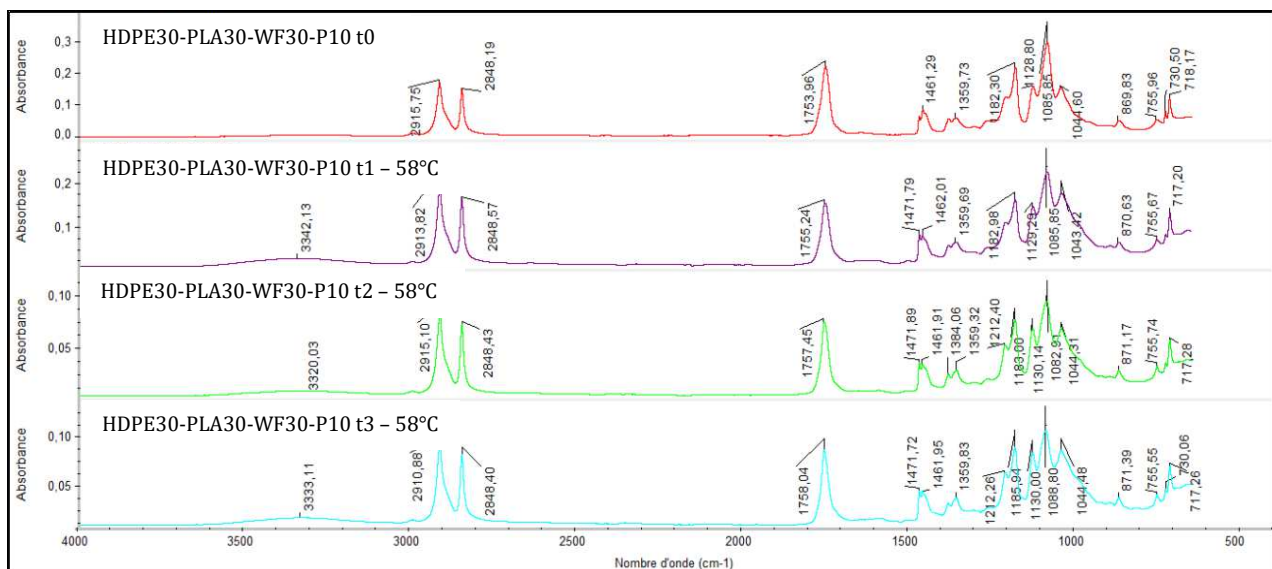


Figure 144: ATR-FTIR spectra of HDPE30-PLA30-WF30-P10 at time 0, 1, 2, 3 of samples placed at 58 °C.

In conclusion, as expected pure HDPE was non-biodegradable, while HDPE60-WF40 and HDPE60-P40 display only degradation of cellulose, lignin and hemicellulose

Neat PLA sample at 35 °C was not very sensitive to degradation processes, but biodegradation was accelerated by the presence of paper and/or wood flour. At 58°C, pure PLA is easily

biodegradable, and signs of biodegradation increase over time. PLA-based composites are characterized by PLA degradation and enrichment in cellulose, less sensitive to biodegradation.

5.12.4 Thermogravimetric Analyses

Thermogravimetric analysis has been performed on pure HDPE and on HDPE composites filled with wood flour and recycled paper, at time 0 and after 30, 60 and 90 days of composting at temperatures of 35°C and 58 °C. Observing thermograms, the presence of fillers reduces thermal stability of samples by lowering the onset temperature degradation compared to neat HDPE. Low degradation temperatures of paper and wood flour are due to the presence of hemicellulose, cellulose and lignin that are sensitive to thermal degradation [45-48].

HDPE, for all time, as reported in literature [45-48], is thermally stable up to temperatures of about 450 ° C and then quickly starts to degrade, with a maximum weight variation speed around 480 ° C. Samples do not display significant variations in both onset temperature and temperature of the maximum weight variation for HDPE. The degradation leads, in all cases, to a total loss of mass because of thermal cracking ending around about 500 ° C [45-48] (Figure 146 for samples buried at 35°C and Figure 147 for samples buried at 58°C).

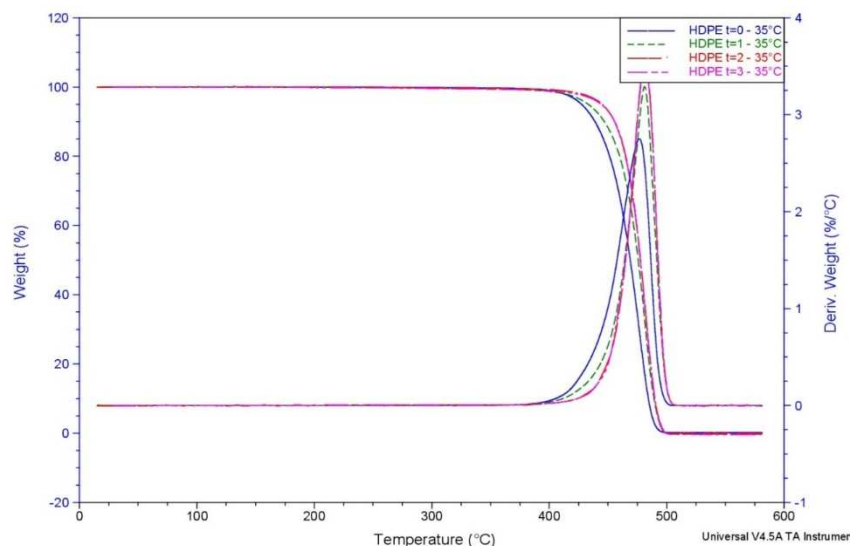


Figure 145: Mass and derivative variations in weight as a function of temperature during degradation of HDPE at time 0, 1, 2, 3 at 35 °C

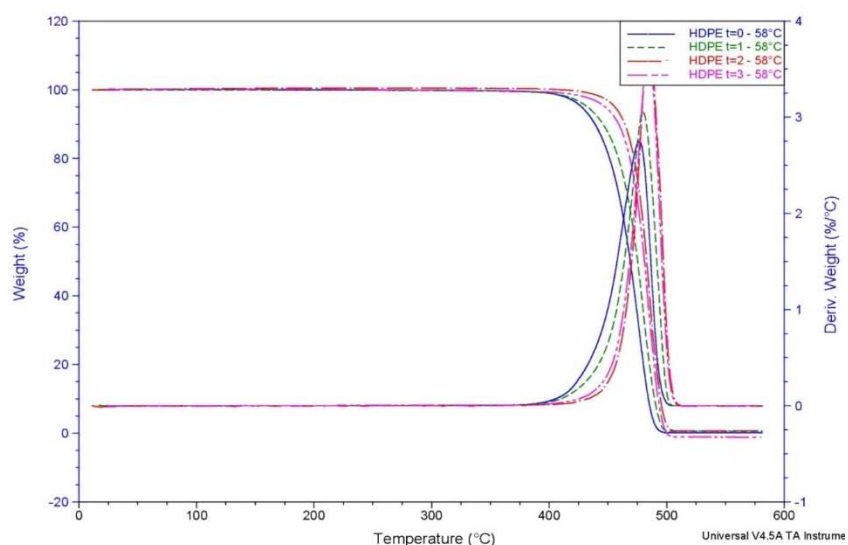


Figure 146: Mass and derivative variations in weight as a function of temperature during degradation of HDPE at time 0, 1, 2, 3 at 58 °C

HDPE60-WF40 and HDPE60-P40 display a multistep thermal degradation (Figure 148 and Figure 149 for HDPE60-WF40 buried at 35°C and 58°C respectively, Figure 149 and Figure 150 for HDPE60-P40 buried at 35°C and 58°C respectively). Firstly, moisture evaporation from room temperature to about 100°C. Secondly, thermal degradation of hemicellulose, the most thermal sensitive component in lignocellulosic fillers [50], occurs around 295°C. Cellulose pyrolysis is displayed at higher temperature range (315-400 ° C) [47-50], and around 350 ° C the maximum thermal degradation rate of cellulose and lignin is displayed. For temperatures higher than 400°C, almost all cellulose is pyrolyzed, while lignin decomposes more slowly, over

400 °C and with a higher amount of solid residue. Samples display, considering composting progression up to time 3, a modest reduction in the initial degradation temperature with a reduction in the residual mass. HDPE60-P40, rich in cellulose, displays a residual mass approximately unchanged at around 5%, while HDPE60-WF40, due to the higher lignin content, displays higher residual mass [50]. Moreover, HDPE60-WF40 displays reduction of residual mass of samples after composting process from 11% to 7%. Probably, biodegradation processes mainly affect hemicellulose and lignin, in agreement with other results.

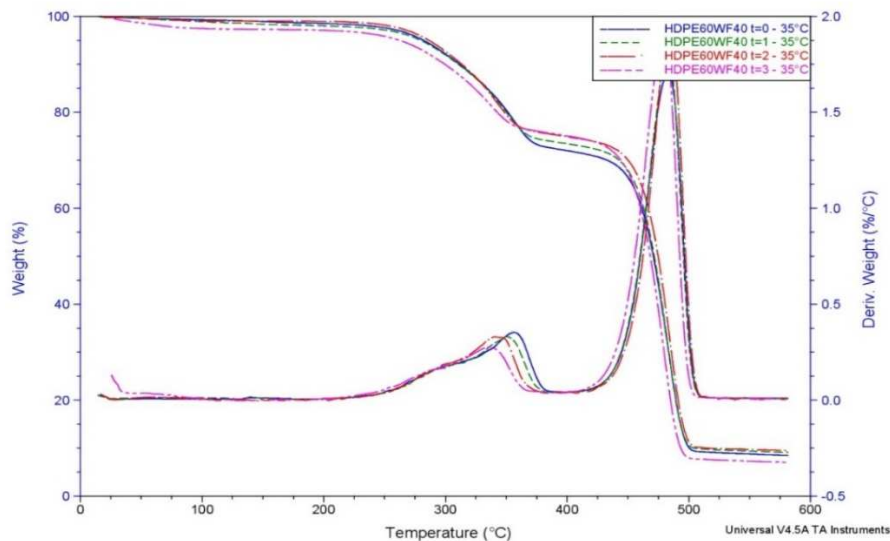


Figure 147: Mass and derivative variations in weight as a function of temperature during degradation of HDPE60-WF40 at time 0, 1, 2, 3 at 35 °C

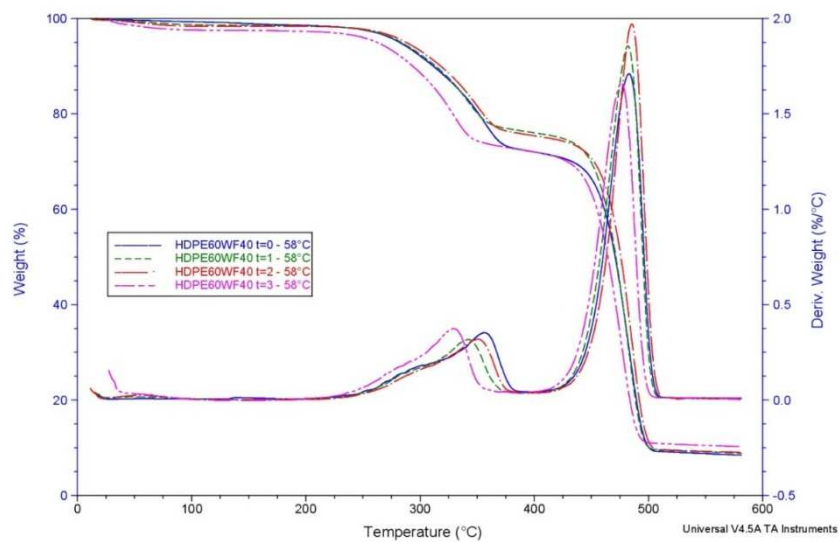


Figure 148: Mass and derivative variations in weight as a function of temperature during degradation of HDPE60-WF40 at time 0, 1, 2, 3 at 58 °C

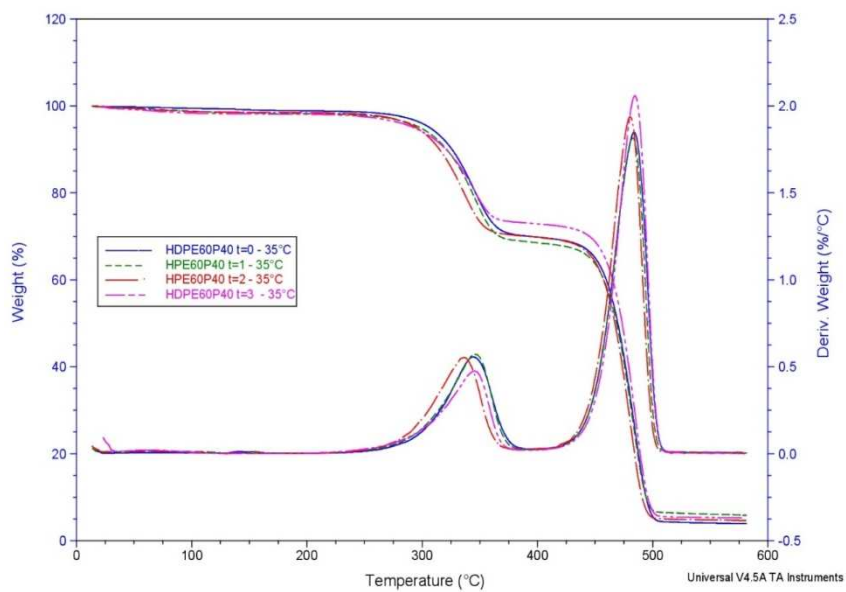


Figure 149: Mass and derivative variations in weight as a function of temperature during degradation of HDPE60-P40 at time 0, 1, 2, 3 at 35 °C

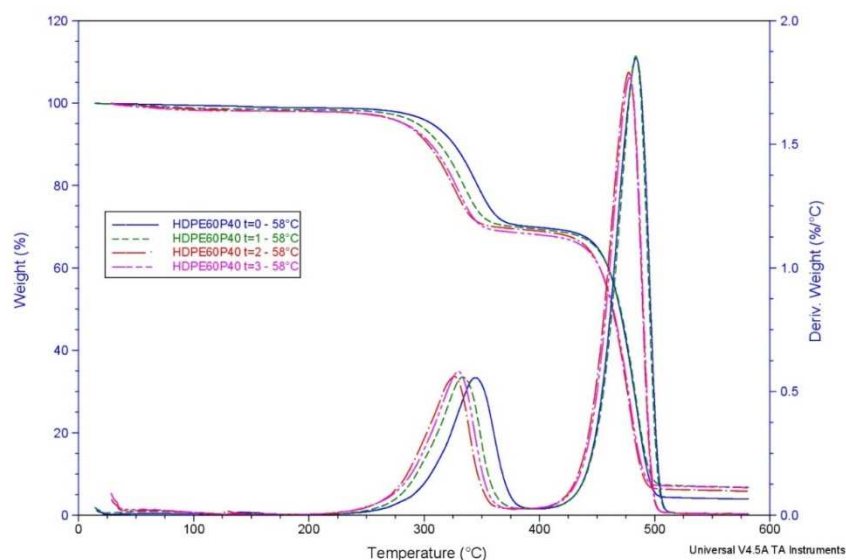


Figure 150: Mass and derivative variations in weight as a function of temperature during degradation of HDPE60-P40 at time 0, 1, 2, 3 at 58 ° C

TGA has been performed also on PLA, PLA60-WF40, PLA60-P40, PLA60-WF30-P10 and HDPE30-PLA30-WF30-P10 at time 0 and a composting follow-up after 30, 60 and 90 days at a temperature of 35 ° C and 58 ° C.

TGA curves of PLA display, over time, a significant difference in thermal stability between samples at 35 ° C (Figure 151) compared to 58 ° C (Figure 152). Mesophilic conditions display a reduction of thermal stability only at time 3. Graphs display a single peak of maximum decomposition rate which starts at about 320 ° C and at 350 ° C PLA is completely degraded with no residual mass. Samples after burying at 58 ° C, on the other hand, display a thermal stability reduction over time, possibly related to the presence of shorter macromolecules compared to time 0, because of degradation process [51]. The onset temperature at time 3 is about 240 ° C and, at 300 ° C, PLA is completely degraded with no residual mass.

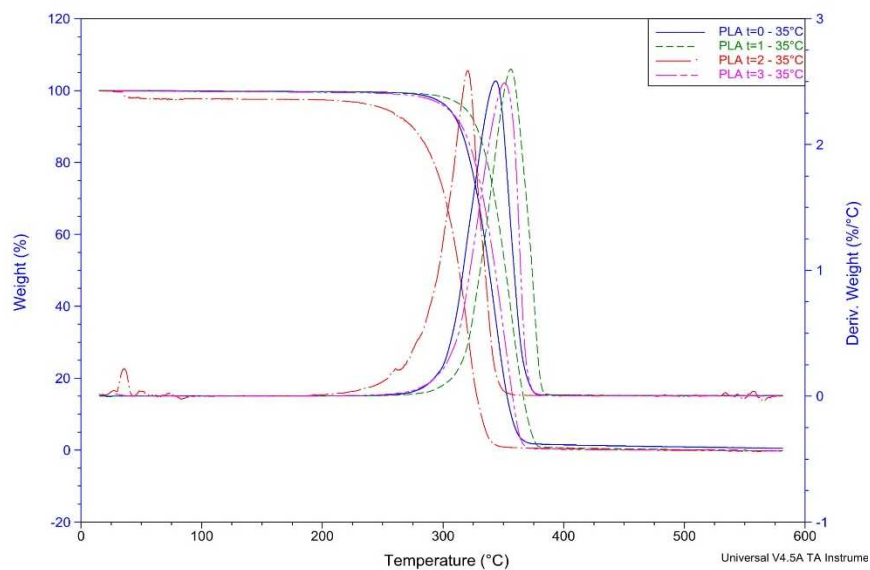


Figure 151: Mass and derivative variations in weight as a function of temperature during degradation of PLA at time 0, 1, 2, 3 at 35 °C.

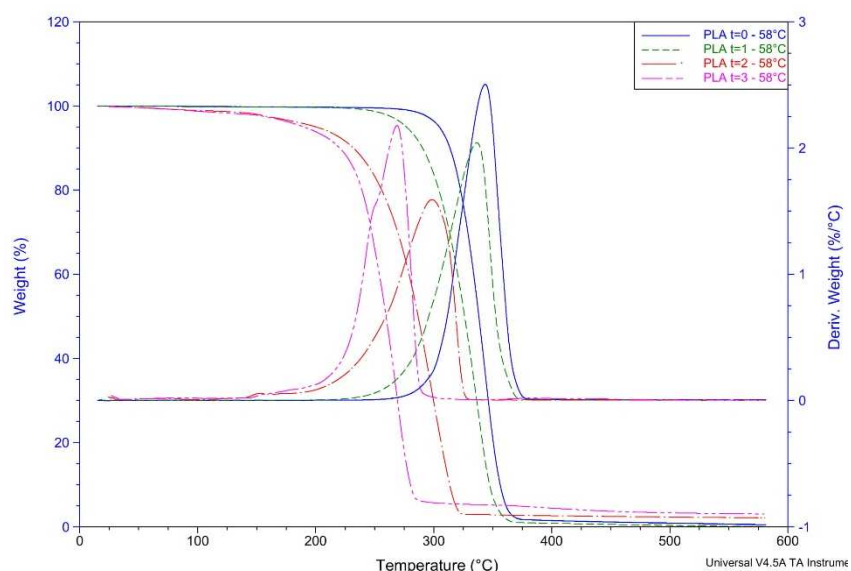


Figure 152: Mass and derivative variations in weight as a function of temperature during the degradation of PLA at time 0, 1, 2, 3 at 58 °C.

The addition of wood flour, for samples buried at 35°C (Figure 153), reduces thermal stability of the composite compared to neat PLA. Samples buried at 58°C (Figure 154), on the other hand, display a progressive reduction of stability over time, but higher than neat PLA. This trend is due to the hemicellulose and PLA degradation during composting process. Thermograms display that thermal decomposition of PLA60-WF40 composite occurs between 150 and 450°C. In mesophilic and even more evident in thermophilic conditions, the presence of "shoulders" due to the overlapping of cellulose and lignin bands is highlighted. PLA, under composting

conditions, displays a reduction in onset temperature degradation and sample is progressively more enriched in cellulose. As a consequence, after composting process two separate peaks are visible, the first refers to PLA and the second to cellulose [52]. A residual mass is displayed at the end of thermal degradation, decreasing over time.

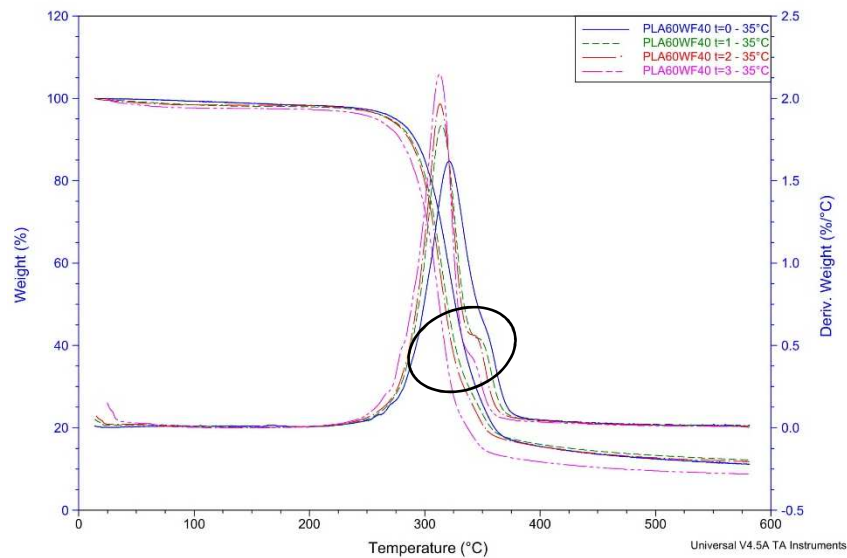


Figure 153: Mass and derivative variations in weight as a function of temperature during the degradation of PLA60-WF40 at time 0, 1, 2, 3 at 35 ° C.

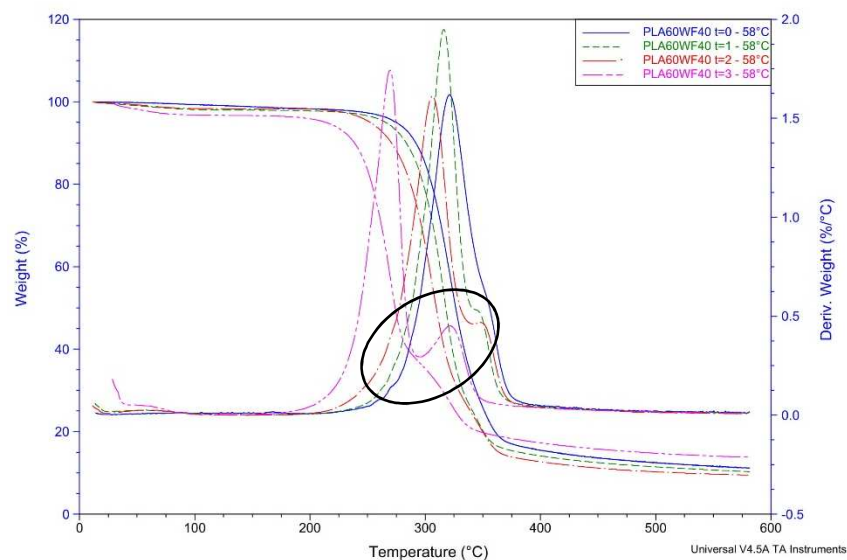


Figure 154: Mass and derivative variations of the weight as a function of the temperature during the degradation of PLA60-WF40 at time 0, 1, 2, 3 at 58 ° C.

PLA60-P40 displays a reduction in thermal stability with respect to neat PLA. Thermograms display a single peak for samples buried at 35°C (Figure 155), with a slight decrease in thermal stability over time. Samples at 58°C (Figure 156) display higher reduction of thermal stability and the appearance of shoulder, already displayed for PLA60-WF40, becomes more visible over time. All samples display a reduction of onset temperature with respect to PLA60-WF40, possibly associated with the lower presence of hemicellulose in paper. A residual mass is displayed at the end of thermal degradation, in lower amount than PLA60-WF40, which remains stable over time due to the lower presence of lignin and hemicellulose [53].

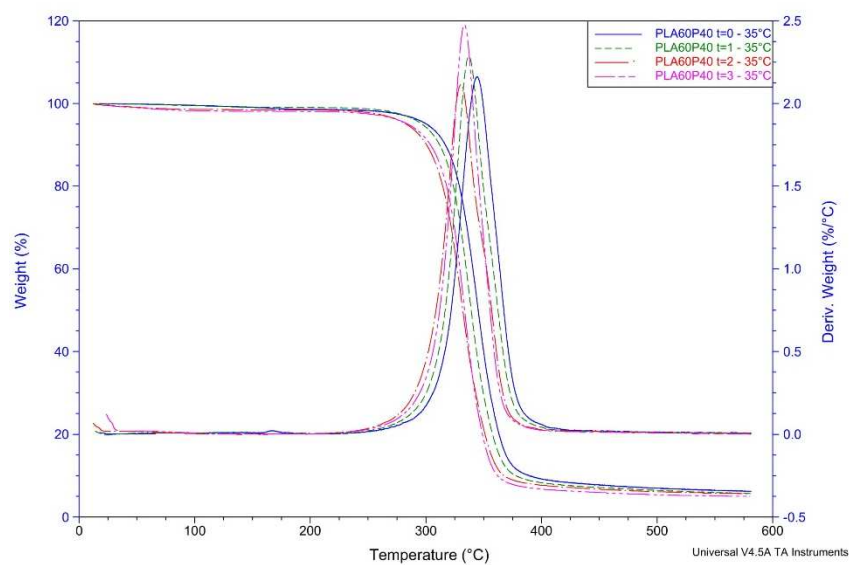


Figure 155: Mass and derivative variations in weight as a function of temperature during the degradation of PLA60-P40 at time 0, 1, 2, 3 at 35 ° C.

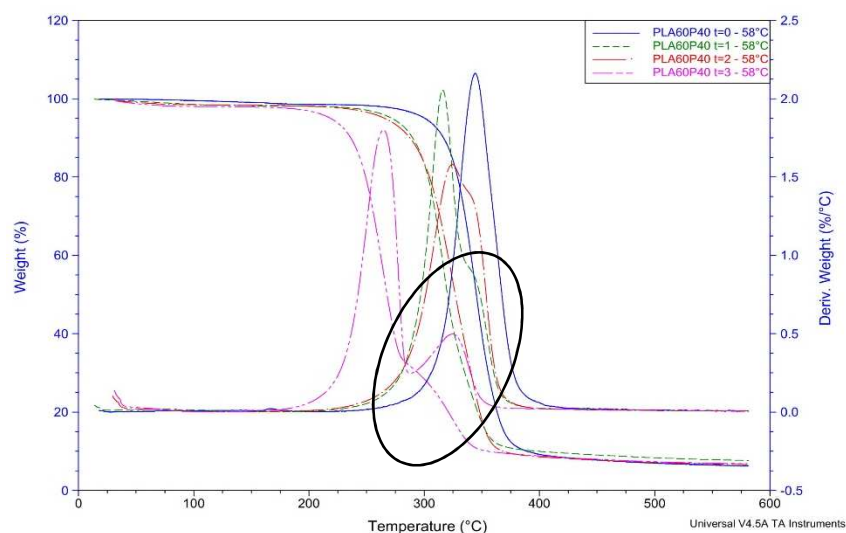


Figure 156: Mass and derivative variations in weight as a function of temperature during the degradation of PLA60-P40 at time 0, 1, 2, 3 at 58 ° C.

HDPE30-PLA60-WF30-P10 compared to neat PLA displays a reduction of the onset degradation temperatures for all samples, both at 35 ° C (Figure 157) and at 58 ° C (Figure 158). Observing thermograms, two distinct phases are highlighted. At 35°C the first phase is characterized by a peak between 180 and 400 ° C, due to the overlap of hemicellulose, PLA, cellulose and lignin. Over time, a slight decrease in initial degradation temperature is observed, while after burying at 58°C, in this first phase of the degradation process, a lower overlap of the peaks can be observed, with a noticeable decrease in the initial degradation temperature. Two peaks are visible, the first due to the degradation of PLA and the second due to the degradation of cellulose. The second phase shows, in all samples, the peak related to the degradation of HDPE, which remains fairly stable over time, both in mesophilic and thermophilic conditions. The mass loss for each sample at both 35°C and 58 ° C remains stable at about 55%.

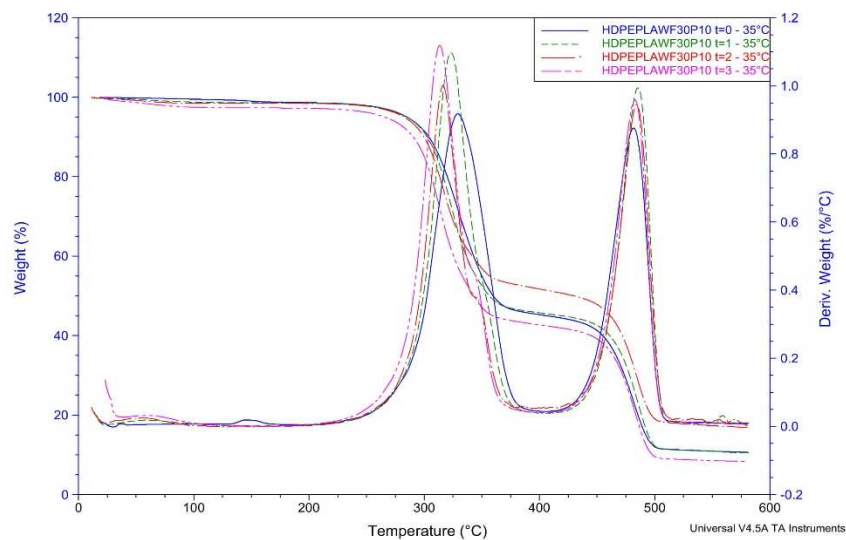


Figure 157: Mass and derivative variations in weight as a function of temperature during degradation of HDPE30-PLA30-WF30-P10 at time 0, 1, 2, 3 at 35 ° C

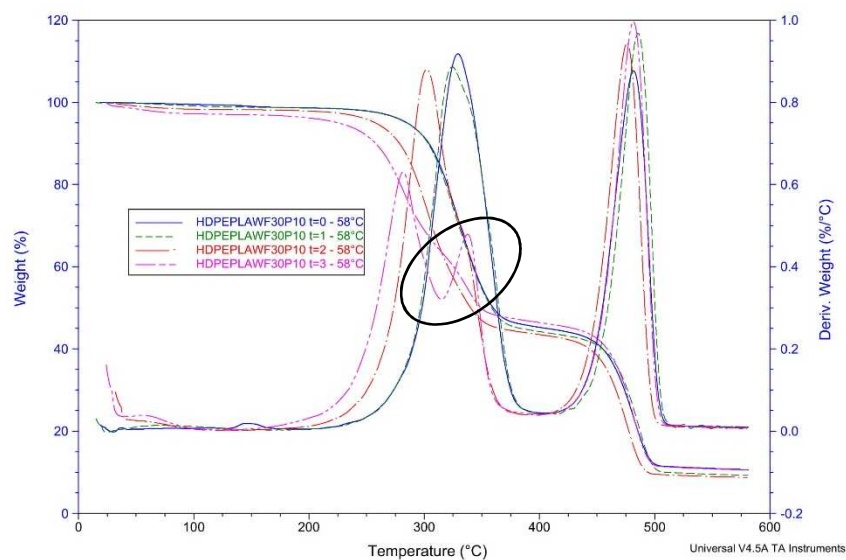


Figure 158: Mass and derivative variations in weight as a function of temperature during degradation of HDPE30-PLA30W-F30-P10 at time 0, 1, 2, 3 at 58 ° C.

To conclude, natural fillers addition reduced thermal stability of HDPE-based composites. Moreover, a reduction of thermal stability has been displayed over time because of hemicellulose and lignin degradation. PLA-based composites displayed a reduction of thermal stability under mesophilic condition because of degradation development. In fact, at 58°C after three months composting, a peak separation of PLA and natural fillers has been detected.

5.12.5 Differential Scanning Calorimetry

DSC analyses allow understanding the influence of natural fillers on both HDPE and PLA, but also the influence of composting process on materials.

HDPE

Neat HDPE display, as expected, no sensitive variation of melting temperature after composting at both 35°C (Figure 159) and 58°C (Figure 160).

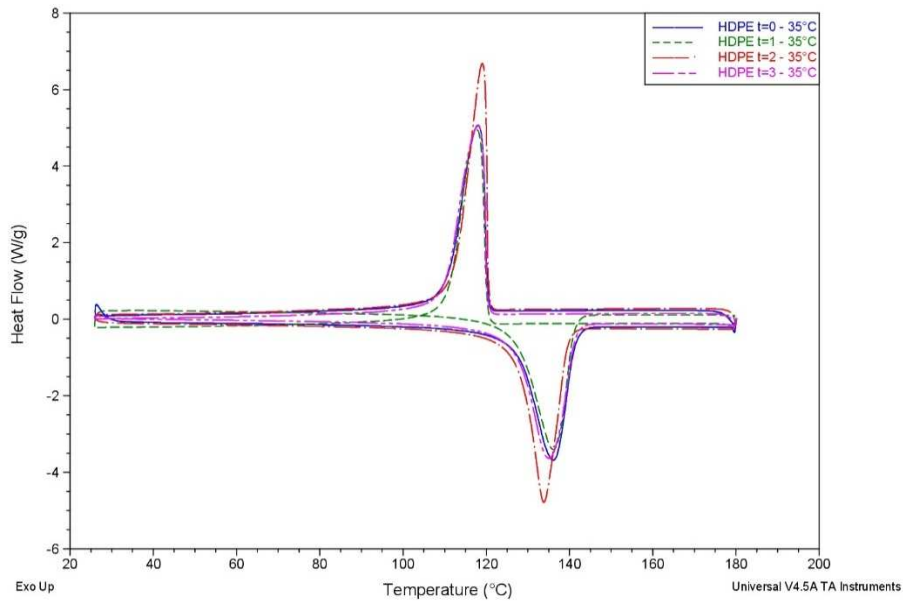


Figure 159: DSC results for neat HDPE after three months buried at 35°C.

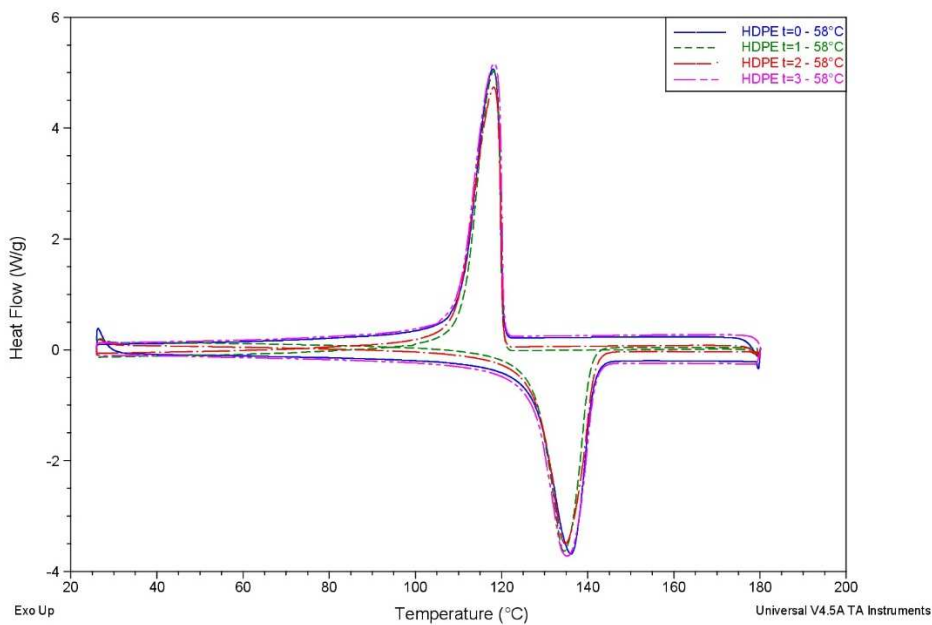


Figure 160: DSC results for neat HDPE after three months buried at 58°C.

HDPE60-WF40

Melting and crystallization enthalpies have higher values compared to neat HDPE. In fact, as analysed also with TOM and $t_{1/2}$, WF seems to act as nucleating agent for HDPE. Similar

observations are in agreement with results of Lee et al., who have studied the influence of different types of softwood in HDPE matrix composites [54]. Figure 161 and Figure 162 display thermograms for samples buried at 35°C and 58°C respectively.

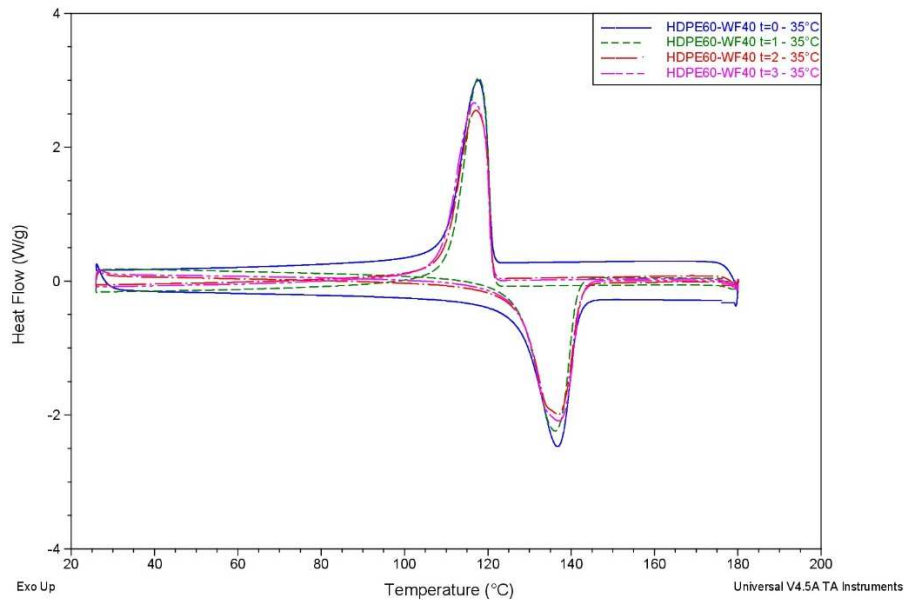


Figure 161: DSC results for HDPE60-WF40 after three months buried at 35°C.

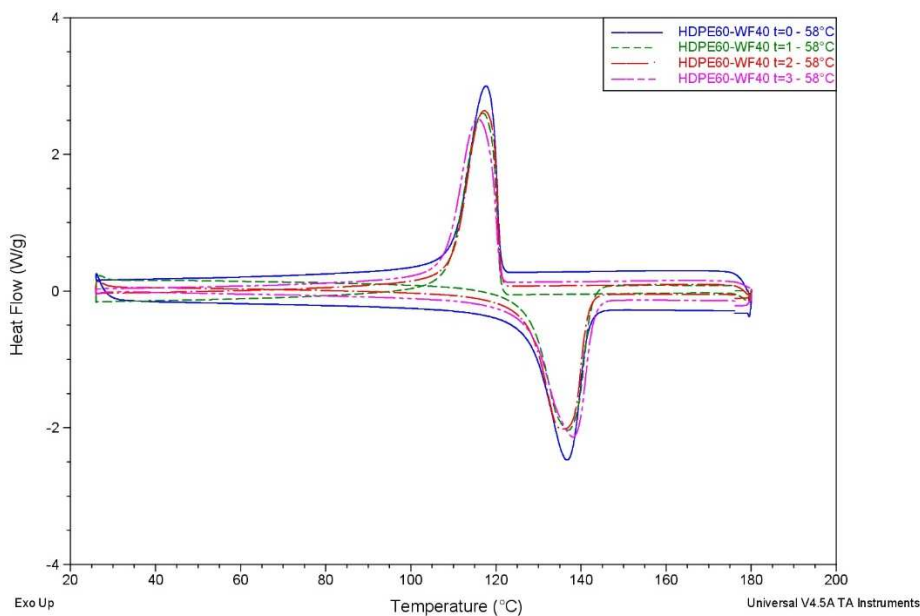


Figure 162: DSC results for HDPE60-WF40 after three months buried at 58°C.

HDPE60-P40

In this case, as previously reported for WF addition, P seems to act as nucleating agent for HDPE. In fact, melting and crystallization enthalpies have values higher than pure HDPE. This effect is

more evident for P than for WF, probably because of morphological differences between P (fibrous) and WF (particulate). Figure 163 and Figure 164 display thermograms for samples buried at 35°C and 58°C respectively.

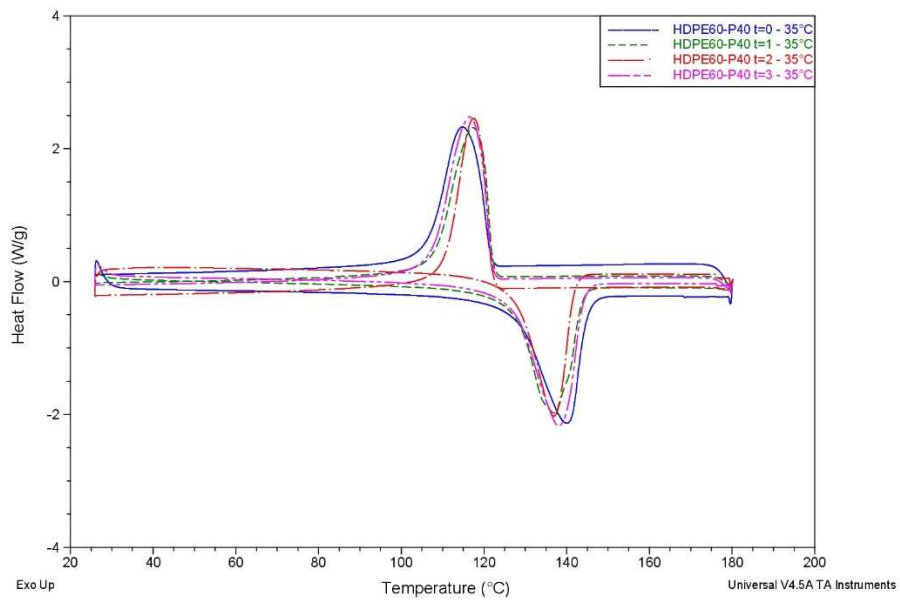


Figure 163: DSC results for HDPE60-P40 after three months buried at 35°C.

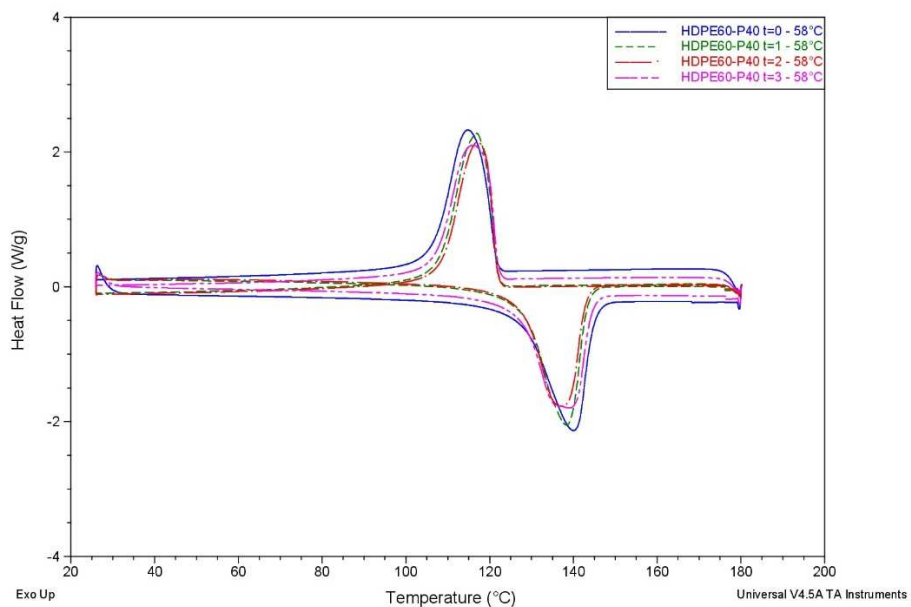


Figure 164: DSC results for HDPE60-P40 after three months buried at 58°C.

No sensitive variations are displayed with DSC analyses for HDPE-based samples, probably because degradation mainly occurs on natural fillers, keeping unchanged HDPE.

PLA

No sensitive variations have been displayed for PLA after composting at 35°C (Figure 165) and the curves are almost superimposable. Samples after composting at 58°C (Table 53), instead, as the composting process proceeds (Figure 166), show a decrease in glass transition temperature (T_g), from 61°C to about 40°C after three months. This result agrees with a reduction of PLA molecular weight due to its degradation under composting condition at 58°C. Moreover, typical cold crystallization temperature (T_{cc}) displays a decrease at 58°C during the degradation process. This reduction may be associated with the formation of oligomers of lactic acid resulting from the cleavage of chains due to hydrolysis during composting. Chains with lower molecular mass crystallize more easily and have lower cold crystallization temperatures [55-57]. No crystallization during cooling has been detected during DSC analyses for neat PLA.

Table 53: DSC results for neat PLA during composting process at 58°C.

	Tm (°C)	ΔH_m PLA (J/g _{PLA})	Tcc (°C)	Tg (°C)	Mw (kDa)
PLA t0	169	48	100	61	40
PLA t1	166	53	94	55	35
PLA t2	148	47	84	45	9
PLA t3	144	45	90	41	5

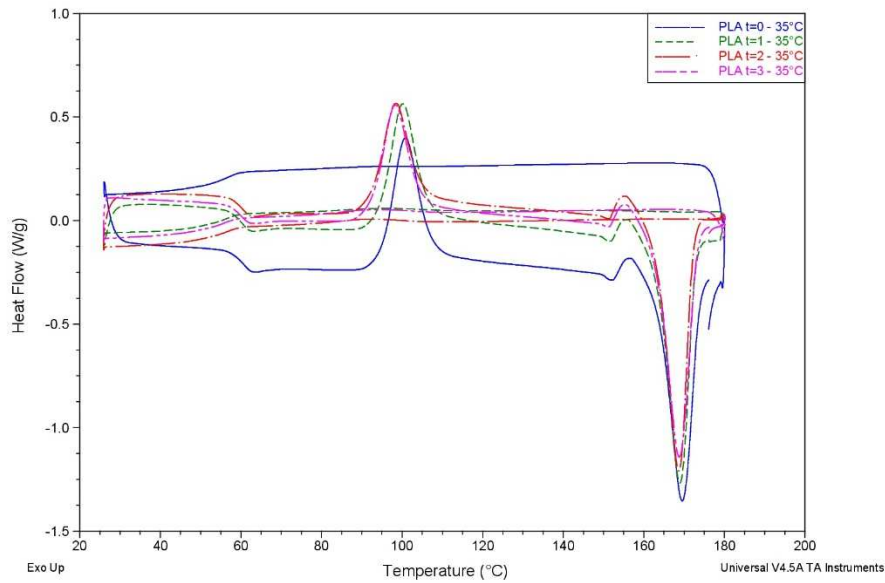


Figure 165: DSC results for neat PLA during composting process at 35°C.

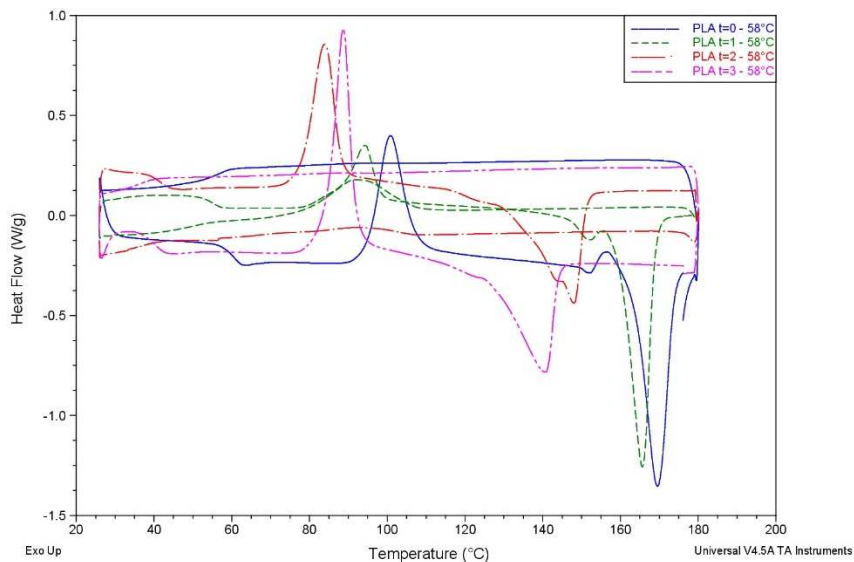


Figure 166: DSC results for neat PLA during composting process at 58°C.

PLA-based composites

The presence of wood flour and recycled waste paper in PLA60-WF40, PLA60-P40, PLA60-WF30-P10 and HDPE30-PLA30-WF30-P10 seems to obstacle cold crystallization, not detected for these samples, because of nucleating effect of natural fillers, facilitating crystallinity from molten state. As a consequence, a formation of two melting peaks was evident, indicating the presence of two crystalline fractions (Figure 167 and Figure 168). Moreover, thermograms of samples buried at 35 ° C are almost superimposable for all composites, while at 58°C there is a displacement of melting peaks towards lower temperatures. In fact, under mesophilic conditions, melting temperature T_m does not show significant variations compared to neat

PLA. Samples buried under thermophilic condition display a significant reduction of T_m over time (Table 54). This reduction is analogous to the one displayed by neat PLA, although compared to the latter, the values are still higher. HDPE30-PLA30-WF30-P10 after three months under thermophilic condition reached a melting temperature very close to HDPE (Figure 169). As a consequence, a separation of these peaks is more complicated. Crystallization enthalpy is not displayed in table 54 because for PLA-base samples is difficult to correctly integrate peaks (baseline is not horizontal, there is a long decreased baseline and it is difficult to detect where crystallization end).

Table 54: DSC results for PLA-based composites during composting process at 58°C.

	T_m (°C)	ΔH_m PLA (J/g _{PLA})
PLA60-WF40 t0	169	54
PLA60-WF40 t1	166	53
PLA60-WF40 t2	156	69
PLA60-WF40 t3	148	45
PLA60-P40 t0	171	53
PLA60-P40 t1	168	59
PLA60-P40 t2	162	62
PLA60-P40 t3	153	56
PLA60-WF30-P10 t0	168	55
PLA60-WF30-P10 t1	167	62
PLA60-WF30-P10 t2	160	69
PLA60-WF30-P10 t3	151	47
HDPE30-PLA30-WF30-P10 t0	168	48
HDPE30-PLA30-WF30-P10 t1	168	48
HDPE30-PLA30-WF30-P10 t2	162	41
HDPE30-PLA30-WF30-P10 t3	-	-

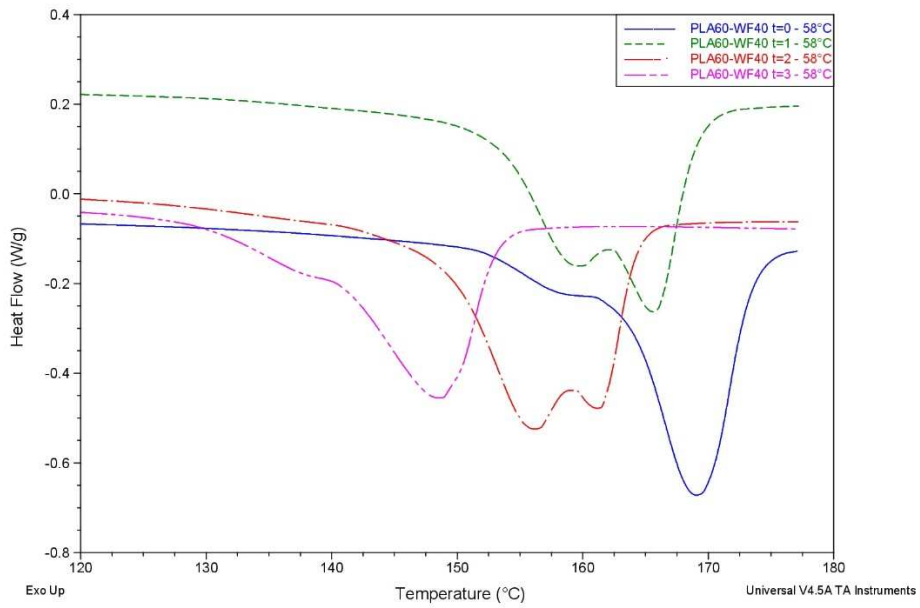


Figure 167: Melting peak of PLA60-WF40 composites during composting process at 58°C.

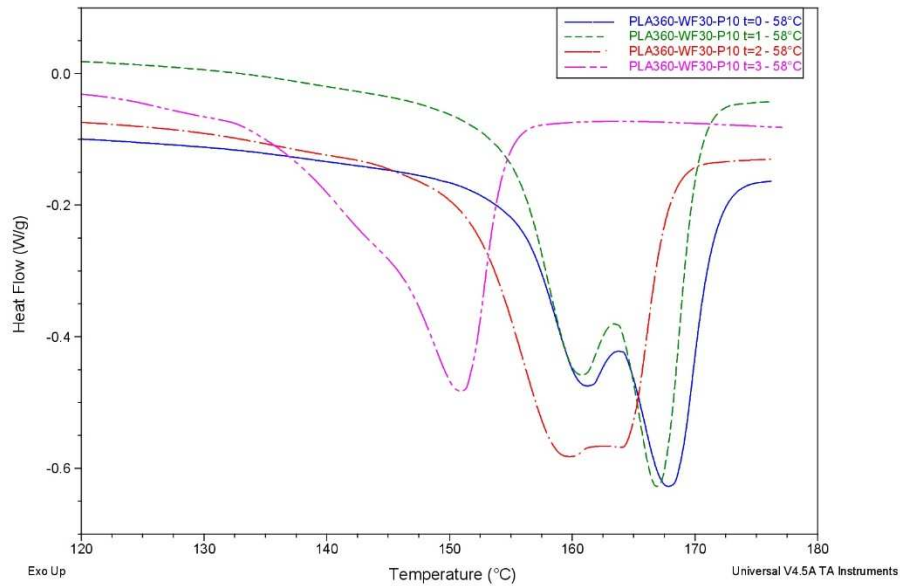


Figure 168: Figure 153: Melting peak of PLA60-WF30-P10 composites during composting process at 58°C.

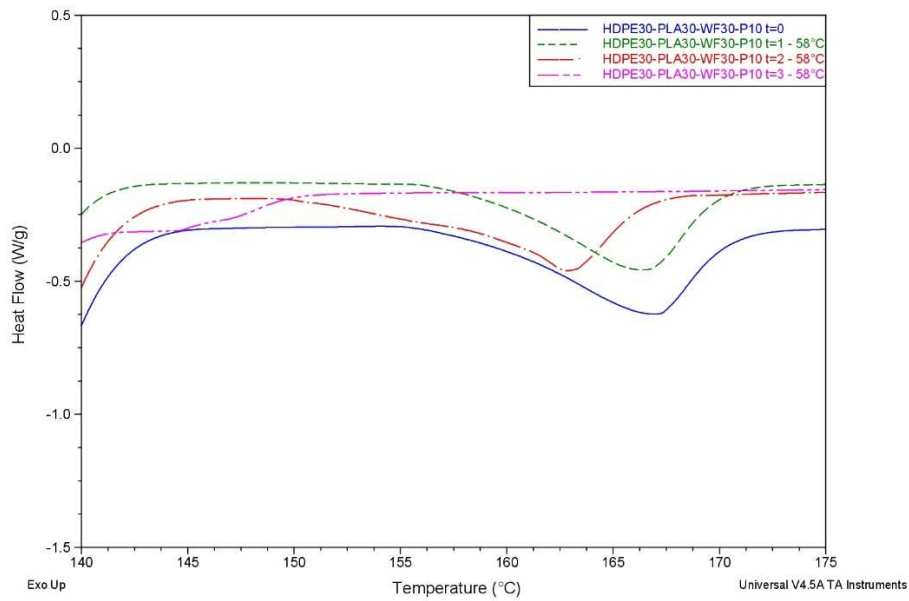


Figure 169: Figure 153: Melting peak of HDPE30-PLA30-WF30-P10 composites during composting process at 58°C.

To conclude, a nucleating effect of WF and P seemed to be evident for both HDPE and PLA matrices. Moreover, a reduction of T_m has been displayed by PLA-based composites over three months composting under thermophilic condition.

A summary of all composting results is displayed in Figure 170.

Figure 170: Summary of composting results.

	HDPE	PLA	HDPE60-WF40	HDPE60-P40	PLA60-WF40	PLA60-P40	PLA60-WF30-P10	HDPE30-PLA30-WF30-P10
Mass variation	No variation after composting at both 35°C and 58°C	No variation after composting at 35°C, sensitive variation after composting at 58°C	Higher variation after composting at both 35°C and 58°C thanks to WF addition	Slight mass variation after composting, minus effect with respect to WF addition	Compared to PLA, higher variation composting at 35°C with WF addition thanks to its biodegradation, lower variation after composting at 58°C	Compared to PLA, higher variation composting at 35°C with P addition thanks to its biodegradation, lower variation after composting at 58°C	Compared to PLA, higher variation composting at 35°C with WF and P addition thanks to its biodegradation, lower variation after composting at 58°C	Compared to PLA60-WF30-P10, lower variation because of HDPE after composting at both 35°C and 58°C. Compared to HDPE-based composites, higher variation, especially after composting at 58°C
ATR-FTIR	No variation after composting at both 35°C and 58°C	No sensitive variation after composting at 35°C, increased intensity of peak referring to -OH groups and C=O groups after composting at 58°C	Peak variation especially for hemicellulose, lignin after composting at both 35°C and 58°C, samples enriched in cellulose, less sensitive to biodegradation	Peak variation of cellulose (predominant in P) after composting at both 35°C and 58°C	Peak variation especially for hemicellulose, lignin after composting at both 35°C and 58°C, samples enriched in cellulose, less sensitive to biodegradation	Peak variation of cellulose (predominant in P) after composting at both 35°C and 58°C	Peak variation especially for hemicellulose, lignin after composting at both 35°C and 58°C, samples enriched in cellulose, less sensitive to biodegradation	Peak variation especially for hemicellulose, lignin after composting at both 35°C and 58°C, samples enriched in cellulose, less sensitive to biodegradation
TGA	No variation after composting at both 35°C and 58°C	No sensitive variation after composting at 35°C, reduction of T_{onset} after composting at 58°C (shorter macromolecules because of degradation)	Reduction of T_{onset} with WF addition, reduction of residual mass (related to pyrolysis of WF) after composting (degradation of hemicellulose and lignin)	Reduction of T_{onset} with P addition, no sensitive variation of residual mass (related to pyrolysis of P) after composting (slow degradation of cellulose)	Reduction of T_{onset} with WF addition, no sensitive variation after composting at 35°C, reduction of T_{onset} after composting at 58°C higher than neat PLA. Peak separation of PLA and WF degradation after composting especially at 58°C.	Reduction of T_{onset} with P addition, no sensitive variation after composting at 35°C, reduction of T_{onset} after composting at 58°C. Peak separation of PLA and P degradation after composting especially at 58°C.	Reduction of T_{onset} with WF and P addition, no sensitive variation after composting at 35°C, reduction of T_{onset} after composting at 58°C higher than neat PLA. Peak separation of PLA and WF P degradation after composting especially at 58°C.	Reduction of T_{onset} with WF and P addition, no sensitive variation after composting at 35°C, reduction of T_{onset} after composting at 58°C higher than neat PLA. Peak separation of PLA and WF P degradation after composting especially at 58°C. HDPE degradation do not display sensitive variation
DSC	No variation after composting at both 35°C and 58°C	Reduction T_m , T_{cc} and T_g after composting at 58°C	Nucleating effect of WF, no variation after composting at both 35°C and 58°C	Nucleating effect of P, no variation after composting at both 35°C and 58°C	Nucleating effect of WF, reduction of T_m after composting at 58°C	Nucleating effect of P, reduction of T_m after composting at 58°C	Nucleating effect of WF and P, reduction of T_m after composting at 58°C	Slight reduction of T_m after composting at 58°C, disappearance of PLA melting peak after three months burying at 58°C
SEC		Mw decreased from about 40kDa to 5 kDa after composting at 58°C, No variation after composting at 35°C			Mw decreased from about 40kDa to 5 kDa after composting at 58°C, No variation after composting at 35°C	Mw decreased from about 40kDa to 5 kDa after composting at 58°C, No variation after composting at 35°C	Mw decreased from about 40kDa to 5 kDa after composting at 58°C, No variation after composting at 35°C	Mw decreased from about 40kDa to 5 kDa after composting at 58°C, No variation after composting at 35°C

Conclusion

Previously, good balance of properties and amount of bio-derived polymer has been obtained for HDPE-PLA blends, in which the amounts of HDPE and PLA were the same. The addition of wood flour allows a further reduction in the content of oil-based polymer, allowing, at the same time, an improvement in mechanical properties. Unfortunately, wood flour addition also increases matrix defectiveness. The addition of compatibilizers slightly improves matrix homogeneity and interaction with wood flour, modifying, at the same time, thermo-chemical properties of the composites.

In agreement with procedures followed for wood flour, we also analysed the effects of recycled waste paper. As expected, the higher the amount of recycled waste paper, the higher the elastic modulus. The main problem related to recycled waste paper fibres is their tendency to form agglomerates when mixed with polymers, as visible on SEM images.

Previous studies reveal interesting results when mixing fillers with different morphologies in terms of amount of filler and obtained properties. As a consequence, studies have also been carried out on composites with both wood flour and recycled waste paper. In particular, 30wt.% of wood flour and 10wt.% of recycled paper have been selected as an optimal mix. Mix of recycled waste paper (10wt.%) and wood flour (30wt.%) seems to increase both elastic modulus and tensile strength comparing results with the same filler amount (40wt.%) of only recycled waste paper or wood flour. A mix of wood flour, exempt from agglomerates formation, and recycled waste paper fibres, more effective in increasing elastic modulus, can optimize composite properties. The presence of Lotader AX8840, thanks to glycidyl methacrylate groups, seems to reduce matrix defectiveness, increasing at the same time interface with wood flour and recycled waste paper. The presence of Polybond 3029 seems to have a lower effect on matrix homogeneity and improvement of fillers-matrix interfaces.

More accurate analyses have been performed on the effect of wood flour and recycled waste paper on HDPE and PLA separately. A thermo-optical microscope from Zeiss has been used to study crystals growth in both neat HDPE or PLA and polymers with wood flour or recycled waste paper. Images suggest the formation of an individual spherulites row on the surface of the fibres, typical of fibres with moderate nucleating ability. Differential Scanning Calorimetry is one of the techniques to analyse the influence of fillers on polymer matrix crystallinity. Both wood flour and recycled waste paper seem to act as nucleating agents, reducing the half time crystallization $t_{1/2}$.

HDPE-based and PLA-based composites have been tested to analyse the effect of natural fillers (wood flour, recycled waste paper and a mix of both fillers) on polymer degradation. Moreover, samples made of HDPE-PLA blend and a mix of two fillers have also been tested. In fact, PLA is sensitive to temperature and humidity conditions, displaying higher reduction of Mw when composting is performed at 58°C. Moreover, natural fillers seem to influence mass variation, already at 35°C. In fact, degradation of fillers at 35°C allows a mass reduction during composting of composites, while neat PLA do not display any variation. This results are in agreement with other analyses performed (ATR-FTIR, TGA, DSC...), validating natural filler degradation under composting conditions.

5.13 References

- 1 S. Borysiak, A. Grzabka-Zasadzinska, M. Odalanowska, A. Skrzypczak, I. Ratajczak, "The effect of chemical modification on wood in ionic liquids on the supermolecular structure and mechanical properties of wood/polypropylene composites", *Cellulose*, vol. 25(8), pp. 4639-4652, 2018.
- 2 R.K. Donato, M. A. Benevgnù, L.G. Furlan, R.S. Mauler, H.S. Schrekker, "Imidazolium salts as liquid coupling agents for the preparation of polypropylene-silica composites.", *J. Appl. Polym. Sci.*, vol. 116, pp.304–307, 2010.
- 3 S. Zhu, Y. Wu, Q. Chen, Z. Yu, C. Wang, S. Jin, Y. Ding, G. Wu, "Dissolution of cellulose with ionic liquids and its application: a mini-review", *Green Chemistry*, vol. 8, pp. 325-327, 2006.
- 4 S. Livi, J. Duchet-Rumueau, J.F. Gérard, "Nanostructuration of ionic liquids in fluorinated matrix: influence on the mechanical properties.", *Polym*, vol. 52, pp.1523–1531, 2011.
- 5 A. Sankri, A. Arhaliass, I. Dez, A.C. Gaumont, Y. Grohe, D. Lourdin, I. Pillin, A. Rolland Sabaté, E. Leroy, "Thermoplastic starch plasticized by an ionic liquid" *Carbohydr.Polym.*, vol. 82, pp. 256–263, 2010.
- 6 L.C. Branco, G.V.S.M. Carrera, J. Aires-de-Sousa, I. Lopez Martin, R. Frade, C.A. Afonso, "Physico-chemical properties of task-specific ionic liquids, In: Ionic Liquids: Theory, Properties, New Approaches." Ed. Kokorin, A. InTech, Zagreb, Croatia., pp. 61–94. 2011.
- 7 B.K. Chen, T.Y. Wu, Y.M. Chang, A.F. Chen, "Ductile polylactic acid prepared with ionic liquids.", *Chem. Eng. J.*, vol. 215, pp. 886–893, 2013.
- 8 S. Livi, J. Duchet-Rumueau, J.F. Gérard, "Supercritical CO₂-ionic liquid mixtures for modification of organoclays.", *J. Coll. Inter. Sci.*, vol. 353, pp.225–230, 2011.
- 9 S. Livi, J. Duchet-Rumueau, J.F. Gérard, "Synthesis and physical properties of new surfactants based on ionic liquids: improvement of thermal stability and mechanical behavior of high density polyethylene nanocomposites", *J. Coll. Inter. Sci.*, vol. 354, pp. 555–562, 2011.
- 10 A.A. Shamsuri, R. Daik, "Utilization of an ionic liquid/urea mixture as a physical coupling agent for agarose/talc composite films.", *Materials*, vol. 6, pp. 682–698, 2014.

- 11 S. Livi, J. Duchet-Rumueau, T.N. Pham, J.F. Gérard, "A comparative study on different ionic liquids used as surfactants: effect on thermal and mechanical properties of high-density polyethylene nanocomposites.", *J. Coll. Inter. Sci.*, vol. 349, pp. 424-443, 2010.
- 12 Z.Bai, Q. Dou, "Non-isothermal crystallization kinetics of polypropylene/poly(lactic acid)/maleic anhydride-grafted polypropylene blends", 2016, *J Therm Anal Calorim*, vol. 126 (2), pp. 785-794.
- 13 M. Poletto, A.J. Zattera, R.M.C. Santana, "Structural differences between wood species: Evidence from chemical composition, FTIR spectroscopy and thermogravimetric analysis. *J. App. Polym. Sci*, vol. 126(S1), pp. E337-E344, 2012.
- 14 X. Liu, S. Khor, E. Petinakis, L. Yu, G. Simon, K. Dean, S. Bateman, "Effects of hydrophilic fillers on the thermal degradation of poly(lactic acid)" *Thermochim acta*, vol. 509, pp. 147-151, 2010.
- 15 M. Valente, A. Quitadamo, "Polymeric matrix composites at reduced environmental impact", *Polym Eng Sci*, vol. 57 (2), pp. 651-656, 2017.
- 16 M. Xanthos, "Polymers and Polymer Composites", in *Functional fillers for plastics, 2nd ed.*, Ed. M. Xanthos, Wiley, NJ, USA, 2009.
- 17 M.A. Al-Maadeed, S. Labidi, "Recycled polymers in natural fibre-reinforced polymer composites", in *Natural fibre composites*, Ed. Hodzic, A.; Shanks, R, Woodhead publishing, Cambridge, UK, 2014.
- 18 J.R. Araujo, W.R. Waldman, M.A. De Paoli, "Thermal properties of high density polyethylene composites with natural fibres: coupling agent effect.", *Polym Degrad Stabil*, vol. 93, 1770-1775, 2008.
- 19 S. Serizawa, K. Inoue, M. Iji, "Kenaf-fiber reinforced poly(lactic acid) used for electronic products", *J App Polym Sci*, vol. 100, pp. 618-624, 2006.
- 20 L.A. Baldenegro-Perez, D. Navarro-Rodriguez, F.J. Medellin-Rodriguez, B. Hsiao, C.A. Avila-Orta, I. Sics, "Molecular weight and crystallization temperature effects on poly(ethylene terephthalate) (PET) homopolymers, an isothermal crystallization analysis", *Polymers*, vol. 6, pp. 583-600, 2014.
- 21 L. Lin, Y. Xu, J. Qin, S. Wang, M. Xiao, Y. Meng, "Correlation between crystallization behaviour and mechanical properties of biodegradable poly(caprolactone-co-cyclohexene carbonate)", *Polymer-Plastic Technology and Engineering*, vol. 57, pp. 1530-1541, 2017.
- 22 J. Varga, A. Menyhard, "Thermooptical microscopy (TOM) for the investigation of the crystallization, melting and supermolecular structure of polypropylene and their multicomponent systems", *Curr Micr Contr Adv Sci Tech*, 2012.
- 23 T. Ke, X. Sun, "Melting behaviour and crystallization kinetics of starch and poly(lactic acid) composites", *J App Polym Sci*, vol 89, pp. 1203-1210, 2003.
- 24 Y. Orhan, J. Hrenovic, J.H. Buyukgungor, "Biodegradation of plastic compost bags under controlled soil conditions.", *Acta Chimica Slovenica*, 51(3), 579-588, 2004.
- 25 Y.G.C. Queirós, K.J.A. Machado, J.M. Costa, E.F. Lucas, "Brazilian synthesis, characterization, and in vitro degradation of poly(lactic acid) under petroleum production conditions", *J. Petrol. Gas*, vol. 7 (2), pp. 57-69, 2013.
- 26 B.S. Ndazi, S. Karlsson, "Characterization of hydrolytic degradation of polylactic acid/rice hulls composites in water at different temperatures." *EXPRESS Polym. Lett.*, Vol.5(2), pp. 119-131, 2011.
- 27 V.K. Gupta, A. O'Donovan, M.G. Tuohy, G.D. Sharma, "Trichoderma in bioenergy research: An overview", in: *Biotechnology and Biology of Trichoderma*, Ed. Druzhinina I.; Herrera-Estrella, A.; Gupta, V.K.; Tuohy M.G., 2014

- 28 R. Liu, J. Cao, L. Ouyang, "Degradation of wood flour/poly (lactic acid) composites reinforced by coupling agents and organo-montmorillonite in a compost test.", *Wood Fiber Sci*, vol. 45(1), pp. 105-118, 2018.
- 29 R.B. Santos, E.A. Capanema, M.Y. Balakshin, H. Chang, H. Jameel, "Lignin Structural Variation in Hardwood Species"; *J. Agr. Food Chem*, vol. 60, pp. 4923-4930, 2012.
- 30 G. Giacchi, B. Pizzo, I. Santoni, "Caratterizzazione chimica del degrado di campioni di legno archeologico imbibito: confronto fra diverse tipologie di analisi"
- 31 N.M. Stark, L.M. Matuana, "Characterization of weathered woodeplastic composite surfaces using FTIR spectroscopy, contact angle, and XPS." *Poly. Degr. Stab.*, vol. 92 pp. 1883-1890, 2007.
- 32 P. Calvini, A. Gorossini, "FTIR - Deconvolution Spectra of Paper Documents, Restaurator", *Internazionale Journal for the Preservation of Library and Archival Material*, Vol. 23 (1), pp. 48-66, 2003.
- 33 N.M. Stark, L.M. Matuana, "Surface chemistry changes of weathered HDPE/wood-flour composites studied by XPS and FTIR spectroscopy.", *Poly. Degr. Stab.*, Vol.86 pp. 1-9, 2004.
- 34 H. Kaddami, A. Magnind, A. Dufresne, A. Ahmad, "Bio-based polyurethane reinforced with cellulose nanofibers: A comprehensive investigation on the effect of interface.", *Carb. Polym.*, vol. 122, pp. 202-211, 2015.
- 35 A. Gorassini, P. Calvini, A. Baldini, "Fourier Transform Infrared Spectroscopy (FTIR) Analysis of Historic Paper Documents as a Preliminary Step for Chemometrical Analysis CMA4CH", 2008.
- 36 Q.H. Xu, Y.P. Wang, M.H. Qin, Y.J. Fu, Z.Q. Li, F.S. Zhang, J.H. Li, "Fiber surface characterization of old newsprint pulp deinked by combining hemicellulase with laccase-mediator system"; *Bioresource Technol.*, vol. 102(11), pp. 6536-6540, 2011.
- 37 J. Siroky, R.S. Blackburn, T. Bechtold, J. Taylor, P. White, "Attenuated total reflectance Fourier-transform Infrared Spectroscopy analysis of crystallinity changes in lyocell following continuous treatment with sodium hydroxide"; *Cellulose*, vol.17, pp.103-115, 2010.
- 38 S. Yildiz, E. Gümü Kaya, "The effect of termical modification on crystalline structure cellulose in soft and hardwood"; *Elvesier, Buildin and Environment* 42, pp.62-67, 2007.
- 39 M. Fan, D. Dai, B. Huang, "Fourier Transform Infrared Spectroscopy for Natural Fibres". *Intechopen.com*, 2012.
- 40 F. Lionetto, R. Del Sole, D. Cannoletta, G. Vaspollo, A. Maffezzoli, "Monitoring wood degradation during weathering by cellulose crystallinity", vol.5(10), pp. 1910-1922, 2012.
- 41 K.K. Pandey, A.J. Pitmanfm, "FTIR studies of the changes in wood chemistry following decay by brown-rot and whit-rot fungi"; *Int. Biodeter. Biodegr*, vol. 52, 151 - 160, 2003.
- 42 S. Dharmalingam, "Biodegradation and photodegradation of polylactic acid and polylactic acid/ polyhydroxyalkanoate blendsnonwoven agricultural mulchesin ambient soil conditions" 2014.

- 43 C.M. Chana, L.J. Vandia, S. Pratta, P. Halleya, D. Richardsonb, A. Werker, B. Laycock, "Composites of Wood and Biodegradable Thermoplastics: A Review", *Polym. Rev.*, vol.58(3), pp. 444-494, 2018.
- 44 S. Bhattacharjee, D.S. Bajwa, "Feasibility of Reprocessing Natural Fiber Filled Poly(lactic acid) Composites: An In-Depth Investigation.", *ADV MATER SCI ENG*, 2017.
- 45 A.K. Gupta, M. Biswal, S. Mohanty, S. K. Nayak, "Mechanical and thermal degradation behavior of sisal fiber (SF) reinforced recycled polypropylene (RPP) composites." *Fibres and Polymers.*, vol. 15(5), pp. 994-1003, 2014.
- 46 M. Poletto, A.J. Zattera, M.M.C. Forte, R.M.C.; Santana, "Thermal decomposition of wood: Influence of wood components and cellulose crystallite size.", *Bioresource Tech.*, vol.109, pp. 148-153, 2012.
- 47 R. Banat, M.M. Fares, "Thermo-Gravimetric Stability of High Density Polyethylene Composite Filled with Olive Shell Flour." *American Journal of Polymer Science*, vol.5(3), pp. 65-74, 2015.
- 48 M. Paabo, B.C. Levin, "A Literature Review of the Chemical Nature and Toxicity of the Decomposition Products of Polyethylenes.", *Fire and Materials*, vol. 11, pp.55-70, 1987.
- 49 F. Mengeloglu, K. Karakus, "Thermal Degradation, Mechanical Properties and Morphology of Wheat Straw Flour Filled Recycled Thermoplastic Composites.", *Sensors*, vol.8, pp. 500-519, 2008.
- 50 L.L. Krehula, Z. Katancic, A.P. Sirocic, Z. Hrnjak-Murgic, "Weathering of high density polyethylene-wood plastic composites", *J Wood Chem Technol.*, vol. 34, pp. 39-54, 2014.
- 51 D. Watkins, M.D. Nuruddin, M. Hosur, "Extraction and characterization of lignin from different biomass resources", *Journal of Materials Research and Technology*, Vol. 4(1), pp. 26-32, 2015.
- 52 H. Yang, R. Yan, H. Chen, D. Ho Lee, C. Zheng, "Characteristics of hemicellulose, cellulose and lignin pyrolysis", *Fuel*, vol.86, pp. 1781-1788, 2007.
- 53 H.S. Kim, H.S. Yang, H.J. Kim, H. J. Park, "Thermogravimetric Analysis of Husk Flour Filled Thermoplastic Polymer Composites", *Journal of Thermal Analysis and Calorimetry*, vol.76, pp.395-404, 2004.
- 54 A. Espert, W. Camacho, S. Karlson, "Thermal and Thermo Mechanical Properties of Biocomposites Made from Modified Recycled Cellulose and Recycled Polypropylene," *J. Appl. Polym. Sci.*, vol. 89, pp.2353-2360, 2003.
- 55 Q.J. Liao, Y.C. Jiang, L.S. Turng, C.C. Chen, "Biodegradability of PLA in compost environment.", SPE ANTEC Anaheim, 2017.
- 56 S.H. Lee, S. Wang, "Biodegradable polymers/bamboo fiber biocomposite with biobased coupling agent." *Composites: Part A*, vol. 37, pp. 80-91, 2006.
- 57 M.V.G. Zimmermann, V.C. Brambilla, B.M. Brandalise, A.J. Zattera, "Observations of the Effects of Different Chemical Blowing Agents on the Degradation of Poly(Lactic Acid) Foams in Simulated Soil." *Mat. Res.*, vol.16, pp.1266-1273, 2013.

6 Conclusion

The object of this research is the development of materials with high amount of bio-derived charge as well as study of the influence of the composition on their ability to biodegrade. The pursued strategy is based on both the introduction of natural fibres in oil-based and bio-derived polymers blends as matrix, reducing the amount of non-biodegradable charge in the material.

High density polyethylene have been chosen because it is one of the most representative recycled polymer on the market. Poly(lactic)acid and Soy protein isolate have been selected as bio-derived polymers.

Wood flour is an interesting natural filler, as a diffuse waste material, that can be used to make Wood Plastic Composites (well-known composites materials for their processability, properties and applications).

Recycled paper fibres are derived from industrial paper waste, which can't be subjected to traditional recycling processes. Fibres production from waste paper represents a difficult process in order to obtain dimensions coherent with the proposed application. Recycled paper fibres (average length of about 750 microns and average diameter of about 25 microns) have been obtained thanks to a micronization process working through impact, shear and turbulence. The use of these fibres represents another step, in order to produce a composite at reduced environmental impact. Moreover, an interesting interaction between particles and fibrous fillers have been displayed in previous work, with HDPE matrix, increasing the amount of cellulosic fillers in the composite.

HDPE-PLA blend with equal amounts of HDPE and PLA seems to be the best compromise between mechanical properties and reduction of non bio-derived charge. PE-g-GMA (Lotader AX8840) and PE-g-MA (Polybond 3029) appear to increase homogeneity of the blend. In particular, PE-g-GMA used in this study has proved to be more efficient in toughness improvement than our PE-g-MA. In fact, the higher content of glycidyl methacrylate (8wt.%) in comparison to maleic anhydride content (between 1.5 and 1.7wt%) can explain the higher efficiency of glycidyl methacrylate functional PE. SEM images display a better dispersion of PLA75-Lot25 than PLA75-Poly25. The amount of 3 wt.% of compatibilizer seem to optimize HDPE50-PLA50 strength, plasticity and affinity between HDPE and PLA, confirmed also by SEM images. In fact, neat HDPE50-PLA50 display a typical immiscible morphology, while the

addition of both PE-g-GMA and PE-g-MA increase homogeneity of the blend thanks to interactions between functional groups and PLA, in agreement with FTIR results.

SPI has been tested as possible alternative to PLA. SPI has been processed through extrusion when blended with both functional PE (Lotader AX8840) and HDPE. The use of this technique for SPI-based materials represents a novelty with respect of traditional solvent based processes. Glycerol in the amount of 30 wt.% has been added as plasticizer for SPI. In fact, SPI-PE-g-GMA blends display higher deformation and homogeneity when glycerol is added. FTIR and TGA analysis suggest physical interactions between glycerol and SPI, in agreement with literature results. Similarly to HDPE-PLA blends, first SPI has been blended with PE-g-GMA, obtaining again a good compromise with the equal amount of both polymers. SPI processing is characterized by a sensitive viscosity increase, as also confirmed by rheological measurements. Mechanical properties of HDPE-SPI blends are improved with the addition of glycerol and PE-g-GMA, in agreement with morphologies observed by SEM images. Composting tests, characterized with mass variation, visual observation and FTIR analyses, suggest rapid composting degradation of SPI, while HDPE appears to be stable. HDPE50-SPI50 display modification, suggesting a progression of composting.

Firstly, wood flour (WF) has been added to PLA or PLA-blended with functional PE. Moreover, wood flour has been treated with a phosphonium-based ionic liquid IL (Cyphos 109), in order to modify WF-matrix interfaces. As expected, IL treatment increases thermal stability of PLA filled with WF plus IL, compared to neat WF.

In order to further reduce the amount of oil-based polymer, the highest percentage of wood flour has been added to HDPE50-PLA50 compatibly with production process. Wood flour addition to HDPE-PLA improves mechanical properties, increasing at the same time defectiveness of the matrix. In fact, PE-g-GMA and PE-g-MA compatibilizers (3 wt.%) have been added, to improve matrix homogeneity.

Recycled waste paper has also been added, with the same proportion as wood flour. The higher the amount of recycled waste paper, the higher the elastic modulus, revealing otherwise a tendency to form agglomerates from SEM images.

Composites with a mix of 30 wt.% of wood flour and 10 wt.% of recycled waste paper have been produced. This mix seems to increase elastic modulus and tensile strength with respect to the

same amount of filler (40 wt.%) of only wood flour or recycled waste paper. The addition of PE-g-GMA seems again to be more efficient than PE-g-MA, in agreement with previous results.

The influence of wood flour and recycled waste paper on HDPE and PLA has been analysed through thermo-optical microscope (TOM) and differential scanning calorimetry (DSC). TOM displays the formation of individual spherulites row on the surface of fibres for both HDPE and PLA. DSC analyses reveal a nucleating effect of both wood flour and recycled waste paper on HDPE and PLA, reducing the half time crystallization.

Composites with HDPE and PLA matrix have been tested to analyse the effect of natural fillers (wood flour, recycled waste paper and a mix of both fillers) and temperature on polymer degradation. HDPE, as expected, did not display any relevant variation, confirming its stability under composting condition. PLA is sensibly influenced by temperature and humidity, with higher reduction of Mw when composting is performed at 58°C. Natural fillers seem to influence degradation process of composites, already at 35°C. In fact, degradation of fillers at 35°C allows a mass reduction during composting of composites, while neat PLA do not display any variation.

The main problem related to the development of hydrophobic polyolefins and hydrophilic bio-derived polymer is their miscibility. The addition of chemical compatibilizer, as done in this project, could be a strategy to compatibilize these blends. Another procedure could be the use of physical compatibilization, adding nanometric or sub-micrometric fillers (1,2 or 3D) acting on polymer rheology, interfacial tension and viscosity variation. In particular, the addition of these fillers reduces interfacial tension, increasing interfacial adhesion between polymers, hindering secondary phase coalescence.

Other future studies have to be done in order to complete the study on the effect of both wood flour and recycled waste paper on HDPE and PLA under composting condition. In fact, future development could focus on the analyses of biodegradation products to follow the process and increase the testing period time.

In agreement with the goal of our project, the highest possible amount of fillers should be introduced, compatibility with production process and properties obtained. With this goal, the optimization of the equipment developed by Sapienza research group, turbomixer, could be improve, having higher process control and obtaining optimized samples.



FOLIO ADMINISTRATIF

THESE DE L'UNIVERSITE DE LYON OPEREE AU SEIN DE L'INSA LYON

NOM : Quitadamo	DATE de SOUTENANCE : 01/03/2019
Prénoms : Alessia	
TITRE : Influence of wood flour and cellulose on the properties and the stability of formulations based on polyolefins and bio-based polymers.	
NATURE : Doctorat	Numéro d'ordre : AAAALYSEIXXXX
Ecole doctorale : Matériaux de Lyon	
Spécialité : Ingénierie des Matériaux Polymères	
<p>RESUME : The objective of this research is the development of high-added value materials, with high amount of bio-derived fillers, resulting in a more eco-friendly product. The pursued strategy is based on both the introduction of natural fibres, and the use of oil-based and bio-derived polymers blends as matrices, reducing the amount of nonbiodegradable amount in the material. The thesis project is based on the development of HDPE/PLA blends filled with natural fillers, such as wood flour and recycled paper fibres. High-density polyethylene has been chosen because it is one of the most representative recycled polymers on the market. Poly(lactic)acid has been selected as it is an important bio-degradable polymer on the market. The methodology developed here can be extended to other bio-degradable polymers, such as Soy Protein Isolate (SPI). Wood flour is a diffuse waste material, that can be used for production of Wood Plastic Composites. Recycled paper fibres are derived from industrial paper waste, which cannot be subjected to traditional recycling processes. Additives have been introduced in order to face the problem of different hydrophilicity between oilbase/ bio-derived polymers and with natural fillers. The optimal composition and production processes are challenges, not only for the use of these materials, but also for their disposal. The end-of-life of these samples can be evaluated through controlled bio-degradability and compostability, correlating material structure with the ability to biodegrade. The production of a material at reduced environmental impact with properties consistent with their applications is a first environmental advantage. Obtaining a controlled biodegradability, as a function of the applications, would give enhanced value to our materials. Several characterizations have been performed in order to analyse the effect of different compatibilizers and treatments such as: tensile tests, scanning electron microscopy, differential scanning calorimetry, thermogravimetric analyses, infrared spectroscopy, size exclusion chromatography and composting tests.</p>	
MOTS-CLÉS : Composites, Natural fillers, bio-derived polymer, blend	
Laboratoire (s) de recherche : IMP - Ingénierie des Matériaux Polymères (UMR5223), LIMS Sapienza	
Directeur de thèse: Marco Valente, Valérie Massardier	
Président de jury : Edoardo Bemporad	
Composition du jury : Bemporad, Edoardo, Professeur, Università degli studi Roma Tre Nanni, Francesca, Associate Professor, Università degli studi di Roma Tor Vergata, Robin, Jean-Jacques, Professeur, Institut Charles Gerhardt Montpellier, Bergeret, Anne, Professeur, Ecole des Mines.	